Modeling the past and future dynamic of the vegetation patterns at catchment scale using an ecohydrological Cellular Automata model

by Domenico Caracciolo

January 15, 2014

Cover picture:
Field with Flowers near Arles
by Vincent Willem van Gogh

"The planting of a tree, especially one of the long-living hardwood trees, is a gift which you can make to posterity at almost no cost and with almost no trouble, and if the tree takes root it will far outlive the visible effect of any of your other actions, good or evil."

George Orwell

To Federica, Chiara and Viola

Acknowledgments

I am sincerely grateful to my advisor Dr. Valerio Noto that provided me guidance and encouragement throughout my PhD study. His contribution and feedbacks have been fundamental for this thesis. I am also thankful for the support from my group members: Francesco Lo Conti, Angelo Forestieri, Elisa Arnone, Dario Pumo, Antonio Francipane, Francesco Viola, Carmelo Cammalleri, Antonia Incontrera. I acknowledge also them to have shared with me the lunch time in the "mensa Santi Romano".

I express gratitude to my co-tutor Dr. Erkan Istanbulluoglu for his fundamental contribution to the development of this thesis and his hospitality at the University of Washington.

I would like to thank all my group members and friends during my study in the University of Washington: Omer Yetemen, GU Wenquan, SAI Siddhartha, Xiaochi Zhou, Chris Frans, Ronda Strauch, Nicoleta Cristea, Suvi Kattainen, Olivia Wright.

Thanks and good luck to Valeria Puleo, Enrico Vitanza and Claudia Morici who shared this PhD experience with me.

A thanks to all my friends for being there when I needed them and even when I did not.

Finally I want to thank my girlfriend Federica for her continually support, and my parents, my sister Giuseppina and Paolo, I can not make this far without all your support.

Sommario

La vegetazione è una componente importante degli ecosistemi terrestri, che gioca un ruolo significativo nei processi di bilancio idrologico e nella ripartizione dei flussi di energia. Lo studio degli ecosistemi caratteristici delle zone aride e semi-aride rappresenta un obiettivo particolarmente interessante nell'ambito ecoidrologico, poichè l'acqua è generalmente considerata la causa principale della limitazione delle risorse. Un fattore importante in tale analisi è la topografia, la quale influenza fortemente lo stato e l'organizzazione spaziale della vegetazione attraverso il ruolo regolatore della radiazione solare e la ridistribuzione laterale dei flussi idrici. In particolare, un'area di studio ancora in gran parte inesplorata è data invece dalle dinamiche spaziali con cui la vegetazione si adatta a questi effetti di regolazione, nonchè alle implicazioni legate al bilancio idrologico a scala di bacino. Inoltre, le dinamiche spazio-temporali degli ecosistemi sono strettamente legate ai cambiamenti climatici e alle competizioni tra i diversi tipi di vegetazione.

Lo studio qui presentato si propone di modellare le dinamiche della vegetazione del passato e quelle attese in futuro in diverse aree, utilizzando un modello eco-idrologico basato sugli automi cellulari (CATGraSS). Tale modello pemette lo studio dei *patterns* e delle dinamiche spazio-temporale della vegetazione in funzione delle caratteristiche morfoclimatiche del sito e della disponibilità delle specie vegetali. In questa tesi, sono stati analizzati tre casi studio: la variazione del *pattern* di vegetazione in un bacino del Mediterraneo, determinata dal possibile cambiamento climatico futuro, e l'invasione (*encroachment*) di specie arbustive e arboree nelle praterie del Nord-Ovest dell'America.

Uno dei più importanti temi recentemente proposti nell'ambito dell'ecoidrologia è la previsione della risposta della vegetazione nelle regioni di transizione (*ecotone*) soggette agli ipotetici cambiamenti climatici. Nell'ambito di questa tesi il modello CATGraSS è stato utilizzato, sviluppato e migliorato, per modellare, a scala di bacino, i *patterns* di vegetazione in funzione dell'influenza della distribuzione spaziale della radiazione solare e della precipitazione. Il modello è stato implementato in un piccolo bacino in Sicilia. Tale modello è stato calibrato in modo da ottenere la distribuzione spaziale della vegetazione osservata nel clima attuale. L'analisi dei risultati del modello mostra l'importanza e il ruolo della radiazione solare nella determinazione dei *patterns*

di vegetazione in questo tipo di ecosistema e di clima. Al fine di studiare le dinamiche dei *patterns* di vegetazione legate ai cambiamenti climatici, il modello è stato inoltre utilizzato per la simulazione degli effetti di scenari climatici futuri ottenuti attraverso un generatore stocastico di precipitazione. A tal fine, gli output dei modelli climatici a scala globale (GCM) sono stati sottoposti ad una procedura di *downscaling* in modo da ottenere i parametri statistici della temperatura e della precipitazione future. È stata osservata un'elevata sensibilità della distribuzione della vegetazione alla variazione della precipitazione e della temperatura. In particolare, le simulazioni suggeriscono che i *patterns* di vegetazione osservati possono esistere solo nel clima attuale.

Le dinamiche spazio-temporali possono anche essere analizzate per studiare il fenomeno dell'invasione delle vegetazioni arbustive e arboree (*encroachment*), ovvero l'aumento della densità di alberi o arbusti indigeni nelle praterie del Nord America occidentale, avvenuta nel corso degli ultimi 150 anni. Per riprodurre questo fenomeno, le invasioni della vegetazione arbustiva (*creosote bush*) e del ginepro occidentale, osservate rispettivamente in New Mexico e in Oregon, sono state simulate nel secondo e nel terzo caso studio con l'utilizzo del modello CATGraSS. Le cause prese in considerazione sono: l'aumento del tempo si ritorno del fuoco, l'aumento del pascolo, la dispersione dei semi provocato dagli animali e la competizione tra i diversi tipi di vegetazione. Mentre nel caso studio in Oregon, i risultati del modello riproducono l'invasione del ginepro occidentale su tutta l'area di studio, con la conseguente scomparsa della vegetazione erbacea e arbustiva, nell'area studio del New Mexico, viene invece riprodotta l'invasione degli arbusti con un aumento dal 2% nel 1860 al 42% nel 2010 (percentuale attuale dell'arbusto). I risultati evidenziano come, tra i fattori più influenti nella modellazione dell'invasione, vi siano la riduzione della frequenza del fuoco e l'aumento del pascolo. Inoltre, tali risultati mostrano come il cambiamento climatico futuro possa determinare livelli di invasione che porteranno la diffusione dell'arbusto e del ginepro nelle rispettive aree di studio.

Abstract

Vegetation is an important component of terrestrial systems, playing a significant role in the processes of land-surface water and energy partition. Ecosystems of arid and semi-arid areas represent a particularly interesting object for studies, as water is generally considered to be the key limiting resource. While it is commonly observed that topography strongly affects the state and spatial organization of vegetation through the regulation of incoming solar radiation and lateral redistribution of water and elements, a still largely unexplored area is how plants adjust to these regulating effects relative to their location in a landscape, what are the implications for the water balance, and whether catchment vegetation-hydrology dynamics can be generalized in the form of terrain indices. Moreover, space and time dynamics of ecosystems are tightly related to fluctuations and changes in the climate and to the competition strategies of individual plants for different resources.

The research here presented aims to model the past and future dynamic of the vegetation at different scales using an existing ecohydrological Cellular Automata Model (CATGraSS). Vegetation patterns and dynamics are inseparably linked to initial conditions of site characteristics (i.e., topography, climate) and species availability. We have studied three case studies: the variation of the vegetation pattern in a Mediterranean basin subsequent to probable climate change, and the shrubs and junipers encroachment in the western north America grasslands.

Predicting vegetation response in regions of ecotone transition under a changing climate is one among grand challenges in ecohydrology. The CATGraSS model of vegetation coexistence driven by solar radiation and rainfall has been used, developed and improved here to modeling the vegetation patterns. The model is implemented in a small basin in Sicily. The model is forced first by a representation of the present climate, comparing the vegetation pattern obtained from the model with the current vegetation pattern. The model analysis underscores the importance of solar irradiance in determining vegetation pattern in this type of ecosystem and climate. To understand how can change the vegetation spatial patterns in the future as result of the climatic changes, the model has been forced with future climate scenarios generated using a stochastic weather generator. A downscaling procedure allows for the downscaling of an ensemble of climate model outputs deriving the frequency distribution functions of factors of change for several statistics of the temperature and the precipitation from a multi-model ensemble of outputs of

General Circulation Models (GCMs). A high sensitivity of the vegetation distribution to variation of rainfall and temperature has been observed. In particular the simulations suggest that the observed vegetation patterns can exist only in the current climate.

Spatio-temporal vegetation dynamics can be also discussed for studying the shrub and tree encroachment phenomenon that is an increase in density, cover and biomass of indigenous trees or shrubby plants occurred in the grasslands of western North America over the last 150 years. In order to reproduce this phenomenon, creosote bush and western juniper encroachments in New Mexico, and in Oregon have been simulated with the CATGraSS, respectively, in the second and third case study. The causes that have been considered for the encroachment in these case studies are: the fire return period increase, the grazing increase, the seed dispersal caused by animals and the plant type competition. While in the Oregon case study, the western juniper encroaches all the study area and the shrub and grass disappears, in the New Mexico site, the model is able to reproduce the shrub encroachment, simulating its increasing from 2% in 1860 to 42% (i.e., current shrub percentage) in 2010 highlighting among the most influent factors the reduced fire frequency and the increased grazing intensity. Moreover the future climate change will increase the encroachment and the shrub and juniper could settle in all the study areas.

Table of Contents

List of Figures

List of Tables

Introduction

The processes within the terrestrial biosphere and atmosphere are intrinsically coupled with the hydrological cycle. Vegetation is an important component of terrestrial systems, playing a significant role in the processes of land-surface water and energy partition. Ecosystems of arid and semi-arid areas represent a particularly interesting object for studies, as water is generally considered to be the key limiting resource. Interactions and feedbacks between the climate and biosphere have been the subject of a number of studies (e.g., Dickinson, 2000; Wang and Eltahir, 2000; Pielke, 2001). Recently, a multi-outcome interplay between vegetation, climate, and soil has been illustrated in a series of papers: Rodriguez-Iturbe et al. (1999), D'Odorico et al. (2000), Laio et al. (2001), Ridolfi et al. (2000), Van Wijk and Rodriguez-Iturbe (2002), Caylor et al. (2005), Ivanov et al. (2008a, b), Istanbulluoglu et al. (2012). Understanding the basic processes and feedbacks in the vegetation-hydrology system is the crucial link to characterizing the existence of different biomes and hydrological mechanisms that underlie the coupled dynamics. As pointed out by a number of researchers (e.g., Eagleson, 1978; Rodriguez-Iturbe, 2000; Mackay, 2001), the fundamental variables determining the vegetation structure and function are light (i.e., energy), soil moisture, and nutrient supplies. Besides vegetation itself, they represent the diagnostic variables of climate, soil, and topography, the key factors affecting their spatio-temporal dynamics. Explicit modeling of each one of these factors requires the simultaneous treatment of the others. Significant variations and feedbacks, which may occur over a wide range of temporal and spatial scales, must be considered. If some of the hydrological or vegetation components are not considered, the lack of dynamic feedbacks could seriously alter the modeled system's behavior (Band et al., 1993). Despite the recognition of the principal factors and their coupled nature, hydrology-vegetation modeling has been extremely simplified in at least one of the following contexts: the effects of climate forcing, soil spatial/vertical heterogeneity, and the impact of topography on lateral fluxes in the system and light exposure. Vegetation itself is considered as a static component with prescribed characteristics in most hydrology models. Therefore, hydrologic modeling has generally ignored the importance of vegetation as an important spatio-temporal dynamic component in the land-surface hydrological cycle and the existence of topographic controls on plant spatial distribution. Past simplifications are due to the overall extreme

complexity of the problem and differences in opinion among ecologists and hydrologists about what simplifications are necessary. While ecologists tend to over-simplify the hydrological mechanisms involved in vegetation function, hydrologists choose to neglect the dynamic features of vegetation.

Vegetation dynamics have temporal and spatial aspects. Indeed, time and space are related, in that forcing functions for vegetation change over large areas tend to be the same as those causing change over long time periods, and likewise for small areas and short time spans the causes of change are similar. Vegetation has been observed to exhibit a degree of spatial organization in a number of ecosystems in space and time. The emergence of these organization patterns is attributable to a range of spatial process such as local interactions between species, localized dispersal abilities and disturbance regime. Previous works suggest that topographic variables related to soil moisture and nutrient status (slope, hillslope position, upslope catchment area, topographic moisture index, topographically modeled soil moisture) are also related to plant species distributions. This mean that the vegetation distribution and pattern is mainly influenced by topography (e.g., Florinsky and Kuryakova, 1996; Sternberg and Shoshany, 2001; Walton et al., 2005; Dietrich and Perron, 2006; Franz et al., 2012; Pizzolla et al, 2012b; Manfreda et al., 2013; Zhou et al., 2013). While it is commonly observed that topography strongly affects the state and spatial organization of vegetation through the regulation of incoming solar radiation and lateral redistribution of water and elements, a still largely unexplored area is how plants adjust to these regulating effects relative to their location in a landscape, what are the implications for the water balance, and whether catchment vegetation-hydrology dynamics can be generalized in the form of terrain indices.

Vegetation pattern and dynamics are inseparably linked to initial conditions of site characteristics (i.e., topography) and species availability. Moreover, space and time dynamics of ecosystems are tightly related to fluctuations in the climate and to the competition strategies of individual plants for different resources (Bachelet et al., 2001; Walther et al., 2002; Lenihan et al., 2003; Boisvenue and Running, 2006; Nathan et al., 2011; Hanenwinkel et al., 2012). The climatic regime influence species' distributions, often through species-specific physiological thresholds of temperature and soil water potential tolerance. Divergent responses or susceptibilities of individual species to climate change may modify their interactions with others species at the same or adjacent trophic levels as long-term data on both terrestrial and marine organisms indicate (Walther et al., 2002).

Space-time scales can be also discussed in the context of their suitability for studying a phenomenon that influences vegetation systems: the encroachment, that is the increase in density, cover and biomass of indigenous trees or shrubs in various grasslands, especially arid and semiarid grasslands (Buffington and Herber, 1965; Burkahardt and Tisdale, 1976; Archer at al., 1988; Grover and Musick, 1990; Bahre and Shelton, 1993; Archer, 1995; Asner et al., 2003; Miller

et al., 2005; Coop and Givnish, 2007; Browning et al., 2008; Knapp et al., 2008a, b; He et al, 2010). The semiarid and arid grasslands of southwestern North America have changed dramatically over the last 150 years (Buffington and Herber, 1965; Archer et al, 1988; Archer, 1994, 1995; Browning et al., 2008; van Auken, 2009). Most recent studies have attributed the encroachment of shrubs or trees into the semiarid grasslands to an interaction of several factors (van Auken, 2000; 2009; Miller et al., 2005). The major cause of the encroachment of these species seems to be the reduction of grass biomass (fine fuel) by chronic high levels of domestic herbivory coupled to a reduction of grassland fires (Burkahardt and Tisdale, 1976; van Auken, 2000), which would have killed or suppressed trees and shrubs to the advantage of the grasses (Grover and Musick, 1990; Archer, 1995; Coop and Givnish, 2007; van Auken, 2009). The introduction of millions of domestic animals into the grassland and high livels of constant herbivory (van Auken, 2009) have caused the reduction of the aboveground grass biomass and the fine fuel, required for large-scale ecosystem fires. With the reduction of the fuel there was a concomitant decrease in grassland fires (Archer, 1994). Bahre and Shelton (1993) showed that the historical climate change did not influence the encroachment. In fact, links between changing climate since 1870s and tree or shrub encroachment in the semiarid grasslands are weak (Bahre and Shelton, 1993; Van Auken, 2000; 2009). Vice versa the future climate change could become the major cause of encroachment (Allen and Breshears, 1998; Van Auken, 2009). In the future, all of the above factors will probably continue to interact to regulate community composition and structure and the density of trees or shrubs will probably increase (Buffington and Herber, 1965; Bahre and Shelton, 1993; Miller et al., 2008; van Auken, 2009). The encroachment of shrubs in North American deserts, has been particularly well documented in the Sevilleta National Wildlife Refuge (SNWR), located in the northern Chihuahuan desert of the Rio Grande Valley, New Mexico. The SNWR shows a dramatic encroachment front of creosote bush (*Larrea tridentata*) into native desert grassland (He et al., 2010). Other parts of USA experienced a tree encroachment. For example in Oregon, since 1870, the area occupied by western juniper has increased 125 to 625 percent (Gedney et al., 1999; Miller et al., 2005; Miller et al., 2007). The increase of trees was a result of infill into shrub-steppe communities with relatively open low density stands of trees and expansion of juniper into sagebrush-steppe communities that previously did not support trees (Miller and Rose, 1995). This has also implications for future changes that will occur within these areas in the next 30 to 50 years (Miller et al., 2008). In the absence of disturbance or management, the majority of these landscapes will become closed woodlands resulting in the loss of understory plant species and greater costs for restoration (Miller, 2001). It is important to underlain that, even if the topic is strongly studied in literature, there are not studies that use hydrological or ecohydrological models in order to model and reproduce the phenomenon.

Moreover, in this context, regions of ecotone transitions, that are strongly interested to the phenomena above described, are also known to be highly sensitive to climate fluctuations (Zhou et al., 2013). In fact, the ecotone boundary is where plants actively migrate in space with changing environmental and climate conditions. Local competition processes have not received enough attention in ecological/hydrological climate change research because the existing models are typically simplistic and they do not explicitly model biomass dynamics in space. Therefore, traditional ecohydrological models are not able to predict how climate change could influence ecotone boundaries; this aspect makes our ability to predict such changes at the catchment and regional scales still limited. The importance of understanding and predicting climate change has been emphasized in many studies (IPCC, 2013). Climate change has potentially significant implications on the hydrological cycle and water resources (Bouraoui et al., 1999; Burlando and Rosso, 2002; Christensen et al., 2004; Liuzzo et al., 2010; Fatichi et al., 2013) and vegetation. In this context, research on climate change impacts on the ecohydrology is urgently needed as testified by many studies on the topic (Merritt et al., 2006; Bae et al. 2008; Bavay et al., 2009; Mooney et al., 2009; Manning et al., 2009; Morin and Thuiller, 2009; Pumo et al., 2010; Hirschi et al., 2012). Downscaling techniques were therefore developed to downscale information from General Circulation Models (GCMs) to local scales (Semenow and Barrow, 1997; Schmidli et al., 2006; Kilsby et al., 2007; Burton et al., 2010; Fatichi et al., 2011; 2013). Time series of meteorological variables representative of climate change scenarios can be subsequently used to analyze the influence of the climate change on the vegetation spatial patterns and biodiversity, at local or catchment scale. The climate change and the global warming is considered to be a major potential threat to change in hydrologic cycle, water resources and vegetation dynamics. Also biodiversity, that is the degree of variation of vegetation life (i.e., the number, variety and variability of plants in a particular area or region), is threaten by climate change (Gitay et al., 2005; Kannan and James, 2009). However, while potential adverse effects of climate change on biodiversity were typically claimed, evidence supporting this statement is tenuous. Increasing atmospheric carbon dioxide certainly affects plant physiology (Ainswort and Long, 2004; Norby and Zak, 2011; Fatichi and Leuzinger, 2013) and temperature affects species ranges (Loarie et al., 2009; Randin et al., 2013), phenology (Hegland, 2009; Körner and Basler, 2010; Richardson et al., 2013), and weather (e.g., Min et al., 2011) but quantification of the impacts in biodiversity is still challenging (McMahon et al., 2011). It is difficult to document major extinctions, even though climate change drastically altered the biology of many species.

In scientific literature the phenomena above described (i.e., dynamics of vegetation patterns) are often studied with cellular automata (CA) models that describe dynamics of local plant interactions by mathematical rules over a

domain of regular grids (e.g., Jeltsch et al., 1996; Jeltsch et al., 1998; van Wijk and Rodriguez-Iturbe, 2002; Caylor et al., 2004; Scanlon et al., 2007; Manfreda and Caylor, 2013; Zhou et al., 2013). Most CA model applications have emphasized biological processes including seed production, dispersal, and stem growth (e.g., Jeltsch et al., 1996, 1998; van Wijk and Rodriguez-Iturbe, 2002; Fernandez-Illescas and Rodriguez-Iturbe, 2004). Some recent ecohydrological CA models have linked plant competition to plant water stress, driven by rainfall characteristics (e.g., van Wijk and Rodriguez-Iturbe, 2002; Fernandez-Illescas and Rodriguez-Iturbe, 2004), leading to links between the statistical properties of vegetation cluster sizes and inter-annual rainfall variability. Patterns of vegetation on the landscape are mainly a function of the availability of different factors that support plant growth: light (Ricard and Messier, 1996; Martens et al., 2000), nutrients (Tilman, 1987; Lejeune et al., 2002; Rietkerk et al., 2004), water availability (Klausmeier, 1999; Couteron and Lejeune, 2001), and other environmental conditions that determine the timing and length of the growing season, such as temperature and snow (Myneni et al., 1997; Dunne et al., 2003). Therefore, plant types and patterns on the landscape are mostly controlled by climate at the regional scale, and soil texture, nutrients and site history at the local scale (Larcher, 1995; Svoray and Karnieli, 2010). Despite the potential important role of topography on water, nutrient and energy distribution, few studies have related topographic controls on the dynamics and patterns of plant co-existence (Caylor et al., 2005; Ivanov et al., 2008b; Franz et al., 2012; Manfreda and Caylor, 2013; Zhou et al., 2013). Especially in semiarid systems, topography mediates patterns of soil moisture feeding back on plant productivity, and could lead to specific vegetation patterns in certain hillslope with specific aspects and morphologies (e.g., Istanbulluoglu et al., 2008; Forzieri et al., 2011; Hwang et al., 2011; Svoray and Karnielli, 2011; Flores-Cervantes et al., 2013). Despite an explicit representation of topographic effects has been introduced in some recent ecohydrological models at the catchment scale (Tague and Band, 2004; Ivanov et al., 2008a; 2008b; Fatichi et al., 2012), these models have limited capacity to represent transitional plant dynamics and life histories (seed dispersal, establishment, age), which can critically dictate plant response to climate change and disturbances. As a result, there is a growing need to develop spatially-explicit transitional ecohydrologic CA models to predict: (1) the role of spatially varying resources (i.e., soil moisture and nutrients on vegetation responses); (2) shifts in ecosystem boundaries due to climate change and anthropogenic disturbances over complex terrain; and (3) spatially varying geomorphic responses which are tightly coupled with vegetation dynamics. While, climate change biogeoscientific studies concentrated on vegetation at large scales and mostly on carbon fluxes and storage, changes in species composition and ecotone boundaries were simulated crudely or almost neglected. In order to fill this gap and represent local processes enhanced CA models can be adopted.

Therefore, with regard to the ecohydrological analysis and modeling of the above mentioned processes there is still a vast field to explore, study and analyze. In this context, in this work, we used and further developed a spatially-explicit *Cellular Automata Tree-Grass-Shrub Simulator* (CATGraSS) that try to bridge the gap between the process representation required for dynamic vegetation modeling and CA rules to simulate species competition for space (Zhou et al., 2013). The CATGraSS model is here developed to analyze three case studies: the current vegetation pattern and its future variation in a Mediterranean basin subsequent to probable climate change, and the shrub and juniper encroachment in the western north America grasslands.

In the first case study the CATGraSS model is developed, first, to reproduce the current vegetation distribution and pattern and then to analyze how the vegetation distribution could change with the climate change in a region composed of different ecotones. Topographic effects on solar radiation are explicitly solved, leading to spatial variability in evapotranspiration, soil moisture, and plant water stress. Plant growth is simply driven by evapotranspiration through the Water Used Efficiency (WUE) concept, and both plant establishment and mortality are linked to plant water stress, assuming no nutrients limitation. CATGraSS is tested in a small Sicilian basin (Italy), characterized by a vegetational spatial pattern strongly controlled by aspect, with north-facing slopes characterized by oaks, and south-facing slopes by Indian fig Opuntia (evergreen perennial species drought tolerant) and grasses. The model is calibrated to reproduce the observed ecotone with a 5,000 years *base run* simulation. The calibrated CATGraSS model is used with the future climate change forcings to analyze potential shifts in vegetation distribution and changes in catchment biodiversity. In order to assess these future climate change forcings, a transient climate scenario from 2001 to 2100 has been generated using the stochastic *Advanced WEather GENerator* (AWE-GEN) (Ivanov et al., 2007; Fatichi et al., 2011; 2013). A downscaling procedure is applied to an ensemble of climate model realizations deriving the probability distribution functions of factors of change for several statistics of temperature and precipitation from a multi-model ensemble of GCMs' outputs (Fatichi et al., 2011; 2013). Specifically, the stochastic downscaling is carried out using realizations from twelve GCMs used in the fourth IPCC assessment report (4AR) for the future scenarios 2046-2065 and 2081-2100. Future increase in CO_2 concentration has been also taken into account by introducing a change in vegetation WUE and stomatal resistance. This study tries then to highlight the importance of understanding local scale plant interactions and the role of climate variability in determining impacts on vegetation dynamics.

In the second and third case studies the CATGraSS model is developed to reproduce and analyze, for the first time in literature, the shrub and juniper establishment and encroachment in two arid grassland areas in *Sevilleta National Wildlife Refuge* (SNWR, New Mexico) and in the Ochoco National Forest

(Oregon), respectively. Creosote bush and western juniper encroachment in the southwestern North America grasslands have been here simulated using a new version of the CATGraSS here developed and implemented. A fire cellular automata component has been introduced to simulate the fire effect. For each plant type, the probability of be ignited and killed by fire is a function of the fuel availability and of the vulnerability to fire. CATGraSS is also improved with grazing and seed dispersal functions, and its plant establishment algorithm has been modified. The causes here considered for the encroachment analysis are: the fire return period increase, the grazing increase, the seed dispersal caused by animals and the plant type competition. In order to understand if the wind direction could have influenced the shrub encroachment direction, the role of wind direction has been analyzed. First the model has been calibrated to reproduce the initial vegetation percentage in the study areas before encroachment in 1860 (in SNWR) or 1870 (in Oregon) with a 5,000 years simulation without encroachment causes. Then the CATGraSS has been run with the encroachment causes for 150 (or 140) years in order to obtain the vegetation distribution in 2010 (i.e., current vegetation distribution).

This thesis can be considered the first application of an ecohydrological CA model to examine the current vegetation composition and the future vegetation dynamics within ecotone boundaries under future climate scenarios and the encroachment phenomenon. We want to demonstrate how this research field has found new focus and new directions, and how it can play a pivotal role in decision making at many scales in order to decide the best actions to reduce and control the encroachment and the vegetation pattern change.

The manuscript is divided into two main parts: a theoretical part which includes the description of the phenomena, the state of the art and the models used for the analysis (three chapters); and an experimental part in which the three study cases are described and discussed (two chapters). A detailed description of each chapter is given below.

Chapter 1 will provide a description of the phenomenon of changes in vegetational types in both time and space, describing the influence of slope and aspect on the spatial vegetation distribution at catchment scale, and providing an analysis of the influence of climate on the vegetation distribution at catchment scale. Chapter 2 will provide a detailed description of the shrubby encroachment analyzing also the causes of it, provides an overview of the state of the art about the juniper (i.e., tree) encroachment in the western North America; moreover an overview of the state of the art and the research about this phenomenon will be shown. While Chapter 3 describes models and methods used in this thesis; in detail the ecohydrological Cellular Automata model, CATGraSS, the weather generator model, AWE-GEN, the General Circulation Models (GCMs) and the downscaling procedure will be discussed and shown, Chapter 4 will present the study case about the prediction of the impacts of the climate change on plant dynamics and tree-grass-shrub competition using the CATGraSS model in a

Mediterranean catchment in Sicily. Finally, Chapter 5 will present the study cases about the shrub and juniper encroachment in SNWR (New Mexico) and in the Ochoco National Forest (Oregon), respectively.

Part I

Theory

Chapter 1

Spatial and temporal vegetation dynamics

The processes within the terrestrial biosphere and atmosphere are intrinsically coupled with the hydrological cycle. This coupling is non-linear and multi-directional, implying that an individual component of the system is both under the influence of, as well as impacting upon the remaining parts of the system (Eagleson, 1978; Eagleson, 2002). Vegetation is one of the essential components that significantly influences the water and energy balances, establishing bi-directional links with the climate (Foley et al., 2000). For instance, Arora and Boer (2002) show that on a global average, the combined evaporation from leaves and transpiration account for about 72% of the total evaporation from the land surface. Interactions and feedbacks between the climate and biosphere have been the subject of a number of studies (e.g., Dickinson, 2000; Wang and Eltahir, 2000; Pielke, 2001). Recently, a multi-outcome interplay between vegetation, climate, and soil has been illustrated in a series of papers: Rodriguez-Iturbe et al. (1999), D'Odorico et al. (2000), Laio et al. (2001), Ridolfi et al. (2000), Van Wijk and Rodriguez-Iturbe (2002), Caylor et al., (2005), Ivanov et al. (2008a, b), Istanbulluoglu et al. (2012).

Understanding the basic processes and feedbacks in the vegetation-hydrology system is the crucial link to characterizing the existence of different biomes and hydrological mechanisms that underlie the coupled dynamics. As pointed out by a number of researchers (e.g., Eagleson, 1978; Rodriguez-Iturbe, 2000; Mackay, 2001), the fundamental variables determining the vegetation structure and function are light, soil moisture, and nutrient supplies. Besides vegetation itself, they represent the diagnostic variables of climate, soil, and topography, the key factors affecting their spatio-temporal dynamics. Explicit modeling of one of these factors requires the simultaneous treatment of the others. Significant variations and feedbacks, which may occur over a wide range of temporal and spatial scales, must be considered. If some of the hydrological or vegetation components are prescribed, the lack of dynamic feedbacks could seriously alter

the modeled system's behavior (Band et al., 1993). Despite the recognition of the principal factors and their coupled nature, hydrology-vegetation modeling has been extremely simplified in at least one of the following contexts: the effects of climate forcing, soil spatial/vertical heterogeneity, and the impact of topography on lateral fluxes in the system and light exposure. Topography, observed to have a significant influence on vegetation distribution (e.g., Florinsky and Kuryakova, 1996; Franklin, 1998; Meentemeyer et al., 2001; Dirnbock et al., 2002; Kim and Eltahir, 2004), is particularly often disregarded in modeling analysis. Vegetation itself is considered as a static component with prescribed characteristics in most hydrology models. Therefore, understanding the impact of climatic disturbances, topography and soil variability on vegetation, however, requires dynamic vegetation modeling across the landscapes.

In this context, coupling of a vegetation model that explicitly considers plant dynamics to a spatially-distributed hydrological model should provide a necessary step towards an integrated approach. The hydrological model will provide the framework to account for the spatial variability of the topography-controlled continuous rainfall-runoff process, subject to stochastic climatic forcing. In this spatially explicit scheme, vegetation will grow and die, reflecting its biophysical and biochemical characteristics, seasonal and interannual climate forcing, and the competition for vital life resources. Such a framework offers a variety of opportunities to explore the bi-directional interactions between vegetation and hydrological mechanisms and represent an important advancement toward integrated ecohydrological modeling. Ecosystems of arid and semi-arid areas represent a particularly interesting object for studies, as they comprise some of the major biomes of the world, often exhibiting a delicate equilibrium between their essential constituents. In these systems, soil water is generally considered to be the key resource affecting vegetation structure, distribution and composition (Ivanov et al., 2008b). The mechanisms through which water limitation affects ecosystems are related to carbon assimilation via the control of photosynthesis and stomatal closure. Many important issues depend on the quantitative understanding of dynamics inherent to these ecosystems including human interference, climate change, environmental preservation, and proper management of resources.

With regard to the potential constraints to the vegetation pattern at global scale, Nemani et al. (2003) constructed a map of the relative contributions of climatic controls on global vegetation, assuming no nutrient limitation. They used long-term monthly climate statistics to build simple bioclimatic indices. From these indices, they estimated that water availability most strongly limits vegetation growth over 40% of Earth's vegetated surface, whereas temperature limits growth over 33% and radiation over 27% of Earth's vegetated surface (Figure 1.1). These factors tend to be colimiting. For example, cold winter temperatures and cloudy summers limit high-latitude Eurasian vegetation,

whereas cold winters and dry summers limit vegetation in western North America. Tropical areas are never limited by low temperatures but may have either a sustained dry season or nearly perpetual cloud cover that limits solar radiation.

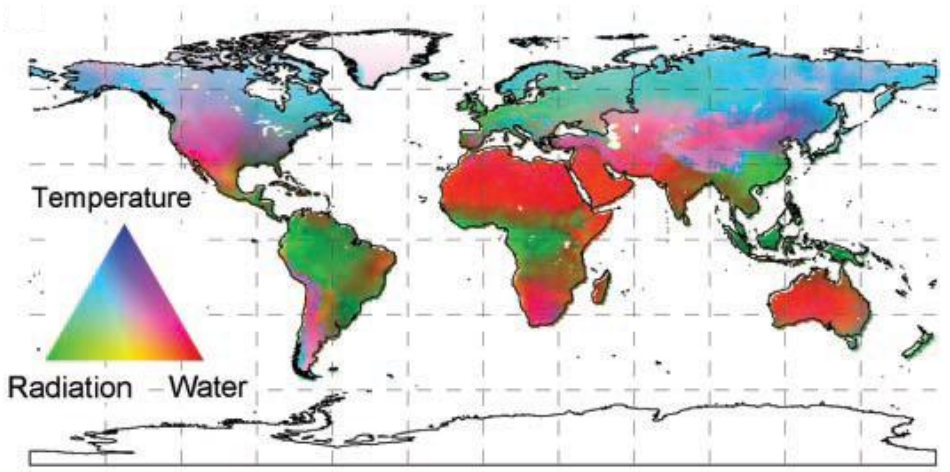

Figure 1.1. Geographic distribution of potential climatic constraints to plant growth derived from long-term climate statistics (Nemani et al., 2003).

Following the classification above described, in this thesis we worked in water limitated environments, moreover assuming no nutrients limitation.

This chapter tries to highlight aspects of the vegetation dynamics related to water availability giving particular attention to two important aspects: the influence of the morphology and of the climate and of the possible climate changes on the spatial vegetation distribution. The chapter provides in section 1.1 an ecological description of the phenomenon of changes in vegetational types in both time and space (plant *succession*), in section 1.2.1 a description of the influence of slope and aspect on the spatial vegetation distribution at catchment scale, trying to point out, in section 1.2.2, the influence of climate on the vegetation distribution at catchment scale.

1.1. Plant succession

1.1.1. Prediction of vegetation change

What kind of plant communities occur in an area? How does the composition of a plant community change over time? These were the kinds of questions posed by pioneering plant ecologists. As explanations began to accumulate, it

became increasingly clear that the distribution and dynamics of vegetation were complex and intricate phenomena. What causes these diverse spatial and temporal patterns? One approach to answer to this question is to examine the proximate causes of the distribution of populations of species in space and time. This approach assumes that all macro or community-level features represent a collection or summation of micro- or population-level phenomena. In other words, community-level changes (*succession*, fluctuation, maturation) are ultimately the results of populations becoming established and spreading, the growth of individuals in those populations, and populations becoming extirpated (van der Valk, 1985; Glenn-Lewin et al., 1992). *Succession* is the term used to describe the phenomenon of changes in vegetational types in both time and space (Glenn-Lewin et al., 1992).

The broadest goals of scientific theory are the understanding and explanation of observed reality through a system of concepts, laws and empirically based generalizations. An important means of testing the fit between theory and observed phenomena is prediction (Pickett and Kolasa, 1989). Prediction is used for testing the component models and for evaluating the appropriate scope of theory in vegetation science. Prediction, either as a means for testing theory or as a goal itself, is particularly important to the field of vegetation dynamics.

Beyond the scientific goal of relating observed patterns of vegetation change to an explanatory theoretical framework, there are numerous practical reasons for predicting vegetation change.

In the context of growing concern over the possibility of climate change resulting from global anthropogenic atmospheric changes, the need to be able to predict vegetation change at a variety of spatial and temporal scales has never been more urgent.

The preservation of plant and animal species, biotic communities, and productive and aesthetically pleasing landscapes is unlikely without a thorough knowledge of the patterns and processes of vegetation change (Glenn-Lewin et al., 1992).

Although humans have long recognized the phenomenon of *succession*, the scientific study of *succession* began only at the end of the nineteenth century. Many of the themes and problems recognized by plant ecologists during the first two or three decades of the twentieth century are still important research objectives in the modern field of vegetation dynamics.

Clements (1904; 1916) viewed *succession* as a highly orderly and predictable process in which vegetation change represented the life history of a plant community that assumed organism-like attributes. From initially distinct, environmentally determined starting points, communities were believed to converge through *succession* towards a *climax* vegetation, whose characteristics were controlled solely by the regional climate. According to this viewpoint, the *climax* was a condition of great stability in which the vegetation had reached an equilibrium with the present climate. Clementsian successional theory was an

equilibrium viewpoint in its assumption that successional change necessarily progressed towards the development of a stable vegetation type in equilibrium with the regional climate.

Clements (1904; 1916) developed a scheme of processes that drive *succession*:

1. *nudation*, which is the creation of bare area or partially bare area by the disturbance which initiates *succession*;
2. *migration*, arrival of organism at the open site;
3. *ecesis*, the establishment of organisms at the site;
4. *competition*, the interaction of organisms at the site;
5. *reaction*, the modification of the site by the organisms thereby changing the relative abilities of species to establish and survive;
6. *stabilization*, the development of a stable climax.

Community dynamics are characterized by a complexity of processes, patterns and mechanisms, and repeated disturbance is important in many systems.

In the 1960s Ramond Margalef and Eugene Odum attempt to draw together the disparate observations of successional phenomena into unifying theories of *succession*. Margalef (1958; 1963; 1968) applied information theory to ecological systems as a strategy for seeking and explaining universal patterns of successional change. He argued that the linkages among trophic levels and populations represented information and that *succession* represents a natural trend towards the accumulation of greater information in an ecosystem. He believed *succession* is driven from simple ecosystems towards more complex ecosystems with more trophic levels and greater diversity of species and life-forms.

Odum (1969) summarized a number of successional trends in community- and ecosystem-level properties (e.g., biomass, diversity) which he postulated result from the tendency of ecosystems to develop towards greater homeostasis. He urged that, within the limits set by the physical environment, *succession* necessarily proceeds towards an ecosystem of maximum biomass and diversity.

Both theories include developmental schemes where successional change is viewed largely as the consequence of relationships and interactions within a community, whereas external influences such as large-scale disturbance, climate variation, and immigration of new species are either relegated to minor roles or are assumed to be constant.

Therefore since its initial development in the late nineteenth century, the study of vegetation dynamics has cycled through periods of active study and quiescence. In the last four decades, advances in our knowledge of the nature of communities, the dynamics of populations, and the structure and function of ecosystems, along with our greatly increased capability for quantitative analysis and modelling of vegetation phenomena, have led to another re-examination of the conceptual basis of vegetation dynamics.

By the early 1970s, ecologists recognized the inadequacy of both Clementsian successional theory and the Margalef-Odum synthesis. There was an increased appreciation of the need for site-specific information on the mechanisms, or approximate causes, of vegetation change.

Since 1970 two major conceptual trends have dominated research on vegetation dynamics: a shift away from holistic explanations of successional phenomena towards reductionist and mechanistic approaches emphasizing proximate causes of vegetation change; and a shift away from equilibrium towards non-equilibrium paradigms. Predictions are derived empirically from knowledge of the mechanisms of vegetation change which apply to a particular local habitat instead of being deductively derived from a universally applicable theory (Pickett et al., 1987).

The view of *succession* as primarily a species replacement process driven by reaction, or plant-controlled environmental modification, has been rejected (Peet and Christensen, 1980). It has been superseded by several non-mutually exclusive hypotheses that may all apply in varying degrees to any one successional sequence. The hypotheses represent *succession* as gradients in time or resource availability (Tilman, 1985; 1988), the consequence of differential longevity and other population processes (Peet and Christensen, 1980), the result of differences in life history characteristics (Noble and Slatyer, 1980) or as a stochastic process (Horn, 1976). Common to all of these hypotheses is a reductionist perspective emphasizing life histories and competitive interactions of the component species rather than emergent properties of communities (Peet and Christensen, 1980). Contemporary ecologists view vegetation changes as the outcome of populations interacting within fluctuating environmental conditions. Thus, parameters such as birth and death rates, and plant growth rates under varying environmental conditions form the core of quantitative models of vegetation dynamics. For long-lived plants, the lack of data on demographic parameters is often a serious constraint for the calibration of these models (Glenn-Lewin et al., 1992).

The modern view of vegetation changes emphasizes the importance of repeated, relatively frequent disturbance and accepts continuous change in vegetation as the norm (Pickett and White, 1985). Indeed, we have come to accept a view very much like the one articulated by Cowles (1901), who defined *succession* as a ‘variable approaching a variable rather than a constant’.

1.1.2. Vegetation dynamics in space and time

Vegetation dynamics are characterized by both temporal and spatial aspects deeply analyzed in the following sub-sections. Indeed, time and space are related, in that forcing functions for vegetation change over large areas tend to be the same as those causing change over long time periods (Austin, 1981; Glenn-Lewin et al., 1992). The course of vegetation dynamics depends upon the spatial scale of the vegetation and any disturbance.

Conversely, spatial patterns of vegetation change with *succession*. The latter is a vegetation gradient in time and space, and different dynamic patterns can be ordered over the scale of time: *fluctuations*, *patch dynamics*, *cyclic succession* or log-term *succession*.

Vegetation dynamics are based on the population processes of the constituent plants. It is in the population processes that one could find the mechanisms of vegetation dynamics, and the explanations for the patterns observed. Successional histories typically exhibit multiple pathways, and may also show community patterns such as convergence, divergence or cycles, which will depend not only upon the initial conditions and mechanisms of *succession*, but also on community circumstances such as species diversity, landscape complexity and community isolation.

1.1.2.1. Temporal aspects of dynamics

The temporal aspects of vegetation dynamics could be segmented in: (1) short term, or the domain of *fluctuations*; (2) long term, the domain of vegetation history on time scales of millennia; and (3) the middle range, or what is, usually, the domain of *succession*.

Fluctuations are impermanent vegetation changes that comprise the natural temporal variation in plant abundance or aspect in a community over short time periods (Miles, 1979; Vale, 1982). Variation in an equilibrium state would be around a mean composition, but it is perhaps more likely that fluctuations will be around some kind of temporal trend in the vegetation. Many fluctuations in vegetation occur because of environmental changes on the same time scales, such as fluctuations in precipitation (Albertson and Tomanek, 1965) or growing season temperature. Mild disturbances on a short time scale might also produce what appear to be fluctuations (Gloaguen, 1990).

In a shifting mosaic, species increase or decrease at any particular position, but the original average remains more or less constant. What appears to be a fluctuation on a small or meso-scale, might at the same time be part of a shifting mosaic such that over a large scale, the average composition changes little.

Succession is compositional change, usually evident over a few decades to a few centuries. The change is in some way directional (Miles, 1979; 1987), uni- or multidirectional, although the directions followed may be determined only after the fact. Long-term change occurs over many centuries or millennia, and results from equally long-term environmental changes such as climatic change or soil development, from species' migration, or from other long-term forces.

The distinction between *fluctuation* and *succession* is arbitrary in that a large enough fluctuation over a long enough period of time becomes *succession* (Austin, 1981; Bornkamm, 1988). Vegetation cycles over a long enough period can, nevertheless, be thought as fluctuations. Distinguishing succession from long-term changes requires a similar arbitrariness. Species range changes are individualistic and probabilistic; vegetational composition and structure are not

stable over periods of centuries to millennia, nor are community boundaries stable. The underlying processes of plant population dynamics are the same for fluctuation, succession and long-term change.

1.1.2.2. Spatial aspects of dynamics

One can conceive of vegetation dynamics as a regional process, as development and change of vegetation in a landscape. Or, if we wish to consider only an area large enough for compositional change actually to occur, *succession* can occur in very small area. Thus, again vegetation dynamics exhibits a continuum, this one of horizontal scale: fine-scale gap phase processes, regeneration, community-wide dynamics, landscape dynamics. A community can be viewed as a changing mosaic of patches of different size, age, structures, and composition (Martinez-Ramos et al, 1989). This means that spatial patterns are important for an understanding of community change and cannot be ignored as random noise (Austin, 1981).

The significance of spatial process in vegetation dynamics can be illustrated in several ways. In the nucleation concept of Yarranton and Morrison (1974), *succession* proceeds by the expansion and coalescence of initially small *nuclei* of a vegetation element. Other studies include:

1. differential colonization resulting from both environmental heterogeneity (McDonnell, 1988) and the locations of seed sources;
2. neighbourhood effects on establishment at a particular point (Ryser, 1990);
3. the influence of spatial heterogeneity on disturbances such as fire and grazing (e.g., Tutner and Bratton, 1987).

Some of the most successful models of vegetation dynamics function by summing over small-scale or gap processes (Botkin, 1992) to produce a profile of community *succession*. Busing (1991) has developed a spatial model of forest dynamics that is based on gap theory, and the heathland dynamics model of Prentice et al. (1987) is explicitly spatial in that points given by spatial coordinates are covered by individual species.

1.1.2.3. Vegetation dynamics as a gradient in time

One of the difficulties in dealing with vegetation dynamics theory is that more than one thing may be changing (Glenn-Lewin et al., 1992). Miles (1979; 1987), considers vegetation change to be the essence of *succession*. Contrast this with, Odum (1969) and Austin (1981), who treat *succession* more broadly as change in any measure of ecosystem character.

Most communities exhibit multiple vertical strate. Some layers may undergo significant change while others show little change. For instance, a ground fire may initiate or modify change in the herbaceous layer, while having little direct effect on the canopy layer. Once again, if we accept that vegetation dynamics are population-based processes, we conclude that there is no fundamental ecological

reason to exclude any change in a community, regardless of kind or vertical distribution, from our concepts and models of vegetation dynamics.

Succession can be thought of as a compositional gradient in time, either of species or of other community characters (Peet and Christensen, 1980). If the spatial axis of traditional gradient analysis is replaced by a temporal one, then the rise and fall of the species' abundance curves represent the dynamics of plant populations and the shape of the curves will reveal the rates and degrees of change. With the concept of a temporal gradient, fluctuations and cycles will show up as repeating patterns: fluctuations will appear as periodic compositional change. Species replacement during *succession* will appear as aperiodic compositional change (Glenn-Lewin et al., 1992).

Changing communities exhibit individualistic behaviour, and vegetation dynamics are population-based processes (Peet and Christensen, 1980). Consequently, community dynamics can be made more sensible if we directly address population-based change in the context of what is changing (e.g., structure, composition), the character of the environment and the scales, both physical and temporal, at which changes occur. For instance, treating changes in relative abundances (due to the differential plant growth) separately from species replacement processes has the advantage of separating growth-based, quantitative changes from those requiring immigration and establishment in an existing vegetation, or in a gaps in an existing vegetation (van der Valk, 1985). Such immigration and establishment reflect the invasive ability of the plants and the resistance to invasion of the existing vegetation.

1.1.3. Mechanisms

It is fruitful to examine the population mechanisms that lead to vegetation variation and distribution in time and space.

The mechanisms that lead to community-level pattern are: *colonization*, *competition*, *species interaction* (inhibition, tolerance), *disturbance*. Then the mechanisms may result, on the one hand, from the properties of the plants themselves, such as colonization abilities, growth and development and life-history characteristics. On the other hand, the mechanisms may result from plant interactions, which may be studied at the plant-plant level, or as net effects, or may be mediated by third parties (Grubb, 1988; Glenn-Lewin et al., 1992).

1.1.3.1. Colonization

Colonization results from interaction between the presence or immigration of the plants, the spatial patterns of the environment and existing vegetation, and the morphology and physiology of the plants. The presence or immigration of plants will reflect the varying contributions of seed banks, seedling banks and differential seed dispersal. Distance to seed sources, spatial distribution of seed source, neighbourhood influences on establishment and the movement of seed

from productive areas into unproductive ones, thereby maintaining populations in the unproductive sites are all important in determining the outcome of colonization. The colonization ability of organisms depends upon their morphological, physiological and reproductive characteristics.

1.1.3.2. Competition

In the *competitive hierarchy* model of Horn (1981), late *succession* plants are increasingly dominant by virtue of their competitive *succession* with early species, but the late successional species can also invade in the earliest stages of *succession*. Pattern of replacement, then, are determined by the outcome of the competition among the various species. However, if in a changing or non-constant environment, the competitive relationships of the species are likely to change, the outcome of *succession* by this mechanism cannot be predicted (Connel, 1978).

1.1.3.3. Changes due to species interactions

Vegetation change resulting from the effects of particular species on other species, either directly or through environmental modification, has long been a central theme of *succession*. Connell and Slatyer (1977), in a seminal work summarized species' interactions during *succession* into three processes: facilitation, inhibition and tolerance.

Facilitation describes a situation in which one or more species enable the establishment, growth or development of other species. Facilitation may be caused by environmental changes that are favourable to future species. For example, in Alaska, the roots of shrubby plants contain nitrogen-fixing bacteria, which greatly increase the amount of inorganic nitrogen present in soils. This increased availability of nitrogen aids the growth of willow (i.e., *Salix*, a deciduous tree) seedlings in areas without other competition. Eventually, however, willows grow more rapidly than the shrubby plant, leading to a reduction in the abundance of the pioneer species.

Inhibition is the prevention of plant maturation or growth, or, especially, the prevention of plant establishment, by existing plants. All of these constitute negative effects. An example of inhibition is the *allelopathy*, i.e., a biological process by which one plant produces one or more biochemicals that limit the growth, survival, and reproduction of other plants (Rizvi and Rizvi, 1992). Went (1955) first suggested that the creosote bushes (i.e., shrub), through its root, excretes toxic substances that kill seedlings of other plants (e.g., grass). Knipe et al. (1966) further analyzed the germination and growth of semi-arid grassland species treated with aqueous extract from creosote bush. Their data indicate that the germination of grasses (e.g., black grama) is significantly reduced, while shrub species were not affected.

Tolerance describes the situation where one or more species neither inhibit nor enable other species during *succession*. It represents a zero net outcome of species' interactions.

1.1.3.4. Disturbance

We have to distinguish among a number of different ways in which *disturbance* has been defined. Grime (1979) defines it as 'the mechanisms which limit the plant biomass by causing its partial or total destruction'. Forman and Godron (1986) identify disturbance as 'an event that causes a significant change from the normal pattern in an ecological system'. A third approach to disturbance defines it as processes which either the survivors of disturbance or new colonists respond (Runkle, 1989). Thus, accelerated growth of small individuals that are released from competition is one pattern of response to disturbance. Another is the creation of bare ground, loose soil, light gaps, or other situations which form microsites in which recruitment can occur.

Three not entirely independent dimensions of disturbance are space, time and magnitude. The spatial dimension is the extent of the disturbance, the physical dimensions of area and volume, and location, in particular in relation to environmental gradients. The temporal dimension includes frequency and predictability. These temporal factors combine in the concept of turnover and return time (White and Pickett, 1985). In the case of fire, and probably other kinds of disturbance as well, the season of the disturbance is another important aspect of the temporal dimension of disturbance. The magnitude is the force of the event, or the severity as reflected by the effects on the vegetation (White and Pickett, 1985). The severity of disturbance will depend upon the character of the disturbance force and the nature of the existing vegetation, especially its sensitivity to disturbance.

1.2. Ecohydrological approaches for vegetation dynamics

As previously seen, the study of the vegetation dynamics is related to a complex multidisciplinary approach, which tries to take into account all the aspects that we have referred above.

Since this thesis tries to highlight aspects of the vegetation dynamics related to water availability through approach that nowadays can be defined *ecohydrological*, particular attention is here given to two important *ecohydrological* aspects: the influence of the morphology which impacts on the hydrologic balance (section 1.2.1) and of the climate and of its possible changes (section 1.2.2) on the spatial vegetation distribution.

Ecohydrology is the science that studies the mutual interaction between the hydrologic cycle and the ecosystems. The main purpose of *ecohydrology*, that is

to join together concepts and theories of two different disciplines, is, in part, contained in the etymological interpretation of its name, that derives from the crossing between the terms ecology (the science of the interrelationships between living organisms and their environment) and hydrology (the science of the hydrological cycle, dealing with the properties, distribution, and circulation of water in the environment). Thus, *ecohydrology* bridges the fields of hydrology and ecology and proposes new unifying principles derived from the concept of natural selection (Eagleson, 2002). In fact, natural ecosystems are complex structures whose peculiarities and properties depend on three fundamental factors, interacting with each other: climate, soil and vegetation. The first aim of *ecohydrology* is thus to understand the various and numerous characteristics and relationships of these factors.

1.2.1. Influence of slope and aspect on the spatial vegetation distribution at catchment scale

Topography is the major driver of irradiation distribution and hydrologic processes across a landscape (Nichols et al., 1998; Yeakley et al., 2000; Pierce et al., 2005; Suzaki et al., 2005; Gallardo-Cruz et al., 2009; Pizzolla et al, 2012a). Patterns of incoming solar radiation cause shifts in available energy, evapotranspiration and water balance conditions, which, in turn, are responsible for major changes in vegetation structure, diversity and pattern (Armesto and Martınez, 1978; Franklin et al., 2000; Martinez-Yrızar et al., 2000; Urban et al., 2000; Vogiatzakis et al., 2003; Hietel et al., 2004; Caylor et al., 2005; Ivanov et al., 2008b; Pizzolla et al., 2012a, b; Manfreda et al., 2013; Zhou et al., 2013). In fact, the amount of solar radiation is one of the primary variables influencing evapotranspiration and thus soil moisture in semi-arid regions (Monteith, 1973).

The importance of slope, aspect, and topographic variations to the distribution of terrestrial plant communities has been noted and analyzed by many authors (Cantlon, 1953; Yeaton and Cody, 1979; Lieffers and Larkin Lieffers, 1987; Kutiel, 1992; Florinsky and Kuryakova, 1996; Sternberg and Shoshany, 2001; Walton et al., 2005; Ivanov et al., 2008b; Caylor et al., 2009; Franz et al., 2012; Pizzolla et al, 2012b; Manfreda et al., 2013; Zhou et al., 2013). Mapping of vegetation spatial patterns at large scales based upon moisture and calculated solar radiation has been attempted with remote sensing technology (Dymond and Johnson, 2002). In Figures 1.2, 1.3, 1.4 three examples of vegetation patterns in relation to topography are shown for different sites in USA.

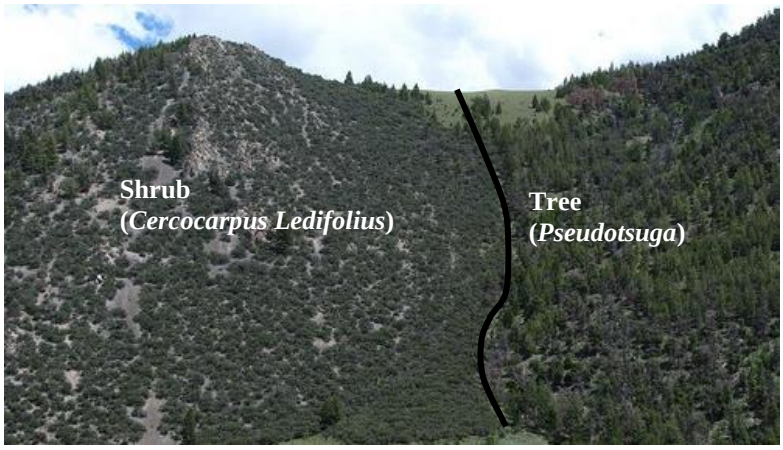

Figure 1.2. Distribution of plant types in relation to topography in Lost River Range (Idaho).

Figure 1.3. The coastal sagescrub community of southern California's Santa Monica Mtns. The slope on the left side is north-facing, thus moister and dominated by *Ceanothus sp.*. The south-facing slope on the right side is much drier (receiving more direct sun), and is more sparsely vegetated with the more drought tolerant *Artemisia californica* and *Yucca whipplei*.

Figure 1.4. Vegetation pattern in relation to slope and altitude in South Baldy, New Mexico.

The available solar radiation that depends on climatic conditions and morphology, may strongly modify hydrological processes at the local scale.

Basin morphology, in fact, modifies the amount of direct solar radiation, and also the amount of diffuse and reflected solar radiation received by a given point of an area. The slope angle, aspect and elevation of surfaces affect the amount of direct solar radiation which is incident upon them. The effect of slope may be related to Lambert's cosine law by which, for direct solar radiation, the angle between the solar beam and the sloping surface determines its intensity (Figure 1.5). The orientation of such a slope, referred to as its aspect, also affect the intensity of solar radiation upon it.

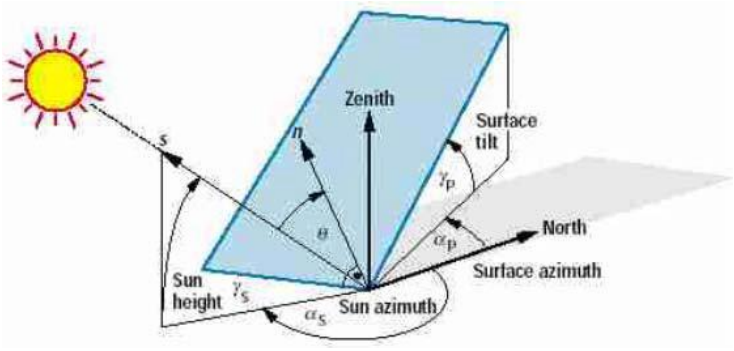

Figure 1.5. Surface orientation.

In Figure 1.6 the solar radiation intensity as function of slope and aspect is shown. In this area, south-facing slopes receive higher solar radiation than the

north-facing slopes. Using the analytical model developed by Allen et al. (2006a), it is possible to describe the radiation balance taking into consideration the effects of basin morphology. This approach is extremely useful to describe the spatial distribution of solar radiation and the maps of potential evapotranspiration. The amount of solar radiation influences the potential evapotranspiration (PET) (or maximum evapotranspiration) of each vegetation type in the space. In fact, the Penman-Monteith equation (Monteith, 1965) used to calculate the PET is strongly related to the net solar radiation: fixed the other parameters of the equation, increasing the solar radiation the PET increases. But the actual vegetation evapotranspiration is function not only of the PET but also of the soil moisture available and then of the rainfall that falls in the study are. The plant evapotranspirates as function of the water available in the soil: more the water available in the soil and more the evapotranspiration of the plant. The actual evapotranspiration is critical in the characterization of soil moisture and vegetation water stress, which, in turn, have important implications on plant growth and stress leading to vegetation patterns formation.

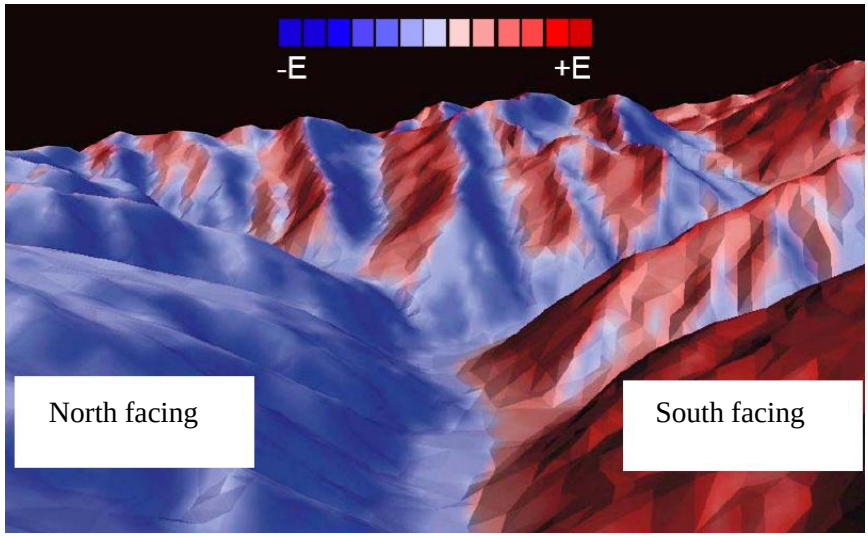

Figure 1.6. Solar radiation intensity in function of slope and aspect.

In order to easy describe the influence of the topography on the spatial vegetation distribution in a basin, the hydrological phenomenon is described in Figure 1.7 (Manfreda et al., 2013): the morphology causes the solar radiation spatial distribution (Figure 1.7a), the solar radiation distribution influences the evapotranspiration spatial distribution (Figure 1.7b) that, in turn, influences the soil moisture and water stress spatial distribution through the water balance (Figure 1.7c), and finally determines the vegetation spatial distribution (Figure 1.7d).

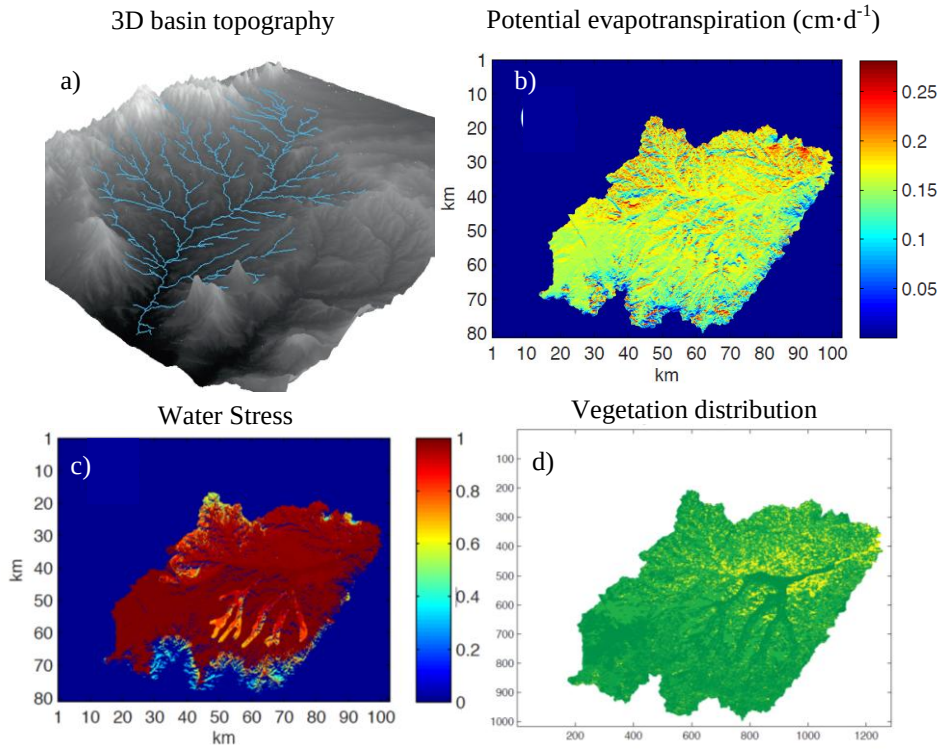

Figure 1.7. Morphology-vegetation distribution relationship. (a) basin topography; (b) potential evapotranspiration; (c) water stress; (d) vegeatation distribution (Manfreda et al., 2013).

In analyzing topography-related vegetation regional patterns, ecologists often overlook the fact that insolation regimes are not exclusively linked to local terrain features such as altitude and surface orientation, i.e., inclination and aspect (Daubenmire, 1968; Pianka, 2000; Ricklefs and Miller, 2000; Gallardo-Cruz et al., 2009), but that they also depend upon the latitudinal position on the Earth of the mountain under study (Holland and Steyn, 1975; Stoutjesdijk and Barkman, 1992). Perhaps, for this reason, it is difficult to generalise the effect of aspect on plant communities of tropical regions. At mid and high latitudes, slopes facing the Equator receive more radiation than slopes facing the closest Pole (Stoutjesdijk and Barkman, 1992). Unlike such predictions related to the geographic distribution of species, it is more difficult to make equivalent generalizations regarding vegetation development. This is so because the vegetational asymmetry is highly dependent upon the regional climate; for example, the observation that vegetation is better developed on the north slope in relatively dry regions of the northern hemisphere (Beaty and Taylor, 2001;

Sternberg and Shoshany, 2001) may not be applicable in areas that do not experience water limitations (Sharma and Baduni, 2000).

The radiation balance should be equal between the north- and south-facing slopes of a symmetric mountain located right on the equator, whereas in mountains located between the Equator and the Tropics of Cancer and Capricorn, both slopes receive direct insolation but during periods of very variable lengths throughout the year (Walter, 1973). Particularly, in seasonally dry regions of tropical latitudes of the northern hemisphere, the longest exposure of south-facing slopes to direct solar radiation usually coincides with the unfavourable period of low precipitation, a combination that results in a large water stress in plants. A different situation appears to take place in north-facing slopes, as they may be more suitable for plant growth because the season of higher energy for photosynthesis is synchronic with the period of positive water balance of the year. Thus, in these regions one may expect differences in floristic composition between slopes, along with a better developed vegetation on the slope facing north.

Vegetation patterns as affected by slope and aspect in the Chihuahuan desert were investigated by Mata-Gonzalez et al. (2002) and Zhou et al. (2013) (Figure 1.8). They concluded that topographic variations are an important influence on plant distributions and there is a correspondence between life cycles, senescence and solar radiation timing. Solar radiation and potential evapotranspiration were highly correlated and both offered essentially the same prediction of plant distributions. Flat and slightly sloping areas receive the most sunlight during the summer solstice. North-facing slopes may receive no solar radiation in winter and extended day lengths in the summer. At winter solstice, south-facing slopes receive the most radiation. Interestingly, south-facing slopes receive low solar radiation at the summer solstice and high radiation during the winter, leading to lower seasonal changes in solar radiation.

In the Mediterranean basin region, south-facing slopes receive higher solar radiation thus affecting temperature, soil moisture, nutrients and soil aggregation processes which, in turn, affect the vegetation (Klemmedson and Wienhold, 1992; Olivero and Hix, 1998; Kutiel and Lavee, 1999). In contrast, north-facing slopes generally receive lower solar radiation flux density, resulting in lower evapotranspiration rates and lower daily maximal temperatures during summer water stress periods. These differences are significant in Mediterranean plant communities where water availability is an important limiting factor. In view of favorable growing conditions in north-facing slopes in Mediterranean basin ecosystems, it is possible to hypothesize that plant community characteristics such as percentage cover, biomass, volume and density would be greater in this aspect than in opposing slopes.

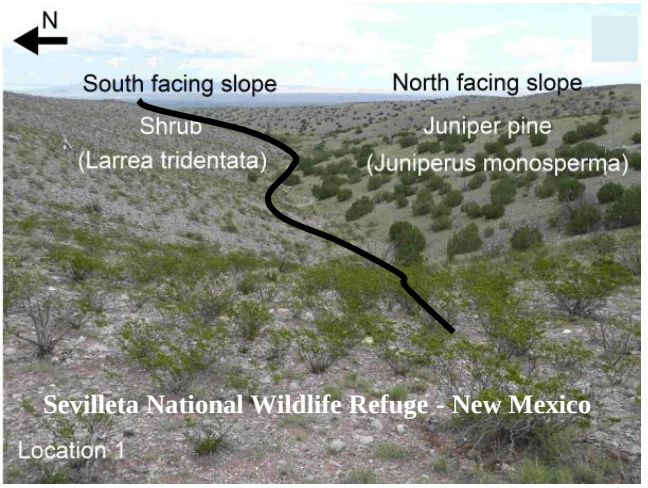

Figure 1.8. Vegetation distribution in relation to topography in Sevilleta National Wildlife Refuge (New Mexico) (Zhou et al., 2013).

Altitude, the second major component of topography, introduces further complexity into this scheme (Rahbek, 1995) (Figure 1.9). Numerous studies analysing altitudinal gradients in tropical mountains have established the magnitude of vegetational changes in response to environmental heterogeneity along this axis (Kappelle et al., 1995; Lieberman et al., 1996; Lovett, 1999; Grytnes and Vetaas, 2002; Grytnes and Beaman, 2006). Nevertheless, they have also shown the difficulty to predict the individual behaviour of each environmental factor with altitude (Bruijnzeel and Veneklaas, 1998). Water availability on the Earth's surface is related to altitude as a result of two processes. For one, evapotranspiration rates decrease with altitude as a result of the corresponding temperature reduction (Stoutjesdijk and Barkman, 1992; Luttge, 1997; Bruijnzeel and Veneklaas, 1998). In addition, gravity-driven runoff causes a larger moisture accumulation in the lower topographic positions (Clark et al., 1999). Despite the vast number of studies analysing separately vegetation responses to either aspect or altitude (Cantlon, 1953; Vazquez and Givnish, 1998), the combined effects of these two factors have not been sufficiently examined.

In scientific literature, several studies are available with regard to the influence of the morphology on the spatial vegetation distribution. These studies can be schematically split in studies which use statistical technique starting from observed data and studies based on numerical models (i.e., hydrological and ecological model).

Figure 1.9. Vegetation pattern in relation to slope and altitude in Karakorum, Pakistan.

1.2.1.1. Qualitative studies and statistical techniques

Isard (1986) demonstrated that slope-aspect influenced evapotranspiration, soil desiccation and vegetation distribution in the Niwot Ridge, Front Range, Colorado, through the control of the radiation. South- and east-facing sites received 18 and 14% more net radiation than the north-facing slope on clear sky and more typical summer days, respectively. West-facing slopes experienced moderate radiation loads. Water loss during two drying sequences for east-, west-, and north-facing slopes was 80%, 80%, and 60%, respectively, of evapotranspiration from the south-facing slope. Consequently, soil at the south-facing site dried faster than soil on other slopes of the knoll. *Dryas octopetala* (i.e., grass) prefers more moist northern slopes on illustrating the importance of topoclimatic controls over soil moisture to vegetation distribution in the fellfield. Water relations during the growing season influence vegetation distribution within topographic depressions on Niwot Ridge. Where meltwater is supplied throughout the growing season wet meadow and moist shrub tundra occur.

Sternberg and Shoshany (2001) investigated the effects of slope aspect on plant community characteristics such as plant cover, species composition and above-ground biomass production in Mediterranean trees and shrubs in two climatological regions. Two experimental sites were selected in a climatic gradient that runs from the foothills of the Judean Hills to the northern Negev desert in Israel (Figure 1.10). In each site, 16 quadrats of 10m·10m (eight south-facing and eight north-facing slopes) were established and the vegetation was recorded. Dominant tree and shrub species were measured using allometric parameters of area and volume, and representative branches were cut and weighed. Species studied were *Quercus calliprinos*, *Phillyrea latifolia*, *Pistacia lentiscus*, *Cistus creticus*, *Coridothymus capitatus*, and *Sarcopoterium spinosum*.

The results showed that slope aspect had significant effects on the composition, structure and density of the plant communities developing in both sites. Vegetation structure within a site changed significantly in the short distance separating the north and south-facing slopes, and that pattern remained generally constant when comparing the two sites along the rainfall gradient.

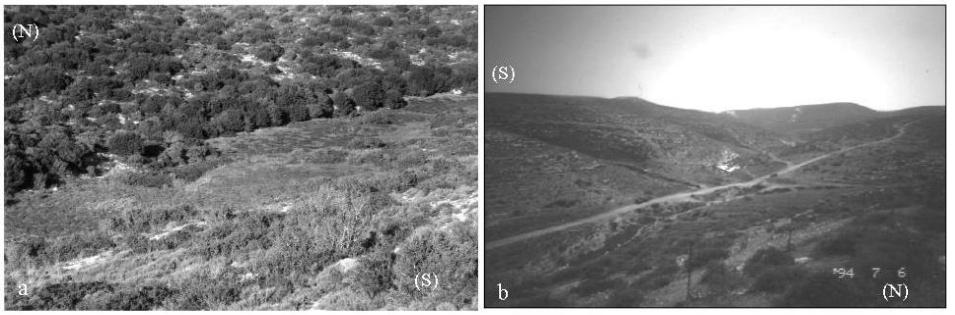

Figure 1.10. Photographs of the study sites showing vegetation differences between slope aspects. (a) Ramat Avisur, representing Mediterranean maquis and (b) Lehavim, characterizing dwarf shrublands. (N) North-facing slope; (S) south-facing slope (Sternberg and Shoshany, 2001).

Walton et al. (2005) examined timing and amount of solar radiation as factors influencing the distribution of seven perennial plants on a small mountain located in the Indio Mountains, in the Chihuahuan desert (Texas). Average direct beam solar radiation fluxes at differing times throughout the day and year were estimated with computer calculations. Principal components analysis was used to reduce the number of solar radiation parameters and include the maximum available information with a manageable number of variables. The remaining solar radiation parameters were compared to plant distributions using redundancy analysis and generalized additive models. Unimodal, bimodal, and monotonic responses were all found depending upon the species and solar radiation parameter. Niche separation at this location depended upon the timing as well as the amount of solar radiation. The research results clearly demonstrated that the timing of solar radiation is an important factor in the topographic distribution of vegetation. Solar radiation alone was able to predict 38.5% of the variation in plant distributions. The statistical observations showed that dynamic water stress is an important factor in plant distributions in the desert.

Another important contribution was also given by Gallardo-Cruz et al. (2009), who assessed that patterns of incoming solar radiation affect energy and water balances in Mexico, resulting in changes in vegetation attributes. They, first, modeled potential energy income for N- and S-facing slopes of Mt. Cerro Verde (Oaxaca) and then they examined the response of vegetation structure to slope aspect and altitude. Vegetation survey and modeling of potential energy

income were based on 30 plots equally distributed among three altitudinal belts defined for each slope of the mountain; combining the three altitudinal belts and two slopes produced six environmental groups, represented by five vegetation plots each. Potential energy income was about 20% larger on the S than on the N slope (9.735 versus 8.138 $MJ \cdot m^{-2}$), but it did not vary with altitude. In addition, the temporal behavior of potential energy income throughout the year differed greatly between slopes. The results of this study demonstrated a differential response of vegetational attributes to environmental heterogeneity along a short altitudinal gradient and between two contrasting aspects. The structure did not show significant changes linked to the environmental gradients, but altitude and aspect did affect species composition.

1.2.1.2. Numerical ecological and hydrological models

In order to explore topographic controls on vegetation, Ivanov et al. (2008b) employed a numerical model to analyze the dynamics of a generic C_4 grass growing in the water-limited conditions of the semiarid climate of central New Mexico. A fully coupled dynamic model of vegetation-hydrology interactions known as tRIBS+VEGGIE was used (Ivanov et al., 2008a). The model mimics principal water and energy processes over the complex topography of a river basin and links them to the essential plant biochemical processes and phenology. Topography and drainage network of a domain of interest are represented using *triangulated irregular network* (TIN) of points. A set of numerical experiments were carried out for two small-scale synthetic domains that exhibited different landscape geometries. Linkages between landscape geometric characteristics and patterns of grass productivity and water balance components were examined. A conceptual procedure was used to partition the space in aspect-slope classes. The interplay among vegetation energy, and water processes led to a much more complex dependence of grass *aboveground net primary productivity* (ANPP) on site characteristics. It follows from above that in order to understand the effect of topographic features on grass productivity, both the water and energy aspects of hydrology-vegetation dynamics need to be considered. The results led to a conceptual relationship linking vegetation-hydrology quantities at different landscape locations. Certain topographic locations favored vegetation growth as compared to a flat horizontal surface. Moreover, grass ANPP for sites of a given aspect was completely determined by site slope. Figure 1.11 shows as the topography influences the solar radiation distribution which, in turn, influences the ANNP causing a vegetation pattern in function of the topography.

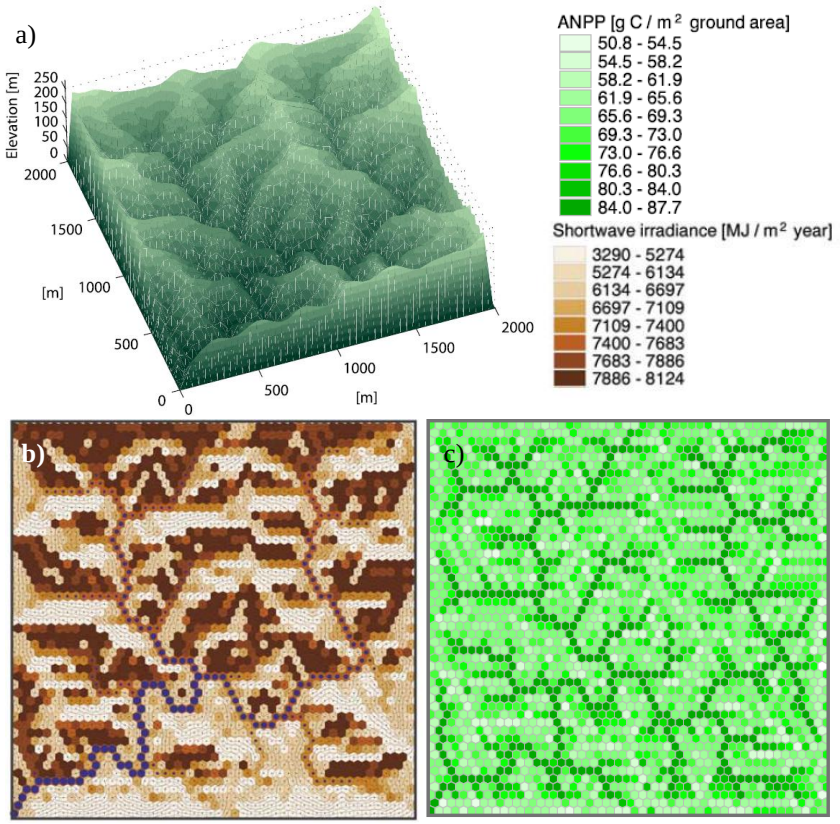

Figure 1.11. Influence of topography on solar radiation and vegetation production at catchment scale: (a) topography, (b) solar radiation map, (c) vegetation aboveground net primary productivity (Ivanov et al., 2008b).

In Figure 1.12 the mean annual ANPP of C_4 grass in function of the irradiance is shown. The three curves are related to three different aspect classes (i.e., north facing, east-west facing and south facing). For each curve, increasing the slope the ANPP decreases. Symbols with lighter color denote the data points for the *CV* domain (i.e., fluvial erosion dominated landscape that exhibits shorter hillslopes and higher drainage density), while the darker color corresponds to the data points for the *CX* domain (i.e., diffusion erosion dominated landscape that exhibits longer hillslopes and lower drainage density). The highest rate of decrease in the incoming solar radiation per unit slope angle is observed for north facing sites. Maximum ANPP occurs on sites of northerly aspect as a result of the trade-off between favorable (a reduction in the incoming radiation) and unfavorable (a decrease in precipitation) effects exerted by slope on grass dynamics. East facing sites show a minor increase (with respect to a flat surface) in productivity for very shallow slopes. For steeper slopes, ANPP continuously

decreases. Estimated ANPP for westerly slopes shows a continuous reduction with growing slope. The grass productivity for south facing sites exhibits a sharp continuous decrease with respect to the ANPP for a flat horizontal surface. Therefore, one can notice the strongly dependence of the surface irradiance and then of the ANPP on the aspect classes (Ivanov et al., 2008b).

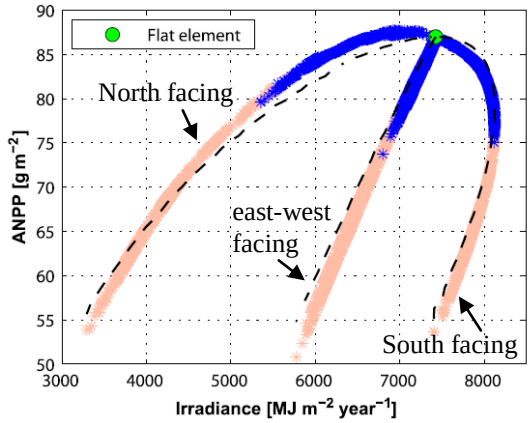

Figure 1.12. The mean annual aboveground net primary productivity (ANPP) of C_4 grass in function of the irradiance (Ivanov et al., 2008 b). Symbols with lighter color denote the data points for the *CV* domain while the darker color corresponds to the data points for the *CX* domain.

Using the approach of Allen et al. (2006a) with the analytical form of the soil water balance equation proposed by Laio et al. (2001), Pizzolla et al. (2012a) demonstrated that basin morphology significantly affects the spatial distribution of vegetation water stress increasing its variability. The variability of the water stress increased taking into consideration the initial conditions for the simulation, because during the winter period differences in the radiation balance were generally larger that during the growing period.

Franz et al. (2012) developed a spatially explicit daily ecohydrologic model that investigates the processes that affect the organization of vegetation and the spatial structure of vegetation on hillslopes. Using observations from a dryland ecosystem in central Kenya where symmetry-breaking instabilities govern the observed vegetation patterns, they constructed a parsimonious spatially explicit daily ecohydrological model that is able to demonstrate a range vegetation patterns observed across this ecosystem. Of particular importance in this ecosystem and many dryland ecosystems, is the effect of redistribution of surface waters to downslope vegetation patches as a result of Hortonian runoff and overland flow. They used a rule-based method based on a complex adaptive systems approach to generate the basic patterns. In order to compare different possible static spatial vegetation patterns that exist, they constrained the hillslope

model to the growing season water balance. Using the dryland resource trade-off hypothesis governing dryland vegetation patterns, proposed by Caylor et al., (2009), they were able to compare the different static patterns according to their hillslope water use efficiency. Starting with the same initial conditions and simulating a series of growing season daily precipitation events, they evaluated the changes in the growing season water balance between different static spatial patterns of vegetation with the same fractional cover. In addition, they varied the strength of the local facilitation and long-range competition effects by varying the model parameters that control the effectiveness of surface flowpath convergence and root to canopy ratios, respectively. By changing these two parameters they were able to demonstrate a range of most efficient static spatial patterns from highly organized to random, which maximizes hillslope water use efficiency.

Manfreda et al. (2013) studied the mutual relationship between climate, vegetation and soil water budget within an ecohydrological framework. They investigated the influences of soil moisture, solar radiation distribution and seasonality of climatic forcing on the spatial organization of vegetation. To this end they adopted a coupled hydrological/ecological model to describe simultaneously soil water budget and vegetation pattern evolution in the semiarid Upper Rio Salado basin. The basin is characterized by a marked heterogeneity in vegetation composition that is influenced by the basin topography. Analyses have been carried out using a soil water balance model based on the soil moisture scheme proposed by Laio et al. (2001) coupled with a vegetation model for the description of the spatial organization of vegetation. They used a simple cellular automata approach to model the steady state conditions of a vegetation mosaic, initiated from a random condition containing 1/3 each of trees, shrub and grass. In each model, the initial random vegetation mosaic is modified through the iteration of local interactions that occur between adjacent locations. Using this approach, they identified the dynamic water stress of vegetation during the growing season, taking into account effects of morphology on the spatial distribution of solar radiation. The impact of solar radiation was studied paying particular attention to the effects of basin morphology on the distribution of incoming radiation at the local scale using the analytical model of Allen et al. (2006a). The solar radiation distribution influences the potential evapotranspiration that is critical in the characterization of vegetation water stress. Results showed that the observed vegetation patterns in the Upper Rio Salado basin are significantly affected by the basin morphology and emerge from the minimization of dynamic water stress and the maximization of vegetation water use.

Finally, Zhou et al. (2013), using the ecohydrological CATGraSS model (see chapter 3 for a more detailed description) demonstrated the importance of solar irradiance in determining vegetation composition over complex terrain under a water limited ecosystem. They implemented CATGraSS in a semiarid basin

within the Sevilleta National Wildlife Refuge (SNWR), New Mexico (USA), where plant distribution is strongly controlled by topographic aspect, juniper and dense black grama co-existing in the north-facing slopes, and creosote bush dominating the south-facing slopes.

1.2.2. Influence of climate and its possible changes on the vegetation distribution

As previously mentioned, patterns of vegetation on the landscape are mainly a function of the availability of light (Ricard and Messier, 1996; Martens, 2000), soil moisture (Klausmeier, 1999; Couteron and Lejeune, 2001) and nutrients (Tilman, 1987; Rietkerk et al., 2004) that support plant growth, and other environmental conditions, such as temperature, that determine the timing and length of the growing season (Myneni et al., 1997; Dunne et al., 2003).

Therefore, plant types, species richness, structure and distribution of vegetation are under the influence of climate at the regional scale (Scheiner et al., 1994; Nemani et al, 2003), and resources availability (including water, nutrients), soil type and surface morphology at the local scale (Kramer and Boyer, 1995; Larcher, 1995). Vegetation patterns could have an important role in the coupled dynamics of water, energy, and carbon in a region (Levis et al., 1996; D'Odorico et al., 2008).

Vegetation, as interface between soil and atmosphere, plays a key role in biogeochemical cycles through photosynthesis and the subsequent production of oxygen and organic matter (Pignatti, 1994; Manfreda, 2009). It exerts important control on the entire water balance recycling more than one half of the annual precipitation (Chahine, 1992). Consequently change in land cover, such as deforestation in the lowland tropics as well as grazing in semiarid regions, can induce a reduction of the precipitation amounts and an increase of temperatures (Dickinson and Kennedy, 1992; Lean and Rowntree, 1997). Vice versa, a change in climatic conditions may modify the spatial patterns of vegetation in a way that is not fully understood.

Climate controls vegetation through direct effects on establishment and growth, indirect effects mediated by soils, and effects on the disturbance regime. These effects modify the internal dynamics of vegetation, producing both geographic patterns and long-term changes in vegetation.

If climate were stationary, vegetation dynamics would consist of fluctuations due to year-to-year weather variation, *succession* triggered by disturbances and gap-phase regeneration. These are stochastic processes, but their average behaviour can be predicted from physiological and life-history characteristics of the available species and information on climate and natural disturbance. Vegetation processes vary spatially in response to the broad-scale pattern of climate, and change through time in response to long-term variations in climate.

Vegetation can similarly be considered as an interacting system (Prentice, 1986) that responds to external forcing. Climate provides the changing boundary conditions to which the vegetation adjusts through a combination of processes with different response times. The nature of vegetation's response to climate change depends on the space and time scales on which it is observed (McDowell et al., 1991). The mode of response (stationary, dynamic equilibrium or disequilibrium) depends on the product of the forcing frequency and the system's response time (Webb, 1986). Vegetation can be observed on time scales ranging from years to millions of years and on spatial scales ranging from the sample plot up to the globe. Different frequencies and strengths of climate change are important on different time scales, and different response times apply to the different spatial scales.

Therefore, a major challenge facing ecologists today is to predict how ecosystems and vegetation patterns will respond to forecast environmental changes and to evaluate the consequences of those responses (Turner, 1989; Walther et al., 2002; Zhou et al., 2013). Future changes in climate are projected to cause changes in vegetation distribution (Bachelet et al., 2001; Bakkenes et al., 2002; IPCC, 2007; Kelly and Goulden, 2008; Lenihan et al., 2008).

Even in this case ecohydrology suggests a renewed interdisciplinary approach that aims to provide a better comprehension of the effects of climate and its possible changes on terrestrial ecosystems.

The assemblages of species in ecological communities reflect interactions among organisms as well as between organisms and the abiotic environment. We might expect, therefore, that rapid climatic change or extreme climatic events can alter community composition. In the Sonoran desert of the southwestern United States, for example, recent increases in woody shrub density have been attributed also to regional climatic shifts (Brown et al., 1997; Walther et al., 2002).

In this context, there is a growing interest on the impacts of climate on the interplay between vegetation and water availability. The latest report on climate change of the Intergovernmental Panel on Climate Change (IPCC) (IPCC, 2013) shows, on a global scale, a linear trend of increase in global average temperature of the last one hundred years (1901-2012) of about 0.89° C, and important changes in precipitation strongly heterogeneous in space. It is also virtually certain that maximum and minimum temperatures over land have increased on a global scale since 1950. Central Europe and the Mediterranean basin represent a vulnerable area, where rainfall reduction and increased temperatures may affect plant and animal species, regulating environmental characteristics.

The plant species may respond to climate change adapting to new conditions, using their plasticity, or through the selection of genetic variants whose physiology allows survival under the new climatic conditions. An alternative or complementary response of some species is the shift in time of the phases of the life cycle, or in space and depth of the rooting system. The sensitivity of

different species to climate change can cause the abundance of common species and, conversely, the disappearance of the rarest (Körner and Walther, 2001). This process, together with a highly uneven distribution of species undermines vegetational biodiversity (i.e., the degree of variation of vegetation life).

The preservation of environmental diversity is necessary for the regulation of the hydrological cycle and biogeochemical cycles of nitrogen and carbon, flood protection, the availability of genetic diversity in agriculture, the natural pollination and the stability of ecosystems (Duffy and Stachowicz, 2006). Leaving aside the processes of biological evolution, the effects of climate change on species and ecosystems can be grouped into the following categories: impacts on the physiology and behavior of species, impacts on the lifecycle, impacts on the composition and interactions of species in ecological communities, impacts on the geographical distribution (Hughes, 2000; Walther et al., 2002).

If changes on physiology and life cycle may increase the resilience of ecosystems, changes in composition and distribution of vegetation patterns may deteriorate the environmental diversity.

Several authors have investigated the effects of climate change on the spatial structure of vegetation. Some of these works relate the trends of precipitation and temperature with NDVI index (*Normalized Difference Vegetation Index*) and phenological measures. This type of analysis showed a negative effect of the decline in rainfall of Mediterranean forests, a positive effect due to the increase in temperature of mountain forests (Maselli et al., 2007) and an anticipation of the growing season and delayed senescence (grass and shrubs of the Alps and Central Europe) (Menzel et al., 2001; Studer et al., 2005).

Poiani and Johnson (1993) constructed a Cellular Automata (CA) model of vegetation dynamics for semi-permanent prairie wetlands that considered seven dynamically evolving species, responding to changes in the hydrologic regime. The study evaluated the potential effects of climate change on wetland resources, with hydrologic components simplified by empirical relationships established for the region of interest.

In coming decades, climate changes are expected to produce major shifts in vegetation distributions at unprecedented rates, in large part due to mortality. The responses of vegetation to variations in climate are expected to be most rapid and extreme at ecotones, the boundaries between ecosystems, with semiarid ecotones considered to be among the most sensitive. Allen and Breshears (1998) showed the most rapid landscape-scale shift of a woody ecotone ever documented taken place in response to climate change in northern New Mexico in the 1950s (from 1954 to 1963). This shift has persisted for 40 years. Using *GIS* tools and historical photographs of the area (1935, 1954, 1963, 1975) they demonstrated that the ecotone between semiarid *ponderosa pine* forest and *pinõn-juniper* woodland shifted extensively (2 km or more) and

rapidly (<5 years, from 1955 to 1959) through mortality in response to a severe drought (Figure 1.13).

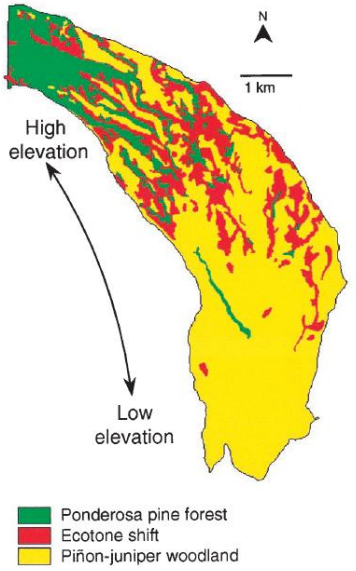

Figure 1.13. Changes in vegetation cover between 1954 and 1963 in the study area in the Jemez Mountains of northern New Mexico, showing persistent ponderosa pine forest (365 ha), persistent pinõn-juniper woodland (1527 ha), and the ecotone shift zone (486 ha) where forest changed to woodland (Allen and Breshears, 1998).

Bachelet et al. (2001) have developed a model to simulate vegetation *succession* in the United States. A multitude of future climate scenarios has been used to produce a big variety of simulated ecological responses. Their objectives were to use an equilibrium model (Mapped Atmosphere-Plant-Soil system) and a dynamic model to simulate changes in potential equilibrium vegetation distribution under historical conditions and across a wide gradient of future temperature changes. Both models agreed that a moderate increase in temperature produces an increase in vegetation density across most of the US with small changes in vegetation types. Vice versa, a large increase in temperature causes losses of *C* with large shifts in vegetation types. In the western states, particularly southern California, precipitation and thus vegetation density increase and forests expand under all but the hottest scenarios. In the eastern US, particularly the Southeast, forests expand under the more moderate scenarios but decline under more severe climate scenarios, with catastrophic fires causing rapid vegetation conversions from forest to savanna.

Bakkenes et al. (2002) demonstrated that the future climate change can strongly influence the diversity and distribution of species and, therefore, affect ecosystems and biodiversity. In order to assess these changes they developed a

model, called *Euromove*. The model uses climate data from 1990 to 2050 and determines climate envelopes for about 1400 plant species by multiple logistic regression analysis. The climate envelopes were applied to the projected climate to obtain predictions about plant diversity and distributions by 2050. For each European grid cell, *Euromove* calculated which species would still occur in forecasted future climate conditions and which not. The results showed major change in biodiversity by 2050. On average, 32% of the European plant species that were present in a cell in 1990 would disappear from that cell. Vegetation species will change in the 44% of the modeled European area. Individual responses of the plant species were diverse.

Lenihan et al. (2008) simulated the response of vegetation distribution to three scenarios of future climate change for California using the *Dynamic General Vegetation Model*. To generate the three future climate scenarios (period 2004-2100), they used monthly output generated by the general circulation models (GCMs): the *GFDL* model (*B1* and *A2* scenario) and the *PCM1* model (*A2* scenario). The response of vegetation class distribution under the three future climate scenarios was determined by comparing the distribution of the most frequent vegetation type simulated for the 30-year historical period (1961-1990) against the same for the last 30 years of the future scenarios (2071-2100). The simulated response of the vegetation classes in terms of changes in percentage coverage was surprisingly similar under the three future climates. Under all three scenarios, Alpine/Subalpine Forest cover declined, and increases in the productivity of evergreen hardwoods led to the displacement of evergreen conifer forest by mixed evergreen forest. Grassland expanded, largely at the expense of woodland and shrubland, even under the cooler and less dry climate scenario where increased woody plant production was offset by increased wildfire. The uncertainty due to differences among future climate scenarios and to unrepresented or poorly understood processes precludes the use of these simulations as unfailing predictions of the future. Nevertheless, the results underscore the potentially large impacts of climate change on California ecosystems, and the need for further analyses of both future climate change and terrestrial ecosystem responses.

Therefore, there is a clear need to develop conceptual models that are capable of interpreting and predicting spatial pattern formation especially in dryland (and similar ecosystems) that are the most vulnerable environments to eventual climatic change (Smith and Goodman, 1987; Jeltsch et al., 1999).

The CA ecohydrological models (see section 3.1.6) represent a useful tool to describe the effects of climate on natural ecosystems and landscape. Manfreda and Caylor (2013) explored the potential of this model using different climatic scenarios to explore the impact of changes on the climatic forcing on semiarid environments simulating vegetation pattern evolution and hydrological water budget at the basin scale using as test site the Upper Rio Salado basin. This enables quantitatively assessing the effects on soil water availability on future

climatic scenarios. They generated a number of synthetic vegetation patterns over the basin. Results highlighted that the relationship between climatic forcing (water availability) and vegetation patterns is strongly non-linear. This implies, under some specific conditions which depend on the ecosystem characteristics, small changes in climatic conditions may produce significant transformation of the vegetation patterns. In the basin, morphological characteristics (local elevation, basin aspect ratio, and local slope) seem to be relevant controlling factors even if it is an arid river basin, while soil texture has a minor role.

Simulations have been carried out assuming different combinations of rainfall parameters, α and λ, with the same temperature values observed in the period 1990-2001 during the growing season. The authors focused on the impact of rainfall variations instead of modifying the potential evapotranspiration through the mean temperature of the season. They simulate different climatic conditions varying rainfall parameters α and λ. In particular, a mean spatial value of the parameter α varying from a minimum value of 0.403 cm to a maximum value of 0.688 cm, while the mean value of the parameter λ (rainfall frequency) varies from 0.196 day^{-1} to 0.481 day^{-1}. Rainfall parameters have been modified producing 20 equally spaced values within the cited intervals that in total produce 400 climatic scenarios. The parameter space was set around the reference conditions of the Rio Salado Basin, which are described by α=0.575 cm and λ=0.284 day^{-1}. Consequently, the CA network model produced 400 patterns of steady state vegetation maps.

The percentages of each land cover types (tree, shrub, grass, and bare soil) as a function of the different climatic conditions are given in Figure 1.14. In particular, Figures 1.14a, d, which describes percentage cover of bare soil and trees, show a complementary behavior with an increase of trees when bare soil declines. The percentage of trees, in fact, increases with the increase of mean rainfall (greater frequency of rainfall λ, and greater mean daily rainfall depth α), up to a condition of stable equilibrium. In contrast, the percentage of bare soil tends to decrease with the increase of total rainfall. Different behavior is observed for shrub and grass that tends to prevail for intermediate values of the climatic conditions (Figures 1.14b, c).

A synthesis of the landscape modifications is given in Figure 1.15 that describes the Shannon's index (i.e., index commonly used in landscape diversity measurement and it accounts both abundance and evenness of species) for all range of parameters investigated for the Upper Rio Salado. The index shows a rapid and marked decrease with the reduction of both rainfall rate and mean rainfall depth. More humid climatic conditions favor the growth of the index that tends to a maximum and after a certain value it slight decreases up to a condition of equilibrium. It is useful to remind that SHDI increases as the number of different patch types increases and/or the proportional distribution of area among patch types become more equitable.

Analyses show that the spatial distribution of vegetation is mainly controlled by local climate and basin morphology that play a dual role, influencing the soil water balance at the local scale and the interaction between species. The landscape analyses show that landscape composition changes non-linearly with climate changing from dry to humid evidencing different sensitivities of the vegetation patterns to the climatic conditions.

The main outcomes of their work can be summarized in the following points: the landscape analyses, based on the modeling applications, show that reduction of landscape diversity (described by the Shannon's Index) may occur rapidly for small changes in the rainfall characteristics; these changes are exacerbated when rainfall modifications are due to reduction in the mean rainfall depth; the impact of climate change on the vegetation pattern depends on the vulnerability of a system with respect to the expected changes. These results are consistent with the analyses carried out by Walther et al. (2002) that evidenced how the responses to relatively low average rates of climate change may be significant, raising several concerns about its ecological and socio-economic consequences.

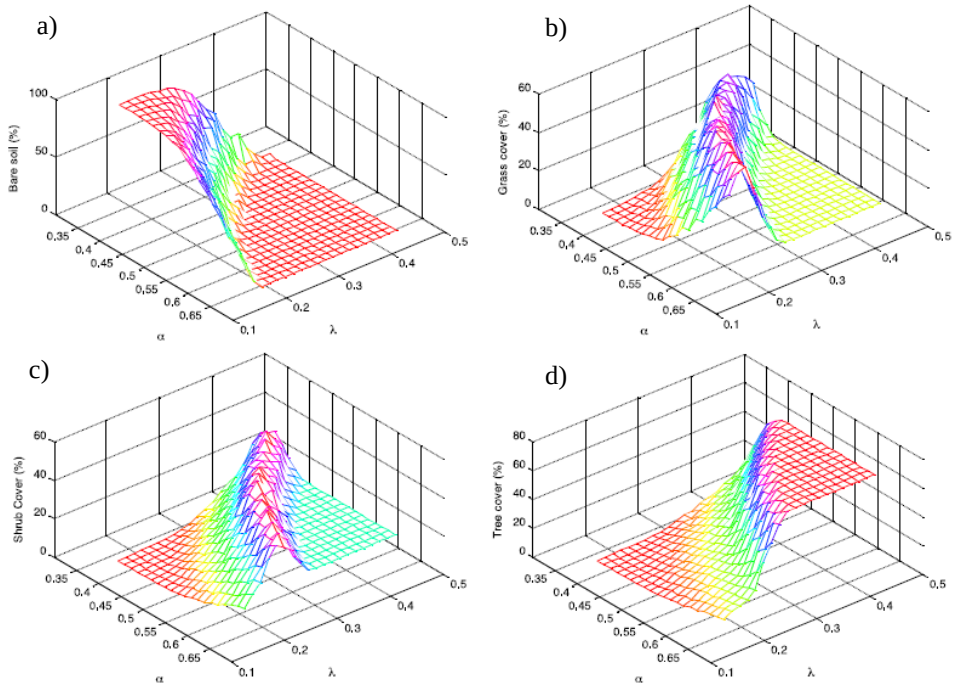

Figure 1.14. Distribution in percentage of the types of soil cover as a function of the climatic conditions described by rainfall parameters α and λ. Percentage of (a) bare soil, (b) grass, (c) shrub, and (d) tree (Manfreda and Caylor, 2013).

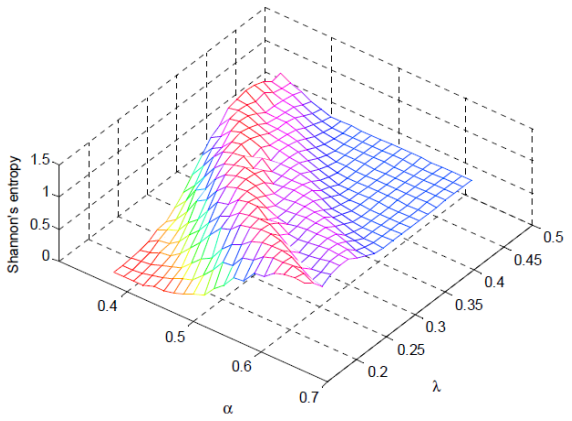

Figure 1.15. Distribution of the Shannon's Index computed on the simulated vegetation patterns as a function of the climatic conditions described by the rainfall parameters α and λ (Manfreda and Caylor, 2013).

Zhou et al. (2013) analyzed how change the vegetation distribution varying the storm characteristics (rainfall frequency-magnitude statistics, and seasonality) in a small basin in the Sevilleta National Wildlife Refuge (SNWR), New Mexico, (in which a reduction of 25% of the mean annual precipitation in 2100 is forecasted) using the ecohydrological CATGraSS model. In this basin plant distribution is strongly controlled by topography (aspect and slope), with juniper pine and grass savanna co-existing in the north-facing slopes, and shrub dominating the south-facing slopes. They analyzed the following storm cases: increased mean time between storms, decreased mean time between storms; enhanced monsoon precipitation, uniform climate. They kept the mean annual precipitation constant (250 $mm \cdot yr^{-1}$). In Figure 1.16 the final vegetation distribution maps obtained with the current climate (Figure 1.16a) and the four fictitious climates (Figures 1.16b, e) are shown. A 20% increase in the mean interstorm time (higher magnitude and lower frequency storms) reduces the shrub percentage and increases grass and tree percentage (Figure 1.16b). When the mean interstorm time is decreased by 20%, creosote bush becomes the dominant plant type (Figure 1.16c). A stronger monsoon is obtained increasing (decreasing) the wet (dry) season total rainfall by 50%, leading to an equivalent of 75% MAP falling in the monsoon season (180 mm of rain in 3 months). Under this scenario (Figure 1.16d) grass expands in the basin rapidly, while juniper pine and creosote bush die off. Under no seasonality scenario (Figure 1.16e), with rainfall evenly distributed, juniper pines rapidly extends in the basin. They analyzed the influence of rainfall seasonality by forcing the model with a mediterranean climate (wet season: from November to January). The simulated vegetation pattern shows the dominance of the juniper pine. The sensitivity runs suggest that the observed vegetation pattern exists only in the

current climate (Figure 1.16a), and changes in the storm characteristics could lead to a dramatic reorganization of the plant composition on topography.

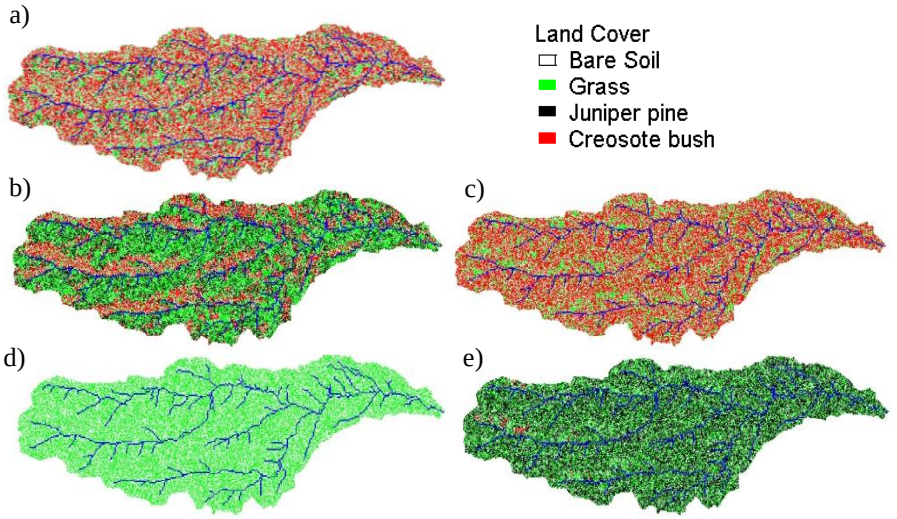

Figure 1.16. Vegetation distribution maps for: (a) current climate, (b) increased mean time between storms (+20% T_b), (c) decrease in mean time between storms (-20% T_b), (d) enhanced monsoon precipitation (+50% increase), (e) uniform climate (no Monsoon) (Zhou et al., 2013).

Chapter 2

Shrub and tree encroachment in the american grasslands: state of the art

The encroachment can be defined as the increase in density, cover and biomass of indigenous tree or shrubby plants in various arid and semiarid grasslands (Van Auken, 2000; 2009).

Tree or shrubby plant encroachment into grasslands and the 'thickening' of tree or shrubby plant density in rangelands and savannas are well documented (Buffington and Herber, 1965; Burkahardt and Tisdale, 1976; Archer at al., 1988; Grover and Musick, 1990; Bahre and Shelton, 1993; Archer, 1995; Asner et al., 2003; Miller et al., 2005; Coop and Givnish, 2007; Browning et al., 2008; Knapp et al., 2008a, b; Miller et al., 2008; He et al, 2010). This phenomenon has changed dramatically over the last 150 years the semiarid and arid grasslands of southwestern North America (Buffington and Herber, 1965; Archer et al, 1988; Archer, 1994, 1995; Browning et al., 2008; van Auken, 2009) (Figures 2.1, 2.2).

There are many temporal photographs that may show that encroachment has occurred, without showing the possible causes of a such phenomenon. The best evidence demonstrating encroachment is found in studies that, examining a specific grassland area, have shown changes in coverage or density of one or more woody species in time (Knapp et al., 2008a). Most encroachment occurred well before scientists began looking at this phenomenon in a systematic way. In order to analyze the phenomenon, Miller et al. (2005; 2008) examined date of woodland community establishment retrospectively using tree-ring chronologies or dendrochronology. A large number of communities were aged and the ages of the communities were examined as a function of time. When this was done, a large, rapid increase in the number of recently established woodland communities was found. The increase in the number of new woodland communities started in the mid to late 1800s and continued through most of the 1900s (Miller et al., 2005; Miller et al., 2008).

In order to to understand the magnitude of the problem, the pictures in Figure 2.1 show the rapidly western juniper encroachment in the Pecos National Park,

north central New Mexico, from 1916 to 1986, while the pictures in Figure 2.2 show the juniper encroachment into the semiarid grassland of Albuquerque, New Mexico, from 1899 to 1977. Other evidences of encroachment times are provided bu Figures 2.3 and 2.4. In particular the graphic of Knapp et al. (2008b) in Figure 2.3 shows the increase in mean cover of *Juniperus virginiana* in northeastern Kansas. Area began grassland in 1956 and 40 years later it was forest community with +95% cover. The graphic of Miller et al. (2005), in Figure 2.4, shows moreover the number of newly established *Juniperus occidentalis* communities per decade for the past 400 years. There were 801 communities examined in former northern California grasslands. The greater juniper encroachment occurred then from 1900 to 1990.

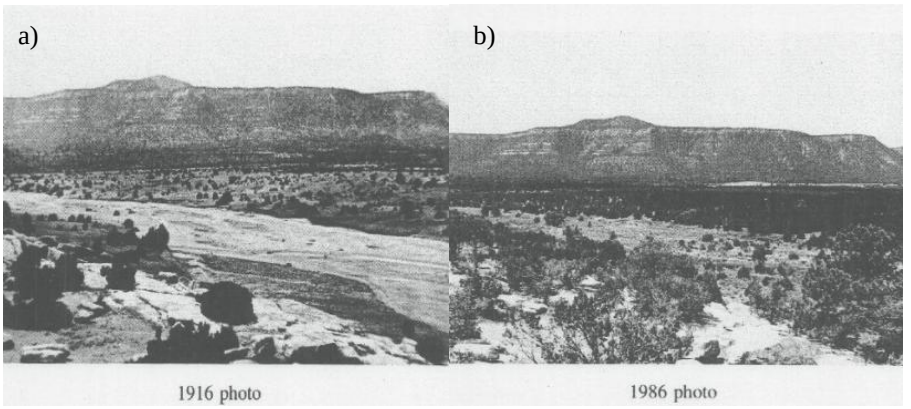

Figure 2.1. Sagebrush steppe has been rapidly changing into woodlands of western juniper and pinyon pine since Euro-american settlement of the West in the middle of the nineteenth century. North central New Mexico, Pecos National Park: (a) 1916, (b) 1986 (Dick-Peddie, 1993).

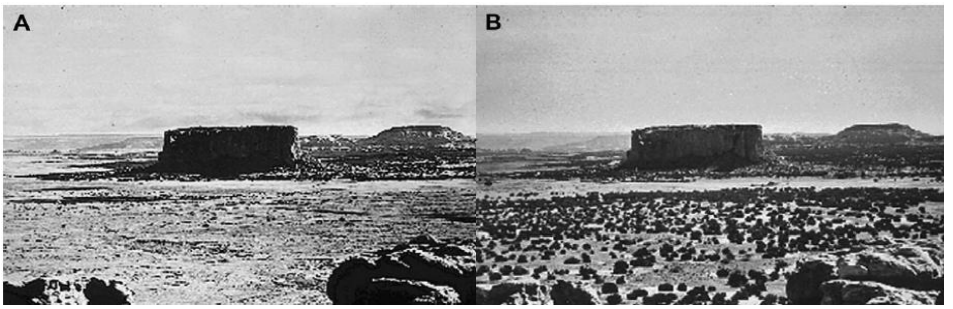

Figure 2.2. Encroachment of juniper plants into semiarid grassland west of Albuquerque, New Mexico: (a) 1899, (b) 1977 (Allen et al., 2002).

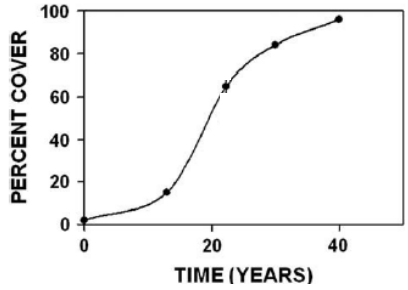

Figure 2.3. Increase in mean cover of *Juniperus virginiana* in northeastern Kansas (Knapp et al., 2008a).

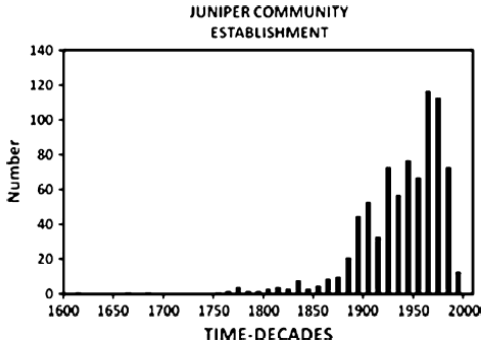

Figure 2.4. The number of newly established *Juniperus occidentalis* communities per decade for the past 400 years (Miller et al., 2005).

This chapter provides in section 2.1 a description of the shrub encroachment and in section 2.2 a description of the tree encroachment. In order to better clarifying the contents of this chapter, a brief distinction of the terms tree, shrub and woody plant is carried out here. Tree is a perennial plant with an elongated stem, or trunk, while shrub is distinguished from a tree by its multiple stems and shorter height, usually under 6 m tall. Plants of many species may grow either into shrubs or trees, depending on their growing conditions. Juniper that is usually a tree can be also considered a shrub when it is young and small. Both tree and shrub can be considered woody plants.

2.1. Shrub encroachment

The grassland communities have not been invaded by non-native shrubby species (*invasion*) but by native species (*encroachment*) (van Auken, 2000). Encroachment of native shrubby species (Figure 2.5) has changed the

appearance and structure of many of these former semiarid grasslands to shrublands (Knapp et al., 2008a, b).

Although some authors have attributed the encroachment of shrub into the semiarid grasslands to only one factor (Burkhardt and Tisdale, 1976), most recent studies have suggested an interaction of several factors (van Auken, 2000; 2009; Miller et al., 2005). Putative causes of increased shrubby plant abundance vary, and include increased grazing intensity, reduced fire frequency, other alterations in local land management practices and rising atmospheric CO_2 concentrations. A second type of factors would include nutrient levels, global climate change, spread of seed by livestock, small animal populations, and combinations of these factors (Archer et al., 1988; Archer, 1994; 1995; Van Auken, 2000; 2009). In Figure 2.6 a conceptual model illustrating the causes of the shrub encroachment (D'Odorico et al., 2010) is shown.

Figure 2.5. Shrub: creosote bush (*Larrea tridentata*)

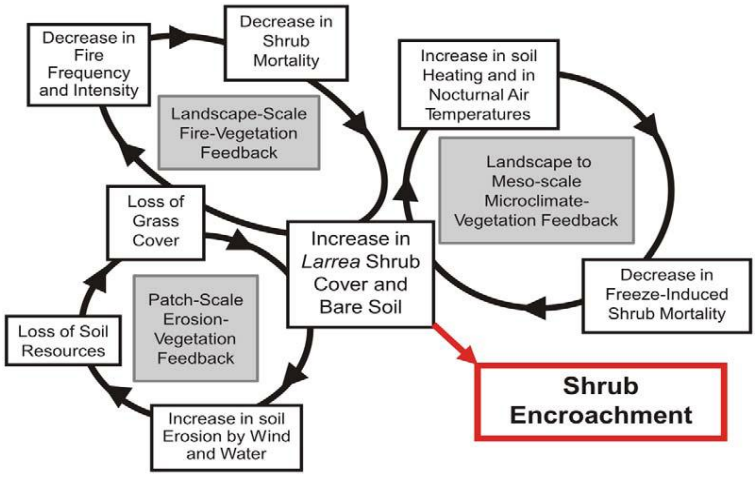

Figure 2.6. Conceptual model illustrating the causes of the shrub encroachment (D'Odorico et al., 2010).

Looking at Figure 2.6, the major cause of the encroachment of these shrubby species seems to be the reduction of grass biomass (fine fuel) by chronic high levels of domestic herbivory coupled to a reduction of grassland fires (Burkahardt and Tisdale, 1976; van Auken, 2000), which would have killed or suppressed the shrubby plants to the advantage of the grasses (Grover and Musick, 1990; Archer, 1995; Coop and Givnish, 2007; van Auken, 2009). The introduction of millions of domestic animals into the grassland and high livels of constant herbivory (van Auken, 2009) have caused the reduction of the aboveground grass biomass and the fine fuel, required for large-scale ecosystem fires. With the reduction of the fuel there was a concomitant decrease in grassland fires (Archer, 1994). Herbivores removed light-fluffy fuel in the form of grass biomass and the grasslands could not burn because there was little fine fuel remaining to burn. However, grassland fires certainly interacted with herbivory, rainfall and temperature to complicate the interpretation of shrubby plant encroachment. These new ecological conditions favored the growth of the shrubby plants and not the grasses that had dominated these communities for thousands years (Miller and Rose, 1999; Miller et al, 2007; van Auken 2009). The role of plant competition and the spread of seeds by introduced domestic herbivores seem to be secondary and probabily modified the rate of change (van Auken, 2000). Moreover, the role of many small native mammals and insects that consume woodly plant seedlings seems to be secondary and possibly localized (van Auken, 2009). Secondary factors probabily modified the rate of change, rather than causing the change (van Auken, 2000; 2009). Elevated levels of atmospheric CO_2 are not necessary to explain shrub encroachment in these semiarid grasslands. Moreover, the earth's orbit which is becoming more circular and less elliptical (Mackenzie, 2003), which is a long-term cyclic change and background to antropogenic chanes occurring today appears to be another factor.

Bahre and Shelton (1993) showed that the historical climate change did not influence the encroachment. In fact, links between changing climate since 1870s and shrub plant encroachment in the semiarid grasslands are weak (Bahre and Shelton, 1993; Van Auken, 2000; 2009). Vice versa the future possible climate change could become the major cause of encroachment (Allen and Breshears, 1998; Van Auken, 2009).

Thus, the shrub plants are not the cause of the changes in these semiarid grasslands as is so often presumed, but they are the result of the effect of changes of other factors on the species in these grassland communities.

The composition of these communities will continue to change in the future (Bahre and Shelton, 1993) but the direction of future change and trends is difficult to predict (Buffington and Herber, 1965). All of the above factors will probably continue to interact to regulate community composition and structure and the density of shrubby plants will probably increase (Buffington and Herber, 1965; Miller et al., 2008; van Auken, 2009). Probably the process will continue

into the future until shrubby plants will encroach into all or most of the grasslands (Bahre and Shelton, 1993; van Auken, 2009).

The study of Buffington and Herber (1965) aimed to show the degree of encroachment of mesquite (i.e., a deciduous leguminous plant of the *Prosopis* genus found in northern Mexico; it can be classify as tree or shrub in function of its size, Figure 2.7) in the Jornada Experimental Range, near Las Cruces, New Mexico.

Figure 2.7. Mesquite plant

The study site is in the drier part of the semidesert grassland area. Vegetation surveys of 1858, 1915, 1928, and 1963 were compared. In this area, fires need to be periodic to keep mesquite under control. The value of fire in maintaining a mesquite-free semidesert grassland is questionable since black grama (i.e., grass) is susceptible to fire damage and mesquite is relatively resistant. Plant competition for space and moisture may have been a factor in keeping the mesquite invasion rate at a minimum under pristine conditions. If plant competition was a factor, any selective grazing by livestock or rodents would weaken the grass and favor the shrubs. In 1858 the Jornada Experimental Range was a great expanse of grass with only isolated spots of mesquite. On the higher areas along the mountains, mesquite was present; however, grass was also good in most places. Since 1858 the grass cover has decreased tremendously, and the mesquite has increased to the point that it was present on the entire study area in 1963. In 1858 good grass was present on more than 90% of the study area. By 1963 less than 25% of the area had good grass. Mesquite has been present on all soil types (Figure 2.8). However, the main invasion of mesquite was on sandy soils. As mesquite began to dominate a sandy site, low dunes form and grass cover was greatly reduced. In 1858 over 6,000 acres had abundant mesquite; by

1963 an area more than ten times as great was dominated by mesquite, with half of that increase occurring after 1928. The authors listed five factors which were responsible for the increase in mesquite: changes in climate, grazing by domestic livestock, effect of rodents, suppression of grassland fires, competition. Fires could have been a factor, however, no extensive fires were reported. Domestic livestock may have used this area prior to the 1880s, but such use would have been only seasonal or intermittent due to lack of water and during the 1880's, the number of cattle increased. Livestock was responsible for the dissemination of mesquite seed since the seed was capable of passing through their digestive tracts without being damaged. The authors concluded that the effect of livestock as a means of disseminating mesquite seed was more a factor in mesquite invasion than the effect of their grazing. Rodents and rabbits also consumed a large amount of range forage and they were also important in dissemination of seed. But authors stated that rodents should be considered only an aggravation of the problem rather than a primary cause.

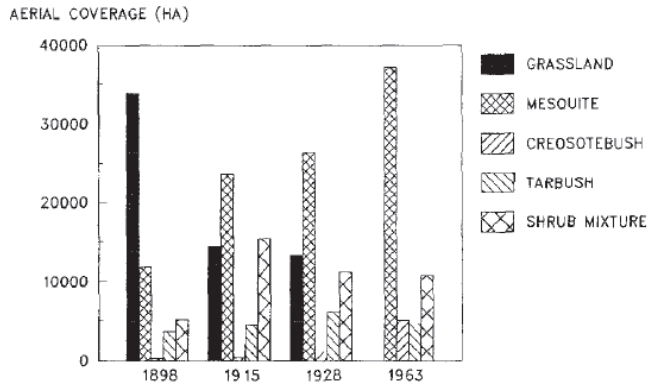

Figure 2.8. Summary of change in the areal coverage (ha) of several vegetation types on the Jornada Erperimental Range (Buffington and Herbel, 1965).

Archer et al. (1988; 1995) stated that dense woodlands occupy what are thought to have been grasslands and savannas prior to settlement of the Rio Grande Plains of Texas. However, the tenet that grasslands have been converted to shrublands and woodlands in recent history is controversial and based largely upon conflicting historical accounts. They hypothesized the two-phase landscapes represented an intermediate stage in the conversion of grassland to woodland. As new shrub clusters were initiated and existing clusters expanded and coalesced, a gradual shift from grassland to savanna to woodland occurred. To address this hypothesis, Archer et al. (1988) inventoried herbaceous interspaces for woody colonizers, quantified the composition and distribution of shrub clusters on upland sites, and compared the structure of clusters to that of adjacent, more mesic areas with continuous woody plant cover. To assess the

physiognomic stability of the two-phase landscapes, cluster size, density, and cover were quantified for 1941, 1960, and 1983 from aerial photographs. They then compared the composition of clusters at advanced stages of development to that of an adjacent stand of closed-canopy woodlands. Three spatially distinct sites within the research area were randomly selected for mapping. Each site was characterized by the same sort of polygonal vegetation pattern. The data suggested that mesquite plants invaded grasslands and served as recruitment foci for bird-disseminated seeds of other 19 woody species previously restricted to other habitats. The result was a landscape composed of discrete chronosequences of woody plant assemblages organized about a mesquite nucleus. Woody plant cover changed significantly over time within portions of the landscape characterized by the two-phase vegetation pattern (Figure 2.9a).

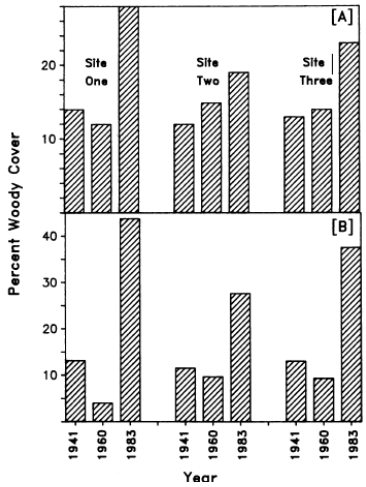

Figure 2.9. (a) Changes in percent woody plant cover within that portion of the landscape characterized by the two phase pattern, sites 1, 2, and 3. (b) Net change in total woody plant coverage resulting from border encroachment and cluster development within the two-phase pattern (Archer et al., 1988).

Percent coverage of woody plants (e.g., *Zanthoxylum*, and *Celtis*, that are evergreen trees or shrubs) , comparable on the three sites in 1941, had increased significantly by 1983. Averaged over sites, woody cover within the two-phase area was 13.0, 13.6, and 23.3% for 1941, 1960, and 1983, respectively. When woody plant cover changes resulting from border encroachment were combined with those changes observed within the two-phase zone, the result was a net increase in area occupied by woody plants of 30, 16, and 24% on Site 1 (S1), Site 2 (S2), and Site 3 (S3), respectively, over the 42 years period (Figure 2.9b). Averaged over the three sites, areal coverage was comparable in 1941 and 1960 (12.6 vs. 7.9%, respectively). By 1983 mean coverage of woody plants had

increased to 36.4%. Border encroachment and changes within the two-phase zone contributed equally to this overall increase in cover, (49% vs. 51%, respectively). The density of clusters and point locations within the two-phase area also changed over time. Cluster densities on S1 (3.7 clusters·ha^{-1}) and S2 (3.7 clusters·ha^{-1}) were twice that of S3 (1.8 clusters·ha^{-1}) in 1941. Cluster density on each of these sites had decreased to 2.1 and 2.8 clusters·ha^{-1}, respectively, by 1960. By 1983 densities had returned to levels comparable to or slightly greater than those of 1941. S3, which began with a low cluster density in 1941, changed little through 1960. However, density increased 42% to 2.7 clusters·ha^{-1} between 1960 and 1983.

Archer's results indicate: (1) mesquite invaded grasslands and served as the nucleus of cluster organization on upland sites; (2) woody plant community development has been highly punctuated by variations in precipitation; (3) the two-phase pattern was moved toward a monophasic woodland. As a result, (4) shrub clusters on uplands represented an intermediate stage in the conversion of grassland to woodland.

Bahre and Shelton (1993) examined long-term directional vegetation changes in the wild landscape of southeastern Arizona since the advent of major Anglo-American settlement in the 1870s and their relation to climate variations (Figure 2.10).

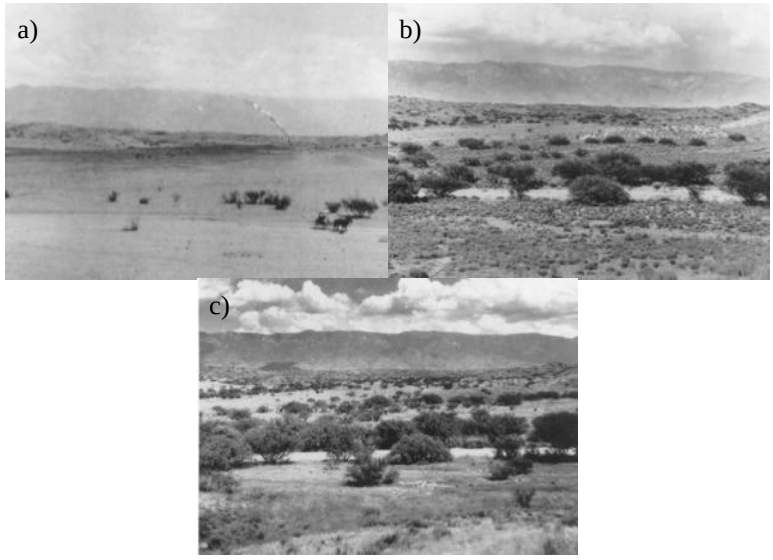

Figure 2.10. Vegetation Change in southeastern Arizona. (a) 1910, (b) 1968, (c) 1988 (Bahre and Shelton, 1993).

Particular emphasis is placed on verifying the purported changes in the distribution of major vegetation types and the link between velvet mesquite

(*Prosopis velutina Woot.*) increases and precipitation trends since the turn of the century. While there is little doubt that climatic oscillations have resulted in short-term fluctuations in vegetation, precipitation variations do not appear to be connected to any major directional vegetation change since 1870 in southeastern Arizona. In fact, no single trend is evident in regional precipitation during this period. Furthermore, there is no clear evidence for the upward displacement along a xeric (i.e., a type of habitat with a moderate or well-balanced supply of moisture)-to-mesic (i.e., a type of habitat with a small amount of moisture) gradient of any major vegetation type, and, except possibly for increases in woody xerophytes such as mesquite, all of the identified long-term vegetation changes appeared to be of anthropogenic origin. Mesquite increases, however, were irregular, showed no clear relation to precipitation variations, and were most likely the result of livestock grazing and/or fire exclusion.

Asner et al. (2003) have documented the local increases in shrub (i.e., mesquite, *Prosopis glandulosa*) cover in arid and semiarid ecosystems worldwide. They used historical aerial photography, contemporary Landsat satellite data, field observations, and image analysis techniques to assess spatial specific changes in shrubby vegetation cover and aboveground C stocks between 1937 and 1999 in a 400 km^2 region of northern Texas, USA.

Remote sensing operations afford comprehensive and repeatable assessments of land cover change at broad spatial scales and yield a suite of tools for mapping and monitoring changes in vegetation cover (Asner et al., 2003). As such, remote sensing plays an increasingly prominent role in estimating terrestrial plant biomass. Quantifying land cover classification accuracy and uncertainty associated with estimates of plant biomass is paramount. One important, yet outstanding challenge associated with estimating biomass from remotely sensed imagery, is to appropriately link field data to remotely sensed estimates of aboveground biomass. Aerial photography provides opportunities to quantify shrubby patch dynamics and stand structure as a link to coarse resolution satellite imagery for improving accuracy of terrestrial biomass and carbon storage estimates.

Browning et al. (2008) used a time-series of aerial photography to (1) quantify rates and dynamics of cover change on two distinct geomorphic surfaces; (2) relate patterns of shrubby cover change to rainfall seasonality and test the hypothesis that shrub cover increases will follow years of relatively high winter precipitation; (3) test the hypothesis that the rate and extent of *P. velutina* encroachment would be highest on coarse-textured soils and lowest on fine-textured soils. To assess the accuracy of using aerial photography to estimate shrub biomass on landscapes, the authors used field data to quantify how much shrubby plant biomass they might be missing. The study was conducted on the Santa Rita Experimental Range, 45 km south of Tucson, Arizona, along the western edge of the semidesert grassland region of the Sonoran Desert. To quantify the extent to which soils influence the rate and extent of shrub cover

change and to minimize potential confounding effects of livestock grazing, fire, and precipitation, they confined their analyses to landscapes with similar land use history, topography, and elevation. Changes in shrub cover were assessed using aerial photography from 1936, 1966, and 1996 from the U.S. Geological Survey (Figure 2.11). The sample unit in their analysis was a shrub patch, defined as a shrubby plant canopy that could represent an individual plant or a cluster of plants with touching or overlapping canopies. Automated image classification protocols were used to delineate shrub patches in geocoded, orthorectified images. Classification accuracies were assessed using a random sample of points stratified by image class. Random points on photographic images were assigned manually to the reference class shrub or non-shrub for 1936 and 1966 images and grass, shrub, or bare soil for the 1996 image. Classification accuracies represent the level of agreement between manual and automated image class assignments and are presented as error matrices along with Cohen's kappa (*k*) statistic, an estimate of accuracy that incorporates agreement that may occur by chance (Cohen 1960). Values of *k* range from 0 to 1.0; values 0.75 indicate strong agreement beyond chance; values 0.40 reflect poor agreement.

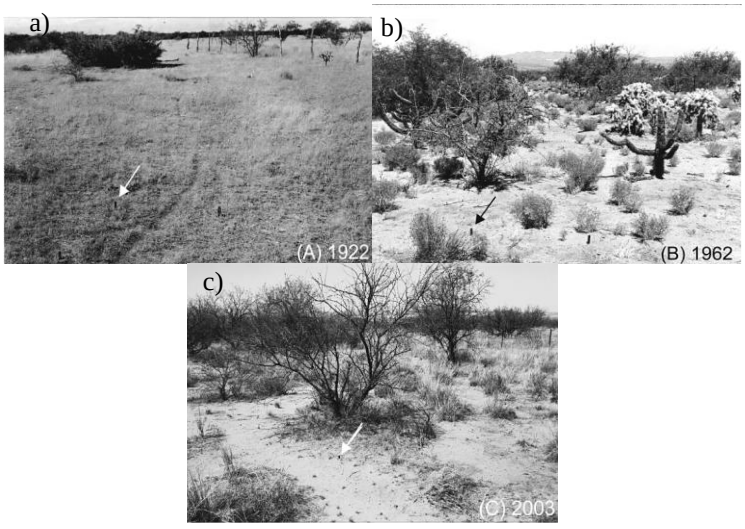

Figure 2.11. Repeat ground photography (1922, 1962, and 2003) of vegetation change on a site in a semidesert grassland in Arizona, USA (Santa Rita Experimental Range). Arrows denote fixed-location rebar. (a) Shrub cover was low in 1922, (b) by 1962, velvet mesquite, cholla, and burroweed abundance had increased markedly, and (c) mesquite abundance remained high through 2003, while cholla and burroweed abundance decline (Browning et al., 2008).

From this database, they extracted canopy dimensions for *P. velutina* (i.e., mesquite, here classified as shrub) plants present in 1948 but absent in 1932.

Thus, the maximum age of selected shrubs would be 16 years. Shrub percent cover on each landscape was determined by dividing the number of cells (i.e., pixels in classified photography) mapped as shrub by total number of cells in each landscape. There was a loose correlation between increases in shrubby plant abundance on aerial photos and periods of increased winter precipitation, a cause-effect assertion is perhaps too simplistic for several reasons. The increase in patch densities observed in their study also coincided with above-average summer rainfall and hence above-average annual rainfall. It could well be that the combination of elevated summer and winter rainfall was key to promoting recruitment. Although recruitment of new shrubs was observed during the 1966-1996 period, rates of recruitment were comparable (sandy sites) to 4.3 times higher (clayey sites), between 1936 and 1966, a period of erratic and relatively non-remarkable fluctuation in winter precipitation; and a period of relatively dry summers. Fifth, although shrub patch density increased during the relatively high-rainfall 1966-1996 period, total cover actually declined.

A better understanding of the relationship between shrub recruitment and climate is needed if we are to confidently forecast vegetation response to future environmental conditions.

2.1.1. Changes in vegetation from mid 1800s

Reports of increased density of shrubby plants in the arid and semiarid grasslands of southwestern North America date to the mid to late 1800s. This encroachment in Arizona is reasonably well documented, but still mostly anecdotal. It appears to be linked or coupled to increased cattle ranching in this area in the 1870s and the concomitant reduction in fire frequency about the same time (Bahre and Shelton, 1993). Additional evidence of dramatic changes in this area during the late 1800s and early 1900s has recently been presented. The shrubby increase is linked to human activity and was probabily caused by rapid expansion of livestock grazing at this time. This would be associated with reduced grass cover, reduced light fuel livel and a concomitant reduction in fire frequency. There is some documentation of the same phenomena in New Mexico and Texas as well, but possibly starting sooner (Archer, 1994). Nonetheless, increased shrubby plant density occurred before the major influx of CO_2 into the atmosphere but the increased density was associated with increasing temperature, which can be considered a background factor.

The area of grassland in southwestern North Americas that has been covered to shrubland is estimated as high as 60 million ha (van Auken, 2000). This encroachment in North American grassland is not limited to the arid and semiarid southwest and some suggest that between 220 and 330 million ha of total grassland have been or are being encroached (Knapp et al., 2008b).

2.1.2. Shrub encroachment causes

As previously mentioned, considerable discussion have centered on the factors that cause shrubby plant encroachment in the dry lands of the world (Archer et al., 1995; Van Auken, 2000; Peters et al., 2006; Knapp et al., 2008a, b; Van Auken, 2009). These debates have included changes in the arid and semiarid grasslands of southwestern North America.

In the following paragraphs a description of the principal causes is shown: herbivory, fire, spread of seed, competition and global change. A synthetic model of shrub invasion is shown in Figure 2.12. The grazing caused the reduction of the perennial grass causing the mesquite and creosote bush invasion. Grass reduction caused the fire suppression that accelerated the perennial grass decline and the shrub encroachment.

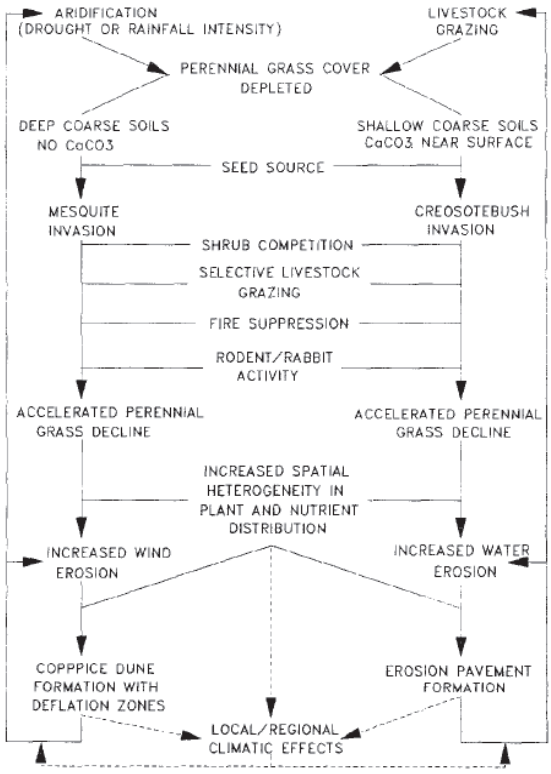

Figure 2.12. Synthetic model of shrubland invasion for the American southwest based on creosote bush and mesquite life histories and the observed consequences of their dominance (Grover and Musick, 1990).

2.1.2.1. Herbivory

Herbivores may reduce the growth of individual plants by damaging the leaves, stems, or roots. Damage to plants by hebivores is determined by the timing of the encounter, location of the tissue eaten, amount of tissue eaten, and frequency of attack (Crawley, 1997). By damaging plant parts, herbivores may alter a plant's ability to obtain resources or selectively eliminate a plant as a competitor, and thereby influence the outcome of species interactions. Damage to individual plants by removal of biomass may lead to changes in plant abundance and distribution through alteration in fecundity or ability to regrow or through changes in mortality. The ability of a plant to regrow after encounters with herbivores is usually reduced, and regrowth of grasses following removal of aboveground parts is usually associated with reductions in belowground growth and biomass. Only grasses are consumed by herbivores (Van Auken 2000; 2009) and then they may be at a disadvantage in their ability to interact with other plant species.

In the semiarid grasslands of the American southwest, brush encroachment has been coincident with or been preceded by development of the livestock industry (Archer, 1994; 1995; Bahre, 1995). Alterations in the grass species composition as well as reductions in herbaceous plant basal area, density, and aboveground and belowground biomass accompany chronic high levels of livestock grazing. Herbivory at low density and frequency may cause little change in a grassland community, but at high density and frequency, it can alter grassland composition, changing it to a shrubland (Archer, 1995).

2.1.2.2. Fire

Periodic burning is required to control or reduce the establishment and growth of shrubby plants in most grasslands: fire interacts with other factors such as topography, soil, herbivores, and amount of herbaceous fuel to determine the nature, density, and location of shrubby plants in a landscape (van Auken, 2009) (Figure 2.13).

Figure 2.13. Fire in Sevilleta.

Fire frequency in the semiarid grasslands has decreased in the past 150 years, while the size and density of shrubby plants has increased and biomass of grass has decreased. Most changes in the composition of the semiarid grasslands in southeastern Arizona, and probably in New Mexico and western Texas as well, occurred after the beginning of large-scale cattle ranching and fire exclusion in the 1870s (Van Auken, 2009). Today, wild-fires are rare. High densities of shrubby plants, low amounts of fuel, and grazing seem to be the cause. In fact the fire return period increased because of fine fuel removal by cattle, sheep, horses.

In the past, the fire return was 10 years (White et al., 2006; Wright et al., 1980; Wright and Bailey, 1982). Wide spread of fire at 5 to 10 years intervals maintained the semiarid grasslands of the pre-1900 (White et al., 2006). Wright et al. (1980), suggested fire return of 5-10 years for the control of shrubby cover in semiarid grasslands. Actual fire return is on a decadal order. Fire return intervals are greater than 10 years, and may actually occur only 1 or 2 times for century (fire return period equal to 100 years) (Parmenter, 2008).

The seedling of many shrubs of the semiarid grasslands are sensitive to fire (Van Auken, 2000). Some will no resprout if their tops are killed, and others are susceptible to fire mortality until reaching an appreciable size. If these plants do not produce seeds before they are 10 years of age, then a fire return time of 10 years or less would keep these semiarid grasslands relatively free of shrubs. Fire-tolerance species would be suppressed by recurring fires and remain in the grassland at a small size (Archer, 1994). However, with a reduction of the fine fuel load by heavy and constant herbivory, fire frequencies would decrease. Further increases in shrubby plant cover and density would follow. Therefore, if intermittent fires do not occur in grassland, they will be converted shrublands. Fire frequency is variable, but there is general agreement that recurring fires are required to control or reduce the establishment, density and growth of shrubby plants in most if not all grasslands (Van Auken, 2009). Moreover, fire frequency and intensity are linked to climate patterns and conditions.

2.1.2.3. Spread of seed

Some large and small mammals, including domestic livestock, feed on the fruit of shrubby plants and act as seed dispersal agents (van Auken, 2000; 2009). The introduction of domestic herbivores may have increased the dispersal of shrubby plant seeds, but many native herbivores could and probably still do the same thing (van Auken, 2009). These increases in shrubs density would not seem to require long-distance seed dispersal by domestic herbivores and could have been dispersed as far by native species.

Miller (1921) considered the role of livestock in causing juniper invasion to be through increased seed dispersal. He claimed that sheep consume quantities of juniper fruits which pass through the digestive tract and are scattered in the droppings. Johnsen (1962) demonstrated that although germination percentage

was not increase, juniper seeds germinated faster after passing through the digestive tract of animals. Parker (1945) pointed out that juniper seed has always been disseminated by birds, rodents, and water.

2.1.2.4. Competition

The importance of competition between grass and shrubs has been demonstrated in many arid and semiarid communities (Fowler, 1986). In addition, interaction between and among species are known to be important in determining community structure and function. Competition between species is considerede one of the major factors determining community characteristics (Wilson, 1998), but it is one of the several factors (Weltizin and McPherson, 1999) and is continually debated.

Changes in competition between grasses and shrubs are implicated in the encroachment of shrubs into semiarid grasslands, where competition is primarily belowground (Van Auken, 2000). Because of the low stature of the plants, relatively low plant density, high belowground biomass, and high root: shoot rations (Van Auken and Bush, 1988; 1997) competitive ability of plants in these communities may depend on root biomass, root density, root branching, root radius, root hair characteristics, mycorrhizae, timing of growth, or interactions with other soil organisms (Van Auken, 2000; 2009). Competition in these semiarid grasslands seems to change depending on the species and environmental conditions. Grasses inhibit the shrubs most during the germination, establishment, and early growth of the shrubby plants (Van Auken, 2000; 2009). However, the interaction seems to be reversed once the shrub root are below the root zone of the grasses.

2.1.2.5. Global change

There is not an evidence that changes in precipitation patterns or temperature in south-western North America since 1860s are linked to the recent shrub encroachment in the semiarid grasslands (Van Auken, 2009).

It has also been proposed that the rising livel of atmospheric CO_2 is the cause of shrub encroachment (Polley et al., 1992). It is based on observations that most shrubs have the C_3 photosynthetic pathway and in the semiarid grasslands, the grasses that are being replaced have the C_4 photosynthetic pathway. Plants with the C_3 photosynthetic pathway have a growth advantage at higher levels of CO_2 compared to plants with the C_4 photosynthetic pathway.

Modeled precipitations of current and future climatic trends in southwestern North America show a warmer drier climate, especially during summer (Solomon et al., 2009). However, links between changing climate since the 1870s and recent shrub encroachment in the semiarid grasslands are weak (Bahre and Shelton, 1993; Van Auken et al., 2000; Van Auken 2009). Precipitation variations do not appear to be connected to any major directional vegetation change since 1870 (Bahre and Shelton, 1993). Moreover, elevated

levels of CO_2 and parallel increases in temperature are background factors and not the principal causes of the encroacment (Van Auken, 2009).

In the future the severity and frequency of drought are expected to increase as the climate continues to get warmer and drier. The future climate change could become the major cause of encroachment (Allen and Breshears, 1998; Van Auken, 2009).

2.1.3. Control and management methods

In the past, the encroaching shrubs were considered alien and invader species with a high degree of aggressiveness. In order to deal with what appeared to be a serious grassland and rangeland problem various mechanical (chaining, rolling, chopping or shredding) and chemical (various herbicide) treatments were used (Scifres, 1980; Miller et al., 2005). Other treatments were tried including fire and biological control without a lot of apparent success. Fire would not work with little fuel. In addition, shrub mortality is size and temperature dependent, with large size plants being fire resistent. As soon as the grasses started to re-grow after treatment, usually after one or more rains, the animals (cattle) were put back on the treated area. The result of this type of treatment was an approximate 20 years cycle of treatment, grass re-growth, shrub encroachment followed by re-treatment.

More recently, combinations of treatments have been used with greater success but difficulties still occur and without fire, treatments are very expensive with limited success. Management usually includes some degree of mechanical or chimical treatment but success is still limited and reversing the process or going from a shrubland to grassland is complex and difficult. Biotic controls are usually more sophisticated, and usually combined with fire and may include genetic manipulation of some of the browsing species (Taylor, 2008).

2.2. Tree encroachment

Tree encroachment into shrublands and grasslands is one of the most pronounced environmental changes observed in rangelands of western North America in recent decades (Burkhardt and Tisdale, 1976; Miller and Rose, 1995; 1999; Miller et al., 2000; 2005). The lack of information on the rates, dynamics, and extent of increases in tree abundance is one of the major source of uncertainty in assessing how this vegetation change has influenced biogeochemical and hydro-ecological cycles.

As previously seen for the shrub encroachment, the fast expansion of tree into neighboring plant communities during the past 150 years has caused considerable concern because of increased soil erosion, reduced stream flows, altered wildlife habitat, reduced forage production, biodiversity, changes in plant community composition, and the replacement of semi-arid plant communities

with woodlands. However, the impacts of tree expansion are not always clear and have led to debate and legal challenges over control projects and management plans (Miller et al., 2005). Tree encroachment in the United States mainly occurred in central and eastern Oregon, southwestern Idaho, northeastern California, northwestern Nevada, in southern Washington and in New Mexico.

Burkhardt and Tisdale (1976), studied the invasion of western juniper into vegetation dominated by perennial bunchgrass on the Owyhee Plateau of southwest Idaho. The encroachment appears to be directly related to cessation of periodic fires (Figure 2.14). Evidence from adjacent climax juniper stands indicated that fires were frequent for at least several hundred years preceding settlement. Fires have been much less frequent during the past century due to active fire control, development of roads and other fire barriers, and reduced fuel because of heavy grazing and shift towards decreased precipitation.

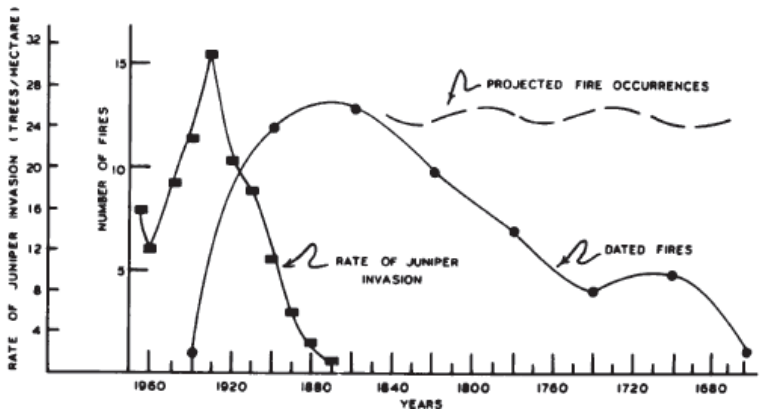

Figure 2.14. Frequency of fires and rate of western juniper invasion on the Owyhe. Plateau of southwest Idaho (Burkhardt and Tisdale, 1976).

Coop et al. (2007) have analyzed tree (i.e., ponderosa pine, blue spruce and aspen) encroachment into montane and subalpine grasslands that has occurred in the Rocky Mountains and many other mountain ranges globally. The timing, rate, and extent of invasion can depend on interactions among topography, positive spatial feedbacks, and temporally variable factors (especially climate, grazing, and fire). They examined spatial and temporal patterns of tree invasion in the Valles Caldera of the Jemez Mountains, New Mexico. They used a GIS analysis of orthorectified aerial photos taken in 1935 and 1996, covering a 40,000-ha study area, to quantify the extent of tree invasion and to assess its relationship to spatial factors. They obtained dates of establishment from 299 increment cores and basal disks from 50 sites to reconstruct temporal patterns of tree invasion. The area of grasslands in the study area declined from 11,747 to 9,336 ha (nearly 18%) between 1935 and 1996. Tree invasion increased with

slope, elevation, and proximity to the previous tree line, but showed no relationship to aspect. Invasion was more rapid and continuous on upper mountain slopes, while the invasion of valley-bottom grasslands below reversed tree lines was more episodic, and appeared to track mean summer minimum temperatures. The rapid and continuous invasion of steep, high-elevation slopes suggested that frequent fire was the single most important factor in maintaining grassy communities in these sites. The slower, episodic invasion of valley-bottom grasslands, and the apparent relationship between increased invasion and years of higher summer minimum temperatures were consistent with the hypothesis that these grasslands have been maintained by low temperatures or frosts damaging to tree seedlings.

In particular, in this section, among all the possible tree encroachment, particular attention is paid to the western juniper encroachment since it represents the encroachment case study analyzed in section 5.2.

The importance of western juniper expansion into sagebrush grassland is due to the possibility to affect the spatial distribution of soil organic matter, nutrients and carbon. The loss of nutrients could also increase if woodland development results in accelerated erosion. Changes in hydrologic processes and water balance as tree abundance and dominance increase are not well understood. Evidence suggests that juniper can impact infiltration rates, sediment loss, and soil water storage and depletion rates.

In order to understand the magnitude of the problem, the photos in Figure 2.15 show the western juniper encroachment over the 34-year period from 1973 to 2007 in the Shoshone Mountains, Nevada (Miller et al., 2008), while the photos in Figure 2.16 show the western juniper encroachment in the Keystone Ranch, east of Prineville, Oregon, from 1890 to 1989. Majority of trees are juniper with a few ponderosa pine. The smaller trees in the foreground of Figure 2.16a appear to be about 10 to 25 years old, and larger trees 60 to 70 years (Miller et al., 2005).

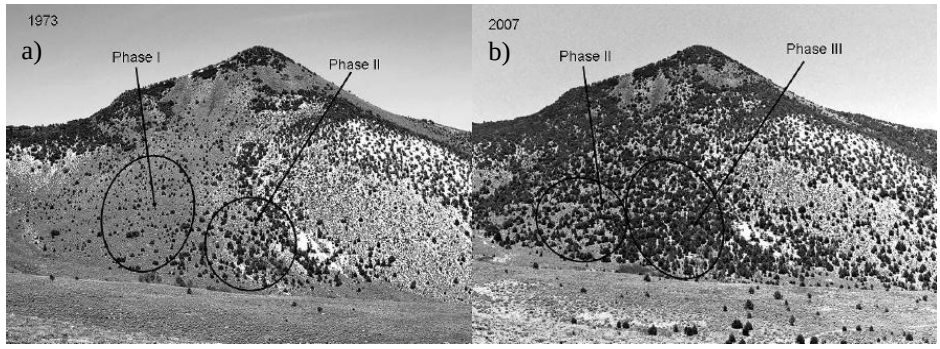

Figure 2.15. Woodlands closure over the 34-year period from (a) 1973 to (b) 2007, resulting in a shift from *phase I* and *II* to *phase II* and *III* in the Shoshone Mountains, Nevada (Miller et al., 2008).

Figure 2.16. Keystone Ranch east of Prineville, Oregon, in Crook County on Ochoco Creek, (a) 1890, (b) 1989 (Miller et al., 2005).

Western juniper (*Juniperus occidentalis* var. *occidentalis Hook.*) (Figure 2.17) which is, together with sierra juniper (*J. occidentalis* var. *australis*), a variant of *Juniperus occidentalis*, occupies 9 million acres in central and eastern Oregon, southwestern Idaho, northeastern California, and northwestern Nevada, and in southern Washington (USDA Forest Service, 1981; Gedney et al., 1999; Miller and Tausch, 2001; Azuma et al., 2004) (Figure 2.18). It represents the northwestern portion of the piñon and juniper region in the Intermountain West. Western juniper is usually the only conifer species occupying a site except where western juniper woodlands adjoin ponderosa pine (*Pinus ponderosa*) forests. Presettlement changes in woodland abundance and distribution are attributed to the increase of the return intervals of fire, long-term changes in temperature, amounts and distribution of precipitation (Davis, 1982; Thompson and Hattori, 1983; Mehringer, 1987; Van Devender et al., 1987; Wigand et al., 1995). Evidence supporting rapid post-settlement expansion is derived from old surveys, photographs, the distribution of relict presettlement woodlands, and tree-ring chronologies. Precipitation across most of the western juniper zone varies between 180 and 500 mm (Gedney et al., 1999), falling during the winter and spring (October through June). It grows over a wide array of environments and occupies elevations ranging from 200 to 2500 m (Sowder and Mowat, 1958; Miller and Rose, 1995; Gedney et al., 1999; Miller et al., 2000).

Figure 2.17. a) Western juniper, b) juniper's leaves.

Sierra juniper (*J. occidentalis* var. *australis*), extends along the eastern slopes of the Sierra Nevada mountain range south of Susanville, California, and east and south from the Anchorite Hills (Nevada) to the San Bernardino mountains (USDA Forest Service, 1981) (Figure 2.18). This species is usually found growing as widely scattered trees mixed with other conifers at elevations between 1,250 and 2,800 m. Recent work has documented small pockets of Sierra juniper growing in the mountains of central and eastern Nevada (Charlet 1996). Although stands typically occur well above Utah juniper (*J. osteosperma*) in this region, mixed stands including hybrids of Sierra and Utah juniper are occasionally found along drainages at lower elevations (Charlet, 1996; Terry et al., 2000).

Western juniper is a long-lived species (more than 1000 years) with a mean age of 800 years and has got an elevation of 4-10 m (mean elevation: 7 m) (Miller et al., 2005). The tree develops male cones in early spring, which attain full size the first summer and mature during the second summer. Seed dispersal of western juniper occurs through gravity, overland flow, and animals. At least 12 species of birds feed on the fruits and as a group are the most important disseminator's of western juniper seed. Western juniper grows on a wide variety of parent materials and soils including materials derived from sedimentary, aeolian and igneous sources. Soil textures range from clay to sandy.

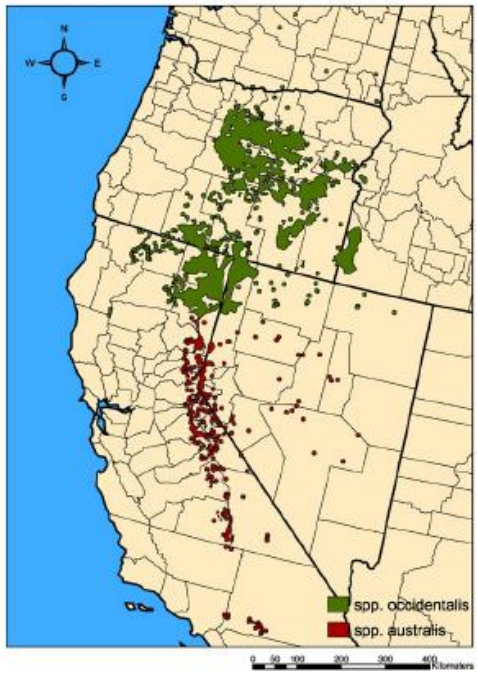

Figure 2.18. Distribution map of western juniper (*Juniper occidentalis* var. *Occidentalis)* and Sierra Juniper (*J. occidentalis* var. *australis*) (Gedney et al. (1999) and USGS: 1:250,000 maps).

Western juniper communities may be separated into presettlement (old-growth) or post-settlement (expansion) communities. Miller et al. (2005) suggest 1870 as a cut-off to separate the two age classes. Western juniper is a long-lived species (more than 1,000 years). Old-growth trees and stands can easily be separated from post-settlement stands based on morphological and stand structure characteristics.

The majority of post-settlement communities are still in a state of transition. The stage of woodland *succession* (defined as *phases I*, *II*, and *III*) directly affects plant community composition, wildlife habitat, and ecological processes including hydrologic and nutrient cycles. As the tree increases, the shrub and grass decrease (Miller et al., 2005). The minimum time for the tree overstory to begin suppressing the understory is 45-50 years and to approach stand closure 70-90 years on cool wet sites (Johnson, 2005) and 120-170 on dry warm sites.

As a result, control of western juniper has been a major concern of land management since the early 1960's. In the 1960's through the early 1970's chaining and dozing were the most common forms of western juniper control. In the 1970's, chainsaws became a widespread tool used for juniper control. In the 1990's, the use of prescribed fire for juniper control also increased (Miller et al., 2005).

2.2.1. Woodland expansion history

2.2.1.1. Presettlement expansion

The distribution and density of western juniper changed across the Intermountain West around the late Pleistocene and into the Holocene. During much of the Pleistocene, 45,000-12,500 years BP (before present), western juniper had a much more southerly distribution, with the northern boundary near Kings Canyon National Park, California (Cole, 1983). Towards the end of the Pleistocene, 12,000-15,500 years BP, its northernmost distribution was the Winnemucca Lake Basin in Nevada (Thompson, 1984). Only prostrate juniper and common juniper occupied southeastern Oregon at the end of the Pleistocene (Wells, 1983). As temperatures warmed during the early Holocene, western juniper began migrating north into its present range. Macrofossils from pack rat middens found in caves at the Lava Beds National Monument in northern California date its arrival around 5,300 years BP (Mehringer and Wigand, 1984). In Oregon, the earliest evidence of western juniper was dated 6,600 years BP in the Fort Rock Basin in south-central Oregon (Bedwell, 1973) and 4,800 years BP at Diamond Craters in eastern Oregon (Wigand, 1987).

Since the arrival of western juniper in central and eastern Oregon, northeastern California, and southeastern Idaho, its abundance and distribution have fluctuated (Mehringer, 1985; Mehringer and Wigand, 1990; Miller and Wigand, 1994). Following a very dry period during the mid-Holocene, 7,500-5,000 years BP, western juniper rapidly expanded into its new range. Precipitation increased while temperatures remained warm between 5,000 and 4,000 years BP (Mehringer, 1986; Wigand, 1987). Between 4,000 and 3,000 years BP climatic conditions were relatively cool and wet. Western juniper continued to increase, but retreated from higher elevations and expanded to lower elevations during this period. Western juniper reached most of its current geographic range approximately 3,000 years BP (Wigand et al., 1995). Severe drought and major fires during the late Holocene, 2,500-1,500 years BP, resulted in regional declines in western juniper (Mehringer and Wigand, 1987; Wigand et al., 1995). Around 1,200 years BP summer precipitation increased, resulting in increases in abundance of both grasses and western juniper. A drying period between 900 and 700 years BP again reduced woodland abundance (Wigand et al., 1995). The Little Ice Age, 700-150 years BP, was the wettest and coolest period during the last half of the Holocene. Increased grass cover during this period (Wigand et al., 1995) probably supported higher fire frequencies (Miller and Rose, 1999), which limited woodland distribution and abundance (Wigand, 1987; Miller and Wigand, 1994). The abundance of juniper pollen has gradually increased since 1500 A.D., fluctuating in the early 1800's and sharply increasing in the mid-1900's (Mehringer, 1987). Since the end of the Little Ice Age around 1850, annual temperatures have been slowly but steadily rising (Ghil and Vautgard, 1991). Relict juniper woodlands, tree age chronology data, down and

dead trees and stumps, and historic documents generally indicate that presettlement western juniper trees were typically confined to rocky ridges, low sagebrush flats, and pumice soils where fine fuels were too low in abundance to carry fire (Burkhardt and Tisdale, 1976; Miller and Rose, 1995; Waichler et al., 2001).

2.2.1.2. Post-settlement expansion

During the past 140 years, western juniper has been expanding within its geographic range at unprecedented rates compared to any other time period during the Holocene (Miller and Wigand, 1994; Miller and Tausch, 2001). Historical expansions of western juniper and other piñon and juniper species throughout the West are well documented in the literature (Burkhardt and Tisdale, 1976; Tausch and West, 1988, 1995; Miller and Rose, 1995, 1999; Gedney et al., 1999; O'Brien and Woudenberg, 1999; Soulé and Knapp, 1999; Tausch and Nowak, 1999; Coppedge et al., 2001; Soulé et al., 2004). For western juniper, evidence supporting rapid post-settlement expansion is derived from old surveys, photographs (i.e., Figures 2.15, 2.16), the distribution of relict presettlement woodlands, and tree ring chronologies. Its rapid increase in abundance and expansion since the late 1800's, has largely been attributed to anthropogenic factors (Miller and Wigand, 1994; Knapp et al., 2001; Miller and Tausch, 2001).

Western juniper woodlands in eastern Oregon with more than 10 % canopy cover increased from 456,000 acres in 1936 (Cowlin et al., 1942) to 2.2 million acres in 1988 (Gedney et al., 1999). Other evidence supporting the post-settlement expansion of western juniper is the sharp rise in pollen in the mid-1900's, which Mehringer (1987) detected in lake sediment cores. The presence of old stumps and logs, which can persist on a site for hundreds of years in this semi-arid climate, are good indicators as to whether woodlands were present on a site prior to the 1860's (Miller and Rose, 1995, 1999; Miller et al., 2000; Miller and Tausch, 2001; Wall et al., 2001).

The strongest evidence for the post-settlement expansion of western juniper is from tree-ring chronologies. These chronologies, which describe the age composition and establishment of woodlands over time, show a rapid increase in establishment since the 1870's (Miller and Tausch, 2001; Soulé et al., 2004). In southeastern Oregon peak establishment in some closed woodland stands occurred between 1900 and 1920 (Miller and Rose, 1999).

A similar pattern of western juniper encroachment has occurred in aspen communities throughout the range of western juniper (Miller and Rose, 1995; Wall et al., 2001). In southeastern Oregon and northwestern Nevada, 12 % of the aspen stands measured were completely replaced by western juniper (Wall et al., 2001). In addition, post-settlement western juniper was the dominant tree species in 23 % of the stands and common to codominant in 42 % of the aspen stands measured. Western juniper began invading aspen stands in the 1890's, with peak

establishment occurring between 1900 and 1940. No western juniper in these aspen stands exceeded 140 years in age.

In much of its range, western juniper has increased the area it occupies by an estimated 10-fold in the past 140 years (Miller et al., 1999a) and has the potential to occupy far more area than it now does (West and Van Pelt, 1986; Betancourt, 1987; Miller et al., 2000). Most of the 9 million acres occupied by western juniper is still in transition from shrub-steppe to western juniper woodland (Miller et al., 2000) and the species continues to expand its range and increase in density (Miller and Rose, 1995, 1999; Wall et al., 2001).

2.2.1.3. Factors affecting post-settlement expansion

Factors most frequently attributed to the increase in both density and area of piñon and juniper are: the reduced role of fire, the introduction of livestock, climate and the industrial increases in atmospheric CO_2 (Figure 2.19).

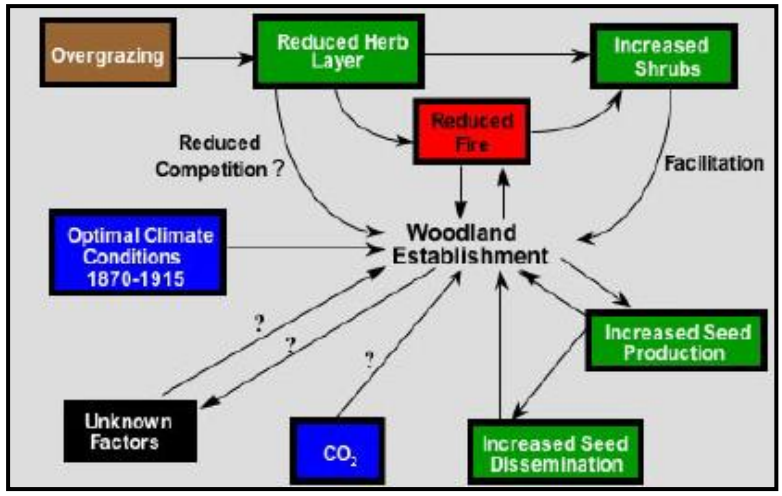

Figure 2.19. Conceptual model illustrating factors influencing the expansion of western juniper since the late 1800's and throughout the 1900's (Miller and Tausch, 2001).

2.2.1.3.1. Fire

Fire is considered to have been the most important factor in limiting conifer encroachment into shrub-grassland communities (West, 1999; Miller and Tausch, 2001). However, only a few studies have documented fire regimes across shrub-steppe communities and woodlands throughout this region. Fire scars on western juniper are occasionally found, but most presettlement trees do not grow on sites representative of more productive deeper-soil sites, which now support expanding postsettlement woodlands. Old-growth western juniper is commonly found on relatively fire-safe sites characterized by low production

with limited fine fuels (Burkhardt and Tisdale, 1976; Vasek and Thorne, 1977; Young and Evans, 1981; Holmes et al., 1986; Miller and Rose, 1995; 1999). Evidence that woodland expansion was limited by fire events prior to settlement includes: (1) sites supporting old-growth trees are usually fuel-limited, (2) most young stands occupy the more productive communities where fine fuel loads could carry a fire, and (3) the time sequence of woodland expansion is synchronous with the decline in fire occurrence.

In productive mountain big sagebrush plant associations in the Northwest, such as those characterized by Idaho fescue (*Festuca idahoensis*), MFRIs (mean fire return intervals) typically ranged between 10 to 25 years and large fires every 38 years.

MFRIs were determined from fire scars collected on ponderosa pine or Douglas-fir (*Pseudotsuga menziesii*) growing in or adjacent to mountain big sagebrush communities. In two studies, where presettlement MFRIs were 12-15 years, fire-free intervals varied between 3 and 29 years (Gruell, 1999; Miller and Rose, 1999). Based on tree growth, age structure, and the scarcity of presettlement trees or the presence of large dead wood, the maximum MFRI in the mountain big sagebrush/Thurber needlegrass (*Stipa thurberiana*) plant association was probably 50-70 years. Fire return intervals up to 50 years were probably adequate to limit western juniper encroachment into the mountain big sagebrush alliance (Burkhardt and Tisdale, 1976; Miller and Rose, 1999). A fire free period of more than 70 years will also increase the potential for leaving large-diameter charred wood consisting of heartwood (that can persist on the site for more than 100 years), resulting from the development of mature trees on the site. In northern California, a plant community identified as a western juniper/ sagebrush/needlegrass (*Stipa occidentalis*) plant association burned in 1856 (Miller et al., 2003). Intact charred wood and fire-killed trees are still present on the site. A number of studies in mountain big sagebrush communities in the Intermountain West have reported significant declines in fire events since the late 1800's (Miller and Tausch, 2001). Several studies have shown a close relationship between the early expansion of western juniper in the late 1800's and the sudden decline in fire occurrences in the mountain big sagebrush alliance (Miller and Rose, 1999; Miller et al., 2001; 2003). MFRIs reported for the low sagebrush/ bluegrass association were considerably longer than for neighboring mountain big sagebrush communities (Young and Evans, 1981; Miller and Rose, 1999). Fire-free periods of 90 (Young and Evans, 1981) and 138 years (Miller and Rose, 1999) were reported for this plant association in northern California and south-central Oregon and it is not unlikely that fire-free periods exceeded 150 years for some sites. This plant association can be characterized by a low density of widely scattered old-growth western juniper, which suggests infrequent fires. Tree growth rates are relatively slow with the average age of a 3-m-tall tree ranging from 75 to 90 years.

2.2.1.3.2. Livestock grazing

Introduction of livestock in the 1860's and the large increase of animals from the 1870's through the early 1900's (Oliphant, 1968; Miller et al. 1994) coincide with the initial expansion of western juniper woodlands. Season-long grazing by the large numbers of domestic livestock during this period is believed to have reduced fine fuel loads, thus contributing to a significantly reduced role of fire in the northern Great Basin (Burkhardt and Tisdale, 1976; Miller and Rose, 1999; Miller and Tausch, 2001). Fire occurrence and fire size declined dramatically in the late 1800's. Miller and Rose (1999) reported a large decrease in fire occurrence in southeastern Oregon shortly after large numbers of livestock were introduced in the late 1860's. The lack of fire and decreased competition from herbaceous species probably contributed to an increase in shrub density and cover, thus providing a greater number of safe sites for western juniper establishment (Miller and Rose, 1995; 1999). The role of livestock as a mechanism for western juniper seed dispersal appears to be also important (Burkhardt and Tisdale, 1976).

2.2.1.3.3. Climatic influences

From 1850 to 1916, winters became milder and precipitation was greater than the current long-term average in much of the Great Basin (Antevs, 1938; Wahl and Lawson, 1970; LaMarche, 1974; Graumlich, 1987). There is some indication that woodland expansion was initiated between 1850 and 1870 (Johnson, 2005). Annual tree ring growth in western juniper is strongly related to local climatic conditions (Pohl et al., 2002). Soulé et al. (2004) reported that western juniper annual ring growth across five sites in eastern Oregon were above-average from the late 1800's through the early 1900's. This wet period coincides with post-settlement establishment and the peak period of woodland establishment for closed stands. Wet, mild conditions promote vigorous growth in western juniper (Fritts and Wu, 1986; Holmes et al., 1986).

2.2.1.3.4. Atmospheric CO_2

Rising levels of atmospheric CO_2 seem to have enhanced the increase in woody species throughout the West (Johnson et al., 1993; Knapp and Soulé, 1999). Increases in atmospheric CO_2 levels do not coincide with the initial increase or peak periods of western juniper establishment (Table 2). However, elevated atmospheric CO_2 during the last half of the 20th century may be an important contributing factor accelerating tree canopy expansion and establishment in some areas (Knapp and Soulé, 1996, 1998, 1999; Soulé et al., 2004).

2.2.1.3.5. Climate and fire

In semi-arid ecosystems, fuels are often limited in abundance and continuity. A series of wet years allows fuels to accumulate and become more contiguous (Miller and Rose, 1999). Wetter than average conditions in the late 1800's would have resulted in the accumulation of fine fuels. However, high livestock stocking rates and season-long or heavy grazing during this period reduced fine fuel accumulations and thus significantly decreased the potential for fire (Burkhardt and Tisdale, 1969; Miller and Rose, 1999). The combination of reduced fire occurrences (Miller and Tausch, 2001) and optimal climatic conditions for conifer establishment (Fritts and Wu, 1986) at the turn of the century were probably the two dominant factors that initiated post-settlement western juniper expansion.

2.2.2. Woodland succession

Most communities occupied by postsettlement western juniper are in a transitional state, ranging from open stands of trees with a dominant understory of shrubs and grasses to mid or late *succession*, where trees are beginning to dominate the site (Miller et al., 2000). It is important to identify the woodland transitional state in resource evaluations or inventories. The state of woodland development directly affects plant community structure, composition, wildlife habitat, and ecological processes. The stage of woodland *succession* will also directly affect the selection of management treatment, response following treatment and treatment cost. Moreover continued changes in structure and composition in developing woodlands over time should be considered when developing resource plans and setting management priorities.

2.2.2.1. Identification of the woodland stage of succession

Woodland *succession* can be separate into three transitional phases (Figure 2.20):

- *phase I*, trees are present but shrubs and grasses are the dominant vegetation that influence ecological processes on the site (Figure 2.21a);
- *phase II*, trees are codominant with shrubs and grasses and all three vegetation layers influence ecological processes on the site (Figure 2.21b);
- *phase III*, trees are the dominant vegetation and the primary plant layer influencing ecological processes on the site (Figures 2.21c, d).

There are several characteristics that can be used to define the phase of woodland development (Miller et al., 2000). Early signs of western juniper domination on a site are canopy mortality of the shrubs in the interspace and the reduction of leader growth on sapling size (less than 3 m tall) trees.

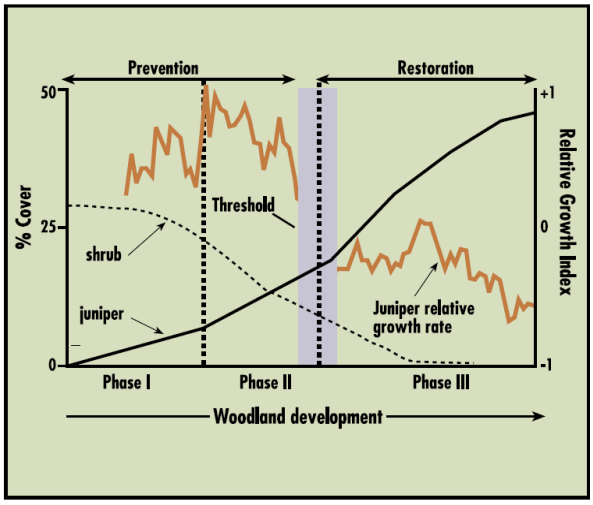

Figure 2.20. A conceptual model illustrating the relationship between shrub canopy cover, tree canopy cover and relative growth rates (Miller et al., 2005).

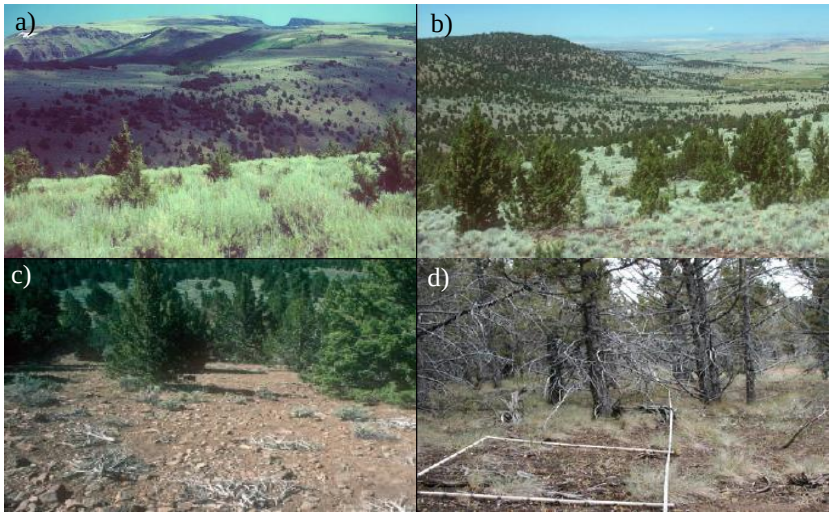

Figure 2.21. Three phases of woodland *succession* in mountain big sagebrush communities: (a) *phase I*, (b) *phase II*, (c) (d) *phase III* (Miller et al., 2005).

2.2.2.2. Rates of woodland development

The rate of woodland *succession* from initial encroachment to entirely developed woodlands is a function of the rates of tree establishment and growth. There is a high degree of variability in woodland *succession* rates across and within plant associations. In eastern Oregon, all three transitional phases of

western juniper stand development can be observed where encroachment began in the late 1800's (Miller and Rose, 1999; Miller et al., 2000).

Dense fully developed post-settlement woodlands that initiated establishment in the late 1800's had reached *phase III* (Figures 2.21c, d) by the 1950's and early 1960's, based on tree growth rates. In closed stands in southwestern Idaho, a significant decrease in growth of annual tree rings occurred during the 1950's, suggesting the onset of intra-species competition.

The primary factor controlling the number of years between initial encroachment and stand closure is establishment rate of tree seedlings. This is largely determined by seed input and the abundance of safe sites for seedling establishment. There may be a lag period of tree establishment immediately following fire, because of the reduction in shrubs (Erdman, 1970; Burkhardt and Tisdale, 1976).

2.2.3. Understory dynamics

2.2.3.1. Shrubs

As western juniper begins to dominate a site, shrubs begin to decrease (Figure 2.20) (Burkhardt and Tisdale, 1969; Adams, 1975; Bunting et al., 1999; Miller et al., 2000; Roberts and Jones, 2000; Schaefer et al., 2003). This has a significant impact on ladder fuels, ground- and shrub-nesting birds, seed pools, and structural complexity of the plant community. At a site near Silver Lake, Oregon, 71 % of the trees established during 1900-1936 (Adams, 1975). The rapid decline in bitterbrush and sagebrush on these sites began in 1948. In the John Day Province near Prineville, Oregon, shrub cover in untreated western juniper plots was 0.4 % compared to 9.4 % cover in adjacent plots cut 18 years earlier (Eddleman, 2002). The decline in mountain big sagebrush is not proportional to the increase in western juniper (Figure 2.20). As western juniper approaches 50 % of maximum potential, sagebrush declines to about 20-25 % of maximum potential (Miller et al., 2000). Tausch and West (1995) also reported a disproportionate decline: shrubs declined to one-fourth of maximum when single-leaf piñon *(Pinus monophylla)* and Utah juniper cover reached 50 % of maximum in Nevada.

2.2.3.2. Grasses and forbs

Even if it is often stated that the grass declines as western juniper increases in dominance, only a few studies have evaluated this relationship for western juniper. Two types of experiments support the hypothesis that western juniper overstory significantly affects production, diversity, and cover of the grass: (1) spatial, comparing different transitional states within plant associations (Bunting et al., 1999; Miller et al., 2000), and (2) temporal, comparing herbaceous

response over time between cut and uncut western juniper plots (Bates et al., 2000; Eddleman, 2002).

Miller et al. (2000) reported that the relationship between herbaceous cover and western juniper canopy cover differed among plant associations. Grass in plant associations characterized by Thurber needlegrass, which often had a restricted subsoil layer or strong argillic horizon, was the most sensitive to increasing tree dominance. Mean herbaceous cover, in early states of woodland development, was 16 %, compared to 5 % in late stages of development. In central Oregon, the presence of western juniper was associated with an increase in bare ground and smaller, more widely spaced grass clumps on relatively shallow soils (Roberts and Jones, 2000) and a significant decrease in ground cover (Knapp and Soulé, 1998). This was consistent with results from southwestern Idaho, where grass also decreased in the mountain big sagebrush alliance as western juniper dominance increased (Bunting et al., 1999). However, changes in species richness across the transitional phases of woodland development were not consistent. In southwestern Idaho and southeastern Oregon, species richness did not change as western juniper increased in dominance (Bunting et al., 1999; Miller et al., 2000). In contrast, species richness declined in Thurber needlegrass communities in Oregon and in Idaho fescue communities in northeast California (Miller et al., 2000). Grass diversity and richness also significantly increased following western juniper removal on a mountain big sagebrush/Thurber needlegrass plant association (Bates et al., 2000).

2.2.4. Inventory of western juniper in Oregon

Gedney et al. (1999) analyzed and summarized a 1988 inventory of western juniper (*Juniperus occidentalis Hook*.) in eastern Oregon. The inventory of all of the forest resources of eastern Oregon, by the *Pacific Resource Inventory, Monitoring, and Evaluation* (*PRIME*) Program of the Pacific Northwest Research Station (Gedney et al., 1989), was intensified to meet increased need for more information about the juniper resource than was available in previous inventories. An earlier inventory of juniper, made in 1936, estimated the area of juniper forest to be 420,000 acres. The 1988 inventory estimated the current area of juniper forest to have increased fivefold. Over half of the area of the present juniper forest became established between 1850 and 1900. After initial stand establishment, the juniper forest increased in density with the greatest increase occurring between 1879 and 1918. This rapid increase in juniper stand establishment occurred during a period of favorable climatic conditions and reduced fire frequency and intensity. Eleven shrub species grew on plots with juniper forest. Shrubs were present on 88 % of the area sampled. The most common shrub was big sagebrush, which was present on 55 % of the juniper forest sampled. On 88 % of the area with shrubs, there were fewer than three shrub species present.

Periodic forest inventories, which have been conducted by the station since the early 1930s, have differed in the amount of information presented about western juniper. The 1936 inventory of eastern Oregon mapped the area occupied by western juniper by crown cover class producing a type map showing the location of juniper stands (Cowlin et al., 1942). Inventories of eastern Oregon made between 1953 and 1977 were less intensive, presenting only statistical information on the area of western juniper forests (Bolsinger and Berger, 1975; Farrenkopf, 1982).

To determine when the present juniper forests of eastern Oregon became established, a chronology was developed based on the age of juniper trees in each of the juniper forest inventory plots. The age when each stand became established was determined from the age of the oldest tree in each field plot. Juniper forests are mostly uneven aged. Over 30 % of the area of juniper forests has trees with a range of ages greater than 100 years. Only 26 % of the juniper forests have trees with a range of ages less than 30 years old.

From the analysis it was concluded that between 1650 and 1800, the annual rate of stand establishment was 2,900 acres a year, increasing to 8,200 acres between 1800 and 1850 (Table 2.1). During the 200 years between 1650 and 1850, 37 % of the present juniper forest became established. In the 50 years between 1850 and 1900, the annual rate of juniper establishment increased sharply to 23,100 acres a year, and more than half of the present juniper forest became established. During the 40-year period from 1900 to 1940, the annual rate of juniper establishment decreased to 6,000 acres a year and a little more than a 10th of the present juniper forest originated.

Gedney et al. (1999) examined the percentage of Juniper forest and savanna by precipitation, elevation, and soil classes to determine if there were influence factors or variables influencing the Juniper encroachment (Figure 2.22). There are more Juniper in the places with precipitation between 254 and 508 mm (Figure 2.22a), and where the elevation is between 1219 and 1524 m (Figure 2.22b). The Juniper percentage is very high in the soil types: *Xeric-Aridic mesic soils on terraces and flood plains* (*S*) and *Xeric frigid soils on grass-shrub uplands* (*Q*) (Figure 2.22c).

Table 2.1. Percentage of western juniper forest between 1650 and 1940, eastern Oregon (Gedney et al., 1999).

Period of origin	Annual rate of stand establishment	Proportion of area established
Years	*Thousand acres*	*Percent*
1900-1940	6.0	11
1850-1900	23.1	52
1800-1850	8.2	18
1650-1800	2.9	19
Total		100

[a] Based on age of oldest tree in stand at breast height plus 30 years for total age.

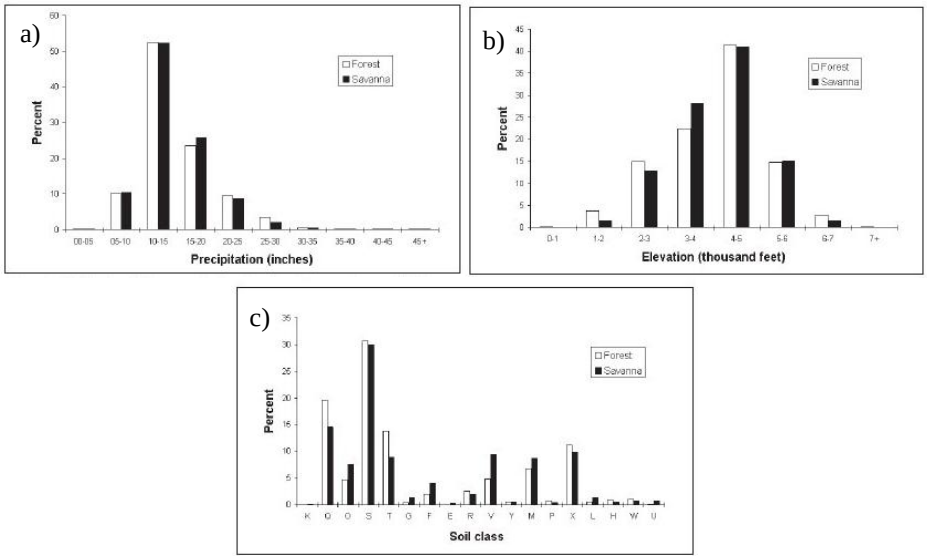

Figure 2.22. Distribution of the area of juniper forest and savanna in the eastern Oregon in 1988 by (a) precipitation classes, (b) elevation classes, and (c) soil classes (Gedney et al., 1999).

2.2.5. Management and control methods

Control of western juniper has been a major concern of land management since the early 1960's. Justifications used for western juniper control include restoration of preinvasion plant communities, increasing forage production and quality, reducing soil erosion, increasing water capture on site, increasing spring and stream flow, increasing biological diversity and improving wildlife habitat (Miller, 2001; Miller et al., 2005; Miller et al., 2007).

In the late 1970's, the *U.S. Bureau of Land Management (*BLM) Prineville district began using chainsaws as its primary method of western juniper control. By the 1980's and 1990's this practice became widespread. Research on the effects of western juniper cutting began in the early 1980's and has quickly expanded. Chemical control of western juniper has been tested but has produced mixed results. In the 1990's, the use of prescribed fire to control western juniper greatly increased. The use of mechanical shears and whole tree chipping of western juniper has increased since 2000 in northeastern California and southcentral Oregon (Lake County). Several studies now provide information from treatments that are older than 10 years. Work in central Oregon provides long-term assessments of vegetation response and successional patterns using several treatment methods (Miller, 2001).

Chapter 3

Methods and Models

This chapter provides in section 3.1 the description of the ecohydrological Cellular Automata model, CATGraSS, used to analyze the influence of topography and climate change on the vegetation spatial distribution and the shrub and tree encroachment, while in section 3.2 the description of the weather generator model, AWE-GEN; finally in section 3.3 the description of the General Circulation Models (GCMs) and the downscaling procedure.

3.1. CATGraSS

The *Cellular Automata Tree-Grass-Shrub Simulator* (CATGraSS) has been implemented by Zhou et al. (2013) and in this thesis it has been furtherly developed and improved with new algorithms and equations that will be described in the following. In particular, the new algorithms that we have implemented are: soil thickness code, described in section 3.1.5, fire component, described in section 3.1.6.3, and encroachment model codes, described in section 3.1.7.

In the CATGraSS catchment topography, soil, and vegetation properties are represented using a regular grid of cells. Each cell can hold a single *Plant Functional Type* (PFT) hereafter denoted by *X* (G: grass, SH: shrub, T: tree) or can be bare soil. Topographic informations needed to the model are retrieved from a *Digital Elevation Model* (DEM). The model combines the functionality of a simplified *dynamic global vegetation model* (DGVM), which includes the dynamics of local water balance (e.g., evapotranspiration), plant life processes (productivity, carbon allocation), and plant mortality (e.g., Kucharik et al., 2000; Sitch et al., 2003) with a rule-based probabilistic cellular automata (CA) component that simulates seed dispersal and plant establishment processes (e.g., Jeltsch et al., 1996, 1998; van Wijk and Rodriguez-Iturbe, 2002). CATGraSS is driven by daily rainfall and maximum (i.e., unstressed) evapotranspiration, ET_{max}, and treat these quantities with a daily or inter-storm time steps in a spatially explicit way using slope and aspect look-up tables. It simulates water budget dynamics for each PFT and their seedlings within each bin of the slope-

area histogram. Local soil and plant dynamics are modeled continuously and include soil moisture, *ET*, net primary productivity (NPP), driven by *ET* with a simple *WUE* approach, assuming no nutrients limitation. The NPP is allocated to aboveground and belowground biomass pools, and plants experience senescence. The age of each plant in each vegetation grid cell is tracked and used in an age-dependent plant mortality function. The Cellular Automaton component of CATGraSS simulates plant spatial processes including seed dispersal and probabilistic seedling establishment which are based on water stress. A flowchart illustrating the CATGraSS components is shown in Figure 3.1.

The model water balance is run at daily or inter-storm time scale, while the plant spatial dynamics (probabilistic plant establishment and mortality algorithms) are run with an annual time step. Earlier work using the point version of the grassland component of this model illustrated that using inter-storm model time step captures soil moisture and biomass (live and dead) dynamics with sufficient accuracy (Istanbulluoglu et al., 2012).

Each of the model components outlined above are discussed in the following sections.

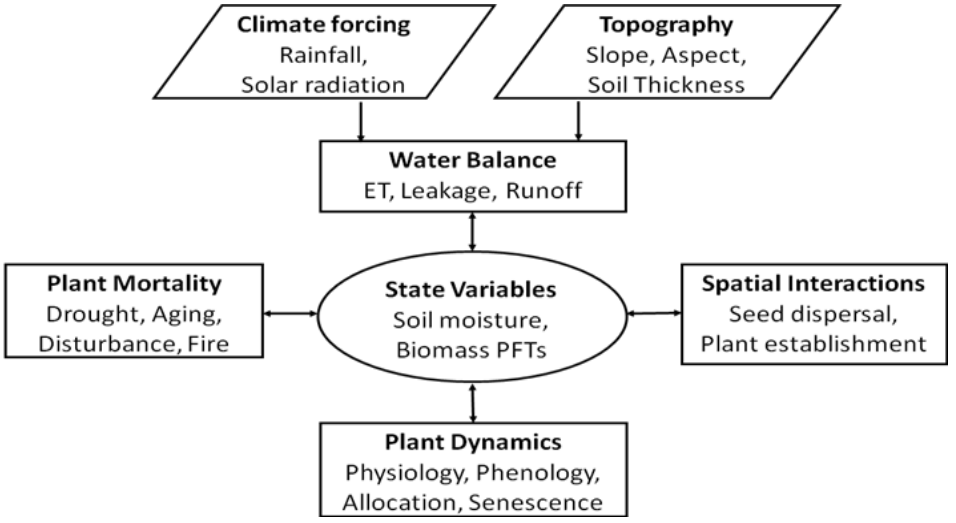

Figure 3.1. Model flowchart illustrating the ecohydrological processes linked to model state variables in the middle. Topography influences the water balance through modulating solar radiation and effective rainfall amount at a point. PFT is plant functional type.

3.1.1. Point water balance

The basis of the CATGraSS model is the depth-averaged soil moisture balance in the root zone represented as (e.g., Eagleson, 1982; Rodriguez-Iturbe, 2000):

$$nZ_r \frac{ds}{dt} = I_a - ET_a(s) - D(s) \tag{3.1}$$

where n [-] is soil porosity, Z_r [mm] is the effective soil rooting depth, s [-] is the degree of soil saturation (volumetric soil moisture normalized by n), t [d] is time, I_a [mm·d^{-1}] is the rate of infiltration, ET_a [mm·d^{-1}] is the actual rate of evapotranspiration, D [mm·d^{-1}] is the rate of drainage from the root zone.

The actual infiltration rate is the amount of rainfall that enters the soil when rainfall depth is larger than canopy interception capacity (daily or inter-storm time scale). When the soil is unsaturated, I_a is determined by the minimum of the rate of rainfall and soil infiltration capacity after the canopy storage is satisfied. Upon soil saturation, infiltration rate is reduced to the rate of drainage D as:

$$I_a = \begin{cases} 0 & P < C_I \\ Min[p, I_c] & 0 \le s < 1, \quad P > C_I \\ D & s = 1, \quad P > C_I \end{cases} \tag{3.2}$$

where I_c [mm·d^{-1}] is infiltration capacity (constant), p [mm·d^{-1}] is the mean rate of rainfall ($p=P/T_r$, where T_r [d] is storm duration), and P [mm] is the depth of rainfall. C_I [mm] is canopy interception capacity. Infiltration is typically higher in under-canopy space than inter-canopy spaces for semiarid ecosystems, and often varies with vegetation types (Reid et al., 1999; Bhark and Small, 2003). To examine the role of variable infiltration in the model, we introduce a canopy-intercanopy infiltration capacity coefficient, R_{in} [-] (equal to 2 for tree and shrub and 1.2 for grass), that scales bare soil infiltration capacity, $I_{c\text{-}b}$, to estimate infiltration capacity of a vegetated area, $I_{c\text{-}v}$ (Bhark and Small, 2003):

$$I_{c-v} = R_{in} I_{c-b} \tag{3.3}$$

The canopy interception capacity C_I is approximated by:

$$C_I = \min(I_{\max} V_t, PV_t) \tag{3.4}$$

where $I_{\max}$ [mm] is the full canopy interception and V_t [-] is the fraction of vegetation cover that includes both dry and live biomass components. V_t is only used for grass model elements and calculated from the total leaf area index, LAI_t [-], (sum of live and dead leaf area) using an exponential function: V_t=1-exp(-0.75LAI_t) (e.g., Lee, 1992). For other vegetation types a constant $I_{\max}$ is used.

In this model, we assume all rain drops fall vertically (P_M, mm), and the actual amount of rainfall (P) intercepted by the ground is calculated by using a cosine correction of the slope angle, S [rad], (Ivanov et al., 2008b):

$$P = P_M \cos(S) \tag{3.5}$$

Maximum unstressed evapotranspiration rate used for solving the soil moisture balance of a model element covered by a PFT of X, $ET_{max\text{-}X}$ [mm·d^{-1}], is defined similar to the model used by Brolsma and Bierkens (2007):

$$ET_{max-X} = \begin{cases} T_{max-X} - C_{I-X}, & LAI_{l-X} = LAI_{max-X} \\ \left[T_{max-X} \dfrac{LAI_{l-X}}{LAI_{max-X}} + E_b \left(1 - \dfrac{LAI_{l-X}}{LAI_{max-X}}\right) \right] - C_{I-X}, & LAI_{l-X} < LAI_{max-X} \end{cases} \tag{3.6}$$

where $T_{max\text{-}X}$ [mm·d^{-1}] is plant maximum transpiration rate of a single PFT. $T_{max\text{-}X}$ is calculated for each PFT using the Penman-Monteith equation (Monteith, 1965) with $LAI_{max\text{-}X}$. E_b [mm·d^{-1}] is maximum soil evaporation. $LAI_{l\text{-}X}$ [-] is the live leaf area index of the canopy and $LAI_{max\text{-}X}$ is maximum $LAI_{l\text{-}X}$ for a PFT of X, given as input to the model. When $LAI_{l\text{-}X} \leq LAI_{max\text{-}X}$, $T_{max\text{-}X}$ is scaled by the $LAI_{l\text{-}X}$ to $LAI_{max\text{-}X}$ ratio, which is assumed to represent the fraction of live vegetation cover in a model cell. The remaining area fraction is assumed to be subject to potential evaporation rate of a bare surface, E_b. To reduce data requirements and keep the model simple, E_b is taken as a fraction (f_b) of the reference grass evapotranspiration rate, $T_{max\text{-}G}$ ($E_b = f_b\ T_{max\text{-}G}$) (e.g., Mutziger et al., 2005; Istanbulluoglu et al., 2012). The value of f_b is set to 0.7 after Istanbulluoglu et al. (2012). The intercepted rainfall of PFT X, $C_{I\text{-}X}$ is assumed to satisfy the initial atmospheric demand for evapotranspiration. For long-term simulations forced by generated rainfall, $T_{max\text{-}X}$ for each PFT is prescribed by a sinusoidal curve ($T_{COS\text{-}X}$) fitted to the calculated $T_{max\text{-}X}$ from historical daily weather data using the Penman-Monteith equation.

With $ET_{max\text{-}X}$ obtained from (3.6), actual evapotranspiration, $ET_{a\text{-}X}$ [mm·d^{-1}], is calculated using a soil moisture limitation approach as:

$$ET_{a-X} = ET_{max-X} \cdot \beta_s(s) \tag{3.7}$$

where β_s [-] is evapotranspiration efficiency term based on the depth-averaged soil moisture in the root zone (e.g., Dyck, 1983; Laio et al., 2001):

$$\beta_s(s) = \begin{cases} 0, & s_h < s \leq s_w \\ \dfrac{s - s_w}{s^* - s_w}, & s_w < s \leq s^* \\ 1 & s_* < s \end{cases} \tag{3.8}$$

where s_h, s_w and s^* [-] are soil moisture levels at hygroscopic capacity, wilting point, and incipient water stress, respectively (Laio et al., 2001). For bare soil, s_w is replaced by s_h.

Surface runoff, R [mm·d^{-1}], is generated when

$$R = \begin{cases} (p - I_a) & p > I_a \\ 0 & p \le I_a \end{cases} \tag{3.9}$$

Drainage from the root-zone is expressed by unsaturated hydraulic conductivity:

$$D(s) = \begin{cases} K_S, & s = 1 \\ K(s) = K_S s^{(2b+3)} & s_{fc} < s \le 1 \end{cases} \tag{3.10}$$

where K_s [mm·d^{-1}] is saturated hydraulic conductivity, s is relative root-zone soil moisture, s_{fc} [-] is field capacity soil moisture, and b [-] is water retention parameter (Campbell, 1974).

In storm generation, we have used the *Poisson Rectangular Pulses* (PRP) model, with a one-parameter exponential distribution for time between storms (T_b) and storm durations (T_r); and a Gamma distribution for rainfall depth h conditioned on T_r (e.g., Ivanov et al., 2007).

3.1.2. Local plant dynamics

Net primary productivity (*NPP*, $g_{DM}\cdot m^{-2}\cdot d^{-1}$) of each PFT is calculated as the difference between gross primary productivity (*GPP*, $g_{DM}\cdot m^{-2}\cdot d^{-1}$) and plant autotrophic respiration (R_e, $g_{DM}\cdot m^{-2}\cdot d^{-1}$). *GPP* is linearly related to daily ET_a by an ecosystem water use efficiency parameter (*WUE*, $kg_{CO2}\cdot kg^{-1}{}_{H2O}$), ratio of the amount of carbon gained for unit water loss (Emmerich, 2003; Williams and Albertson, 2004; Scott et al., 2006).

$$NPP = GPP - R_e = ET_a \cdot WUE \cdot \rho_v \cdot w - R_e \tag{3.11}$$

where ρ_v [kg·m^{-3}] is water density and w [$kg_{DM}\cdot kg^{-1}{}_{CO2}$] converts CO_2 to dry matter. Plant autotrophic respiration (R_e) consists of maintenance (R_m) and growth (R_g) respirations $R_e = R_m + R_g$, which are often related to photosynthesis, Rubisco level, and soil, air, and leaf temperatures (Collatz et al., 1992; Arora, 2002, Fatichi et al., 2012). Through studying the daytime and nighttime net ecosystem CO_2 exchange, Williams and Albertson (2005) found that R_m could take up approximately 29% to 47% of daytime *GPP*. Using the same assumptions of Zhou et al. (2013), we introduced a coefficient μ [-] representing the ratio of R_m to *GPP*, and we assumed that R_g represent the 0.25 of GPP and we assumed R_g is approximately 25% of *GPP*, less of R_m, $R_g=0.25(GPP-R_m)$ (e.g., Ryan, 1991, Sitch et al., 2003). Adding R_m and R_g, and substituting into R_e in (3.11) gives *NPP* as:

$$NPP = 0.75 \cdot (1 - \mu) ET_a \cdot WUE \cdot \rho_v \cdot w \tag{3.12}$$

The partitioning of *NPP* is based on the mass balance concept similar to most DGVMs (e,g. Kucharik et al., 2000; Cramer et al., 2001; Bonan et al., 2003; Sitch et al., 2003; Krinner et al., 2005) and ecohydrological models (Ivanov et

al., 2008a; Fatichi et al., 2012). Dynamics of aboveground green/live (B_l), aboveground dead (B_d), and structural (B_s) biomass ($g_{DM} \cdot m^{-2}$) are modeled based on ordinary differential equations (e.g., Arora, 2002; Montaldo et al., 2005; 2008; Williams and Albertson, 2005; Ivanov et al., 2008a). B_s consists of both root and sapwood biomass for trees and shrubs, and only represents root biomass for grasses.

$$\frac{dB_l}{dt} = NNP\phi_{a-X} - k_{sg}B_l - k_{sf}\xi B_l, \tag{3.13a}$$

$$\frac{dB_s}{dt} = NPP(1-\phi_{a-X}) - k_{ss}B_s, \tag{3.13b}$$

$$\frac{dB_d}{dt} = k_{sg}B_g - k_{dd}\eta_{sd}B_d \tag{3.13c}$$

where k_{sg}, k_{ss}, and k_{dd} [d^{-1}] are decay coefficients for green, structural, and dead biomass respectively. In the simulation, k_{sg} and k_{ss} are used in both the growing and dormancy periods. During dormancy, k_{sg} is doubled to represent unfavorable environmental conditions for growth. *NPP* is partitioned between B_l and B_s using an allocation coefficient, $\phi_{a\text{-}X}$ [-], that depends on available space. The allocation coefficient for grass is taken from Istanbulluoglu et al. (2012), and those for woody plants (e.g., shrubs and trees), are based on Williams and Albertson (2005), respectively:

$$\phi_{a-G} = \left(1 - \frac{LAI_l}{LAI_{\max} - LAI_d}\right), \tag{3.14a}$$

$$\phi_{a-G} = 1 - \frac{LAI_l}{LAI_{\max}} \tag{3.14b}$$

In (3.13a), k_{sf} [d^{-1}] represents the maximum drought induced foliage loss rate (Ivanov et al., 2008a). ξ [-] is plant cumulative water stress during growing season defined by multiplying an index of water stress by its duration (Porporato et al., 2001):

$$\xi = \begin{cases} 1 & \bar{s} < s_w \\ \sum_{n=1}^{N_{is}} \left(\frac{s^* - \bar{s}}{s^* - s_w}\right)^M T_b & s_w < \bar{s} < s^* \\ 0 & \bar{s} > s^* \end{cases} \tag{3.15}$$

where $\bar{s}$ [-] is mean inter-storm soil moisture content, N_{is} [-] is number of inter-storm periods in growing season, T_b [d] is the time between storms. M is an index related with nonlinear effects of water deficit on plants (we used M = 4.0 for all PFTs following Ivanov et al., 2008). In (3.13c), k_{dd} represents the

maximum decomposition rate of dead biomass during the peak of the warm season. The adjustment coefficient for dead biomass loss rate n_{sd} [-] is included to introduce the effect of weather such that the rate of decomposition is at its maximum level when $T_{\text{max-}X}$ reaches a threshold value using the $T_{\text{max-}X}$ / $T_{\text{d-max}}$ ratio:

$$\eta_{sd} = \min(T_{\max -X} / T_{d-\max}, 1) \tag{3.16}$$

where $T_{d\text{-max}}$ [mm·d^{-1}] is a calibration parameter. Application of (3.16) has greatly improved model performance in grasslands (Istanbulluoglu et al., 2012). The specific leaf area for green (c_g) and dead (c_d) biomass are used to calculate live, dead, and total *LAI* respectively as:

$$LAI_l = c_g B_l, LAI_d = c_d B_d, LAI_t = LAI_l + LAI_d \tag{3.17}$$

In *DGVM*s, the onset and the offset of the growing season is often triggered when a set of environmental conditions (e.g., air and soil temperatures, soil moisture, positive net photosynthesis) are satisfied for certain period of time (Cayrol et al., 2000; Sitch et al., 2003; Ivanov et al., 2008a). For simplicity, we used the 30-day-averaged $T_{\text{max-}X}$, $T_{\text{max-}X\text{-}30}$ [mm·d^{-1}], as a surrogate variable for climatic favorability (Istanbulluoglu et al., 2012). The growing season starts when $T_{\text{max-}X\text{-}30}$ is higher than *GT* (growth threshold), and ends when $T_{\text{max-}X\text{-}30}$ falls below *DT* (dormancy threshold). This approach is preferred to minimize the model parameters in long-term model simulations. For evergreen plants growth and dormancy thresholds are not used.

3.1.3. Clear-sky solar radiation on slopes

In this section the clear-sky solar radiation estimation for inclined surface, used for the evapotranspiration evaluation, is detailed. Daily extraterrestrial solar radiation calculation on sloped surface has been established by Allen et al. (2006a). For clear-sky solar radiation, atmospheric absorption and scattering effects has been approximates by applying the empirical method from Bras (1990) for cloud-free conditions.

3.1.3.1. Extraterrestrial solar radiation

Instantaneous extraterrestrial solar radiation R_a is calculated as:

$$R_a = I_{sc} E_0 \cos(\theta) \tag{3.18}$$

in which I_{sc} is solar constant, E_0 is eccentricity correction, θ is solar zenith angle

$$E_0 = \frac{1}{1 + 0.033 \cos\left(\frac{2\pi DOY}{365}\right)} \tag{3.19}$$

where *DOY* is the day of the year and ($2\pi DOY/365$) is in radians.

Estimation of instantaneous angle of incidence for solar radiation on sloped surfaces is based on Duffie and Beckman (1980):

$$\begin{aligned}\cos(\theta) = {} & \sin(\delta)\sin(\Lambda)\cos(S) \\ & - \sin(\delta)\cos(\Lambda)\sin(S)\cos(\gamma) \\ & + \cos(\delta)\cos(\Lambda)\cos(S)\cos(\omega) \\ & + \cos(\delta)\sin(\Lambda)\sin(S)\cos(\gamma)\cos(\omega) \\ & + \cos(\delta)\sin(\gamma)\sin(S)\sin(\omega)\end{aligned} \tag{3.20}$$

where δ is the declination of the earth (positive during northern hemisphere summer), Λ is the latitude of the location (positive for the northern hemisphere and negative for the southern hemisphere), S the surface slope, where S=0 for horizontal and $S=\pi/2$ for vertical slope (S is always positive and represents the slope in any aspect), and γ is the surface aspect angle, where γ=0 for slopes oriented toward south, $\gamma=-\pi$ for slopes oriented toward east, $\gamma=\pi/2$ for slopes oriented due west, and $\gamma=\pi$ for slopes oriented toward north. Parameter ω is the hour angle, where ω=0 at solar noon, ω is negative in morning and ω is positive in afternoon.

Declination of sun δ (radians), is calculated as a function of Day angle Γ, which is estimated as 2π(DOY-1)/365.

$$\begin{aligned}\delta = {} & [0.006918 - 0.399912\cos(\Gamma) - 0.070257\sin(\Gamma) - 0.006758\cos(2\Gamma) \\ & - 0.000907\sin(2\Gamma) - 0.002697\cos(3\Gamma) - 0.00148\cos(3\Gamma)]\end{aligned} \tag{3.21}$$

For horizontal surface, S=0 and (3.20) can be reduced to:

$$\cos(\theta) = \sin(\Lambda)\sin(\delta) + \cos(\Lambda)\cos(\delta)\cos(\omega) \tag{3.22}$$

Daily extraterrestrial solar radiation on horizontal surface $R_{E\text{-}h}$ can be expressed as:

$$R_{E-H} = \int_{\omega_{hr}}^{\omega_{hs}} R_a \tag{3.23}$$

where the integration can be limited by sunrise hour angle ω_{hr} and sunset hour angle ω_{hs}:

$$\omega_{hr} = -\cos^{-1}(-\tan(\delta)\tan(\Lambda)) \tag{3.24a}$$

$$\omega_{hs} = \cos^{-1}(-\tan(\delta)\tan(\Lambda)) \tag{3.24b}$$

Daily extraterrestrial solar radiation on slope area $R_{E\text{-}S}$ can be expressed as:

$$R_{E-S} = \int_{\omega_{sr}}^{\omega_{ss}} R_a \tag{3.25}$$

where the integration limit sunrise hour angle ω_{sr} and sunset hour angle $\omega_{ss,}$ are computed as:

$$\omega_{sr} = \sin^{-1}\left(\frac{ac - b\sqrt{b^2 + c^2 - a^2}}{b^2 + c^2}\right) \tag{3.26a}$$

$$\omega_{ss} = \sin^{-1}\left(\frac{ac + b\sqrt{b^2 + c^2 - a^2}}{b^2 + c^2}\right) \tag{3.26b}$$

where *a*, *b*, and *c* are constants for a given day, latitude, slope and slope azimuth:

$$\begin{aligned} a &= \sin(\delta)\cos(\Lambda)\sin(S)\cos(\gamma) - \sin(\delta)\sin(\Lambda)\cos(S) \\ b &= \cos(\delta)\cos(\Lambda)\cos(S) - \cos(\delta)\sin(\Lambda)\sin(S)\cos(\gamma) \\ c &= \cos(\delta)\sin(\gamma)\sin(S) \end{aligned} \tag{3.27}$$

3.1.3.2. Clear-sky shortwave radiation

Total clear-sky shortwave radiation consists of direct, diffusive and reflected solar radiation. In this model we calculated clear-sky shortwave radiation normal to the surface without cloudiness effect. For both slope area and horizontal surface, clear-sky direct solar radiation R_{dir} (*H*: horizontal, *S*: slope) at the surface is calculated following Bras (1990):

$$R_{dir-H} = R_{E-H}\, f_{di} \tag{3.28a}$$

$$R_{dir-S} = R_{E-S}\, f_{di} \tag{3.28b}$$

in which $f_{di} = \exp(-f_t m(0.128\text{-}0.054\log_{10} m))$, where f_t is turbidity factor varies from 2.0 for clear mountain air to 4 or 5 for smoggy urban areas; *m* is the optical air mass approximated as 1/sin α, in which α is the solar altitude and it varies for time of the day. Daily averaged sin α is calculated based on Allen et al. (2006a) weighted according to R_a.

Diffuse solar radiation on horizontal surface, $R_{dif\text{-}H}$ is computed based on $R_{E\text{-}H}$ following ASCE-EWRI (2005) by multiplying a diffusive coefficient f_{df}:

$$R_{dif-H} = R_{E-H}\, f_{df} \tag{3.29}$$

where f_{df} is determined by ASCE-EWRI based on 49 locations across the U.S.:

$$f_{df} = \begin{cases} 0.35 - 0.36 f_{di} & f_{di} \geq 0.15 \\ 0.18 + 0.82 f_{di} & 0.065 < f_{di} < 0.15 \\ 0.10 + 2.08 f_{di} & f_{di} < 0.065 \end{cases} \quad (3.30)$$

Total clear-sky shortwave radiation for horizontal surface, $R_{c\text{-}H}$ is expressed as:

$$R_{c-H} = R_{dir-H} + R_{dif-H} \quad (3.31)$$

Diffuse solar radiation on sloped surface, $R_{dif\text{-}S}$ is assumed as a fraction of $R_{dif\text{-}H}$ following Allen et al. (2006a):

$$R_{dif-S} = R_{dif-H} f_{ia} \quad (3.32)$$

in which f_{ia} is simulated by applying isotropic approach following Tian et al. (2001):

$$f_{ia} = 0.75 + 0.25\cos(S) - S / 2\pi \quad (3.33)$$

Reflected (or backscatter) solar radiation, $R_{ref\text{-}S}$, is calculated only for slope areas and is estimated by assuming that both the direct and diffuse solar radiation reflect isotropically from a horizontal surface at the foot of the inclined slope (Allen et al., 2006a):

$$R_{ref-S} = \alpha_s (1 - f_{ia}) R_{c-H} \quad (3.34)$$

where α_s is average albedo of surrounding ground surface varies with vegetation coverage.

Total clear-sky shortwave radiation for sloped surface, $R_{c\text{-}S}$ is expressed as:

$$R_{c-S} = R_{dir-S} + R_{dif-S} + R_{ref-S} \quad (3.35)$$

3.1.4. Spatial patterns in evapotranspiration

CATGraSS is designed to perform long-term simulations (greater than thousand years) to examine vegetation pattern development. To improve computational efficiency, topography can be classified into topographically similar slope, aspect (*S-A*) groups. This classification is performed with a Δ_S degree increment for local slopes, and a Δ_A degree increment for aspect, leading to *x* different combinations (*S-A* groups). In each of the *S-A* group, the coupled water balance and biomass production models (from (3.1) to (3.16)) are run for all PFTs separately. Methods used to calculate $T_{\max\text{-}X}$ for different PFTs in each *S-A* group are described below.

CATGraSS can be run both by observed and generated weather data. In the case of the former, the Penman-Monteith equation (Monteith, 1965) is directly used in the model:

$$T_{\max-X} = \frac{\Delta(R_{n-X} - G) + \rho_a c_P (e_s - e_a)/r_{a-X}}{\lambda_v \rho_w (\Delta + \gamma(1 + r_{s-X}/r_{a-X}))} \tag{3.36}$$

where $R_{n\text{-}X}$ [W·m^{-2}] is net radiation. G is the ground heat flux and is neglected for daily estimation (Allen et al., 1998). e_s and e_a [kPa] are saturation and actual vapor pressure at air temperature, respectively. ρ_a [kg·m^{-3}] is air density. c_p [W·°C^{-1}] is the specific heat of the air, Δ [kPa·°C^{-1}] represents the slope of the saturation vapor pressure versus air temperature curve. γ [kPa·°C^{-1}] is the psychrometric constant. $r_{s\text{-}X}$ and $r_{a\text{-}X}$ [s·m^{-1}] represents plant canopy and aerodynamic resistances, respectively. $r_{s\text{-}X} = r_{l\text{-}X} / 0.5LAI_{max\text{-}X}$ where r_l [s·m^{-1}] is stomatal resistance. $r_{a\text{-}X}$ is calculated based on the von-Karman logarithmic profile as a function of vegetation height and heights at which wind and relative humidity were measured (e.g., Allen et al., 1998).

The influence of topography is introduced in the calculation of $R_{n\text{-}X}$. In each *S-A* group, we start with postulating that the daily incoming shortwave radiation on a hillslope element, $R_{s,H}$ [W·m^{-2}], and on a flat surface, $R_{s,F}$ [W·m^{-2}] (from observation), can be related through a radiation factor f_R [-], assuming that both hillslope and flat landscape elements have identical cloud cover (e.g., Dingman, 2002):

$$R_{s,H} = f_R \cdot R_{s,F} \tag{3.37a}$$

$$f_R = \frac{R_{c,H}}{R_{c,F}} \tag{3.37b}$$

where f_R is described as the ratio of the clear-sky incoming shortwave radiation on a hillslope element, $R_{c,H}$, to that of a flat surface, $R_{c,F}$ [W·m^{-2}] (f_R = 1 for flat surface) (Dingman 2002). In each *S-A* group, the model proposed by Allen et al. (2006a) is used to calculate $R_{c,H}$ and $R_{c,F}$ as a function of the DOY, latitude, slope and aspect angles at the mid points of the *S-A* ranges, with the clear-sky atmospheric transmissivity coefficient obtained from (Bras, 1990). Calculated f_R values for the *S-A* groups for each *DOY* are compiled into a look-up table and used in the model in all simulations.

The net radiation $R_{n\text{-}X}$ on the terrain for each PFT is calculated based on the approximation of radiation balance (e.g., Caylor et al., 2005):

$$R_{n-X} = (1 - \alpha_X) R_{s,H} + \sigma T_s^4 - \sigma(T_a + 273.15)^4 \tag{3.38}$$

where α_X [-] is the shortwave albedo, σ is the Stefan–Boltzmann constant (5.67×10-8 Wm^{-2}·K^{-4}), T_a [°C] is the air temperature used to estimate the outgoing longwave radiation, assuming surface and air temperatures are equal. T_s [K] is the apparent radiative temperature of the atmosphere, approximated empirically from (Friend, 1995):

$$T_s = T_a + 273.15 - 0.825\exp(3.54 \cdot 10^{-3} R_H f_R), \tag{3.39}$$

and used to estimate the incoming longwave radiation in (3.38).

In long-term simulations with generated storms, the model is forced by prescribed $T_{max\text{-}X}$, obtained from a cosine function of *DOY*, calibrated to calculated $T_{max\text{-}X}$ ((3.36), using local observed weather data) of flat surface, $T^F_{\max -X}$ (e.g., Small, 2005):

$$T^F_{Cos-X} = \left\{ \frac{\Delta}{2} \cos\left[2\pi \left(\frac{DOY - L_T - N_d/2}{N_d} \right) \right] + \overline{T}^F_{\max -X} \right\} \tag{3.40}$$

where Δ [mm·d^{-1}] is the calibrated difference between the maximum and minimum values of daily T^F_{Cos-X} throughout the year. L_T [d] is the lag between the peak T^F_{Cos-X} and solar forcing. $\overline{T}^F_{\max -X}$[mm·d^{-1}] is the mean annual rate of calculated $T_{max\text{-}X}$ for flat surface (3.36). N_d [d] is the number of days in the year.

With T^F_{Cos-X} obtained from (3.47), $T^H_{\max -X}$ for each *S-A* group is obtained by scaling T^F_{Cos-X} with a maximum transpiration ratio, $f^H_{T\text{-}X}$:

$$T^H_{\max -X} = f^H_{T-X} \cdot T^F_{Cos-X} \tag{3.41a}$$

$$f^H_{T-X} = \frac{\overline{T}^H_{\max -X}}{\overline{T}^F_{Cos-X}} \tag{3.41b}$$

where $f^H_{T\text{-}X}$ [-] is the ratio of the mean daily $T^H_{\max -X}$ on a *S-A* group to the flat-terrain mean daily $T^F_{\max -X}$, both calculated in each *DOY*, for all PFTs, using the historical daily weather data (following (3.36), (3.37), (3.38), and (3.39)). The $f^H_{T\text{-}X}$ ratios are compiled into a look-up table for each PFT, as a DOY and *S-A* group matrix. No year-to-year variation in $f^H_{T\text{-}X}$ is considered.

3.1.5. Soil thickness

In the first version of CATGraSS (Zhou et al., 2013), a spatially uniform soil thickness was assumed, as the case study was located in a catchment developed on an alluvial fan deposits with no distinct bedrock formation below the root zone. Since the landscape may generally show spatial variability of soil thickness, a soil thickness spatial variation has been introduced. Soil depth has been assumed to vary linearly from high values at the basin outlet to low values in the upstream area following the simple soil depth model of Saulnier et al. (1997), whose simple model was preferred over more complex ones (e.g., Pelletier and Rasmussen, 2009) as the first approximation considering a possible absence of any detailed soil depth maps in the region to compare the model results against. In particular the authors modeled the soil thickness, h_i, as function of the elevation:

$$h_i = h_{\max} - \frac{z_i - z_{\min}}{z_{\max} - z_{\min}} \left(h_{\max} - h_{\min} \right) \tag{3.42}$$

where z_i [m] is the local elevation, z_{max} and z_{min} [m] are the maximum and minimum elevation in the analyzed basin, h_{max} and h_{min} [m] are the maximum and minimum soil thickness values obtained from field observations. The elevation, from a computational point of view, can be subdivided in classes and for each class we calculated the soil thickness using (3.42). In the water balance equation the value of Z_r is limited to the minimum of the depth of the plant root of the PFT that occupies a model element and soil depth.

3.1.6. The Cellular Automata (CA) component

Ecohydrological cellular automata (CA) model provides a way of organizing and extending our understanding of the mechanisms and processes of the vegetation dynamics to make prediction.

A CA model consists of a regular grid of cells, each in one of a finite number of states, such as *on* and *off* (in contrast to a coupled map lattice). The grid can be in any finite number of dimensions. For each cell, a set of cells called its *neighborhood* is defined relative to the specified cell. An initial state (time t=0) is selected by assigning a state for each cell. A new generation is created (advancing t by 1), according to some fixed rule (generally, a mathematical function) that determines the new state of each cell in terms of the current state of the cell and the states of the cells in its neighborhood. Typically, the rule for updating the state of cells is the same for each cell and does not change over time, and is applied to the whole grid simultaneously, though exceptions are known, such as the stochastic cellular automaton and asynchronous cellular automaton.

The first example of CA is the *Game of Life* devised by the british mathematician John Horton Conway in 1970 (Gardner, 1970). The *Game of life* is a zero-player game, meaning that its evolution is determined by its initial state, requiring no further input. One interacts with the *Game of Life* by creating an initial configuration and observing how it evolves.

The *Game of Life* is an infinite two-dimensional orthogonal grid of square cells (Figure 3.2), each of which is in one of two possible states, alive (blue cell in Figure 3.2) or dead (red cell in Figure 3.2) . Every cell interacts with its eight neighbours, which are the cells that are horizontally, vertically, or diagonally adjacent. At each time step, the following transitions occur:

- Any live cell with fewer than two live neighbors dies, as if caused by under-population.
- Any live cell with two or three live neighbors lives on to the next generation.
- Any live cell with more than three live neighbors dies, as if by overcrowding.
- Any dead cell with exactly three live neighbors becomes a live cell, as if by reproduction.

The initial pattern constitutes the seed of the system. The first generation is created by applying the above rules simultaneously to every cell in the seed-births and deaths occur simultaneously, and the discrete moment at which this happens is sometimes called a tick (in other words, each generation is a pure function of the preceding one). The rules continue to be applied repeatedly to create further generations.

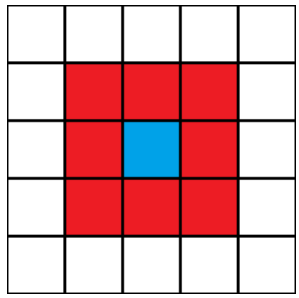

Figure 3.2. Example of CA grid.

In our context, we can find different CA developed and used into an ecohydrological model (Wolfram, 1983; 1984; 1986); these models usually sub-divide the computational domain into a grid of cells, whose size is determined by some typical biological scale (e.g., 5m grid cell resolution is common for individual-based modeling of vegetation dynamics). The necessary biological information for the modeled process is included in the form of heuristic rules, rather than physically-based equations. Evolution of state of any cell depends on its current state and state of its neighboring cells. Most of such models operate at time steps larger than one month, usually ranging between 1-5 years. Because vegetation physiological processes, such as seed production, germination, and survival are dependent on the timing of rainfall and its amount, these processes are accounted for in an implicit manner. CA models thus attempt to recreate complex ecosystem dynamics without explaining the underlying mechanisms of hydrology-vegetation interactions.

Three examples of CA application to the vegetation dynamics are represented by the works of Jeltsch et al. (1996), Van Wijk and Rodriguez-Iturbe (2002) and Perry and Enright (2002). Jeltsch et al. (1996) developed a more elaborate CA model that considered the moisture availability scenarios in the two-layer soil. Driving the ecosystem processes (e.g., growth, mortality, competition, etc.) with yearly rainfall, the dynamics of tree-grass coexistence was studied. Jeltsch et al. (1996) argued that disturbances are likely to be the key processes driving the dynamics of plant community and plant coexistence. A concurrent conclusion was made later by Van Wijk and Rodriguez-Iturbe (2002) using a more hydrologically sound model. Perry and Enright (2002) developed a gridbased model of vegetation dynamics, applied in particular to maquis. Although the

position of vegetation in topography was explicitly considered via simple categories of slope favorability, the role of soil moisture was not explicitly accounted for with the time step of one year.

In CATGraSS, a cell can be occupied by one of the following five plant states: tree, shrub, grass, tree seedling, shrub seedling; or can be bare soil. Seedlings can continue to grow to mature plants or die before they mature. No mixed occupation of PFTs in a single cell is allowed. Spatial changes occur only when a plant dies and leaves the site as bare soil. Plant establishment only occurs on empty (bare soil) cells, and follows a set of rules based on the water stress of neighboring cells with mature plants. The vegetation can die also for the fire event, and the probability of death is a function of the fuel availability and of the vulnerability to fire of each plant type.

3.1.6.1. Plant establishment

As previously mentioned the probabilistic plant establishment algorithm is run once a year at the beginning of the growing season at each bare soil cell, by postulating the probability of establishment ($P_{E\text{-}X}$) as an aggregate measure of seedling availability from the plant community neighboring the bare soil cell, conditioned on their water stress.

For grass plant type, we make the assumption that seeds are available for growth everywhere in the simulation domain. Following the earlier *CA* models of savanna ecosystems, it is assumed that shrubs provide seeds to their first ring of surrounding neighboring cells (8 cells), and trees provide seeds to their both first and second ring of neighboring cells (16 cells) following Jeltsch et al. (1996) and Van Wijk and Rodriguez-Iturbe (2002). Considered vegetation seedlings cannot send seeds until they become mature (Jeltsch et al. 1996).

We postulate that the probability of establishment ($P_{E\text{-}X}$) due to seedling dispersal can be related to the ecohydrological "well-being" of the seedling source in the neighboring plants. In order to measure plant well-being, we introduce a plant live index, φ_X, defined as the complement to one of the water stress index, WS_X [-]:

$$\varphi_X = 1 - WS_X \tag{3.43}$$

where WS_X [-] is defined following Porporato et al. (2001) as the cumulative plant water stress (3.15) normalized by the growing season length, T_{seas} [d], $WS_X = \xi / T_{seas}$. The plant live index φ_X is calculated at the end of each growing season in each model cell in the first ring (*I*), for mature shrub neighbors, and both first (*I*) and second (*II*) rings, for mature tree neighbors, of a bare soil cell (Figure 3.3). Instead of using the values for individual cells, we estimate the cumulative live index of mature shrub neighbors and tree neighbors, to use for the probability of establishment for these PFTs in the bare cell as:

$$\bar{\varphi}_{SH} = \sum \varphi_{SH}^{I} / 8 \tag{3.44}$$

$$\bar{\varphi}_T = \sum \varphi_T^I / 8 + \sum \varphi_T^{II} / 16 \tag{3.45}$$

Since we assume grass seeds are abundant everywhere in the basin (Jeltsch et al., 1996; Van Wijk and Rodriguez-Iturbe, 2002), the live index of grasses is taken as the mean live index of all grass cells within the modeled domain located with similar slope and aspect as the bare cell.

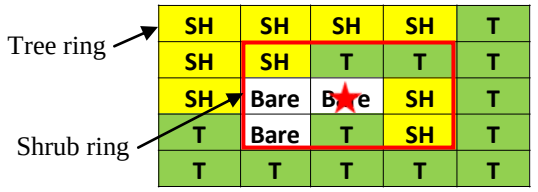

Figure 3.3. Example of CA grid for the establishment.

A second component in the calculation of establishment probability relates with the allelopathy phenomenon, which has also been recognized as a biotic mechanism regulating plant communities in arid and semiarid ecosystems (Went, 1955; Knipe et al., 1966; Fowler, 1986; Esudero et al., 2000). Allelopathy is defined as a biological process by which one plant produces one or more biochemicals that limit or support the growth, survival, and reproduction of other plants (Rizvi and Rizvi, 1992). Went (1955) first suggested that the regular spacing of creosote bushes can be attributed to the fact that its roots excrete toxic substances that kill seedlings of other plants. Knipe et al. (1966) further analyzed the germination and growth of semi-arid grassland species treated with aqueous extract from creosote bush. Their data indicate that the germination of grasses (e.g., black grama) is significantly reduced, while shrub species were not affected.

In the encroachment application (chapter 5) we assume that shrubs (creosote bushes) only influence grasses based on the work of Knipe et al. (1966). Allelopathy is incorporated in CATGraSS by using an inhibitory factor, IN_G, with a subscript G referring to the PFT affected by the allelochemicals produced by shrub, which is limited to grasses in this study. IN_G is defined for each shrub cell. Knipe et al. (1966) indicated that the inhibition effect increases with the concentration of the extract from creosote bush roots. Therefore, a cumulative inhibition effect is calculated as the product of single shrub inhibition factor on grass (IN_G) and the number of shrub cells in the 1st ring (N^I) of a bare soil cell, $IN_G \cdot N^I$.

Finally, the establishment probability for grasses ($P_{E\text{-}G}$), tree ($P_{E\text{-}T}$) and shrub ($P_{E\text{-}SH}$) on a bare soil cell are defined as:

$$P_{E-G} = \min\left(\overline{\frac{\varphi_G}{IN_G \cdot N^I}}, P_{E-G-\max}\right) \quad (3.46a)$$

$$P_{E-SH} = \min\left(\overline{\varphi_{SH}}, P_{E-SH-\max}\right) \quad (3.46b)$$

$$P_{E-T} = \min\left(\overline{\varphi_T}, P_{E-T-\max}\right) \quad (3.46c)$$

A maximal establishment probability value, $P_{E\text{-}X\text{-max}}$ [-] is introduced as an upper limit to prevent unrealistically fast plant colonization rate of a PFT in a bare soil cell during favorable conditions (Jeltsch et al., 1996; Van Wijk and Rodriguez-Iturbe 2002).

The plant establishment processes includes the following two major steps (Figure 3.4). In each iteration of the algorithm, first all bare soil cells are identified, and a "candidate" PFT (tree, shrub or grass) is randomly selected, with an equal chance (33%), to establish in each bare soil cell. Second, $P_{E\text{-}X}$ is calculated for the selected PFTs (3.46) and compared with a uniformly distributed random number ~$U(0,1)$. If the generated number is less than $P_{E\text{-}X}$, the selected PFT in the first step is placed in the cell. If the random number is higher than $P_{E\text{-}X}$ the cell is left bare for a year.

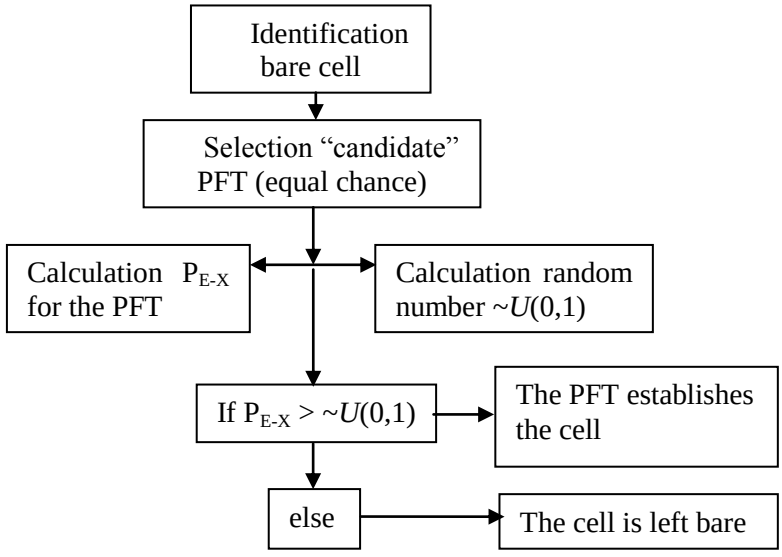

Figure 3.4. A flowchart of the plant establishment algorithm.

3.1.6.2. Plant mortality

In the model application, plant mortality removes the plant from a cell, and sets the cell status to bare soil, opening the cell for competition for establishment. Plant mortality is also treated probabilistically and operates at the end of the year. Annual probability of plant mortality is defined as the sum of three probabilities: mortality due to drought stress ($P_{Md\text{-}X}$ [-]), plant aging ($P_{Ma\text{-}X}$ [-]) and local disturbance ($P_{Mb\text{-}X}$ [-]) such as grazing.

$$P_{M\text{-}X} = \min(P_{Md\text{-}X} + P_{Ma\text{-}X} + P_{Mb\text{-}X}, 1) \quad (3.47)$$

$P_{Md\text{-}X}$ [-] is calculated as difference between WS_X and a PFT specific drought resistance threshold value, θ_X [-] (Van Wijk and Rodriguez-Iturbe, 2002).

$$P_{Md\text{-}X} = \max(WS_X\text{-}\theta, 0) \quad (3.48)$$

Mortality due to aging is caused by the accumulation of physiological changes that are associated with increased susceptibility to diseases and other environmental factors, and finally death with advancing age. Mortality due to aging is only modeled for woody plants (e.g., trees and shrubs), as a piecewise function of plant age (Jeltsch et al., 1998):

$$P_{Ma-X} = \begin{cases} 0 & t_X \le 0.5t_{\max-X} \\ \dfrac{t_X - 0.5t_{\max-X}}{0.5t_{\max-X}} & 0.5t_{\max-X} < t_X < t_{\max-X} \\ 1 & t_X \ge t_{\max-X} \end{cases} \quad (3.49)$$

where $t_{max\text{-}X}$ [yr] is the maximum age and t_X [yr] is the current age of the plant, with the subscript X denoting vegetation type. In this equation, mortality due to age is assumed to be negligible before plant reaches its half-life ($0.5t_{max\text{-}X}$). As aging continues mortality probability grows with plant age linearly.

Finally $P_{Mb\text{-}X}$ [-] is introduced as background probability that could incorporate the influence of disturbances, fires, and diseases. In the implementation of the model P_M is calculated for each plant group and compared with a random number, $U\sim(0,1)$. Plant is removed when $U\sim(0,1)<P_M$.

3.1.6.3. Fire

The probability of death caused by fire will increase with the amount of the grass fuel available (Frost and Robertson, 1987) and it is therefore modeled to increase with an increased number of cells dominated by grass (Jeltsch et al., 1996). In order to avoid too much complexity, we assumed a probability of fire, P_F, (i.e., the reverse of fire return period, T_F) to be compared to a random number, $U\sim(0,1)$, created each year. For each year, if the probability of fire is greater than the random number ($P_F > U\sim(0,1)$) then the fire starts. For each cell, the plant dies (i.e., it is burned) if its vulnerability to fire, $V_{F\text{-}X}$, is greater than a

random number, $U\sim(0,1)$, created each year ($V_{F\text{-}X} > U\sim(0,1)$). For each tree and shrub cell, this comparison between $V_{F\text{-}X}$ and $U\sim(0,1)$ is repeated as many times as the number of neighbor grass cells in the first ring, therefore more are the neighbor grass cells of a tree or shrub cell and more is the probability to be ignited and killed by fire.

3.1.7. Encroachment model codes

In order to analyze the encroachment phenomenon, the new following algorithms have been implemented in the CATGraSS model: fire (section 3.1.6.3), grazing, seed dispersal caused by animals and wind effect. In the new version of the CATGraSS the plant establishment algorithm is modified and described in paragraph 3.1.7.4.

3.1.7.1. Grazing

The grazing effect is limited to the grass. The animals eat only the herbaceous vegetation (herbivores) (Van Auken 2000; 2009). Grazing effect is obtained like Zhou et al. (2013), considering a constant background probability for disturbance factor, P_{Mb}, to be added to the annual probability of plant mortality, P_M.

3.1.7.2. Seed dispersal caused by animals

Dispersal of seeds of woody plants by domestic animals has increased the encroachment (Van Auken, 2000; 2009). Miller (1921) considered the role of livestock in causing juniper invasion to be through increased seed dispersal. He claimed that sheep consume quantities of juniper fruits which pass through the digestive tract and are scattered in the droppings. Moreover, Johnsen (1962) demonstrated that although germination percentage was not increase, juniper seeds germinated faster after passing through the digestive tract of animals. Phillips (1910), Emerson (1932) and Parker (1945) pointed out that juniper seed has always been disseminated by birds, rodents, and water.

The spread of seed probability (*SSP*) represents the probability that a seed can arrive in the bare cell from everywhere caused by the animal that carry the seed (birds, cows or other animals) or through the animal faeces.

The *CA* rules for plant establishment include the following steps:

1. in each annual iteration of the algorithm, all bare soil cells are identified and a "candidate" PFT (tree, shrub or grass) is selected to establish in each of them;
2. the plant establishment probability, P_E, is calculated for the selected PFT (3.46) and compared with an uniformly distributed random number $\sim U(0,1)$;

3. if the generated number is less than P_E, the selected PFT in the first step is placed in the cell; otherwise in a second step the *SSP* is compared with another uniformly distributed random number ~$U(0,1)$;
4. if the generated random number is less than *SSP*, the selected PFT is placed in the cell, otherwise cell is left bare for one year.

3.1.7.3. Wind Effect

In order to consider the wind direction effect on the seed dispersal, before to estimate the mean live index of PFTs (different from grass), the plant live index, φ_X, is multiplied for a pair of coefficients named *wind direction factor*, *WD*. It is an amplification coefficient (i.e., $WD > 1$). One the prevalent wind direction has been identified (for example in Figure 3.5 it is from south-east, SE, to north-west, NW), the plant live index, φ_X, of the cells in the same direction of the prevalent wind direction (blue cells) is multiplied for *WD'*, while the φ_X of the neighbor cells of the cells in the same direction of the wind (red cells) is multiplied for *WD''* (*WD''* < *WD'*). Using this factor, the probability of establishment of the PFTs along the wind direction increases, increasing the encroachment phenomenon along the same direction of the wind.

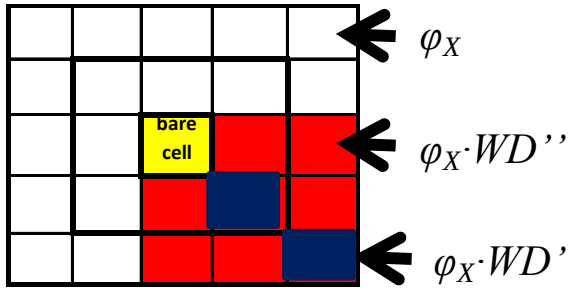

Figure 3.5. Wind speed direction modeling assuming a prevalent wind direction from SE to NW.

3.1.7.4. New plant establishment algorithm

The plant establishment algorithm described in section 3.1.6.1 and used in the case study in Chapter 4 considers the coexistence of the vegetation types and not the competition, in fact the "candidate" PFT (tree, shrub or grass) is randomly selected to establish in each bare soil cell, with an equal chance (33%). The encroachment phenomenon is tightly related to the competition between vegetation types. In order to take into account the competition a new plant establishment algorithm has been implemented.

In order to select the "candidate" PFT in the bare cell the following competition procedure has been used with two vegetation types (shrub, *SH*, and grass, *G*).

The cumulative live index for shrub is:

$$\overline{\varphi_{SH}} = \sum_{1=1}^{N^I} \varphi_{SH}^I / N^I + \sum_{1=1}^{N^{II}} \varphi_{SH}^{II} / N^{II} \tag{3.50}$$

φ_{SH}^I and φ_{SH}^{II} are the shrub plant live index in the first and second ring, respectively. N^I and N^{II} are the number of mature shrub neighbors in the first and second ring, respectively. The mean live index for grass, $\overline{\varphi_G}$, is taken as the averaged live index of all grass cells within the modeled domain located with similar slope and aspect as the bare cell (Zhou et al., 2013).

The total live index is:

$$\overline{\varphi_{TOT}} = \overline{\varphi_{SH}} + \overline{\varphi_G} \tag{3.51}$$

and then the normalized live index is:

$$\overline{\varphi_{SH}}' = \overline{\varphi_{SH}} / \overline{\varphi_{TOT}} \tag{3.52a}$$

$$\overline{\varphi_G}' = \overline{\varphi_G} / \overline{\varphi_{TOT}} \tag{3.52b}$$

A uniform random number ~$U(0,1)$ for shrub probability of selection, P_{SH}, is generated. The probability of grass selection is:

$$P_G = 1 - P_{SH} \tag{3.53}$$

If $P_{SH} < \overline{\varphi_{SH}}'$, shrub is selected, otherwise P_G is less than $\overline{\varphi_G}'$ and grass is selected. Once the plant type is selected, the establishment probability $P_{E\text{-}X}$ is calculated for the selected PFTs and compared with a uniformly distributed random number ~$U(0,1)$. If the generated number is less than $P_{E\text{-}X}$, the selected PFT in the first step is placed in the cell, otherwise the cell is left bare for a year.

Using three vegetations types (grass, *G*, shrub, *SH*, and tree, *T*) the initial selection procedure changes. The total live index is:

$$\overline{\varphi_{TOT}} = \overline{\varphi_{SH}} + \overline{\varphi_G} + \overline{\varphi_T} \tag{3.54}$$

and then the normalized live index is:

$$\overline{\varphi_{SH}}' = \overline{\varphi_{SH}} / \overline{\varphi_{TOT}} \tag{3.55a}$$

$$\overline{\varphi_G}' = \overline{\varphi_G} / \overline{\varphi_{TOT}} \tag{3.55b}$$

$$\overline{\varphi_T}' = \overline{\varphi_T} / \overline{\varphi_{TOT}} \tag{3.55c}$$

A uniform random number ~$U(0,1)$ for shrub, tree and grass probability of selection P_{SH}, P_T, P_G is generated. The normalized random number is calculated:

$$r_{TOT} = P_{SH} + P_T + P_G \tag{3.56}$$

$$r_{SH} = P_{SH}/r_{TOT},\ r_{SH} = P_{SH}/r_{TOT},\ r_{SH} = P_{SH}/r_{TOT} \tag{3.57}$$

If $r_{SH} < \overline{\varphi_{SH}}'$, shrub is selected, otherwise if r_G is less than $\overline{\varphi_G}'$ grass is selected or if r_T is less than $\overline{\varphi_T}'$ tree is selected. If two vegetation type are selected, we compare:

$$\overline{\varphi_{r\_X}}' = (\overline{\varphi_X}' - r_X) / \overline{\varphi_X}' \tag{3.58}$$

The vegetation type with the greater value obtained from (3.58) is taken (X si the PFT: G, T or SH).

3.2. AWE-GEN

Advanced WEather GENerator (AWE-GEN) (Fatichi et al., 2011), is an hourly stationary weather generator. The generator is capable of reproducing low and high-frequency characteristics of hydro-climatic variables and essential statistical properties of these variables. The weather generator employs both the physically-based and stochastic approaches and can be considered a substantial evolution of the model presented by Ivanov et al. (2007).

The main modules of the model are the following: the precipitation module based on the *Poisson-Cluster* process, the module simulating vapor pressure, the wind speed module, the shortwave radiation module, the cloudiness and air temperature components, and the atmospheric pressure module. Furthermore, a procedure to take into account non-stationary change of climate has been incorporated in the AWE-GEN framework. The procedure is based on a stochastic downscaling of GCM predictions (Fatichi et al., 2011; 2013).

The variables simulated by the weather generator at hourly scale are precipitation, cloud cover, shortwave radiation with partition into various type and spectral bands, air temperature, vapor pressure, wind speed, and atmospheric pressure.

Interested readers are referred to Fatichi et al. (2011; 2013) and to the on-line technical documentation available at http://www.umich.edu/ivanov for details concerning the model structure and parameterization. A brief description of each one of the model components is provided in the following sections.

3.2.1. Precipitation

The precipitation component of the AWE-GEN is based on the Poisson-cluster rainfall model (Onof et al., 2000) that was originally introduced by

Rodriguez-Iturbe et al. (1987) and Rodriguez-Iturbe and Eagleson (1987) and was further developed by Rodriguez-Iturbe et al. (1988), Entekhabi et al. (1989), Cowpertwait (1991) and Cowpertwait et al. (1996). Recently, this type of precipitation occurrence has been extended to the two-dimensional space; a third moment theoretical function of the rainfall process has been developed to better fit extreme values; and an overlapping model of two rectangular pulse processes has been proposed to enhance the capability in reproducing finer structure of the process (Cowpertwait, 1994; Cowpertwait, 1995; Cowpertwait, 2003; Cowpertwait, 2007; Baton et al., 2008; Leonard et al., 2008).

3.2.1.1. Neyman-Scott Rectangular Pulse process

The Neyman-Scott Rectangular Pulse (NSRP) approach (Figure 3.6) is used in AWE-GEN to generate the internal structure of precipitation process. The model is primarily based on the approach of Cowpertwait (1998), Cowpertwait et al. (2002), and Cowpertwait (2004). The storm time origin occurs as a Poisson process with the rate λ [h^{-1}]. A random number of cells C is generated for each storm according to the geometrical distribution with the mean μ_c [-]. Cell displacement from the storm origin is assumed to be exponentially distributed with the mean β^{-1} [h]. A rectangular pulse associated with each precipitation cell has an exponentially distributed life time with the mean η^{-1} [hr] and intensity X [$mm \cdot h^{-1}$]. The latter is distributed according to the Gamma distribution with the parameters α and θ. The distributions adopted for the random process within the NSRP model fully define the statistical properties of the aggregated process over an arbitrary time-scale h (Cowpertwait, 1998).

The parameter estimation procedure follows that of Cowpertwait et al. (2002), Cowpertwait (2006), Cowpertwait et al. (2007), i.e., an objective function containing statistical properties of precipitation at different aggregation times is used. After a large number of tests using available data, the following properties are used in the objective function: the coefficient of variation $C_\upsilon = \sqrt{\gamma_{h,0}} / \mu_h$; the lag-1 autocorrelation $\rho(h) = \gamma_{h,1} / \gamma_{h,0}$; the skewness $k(h) = \xi_h / \gamma_{h,0}^{3/2}$; and the probability that an arbitrary interval of length h is dry, Φ(h). The parameters μ_h, $\gamma_{h,l}$, and ξ_h represent the mean, the covariance, and the third moment of precipitation process at a given aggregation time interval h and lag-l. The utilized fitting procedure assumes that hourly rainfall time series are available as the coarsest temporal resolution. The procedure specifically uses the above statistical properties of the rainfall process at four different time scales h: 1, 6, 24, and 72 h. The simplex method (Nelder and Mead, 1965) is used as a minimization method for the imposed objective function. The method has been previously employed by Cowpertwait (1998), Cowpertwait et al. (2007) with good performance in terms of its convergence characteristics. In order to take

into account the seasonality of site climatology, the parameters are estimated on a monthly basis, i.e., six parameters for each month need to be inferred to completely define the NSRP model: λ, μ_c, β, η, α, and θ.

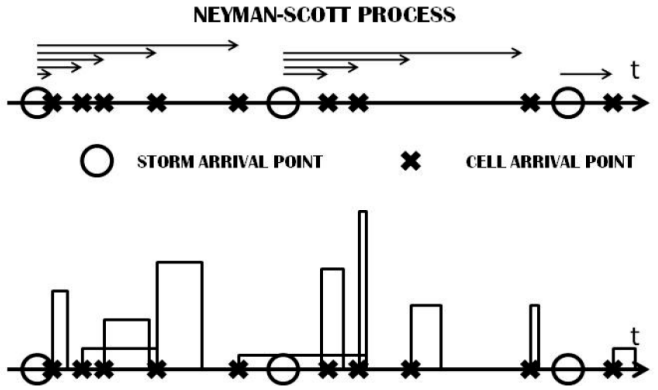

Figure 3.6. Schematic representation of Neyman-Scott model with rectangular pulses.

3.2.1.2. Low-frequency properties of precipitation process

Previous efforts of validation of the NSRP model at larger time intervals, for instance, at the yearly time scales, have indicated that the variance of the simulated process was smaller than the one inferred from observed data (Wilks and Wilby, 1999). This underestimation, sometimes referred to as ‘‘overdispersion’’ (Katz and Parlange, 1998; Wilks, 1999), is probably because of the underlying stationarity assumption of weather generators (Wilks and Wilby, 1999).

In order to introduce the capability for reproducing lowfrequency properties of the precipitation process and overcome the problem of ‘‘overdispersion’’, a numerical procedure of external selection of hourly precipitation series generated with the NSRP model on the basis of the annual precipitation series generated with the model is implemented in the AWE-GEN (Bates et al., 2008). The approach therefore aims to preserve the variance and the autocorrelation properties of the precipitation process at the annual scale, rather than at the monthly scale. It does not undermine the capability of the model to preserve the intra-annual precipitation statistics. The latter is guaranteed by the NSRP model, which is applied seasonally at the hourly scale.

Markov-type models have been commonly used to reproduce annual time series of precipitation (Srikanthan and McMahon, 1982; Srikanthan and McMahon, 2001), though they neglect the possible long term persistency of the process (Wilson and Hilferty, 1931). The inter-annual variability of precipitation at the annual time scale is simulated using an autoregressive order-one model, AR(1), with the skewness modified through the Wilson-Hilferty transformation (Wilson and Hilferty, 1931; Fiering and Jackson, 1971):

$$P_{yr}(i) = \overline{P_{yr}} + \rho_{P_{yr}}(P_{yr}(i-1) - \overline{P_{yr}}) + \eta(i)\sigma_{P_{yr}}\sqrt{1-\rho_{P_{yr}}^2} \quad (3.59)$$

where $\overline{P_{yr}}$ is the average annual precipitation, σ_{Pyr} is the standard deviation, and ρ_{Pyr} is the lag-1 autocorrelation of the process. The term $\eta(i)$ represents the random deviate of the process, which is transformed according to the Wilson and Hilferty (1931) approach. The parameters P_{yr}, σ_{Pyr}, ρ_{Pyr}, and γ_{Pyr} are determined from annual observations.

The NSRP model that captures intra-annual precipitation regime (the high-frequency properties) is coupled with the AR(1) model (Bates et al., 2008) that reproduces precipitation inter-annual variability (the low-frequency properties) in the following manner. First, the NSRP model is used to simulate precipitation series at the hourly time scale for the period of one year. The obtained total precipitation is then compared with the annual value estimated with the autoregressive model (Bates et al., 2008). If the difference between the two values is larger than a certain percentage $\breve{p}$ of the measured long-term mean annual precipitation, the simulated one-year long hourly series are rejected; a new series is generated and the above comparison is repeated. Once the difference between the two values is below the $\breve{p}$ threshold, the NSRP model simulated time series of precipitation are accepted. The entire procedure is repeated until all annual values generated with the model (Bates et al., 2008) have matching hourly series generated with the NSRP model. The rejection threshold $\breve{p}$ can be chosen according to the information about observational errors of annual precipitation.

Given the stationary nature of the NSRP model, the search of ‘‘suitable’’ years can be computationally exhaustive for locations characterized by a high variance of annual precipitation. In order to reach the convergence in a reasonable computational time, an adjustment procedure similar to that proposed by Kysely and Dubrovsky (2005) is introduced after a pre-defined number of iterations without a satisfactory match. Specifically, discarded one-year long hourly NSRP precipitation series are first selected that have the closest match to the precipitation simulated with the AR(1) model. These series are subsequently multiplied by a correction factor to match the annual precipitation simulated with the AR(1) model.

3.2.2. Air temperature component

Air temperature is simulated with a mixed physics-based, stochastic approach developed by Curtis and Eagleson (1982) and Ivanov et al. (2007). AWE-GEN utilizes the same approach with further improvements.

The generation of air temperature $T(t)$ [°C] is simulated as the sum of a stochastic component $dT(t)$ and a deterministic component $\widetilde{T}(t): T(t) = \widetilde{T}(t) + dT(t)$. The deterministic component of air temperature

$d\widetilde{T}(t)/dt$ is assumed to be directly related to underlying physical processes such as the divergence of radiative and eddy heat fluxes. The deterministic time-gradient of temperature $d\widetilde{T}(t)/dt$ is a function of the air temperature itself, and of the incoming long-wave radiation (which exhibits a dependence on cloud cover). It is further related to the site geographic location and Sun's hourly position, used as a proxy for shortwave irradiance (Curtis and Eagleson, 1982).

The stochastic temperature component $dT(t) = T(t) - \widetilde{T}(t)$, is estimated through an autoregressive model. The random deviate exhibits a significant dependence on the hour of the day, with differences noticeable in various statistics of *dT(t)* for morning, midday, afternoon, evening, and night. Consequently, the average of the stochastic component $\overline{dT_h}$ and its standard deviation $\sigma_{dT,h}$ are estimated differently for each hour of the day.

The coefficients and the parameters used to estimate the deterministic and stochastic components are evaluated at the monthly scale. Ivanov et al. (2007) describe the procedure for estimation of the coefficients. The parameters $\overline{dT_h}$; $\sigma_{dT,h}$, and ρ_{dT} (the lag-1 autocorrelation of the stochastic component) are estimated from *dT(t)* using conventional techniques.

3.2.3. Cloud cover component

The cloud cover simulated in AWE-GEN is based on the framework first developed by Curtis and Eagleson (1982) and Ivanov et al. (2007). Cloud cover *N(t)* is the fraction of the celestial dome occupied by clouds. In the model of Ivanov et al. (2007), *N(t)* [-] is considered to be a random variable that has different dynamics during intra-storm and inter-storm periods. During an intra-storm period, the value of cloudiness is assumed to be equal to 1. During an inter-storm period, the existence of the ''fair weather'' region, R_0, is assumed. The region is sufficiently distant from storms, thus the cloud cover can be assumed stationary and fully characterized by the first two statistical moments: the mean $E\{N(t)\}_{t\in R_0} = M_0$ and the variance $VAR\{N(t)\}_{t\in R_0} = \sigma_M^2$ of the process. T_R [h] is the length of the post-storm period after which the cloud cover process can be considered stationary. The second assumption is that the transition of the cloud process between the boundary of a storm and the fair weather period is described through an exponential function *J(t)*. The latter is characterized by two coefficients controlling the transition rates ξ and γ [h^{-1}], and by the average cloud cover of the first hour after a storm and of the last hour of an inter-storm, J_1.

The parameters required for the model are M_0, σ_m^2, $\rho_m(1)$ (lag-1 autocorrelation value for the fair weather region), $\gamma = \varsigma, J_1$, and 11 parameters of the Beta distribution that are used to generate random variables.

3.2.4. Shortwave incoming radiation component

In weather generators, shortwave radiation, R_{sw} [W·m^{-2}], is commonly estimated through regression with other variables (Richardson, 1981; Parlange and Katz, 2000). The likely reason for such an approach is a lack of a conventional methodology for direct estimation of cloudiness and optical properties of the atmosphere. Once the site geographic location and cloudiness are known, several deterministic models with different degrees of complexity can be used to calculate the incoming shortwave radiation for clear-sky and overcast conditions (Gueymard, 1989; Freidenreich and Ramaswamy, 1999; Muneer et al., 2000; Gueymard, 2001; Gueymard, 2008; Ineichen, 2006). These methods use empirical coefficients to determine the atmospheric transmittances and the scattering fractions for direct and diffuse shortwave radiation. The incoming shortwave radiation is estimated with the model *REST2* developed by Gueymard (Gueymard, 2008) for clear sky conditions.

The parameterizations of Stephens (1978) and Slingo (1989) are used to compute transmittances for arbitrary cloudy conditions. The simulation of cloud cover, directly affects the computed shortwave fluxes. The partition of the incoming energy into different spectral bands could be useful for several purposes, such as ecological or eco-hydrological simulations that require the photosynthetically active radiation, PAR, as input. The discussed weather generator considers two bands *K*: the ultraviolet/ visible UV/VIS band, with wavelengths within the interval [0.29-0.70 μm], and the near infrared NIR band, with wavelengths within the interval [0.70-4.0 μm] (Gueymard, 2008). In the first band, ozone, nitrogen dioxide absorption, and Rayleigh scattering are concentrated; the absorption by water vapor and uniformly mixed gases is concentrated in the second band.

The output of the radiation component of the weather generator contains the direct beam, $R_{Bn,\Lambda}$ [W·m^{-2}], and diffuse, $R_{D,\Lambda}$ [W·m^{-2}], radiation fluxes for the ultraviolet/visible UV/VIS [0.29-0.70 μm] and the near infrared NIR [0.70-4.0 μm] bands. PAR is also explicitly computed in AWE-GEN: conversion factors are applied to the first radiation band UV/VIS to compute PAR (Gueymard, 2008). The same factors are applied for both clear and cloudy sky conditions.

The spatial distribution of solar radiation over a terrain is a function of surface geometry: site slope β_T [rad] and aspect ζ_T [rad] alter the daily distribution of incoming energy at the ground. Furthermore, the reflection and shadow effects of the surrounding terrain can strongly influence site radiation fluxes (Dubayah and Loechel, 1997; Rigon and Bertoldi, 2006; Ivanov et al., 2007; Fatichi, 2010).

3.2.5. Vapor pressure component

The vapor pressure is not commonly simulated by weather generators (Semenow et al., 1998). Some weather generators, for instance, include relative

humidity (Sharpley and Williams, 1990; Sheppard et al., 2002) or dew point temperature (Parlange and Katz, 2000; Ivanov et al., 2007). While the conversion of relative humidity or dew point temperature into vapor pressure is mathematically straightforward, it involves non-linearity. Because of that, an accurate simulation of dew point temperature or relative humidity does not necessary imply a good fit for vapor pressure. Dew point or relative humidity outputs of weather generators should therefore be checked before asserting their suitability for applications that require vapor pressure.

This model approaches the simulation of air humidity via the simulation of vapor pressure deficit, Δe [Pa], i.e., the difference between the vapor pressure at saturation e_{sat} [Pa], and the ambient vapor pressure e_a [Pa]. Following Bovard et al. (2005), who pointed out a correlation between vapor pressure deficit Δe and PAR during daylight time, the correlation of vapor pressure deficit with shortwave radiation and temperature has been analyzed. The possibility of such a linkage stems from the observation that specific humidity and vapor pressure, e_a, remain almost constant throughout the day, especially in dry climates. Therefore, the variations of Δe should be well explained by the diurnal cycle of air temperature. The assumption is primarily valid when the atmosphere is stable and the exchange between air masses with different characteristics is limited.

In order to simulate vapor pressure, a framework similar to the one used to model air temperature is used: Δe is simulated as the sum of the deterministic component, Δe, and the stochastic component, $d\Delta e$: $\Delta e(t) = \Delta e(t) + d\Delta e(t)$. The term Δe is related to air temperature through a cubic function, which is essentially an approximation of the commonly used exponential relation between T_a and e_{sat} (Dingman, 1994). From observational data, a significant correlation was also detected with global shortwave radiation, R_{sw} [W m^{-2}], at the lag of one and two hours:

$$\Delta e(t) = a_0 + a_1 T_a^3(t) + a_2 R_{sw}(t-1) + a_3 R_{sw}(t-2) \tag{3.60}$$

where a_i (i = 0,1,. . . ,3) are the regression coefficients. The deterministic component Δe usually shows a minor hourly variance when compared to $\Delta e(t)$. The residuals $d\Delta e(t)$ are modeled with the AR(1) approach. Finally, the ambient vapor pressure e_a is calculated as the difference between e_{sa} and $\Delta e(t)$.

The parameters a_i (i = 0,1,. . . ,3) are estimated on a monthly basis using conventional regression techniques, for example, the least squares approach. The parameters of the stochastic component: the average vapor pressure deficit deviations, $\overline{d\Delta e}$, the standard deviation, $\sigma_{d\Delta e}$, and the lag-1 autocorrelation of the process, $\rho_{d\Delta e}$, are evaluated using the time series of $d\Delta e(t)$ after removing the deterministic component from the observed series of $\Delta e(t)$.

3.2.6. Wind speed and atmospheric pressure components

Several studies highlight that cross-correlation between wind speed and other variables is typically very weak (Curtis and Eagleson, 1982; Ivanov et al., 2007) and thus wind speed is usually modeled as an independent variable.

Fatichi et al. (2011) observed that wind speed exhibits a marked daily cycle in some locations and therefore the assumption of independence may need to be questioned. From a physical point of view, the wind speed daily cycle is related to turbulent fluxes occurring in the surface boundary layer that are enhanced during the daytime by the dissipation of sensible heat. The wind daily cycle is thus more pronounced in dry climates. Starting from this concept, a relation between the global solar radiation and wind speed has been investigated. As found, the maximum correlation between the two cycles is usually shifted by several hours, possibly due to the difference in thermal properties of the ground surface and air.

The method adopted to simulate the wind speed, W_s [m·s^{-1}], is based on representing the process as a sum of the deterministic component W_s and the stochastic component dW_s. This is a new approach as compared to methods developed previously. The deterministic component relates wind speed to the incident global shortwave radiation. The correlation is shifted by several hours (up to 3 h) and the shift strongly depends on the site location, as inferred from our tests:

$$W_s(t) = c_0 + c_1 R_{sw}(t) + c_2 R_{sw}(t-1) + c_3 R_{sw}(t-2) + c_4 R_{sw}(t-3) \tag{3.61}$$

where c_i (i = 0,1, . . . ,4) are the regression coefficients. The stochastic component $dW_s(t) = W_s(t) - W_s(t)$ is modeled with the autoregressive AR(1) model including the Wilson–Hilferty transformation (Wilson and Hilferty, 1931; Fiering and Jackson, 1971). This transformation is necessary to represent the generally positive skewness exhibited by hourly wind speed data (Takle and Broen, 1978; Deaves and Lines, 1997).

The parameters c_i are estimated with conventional regression techniques. The parameters of the stochastic component: the average wind speed deviation, $\overline{dW_s}$, the standard deviation, σ_{dWd}, the lag-1 autocorrelation, ρ_{dWs}, and the skewness of the process, γ_{dWs}, are evaluated using time series of $dW_s(t)$ after removing the deterministic component from the observed series of $W_s(t)$. Wind speed generally does not present marked differences throughout the year, therefore the parameters are derived and assumed to be valid for all months.

The atmospheric pressure P_{atm} [mbar] is generally neglected in weather generators, given its low impact on hydrological and ecological processes. However, it is used in many non-linear equations describing physical phenomena, such as evaporation. This observation implies that using a constant value of atmospheric pressure is theoretically incorrect. In the AWE-GEN, a simple autoregressive model AR(1) is employed with parameters valid for the

entire year. It has been observed that AR(1) model is suitable for reproducing hourly atmospheric pressure dynamics in several different climates.

3.3. General Circulation Models (GCMs) and downscaling procedure

3.3.1. General Circulation Models

The General Circulation Models (GCMs) are complex numerical tools able to simulate globally the climate system of the Earth. GCMs include five components: atmosphere, oceans, land surface, sea-ice and the biological and biogeochemistry cycles. There is a disagreement with regards to the reliability of GCMs skill to reproduce much more than global averages of climatic variables within the Earth system. Since GCMs realizations are the foundation of any climate change prediction study, questioning the reliability of GCMs means questioning the overall possibility of making inferences about future climate and consequently whatever scientific discussion about climate change predictions must be looked as biased from the beginning. But, while climate models provide information that may not be exact in the absolute sense, yet due to their physically-based nature and their global scale of application, they still provide a robust prediction of a tendency, or at least they identify the emergence of a climate change signal. Nonetheless, the possibility that model artifacts can undermine the credibility of the study could not be totally dismissed but currently few alternatives, if any, are available. Moreover, GCMs have two important drawbacks: 1) the realizations spatial resolution is too coarse to be used directly in local studies (each model has a different pixel dimension that range from 130 to 550 km), 2) GCMs realizations are only available at the daily or larger aggregation intervals.

In this thesis, we used the GCMs (atmospheric component) employed in the *Intergovernmental Panel on Climate Change - Fourth Assessment Report* (*IPCC 4AR*) (IPCC, 2007). Specifically, in the *Chapter X* (Meehl et al., 2007) of the Working Group I, climate models are assessed and their projections discussed. The GCMs used in the *IPCC 4AR* are 25 in total including different versions of same climate models (Table 3.1). An overview of availability of GCM outputs used in the *4AR* of the IPCC, can be found on the website of the Program for *Climate Model Diagnosis and Intercomparison* (*PCMDI*) (http://www-pcmdi.llnl.gov/ipcc/about_ipcc.php).

Since projections of climate change depend upon future human activity, climate models are run assuming different scenarios. There are 40 different scenarios, each making different assumptions for future greenhouse gas pollution, land-use and other driving forces. Assumptions about future technological development and future economy are also made for each scenario.

Most include an increase in the consumption of fossil fuels and *Gross Domestic Product* (GDP) all around the world.

The emission scenarios of IPCC (2007) are organized into four families, which contain scenarios that are similar to each other in some respects. IPCC assessment report projections for the future are made in the context of a specific scenario classes. The considered classes are:

- The *A1* storyline and scenario family describes a future world of very rapid economic growth, global population that peaks in mid-century and declines thereafter, and the rapid introduction of new and more efficient technologies. Major underlying themes are convergence among regions, capacity building, and increased cultural and social interactions, with a substantial reduction in regional differences in per capita income. The *A1* scenario family develops into three groups that describe alternative directions of technological change in the energy system. The three A1 groups are distinguished by their technological emphasis: fossil intensive (*A1FI*), non-fossil energy sources (*A1T*), or a balance across all sources (*A1B*).
- The *A2* storyline and scenario family describes a heterogeneous world. The underlying theme is self-reliance and preservation of local identities. Fertility patterns across regions converge very slowly, which results in continuously increasing global population. Economic development is primarily regionally oriented and per capita economic growth and technological changes are more fragmented and slower than in other storylines.
- The *B1* storyline and scenario family describes a convergent world with the same global population that peaks in midcentury and declines thereafter, as in the *A1* storyline, but with rapid changes in economic structures toward a service and information economy, with reductions in material intensity, and the introduction of clean and resource-efficient technologies. The emphasis is on global solutions to economic, social, and environmental sustainability, including improved equity.
- The *B2* storyline and scenario family describes a world in which the emphasis is on local solutions to economic, social, and environmental sustainability. It is a world with continuously increasing global population at a rate lower than *A2*, intermediate levels of economic development, and less rapid and more diverse technological change than in the *B1* and *A1* storylines.

The emission scenarios considered in the *4AR* are only a subset of the forty defined on the *Special Report on Emissions Scenarios* (SRES) and they include the scenario *A2*, *A1B* and *B1* (Meehl et al., 2007). They represent "low" (*B1*), "medium" (*A1B*) and "high" (*A2*) forecasts, with respect to the prescribed concentrations of greenhouse gases and the resulting radiative forcing (Meehl et al., 2007). The *B1* is the closer to the low end of the range of CO_2 emission

projections, (CO_2 concentration of about 550 ppm by 2100), the *A2* is closer to the high end of the range (CO_2 concentration of about 850 ppm by 2100) and the *A1B* is almost in the middle of the range (CO_2 concentration of about 700 ppm by 2100).

Table 3.1. GCMs of the *IPCC 4AR*.

Group	Country	Model
Beijing Climate Center	China	BCC-CM1
Bjerknes Centre for Climate Research	Norway	BCCR-BCM2.0
National Center for Atmospheric Research	USA	CCSM3
Canadian Centre for Climate Modelling and Analysis	Canada	CGCM3.1 (T47)
Canadian Centre for Climate Modelling and Analysis	Canada	CGCM3.1 (T63)
Centre National de Recherches Meteorologiques	France	CNRM-CM3
CSIRO Atmospheric Research	Australia	CSIRO-Mk3.0
CSIRO Atmospheric Research	Australia	CSIRO-Mk3.5
Max Planck Institute for Meteorology	Germany	ECHAM5/MPI-OM
Meteorological Institute of the University of Bonn, Meteorological Research Institute of KMA, and Model and Data group	Germany-Korea	ECHO-G
LASG / Institute of Atmospheric Physics	China	FGOALS-g1.0
US Dept. of Commerce- NOAA - Geophysical Fluid Dynamics Laboratory	USA	GFDL-CM2.0
US Dept. of Commerce- NOAA - Geophysical Fluid Dynamics Laboratory	USA	GFDL-CM2.1
NASA Goddard Institute for Space Studies	USA	GISS-AOM
NASA Goddard Institute for Space Studies	USA	GISS-EH
NASA Goddard Institute for Space Studies	USA	GISS-ER
Instituto Nazionale di Geofisica e Vulcanologia	Italy	INGV-SXG
Institute for Numerical Mathematics	Russia	INM-CM3.0
Institut Pierre Simon Laplace	France	IPSL-CM4
Center for Climate System Research, National Institute for Environmental Studies, and Frontier Research Center for Global Change (JAMSTEC)	Japan	MIROC3.2 (hires)
JAMSTEC	Japan	MIROC3.2 (medres)
Meteorological Research Institute	Japan	MRI-CGCM2.3.2
National Center for Atmospheric Research	USA	PCM
Hadley Centre for Climate Prediction and Research Met Office	UK	UKMO-HadCM3
Hadley Centre for Climate Prediction and Research Met Office	UK	UKMO-HadGEM1

The realizations here used correspond to the A1B emission scenario (IPCC, 2007), in which rapid economic growth, global population that peaks in the mid-century and an efficient use of technologies to reduce emissions are forecasted.

The A1B scenario is an intermediate case between the B1 and A2 and it should supposedly provide an intermediate effect of climate change, that approximately corresponds to the median curve of global temperature increase among all considered scenarios in the *4AR* (IPCC, 2007). Moreover realizations for this scenario are available from almost all *GCMs* used in the *4AR* of the IPCC. Among the 25 General Circulation models that are used in *IPCC 4AR* (Meehl et al., 2007), only a subset of models is usually used for the stochastic downscaling procedure. GCM realizations are obtained from the dataset compiled in the *World Climate Research Programme*'s (*WCRP*'s), *Coupled Model Intercomparison Project* phase 3 (*CMIP3*) (Meehl et al., 2007). The selection of models can be typically based on two criteria: data availability (availability of daily precipitation time series as the principal constraint) and a relative independence among the models (the mutual independence between model realizations is one of the requirements for using the multi-model ensemble approach). Climate models developed by different groups around the world can be assumed to be independent to a certain extent, they can share components or have similar theoretical arguments for their parameterizations (Tebaldi and Knutti, 2007). In order to preserve the relative independence among models, when multiple or updated versions of the same climate model are available, only a single version of such a GCM is used. The same discrimination is usually realized, for different models provided by the same originating group or for models that borrow many components by other ones.

3.3.2. Stochastic downscaling procedure

In the presented approach of stochastic downscaling only precipitation and air temperature are directly considered. But, once precipitation and temperature factors of change are introduced into AWE-GEN, the other variables might be affected as a result of linkages considered by the weather generator.

Various GCMs multi-model ensemble and probabilistic approaches to the analysis of climate projections have been recently proposed, like the Bayesian methods (Tebaldi and Knutti, 2007). The underlying idea is that a performance forecast can be improved by weight-averaging results from multiple models. The multi-model ensemble approach realized in this thesis follows that of Tebaldi et al. (2005) where model combines information coming from several GCMs and observations to determine the probability density functions (*PDF*s) of future changes of different certain climatic variables at the regional scale (Fatichi et al., 2011). In the Bayesian framework, all uncertain quantities are modeled as random variables, with a prior probability distributions. The method assigns weights to climate models, according to two criteria: the *bias* and the *convergence*. The *bias* measures the difference between GCM simulations and the best approximation of the "truth" value of a certain variable for the control scenario, μ. The *convergence* criterion measures the distance between the GCM simulations and the "true" value of a certain variable of the future realizations, v.

Note that for each statistic v represents the expected value of the PDF for the future.

The multi-model ensemble approach of inference is used for all statistical properties of climatic variables that are part of stochastic downscaling, i.e., the mean, the variance, the frequency of non precipitation, and the skewness of fine-scale precipitation (for each month), the coefficient of variation and the skewness of annual precipitation, and the mean monthly air temperature (Fatichi et al., 2011; 2013). Long-term statistics of present climate X_0 are calculated from observed values based on point measurements, which therefore represent a much smaller area as compared to a typical GCM grid cell size. The difference between observations and climate model realizations is accounted for by the bias criterion used to weight different GCM realizations in getting proper downscaling information. This implies that the shape of the probability density functions of the factors of change is somewhat dependent on the observed climate.

In Figure 3.7 a flowchart of the used stochastic downscaling methodology is presented (Fatichi et al., 2011). More specifically, a set of factors of change is computed to reflect changes in the mean monthly air temperature and several statistics of precipitation (e.g., mean, variance, skewness, frequency of no-precipitation) at different aggregation periods (24, 48, 72, 96 h), as a result of comparing historical and projected climate model outputs. The factors of change derived from the ensemble of GCM realizations are subsequently applied to a set of statistics of the observed climate in order to obtain statistics representative of the future climate. Using these statistical properties, an updated set of AWE-GEN parameters can be estimated. Each of these AWE-GEN parameters set is calculated assuming stationary climate for any considered period. Finally, the re-parameterized weather generator is used to simulate hourly time series of hydro-climatic variables that are considered to be representative of the predicted climate. For a more detailed description of the procedure, interested readers are referred to Fatichi et al. (2011) and Fatichi et al. (2013).

It is important to remind that the uncertainties captured by the proposed procedure and quantified by the *PDF*s are only a part of the total uncertainty of climate change predictions. The *PDF*s of factors of change are the result of climate model differences in predicting future; these *PDF*s do not contain any information about other sources of uncertainty (e.g., model structure, different CO_2 emission scenarios, etc.). However, the variation of climate change predictions between different models is probably the most meaningful measure of uncertainty that is presently available, although, this measure is more likely to underestimate than overestimate the total uncertainty.

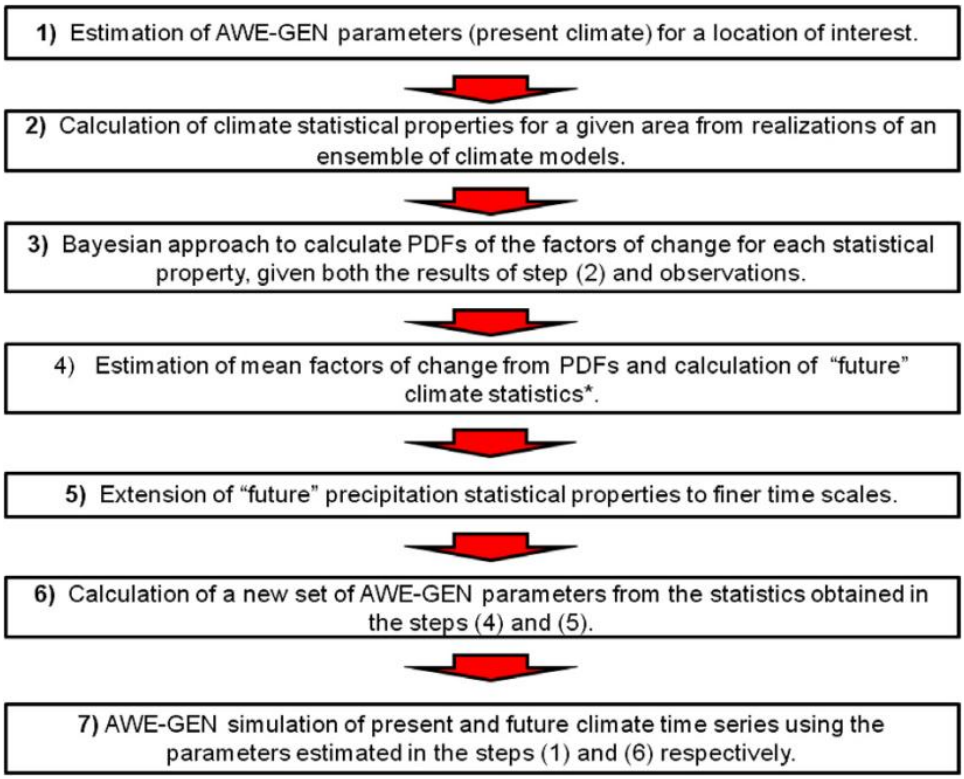

Figure 3.7. A flowchart of the used stochastic downscaling methodology (Fatichi et al., 2011).

3.3.2.1. Factor of change

The factors of change for precipitation (*Pr*) are calculated for each statistic used by the weather generator: the mean $E_{Pr}(h)$, the variance $VAR_{Pr}(h)$, and the skewness $SKE_{Pr}(h)$, where h is the aggregation interval (24, 48, 72, 96 h). The product factor is also applied to the frequency of non-precipitation Φ_{Pr}, following a logit-like transformation: $f(\Phi_{Pr}) = \Phi_{Pr} / (1-\Phi_{Pr})$, as proposed by Kilsby et al. (2007). This transformation allows the linearization of Φ_{Pr} across a wide range of values, reducing inaccuracies in the computation of the product factor. The downscaling of the lag-1 autocorrelation $\rho_{Pr}(h)$ is neglected due to difficulties in finding a proper relationship for the factor of change of this statistic, and due to the weaker sensitivity of weather generator realizations to $\rho_{Pr}(h)$ variations.

The stochastic downscaling uses a Bayesian approach to weight climate model realizations (Tebaldi et al., 2004, 2005; Fatichi et al., 2011) which allows one to derive the probability distributions of factors of change (*FOC*) representative of the ensemble of GCM projections. *FOC* from single climate

models can be calculated as ratios (*FOCR*) or "delta" (*FOCD*), i.e., differences of climate statistics for historical and future periods. The general equation, which using *FOCR* provides the statistical properties *S* at the time aggregation *h* in the future scenario reads:

$$S(h)^{FUT} = \frac{S(h)^{GCM,FUT}}{S(h)^{GCM,CTS}} \cdot S(h)^{OBS} = FOCR \cdot S(h)^{OBS} \tag{3.62}$$

where the superscript *FUT* denotes the future scenario, *OBS* denotes observations, and *CTS* denotes the control scenario, which is the GCMs run representing the current climate. The notation GCM implies *General Circulation Models* outputs. The sought statistical property for future climate, S^{FUT}, is then calculated from the observed statistics of present climate, S^{OBS}, and the product factor of change computed using statistics derived from the control and the future scenarios, $S^{GCM,FUT}/S^{GCM,CTS}$ (obtained from GCM outputs).

In order to include the effects of intra-annual seasonality, the factors of change are calculated on a monthly basis.

Low-frequency effects are important in the detection of climate change impacts, especially when long-term variations in the occurrence and duration of drought or wet periods are likely to be encountered. AWE-GEN is capable of taking into account such features of precipitation regime. Therefore, statistical properties describing the inter-annual variability of precipitation are also downscaled using the derived factors of change from GCM realizations. Specifically, once downscaling is carried out for the mean precipitation at finer aggregation intervals and realized independently for each month, the total annual precipitation $\overline{P}_{yr}^{FUT}$ is obtained as the sum of modified monthly precipitation. The application of independent factors of change on a monthly basis, however, has a not immediately apparent implication: $\overline{P}_{yr}^{FUT}$ may not be exactly equal to $\overline{P}_{yr}^{OBS} \cdot \left[\overline{P}_{yr}^{GCM,FUT} / \overline{P}_{yr}^{GCM,CTS} \right]$, where the expression in the brackets is the factor of change estimated at the annual scale. This outcome is due to the fact that applying the factors of change at the monthly scale is different from applying a factor of change at the annual scale. However, in order to account for seasonality and to be coherent with the factors of change calculated at the aggregation periods smaller than 1 year, $\overline{P}_{yr}^{FUT}$ is used as the mean annual precipitation of the *FUT* scenario. Furthermore, the coefficient of variation and the skewness of annual precipitation must be downscaled using (3.62): the downscaling of the former is necessary in order to introduce changes in the variance of precipitation annual time series. It is necessary to compute a factor of change for the coefficient of variation and not directly for the variance because of the issue of the mean annual precipitation. The autocorrelation property of annual precipitation process is not directly downscaled. The value inferred from observations is kept for simulations of future climate.

With regard to the mean monthly temperature, its statistical properties *S*, is obtained by the following equation, which uses the "delta" factor of change *FODC*:

$$S(h)^{FUT} = S(h)^{OBS} + \left[S(h)^{GCM,FUT} - S(h)^{GCM,CTS}\right] = S(h) + FOCD \tag{3.63}$$

Correcting only the mean does not permit to infer changes of higher order statistics and thus to capture the changes in the daily cycle or frequency of extremes. This limitation is related to the procedure adopted for the estimation of the parameters of the air temperature model. Nevertheless, in many cases intra-daily variation of changes can be considered to have a fairly minor effect on the hydrological dynamics. The correction $FOCD = T_{mon}^{GCM,FUT} - T_{mon}^{GCM,CTS}$ is applied on a monthly basis to air temperature simulated by the weather generator at the hourly scale.

3.3.2.2. Extension of precipitation statistics to finer time scales

Since, several statistics of precipitation in the weather generator are required at the aggregation intervals of 1 h and 6 h, a methodology to infer the factors of change for these periods is necessary. The extension to shorter time scales is straightforward for the mean, i.e., given the linearity of the mean operation, the factors of change are equal at each aggregation period. The extension to shorter time scales is not such a trivial task for the other statistical properties, such as the variance $VAR_{Pr}(h)$, the frequency of non-precipitation $\Phi_{Pr}(h)$, and the skewness $SKE_{Pr}(h)$.

In order to infer VAR_{Pr} at 1 h and 6 h aggregation intervals, a theoretical derivation of Marani (Marani, 2003; Marani, 2005) is applied. The parameters for the $VAR_{Pr}(h)$ of Marani (2003) are estimated from the variance $VAR_{\Pr}^{FUT}(h)$ at different aggregation periods equal to or larger than 24 hours (24, 48, 72, and 96 h). The values of $VAR_{\Pr}^{FUT}(h)$ are thus calculated once $VAR_{\Pr}^{OBS}(h)$ and the factors of change for precipitation variance are known at the aggregation period $h \geq 24h$.

The extension to 1 h and 6 h aggregation periods of the frequency of non-precipitation $\Phi_{\Pr}(h)$ is realized through an exponential function $\Phi_{\Pr}(h) = e^{-\bar{\gamma}h}$, that links $\Phi_{Pr}(\geq 24)$ to $\Phi_{Pr}(<24)$, considering that $\Phi_{Pr}(0) = 1$, by definition. The exponential decay of the frequency of non-precipitation $\Phi_{Pr}(h)$ has been observed in practically all of the analyzed time series. The parameter γ is estimated from $\Phi_{Pr}(24)^{FUT}$ and $\Phi_{Pr}(48)^{FUT}$. The values of $\Phi_{Pr}(h)^{FUT}$ are calculated from the observed $\Phi_{Pr}(h)^{OBS}$ using the factors of change *FC* for logit transformed frequency of non-precipitation. Since the fitting of $\Phi_{Pr}(h < 24)$ is carried out with two values of $\Phi_{Pr}(\geq 24)$, γ is determined using the least squares method.

Skewness $SKE_{Pr}(h)$ is not extended to 1 h and 6 h aggregation periods since no suitable relationship was found for this statistic. The factors of change for 1 h and 6 h skewness are taken equal to one. This implies that the values obtained from observations are employed for generating future scenarios.

Part II

Study Cases

Chapter 4

Modeling the role of climate change on small-scale vegetation patterns in a mediterranean basin using a Cellular Automata model. Case study

4.1. Study catchment

4.1.1. Basin framework

The CATGraSS is applied to the Zafferia catchment located in the Peloritani Mountains area, near the town of Messina, located in the island of Sicily, Italy. In Figure 4.1 the *Google Earth* aerial photo of the basin and its location are shown (38°9' N, 15°29' E). In Sicily climate shows a clear gradient moving from the coast to the mountains and is characterized by a marked seasonal variability, with wet temperate winters, and hot dry summers. The mean annual temperature ranges from 10.5° C (in high elevation areas) to 19.5° C (in the coast) (Viola et al., 2013) while the mean annual precipitation ranges from 380 mm (in the coast) to 1345 mm in the mountains (Di Piazza et al., 2011). The study region has experienced trends in temperature and precipitation in the 20th century. For the period from 1924 to 2006 regional temperature has risen 0.2° C·decade^{-1} (2° C·century^{-1}), a rate higher than the global average (Viola et al., 2013). In the last 25 years the regional data shows a warming twice the long-term trend (0.4° C·decade^{-1} increase). Temperature trend is uniformly distributed over the seasons while rainfall has dropped as much as 2.5 mm·yr^{-1} especially in the winter season (Cannarozzo et al., 2006).

The Peloritani Mountain area is characterized by elevation ranging from 100 to 1374 m above mean sea level (*a.s.l.*). The mean annual temperature ranges from 11° C to 16° C (Viola et al., 2013) and the *MAP* range from 750 to 1500 mm (Di Piazza et al., 2011). The morphology of this region is very complex and is characterized by a long series of peaks, ridges and ravines. The vegetation of this area includes mainly *Quercus ilex* and *Quercus rotundifolia* forests (1405 ha), *Platanus orientalis* and *Liquidambar orientalis* woods (*Platanion orientalis*) (242.5 ha), *Fagus, Taxus and Ilex* forests (195.5 ha), *Quercus suber* forests (114 ha), *Tilio-Acerion* forests (43.5 ha) and *Arborescent matorral* with *Laurus nobilis* (3.5 ha) and *Pinus* (Picone et al., 2008).

4.1.2. Basin description

The Zafferia catchment covers 1.3 km^2 of area, spans an elevation range from 160 m to 866 m a.s.l., with an average slope of 61.1% (31.42°) and a main channel length of 2.42 km (Figures 4.1, 4.2). The mean annual precipitation (MAP) is ~815 mm, with a dry season from May to September (165 mm) and a wet season from October to April (650 mm). The mean annual temperature is 15.4° C. Climatic data have been recorded from SIAS (*Servizio Informativo Agrometeorologico Siciliano*) from January 2002 to December 2011 in the Acquaurtedditi San Pier Niceto (ME) weather station (38°9' N, 15°21' E, 180 m a.s.l.).

Sandy loam texture is the main soil type in the basin (obtained from field data, Figure 4.3). The landscape show spatial variability of soil thickness. Typically soils get shallower as slopes get steeper toward high-elevation areas of the basin.

The vegetation pattern has an evident aspect dependence, with opposing hillslope aspects hosting different and contrasting plant types (Figures 4.1, 4.2). In the *N*-facing slopes, oak (*Quercus Ilex*) is the dominant plant and co-exist with grass C_3. In the *S*-facing slopes, Indian fig Opuntia (*Opuntia ficus-indica)* and grass C_3 are the dominating plant types and co-exist with sparse oaks. Oak and Indian fig Opuntia are evergreen species, while grass C_3 have a strong seasonal phenology. It is important to point out that Indian fig Opuntia is a succulent specie with CAM photosynthesis. The detailed description of the vegetation types is in section 4.1.3.

A 2 m LIDAR DEM, resampled at 10 m (Figure 4.4a), has been used for the modeling study. The slope (Figure 4.4b) and aspect (Figure 4.4c) maps at the same resolution are obtained from the DEM using Spatial Analysis techniques within *ESRI ArcGIS*. The estimated slope within the basin ranges from 0.5° to 58.54° (from 0.87% to 163.5%) (Figure 4.4b). In order to illustrate the role of topography on incoming solar radiation, the mean daily clear-sky radiation over the catchment has been assessed (Figure 4.5) showing as, annually, *S*-facing slope receive as much as twice the solar radiation received by *N*-facing slopes.

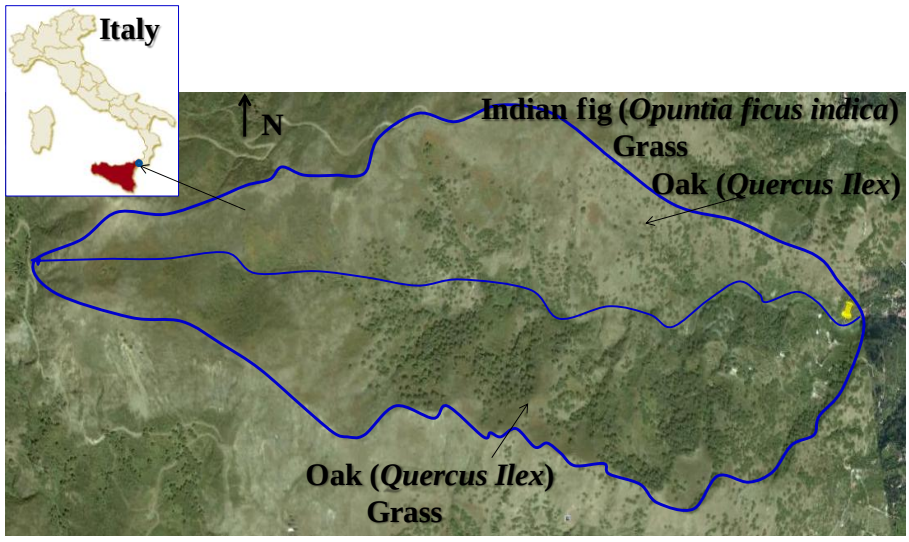

Figure 4.1. Google Earth view of the study catchment and its location in Sicily.

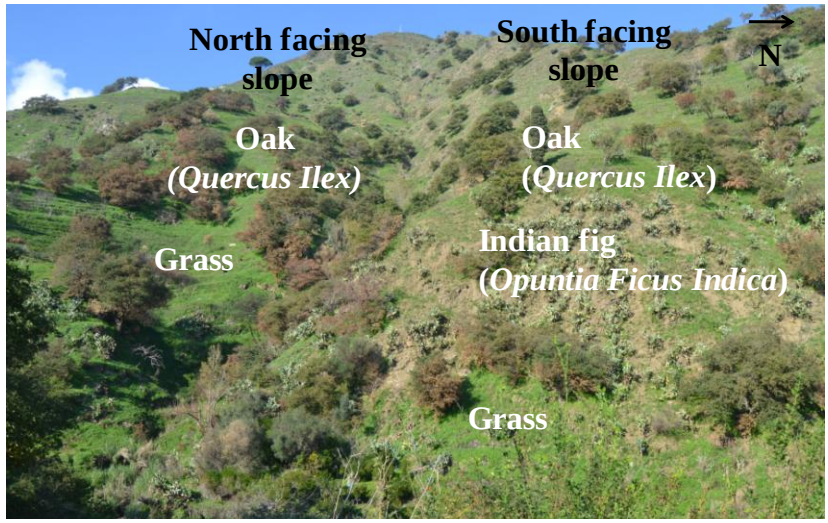

Figure 4.2. Distribution of plant functional types in relation to topography in the basin.

Figure 4.3. Sampled soil in the field site.

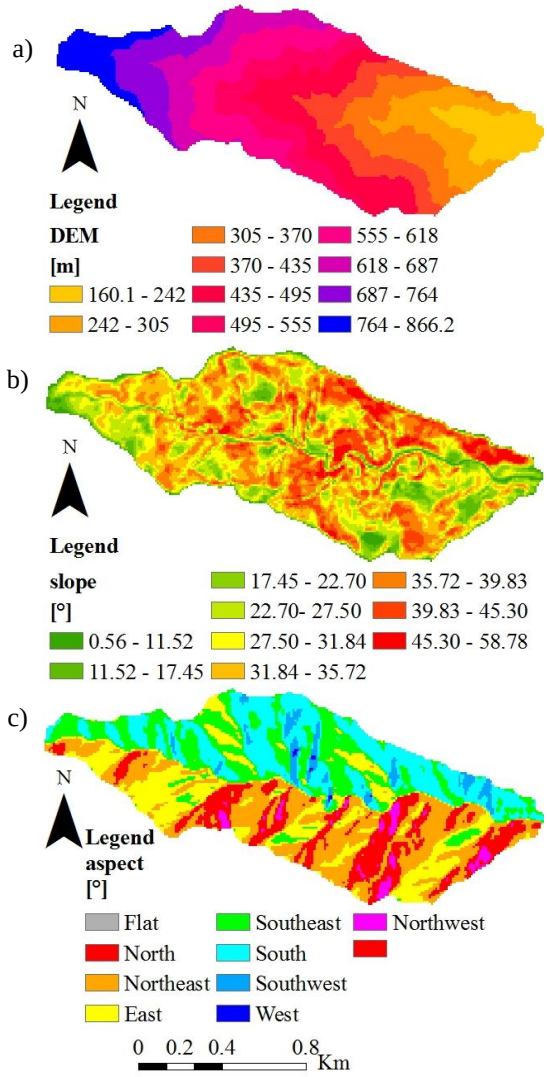

Figure 4.4. Topography of the basin: (a) DEM, (b) slope, (c) aspect.

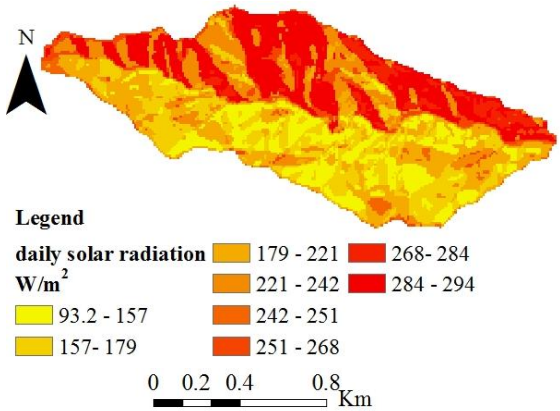

Figure 4.5. Simulated mean daily incoming clear-sky shortwave radiation over the study area over a year.

4.1.3. Vegetations types

In the following section a brief description of the vegetation types is done with a greater focus on the Indian fig Opuntia since it is a typical species of the sicilian environments, and it is rarely modeled in the hydrological and ecohydrological models.

4.1.3.1. Grass and oak

In the basin there are different grass C_3 species with a strong seasonal phenology. Figure 4.6 shows some grass species of the study area.

Quercus ilex (Figure 4.7), the holm oak or holly oak is a large evergreen oak native to the mediterranean region. It is a medium-sized tree (from 4 to 10 meters tall) with finely square-fissured blackish bark and leathery evergreen leaves. The old leaves fall 1-2 years after new leaves emerge. The leaves are dark green above and pale whitish-grey with dense short hairs below. The flowers are catkins, produced in the spring; the fruit is an acorn, which matures in about six months.

Figure 4.6. Grass in the study basin.

Figure 4.7. *Quercus Ilex* in the study basin.

4.1.3.2. Indian fig Opuntia

As previously mentioned *Opuntia ficus-indica* (Figure 4.8) is a drought-tolerant cactus, widely cultivated in arid and semi-arid regions worldwide and exhibits *Crassulacean Acid Metabolism* (*CAM*), with nocturnal stomata opening and CO_2 uptake occurring, typically, from dusk to dawn, when, through phosphoenolpyruvate (*PEP*) carboxylation, malate is formed and stored in vacuoles (Nobel, 1988). Its native area is Mexico but it is cultivated for fruit production in many other countries as in the mediterranean basin, temperate zones of South America, Asia and Oceania, also for vegetable, juices, cattle fodder and forage production (Nobel, 2002). In Sicily, where the prickly pear (i.e., the fruit of the *Opuntia ficus-indica*) is known as *ficudinnia* (the Italian

name being "fico d'India", meaning "indian fig"), the *Opuntia ficus-indica* grows wild and cultivated to heights of 1-5 meters. In these regions, production system has to cope with strong seasonal variations in environmental conditions, which considerably reduce land productivity. Specifically, rainfall distribution is a critical limiting factor as well as extensive and variable dry seasons, high soil-water deficit conditions and dry atmosphere. Thus, the selection of *CAM* cultivars for cropping in stress-prone areas could be a major component in agricultural strategies to improve land management. In particular, *CAM* species thrive in areas with restricted water supply (200 or 300 mm of annual rainfall) or where long periods of drought occur, because of the ecological advantage related to the daily timing of stomata opening. In fact, *CAM* plants open the stomata when lower temperature and water pressure deficit account for a lower evaporative demand (during the night), leading to a twofold to sixfold lower transpiration rate compared with the same degree of stomata opening during the day (Nobel, 1988; San-José et al., 2007). Ultimately, the water use efficiency of the species reaches values of about 250-300 $kg_{H2O} \cdot kg_{DM}^{-1}$ (De Kock, 1980; Le Houèrou, 2000).

Nobel (1988), showed that three weeks of drought conditions are required for halving net CO_2 uptake over 24-h periods, and after 50 days of drought net CO_2 uptake of cladodes (stem-like flattened organs) is around zero (Acevedo et al., 1983). Moreover, three months of drought decreased nocturnal acid accumulation by 73%, essentially abolished transpiration and reduced cladode water content by 45% (Goldstein et al., 1991). However, fruit quality, i.e., fruit size, is reduced by water deficit long before the tree shows any symptom of water stress (Gugliuzza et al., 2002).

Indeed, in the northern hemisphere, most of the fruit development period coincides with long and dry summers, with a water deficit period that may last for 3-4 months (June-September). Nerd et al. (1989) report that in the Negev desert, with an annual rainfall lower than 300 mm, winter irrigation is needed to reach a regular plant fertility at springtime. An annual volume of 60-100 mm of irrigation water, during the fruit development period, coupled with fruit thinning is required to get export-size fruit with regular flesh percent (55-65%), and to increase marketable yield composition (Barbera, 1984; Gugliuzza et al., 2002).

Though irrigation is used and successful in all cultivated area for Indian fig fruit production (Barbera, 1984; Gugliuzza et al., 2002; Nerd et al. 1989; Van der Merwe et al., 1997), its timing and applied volumes are still defined on an empiric basis. Evapotranspiration of cacti have been evaluated using the soil water balance technique (Han and Felker, 1997), and, measurements of mass (CO_2, H_2O) and energy exchanges (solar radiation) for a *CAM* community was reported by Nobel and Bobich (2002) at the *Biosphere 2 Center in Arizona*.

Measurements of gas exchange in Indian fig began in the early 1980s, when Nobel and Hartsock (1983) measured CO_2 uptake on single cladodes, using portable infrared gas-analyzers (*IRGA*), with cuvettes adapted to fit cladode

morphology. At optimal temperature and intercepted radiation, instantaneous values of net CO_2 uptake of 1-year-old cladodes may reach 18 μmol $m^{-2} \cdot s^{-1}$, with a total daily CO_2 uptake of 680 mmol$\cdot m^{-2}$ (Nobel and Bobich, 2002).

The response of Indian fig to water stress, in term of gas exchange rate, has been investigated on individual, terminal or basal, cladodes while there are no data integrating whole-tree behaviour where cladode interactions are more complex (Andrade et al., 2009; Nobel and Bobich, 2002). Cladode succulence acts as a buffer to maintain turgescence in the photosynthetic tissue (chlorenchyma), making it possible for the cladode to continue photosynthesizing during dry periods. Small changes in daily net CO_2 uptake of single cladodes occur during the first 7 days of drought (Nobel and Bobich, 2002); after 17 days of drought, cladode net CO_2 uptake over a 24-h period halved, and became almost zero at 50 days (Acevedo et al. 1983; Nobel and Hartsock, 1984). Drought combined with an increase of daughter cladodes shortened the period of positive net CO_2 uptake and reduced the maximum rates of CO_2 uptake of 1-year-old basal cladodes, while total daily CO_2 uptake does not change if trees are watered (Pimienta-Barrios et al., 2005).

Figure 4.8. *Opuntia ficus-indica* in the study basin.

4.2. Model simulations

4.2.1. Model set up

As mentioned in chapter 3, in order to improve computational efficiency, basin morphology has been classified into topographically similar slope and aspect (*S-A*) groups. In each of the *S-A* group, the coupled water balance (i.e., soil moisture dynamic, evapotranspiration, water stress) and biomass production equations ((3.1) to (3.16)) are used for each PFTs separately (Zhou et al., 2013).

In particular, the influence of topography is explicitly introduced in the calculation of the net radiation using the daily incoming shortwave radiation for each *S-A* group. This classification is performed considering a 14 degree increment for local slopes (5-61°) (5 slope classes) and a 45 degree increment for aspect (0-360°) (8 aspect classes) leading to 40 different combinations (*S-A* groups) in order to get and analyze the effect of the *S-A* group on the vegetation distribution.

In this study case since the landscape shows spatial variability of soil thickness with deep soils in the valleys in low lying areas and shallower soils as slopes get steeper toward high-elevation areas, a soil thickness spatial variation has been introduced. As elevation grows and the soil thickness decreases together with water storage capacity, oak gives way to grass because the former is not able to settle and grow in soil with small thickness. On the basis of observation, soil depth has been assumed to vary linearly from high values at the basin outlet to low values in the upstream area following the simple soil depth model of Saulnier et al. (1997). In particular the authors modeled the soil thickness, h_i, as function of the elevation using (3.42), z_{max} and z_{min} (the maximum and minimum elevation in the analyzed basin) are 866.2 and 160 m, respectively, h_{max} and h_{min} (the maximum and minimum soil thickness values obtained from field observations) are 3 and 0.01 m, respectively.

The elevation, from a computational point of view, was subdivided in 5 classes (elevation increment for each class equal to about 140 meters) and for each class we calculated the soil thickness using (3.42) (Table 4.1). The 5 elevation classes are integrated into the 40 *S-A* groups creating a total of 200 slope-aspect-soil thickness classes. It is important to underline how the choice of elevation classes does not influence the solar radiation assessment but only the soil moisture. In the water balance equation the value of Z_r is limited to the minimum of the depth of the plant root of the PFT that occupies a model element and soil depth.

PFTs and the cellular automaton processes for spatial plant dynamics are represented using a 5m grid cell resolution, which is approximately the size of a mature oak tree. The same resolution was also used in CATGraSS in central New Mexico for simulating juniper pine trees (Zhou et al., 2013) and in a Texas savanna (Van Wijk and Rodriguez-Iturbe, 2002). This finer scale is achieved by dividing each model DEM grid cell into 4 equal-size cells. Identical grid resolution is used for the other two plant types.

Table 4.1. Soil thickness for each elevation class.

class	min *z* [m]	max *z* [m]	mean *z* [m]	thickness [m]
1	160	302	231	3.0
2	302	444	373	2.2
3	444	586	515	1.5
4	586	728	657	0.7
5	728	866.2	797.1	0.01

4.2.2. Model experiments

Two different sets of simulations are performed using CATGraSS: (1) *Base run*: CATGraSS is calibrated for the chosen study site to reproduce the observed ecotone of *N* and *S* facing slopes using a stationary climate, and the model is also run without soil depth limitation to illustrate the role of soil depth on modeled vegetation organization in the catchment. PFTs are initialized randomly in space, with identical random initial cover fractions (33.3% grass, 33.3% Indian fig, 33.3% tree). The simulation is run for 5,000 years, forced by statistically generated storms using a Poisson process and a cosine function to reproduce the annual cycle of the potential evapotranspiration. (2) *Future run*: CATGraSS is run for 100 years with 50 realizations of future climate scenarios generated with a stochastic downscaling procedure using GCMs output and the AWE-GEN model. The initial vegetation spatial distribution is that provided by the *base run* after simulating 5,000 years. This simulation is designed and carried out with the aim to understand how the vegetation spatial pattern could change in the future as result of the expected climatic changes.

4.2.2.1. Weather forcings

In this section before to describe the *Base run* (section 4.2.2.1.2) and *Future run* (section 4.2.2.1.3) weather forcings, a briefly example of the results obtained with the AWE-GEN in the current climate and stationary conditions using the SIAS weather station data is shown (section 4.2.2.1.1).

4.2.2.1.1. AWE-GEN results in stationary conditions and current climate

In order to test the AWE-GEN model the current climate has been simulated in stationary conditions using the data of the SIAS weather station in San Pier Niceto (ME) with 10 years of hourly weather data (2002-2011). A description of the results is shown below.

In Figure 4.9 the observed and simulated monthly precipitation are shown. In Figures 4.10 and 4.11 a comparison between observed and simulated monthly statistics of precipitation (mean, variance, lag-1 autocorrelation, skewness, frequency of non precipitation, transition probability wet-wet), for the aggregation period of 1 hour and 24 hours, respectively, are shown.

In Figure 4.12 the annual precipitation simulated with the NSRP model after the external selection based on the AR(1) precipitation series has been carried out. In Figure 4.13 the observed and simulated values of extreme precipitation at 1-hour and 24-hour aggregation periods and extremes of dry and wet spell durations are shown.

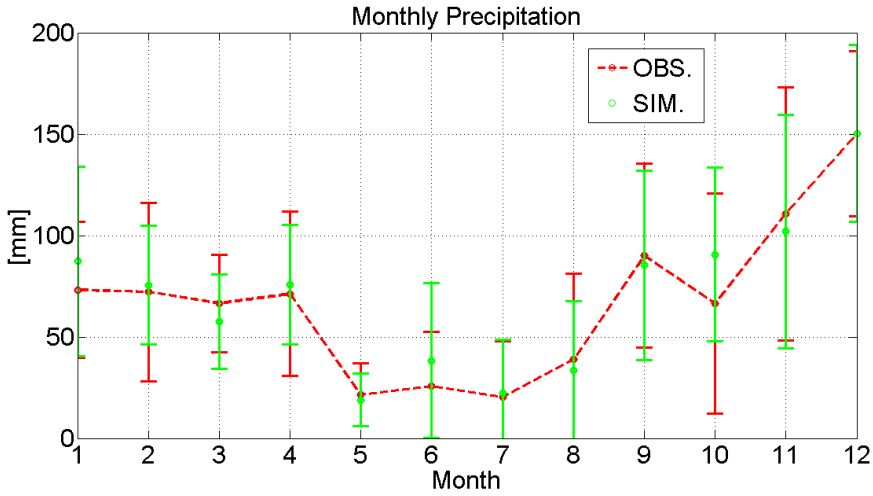

Figure 4.9. A comparison between observed (red) and simulated (green) monthly precipitation. The vertical bars denote the standard deviations of the monthly values.

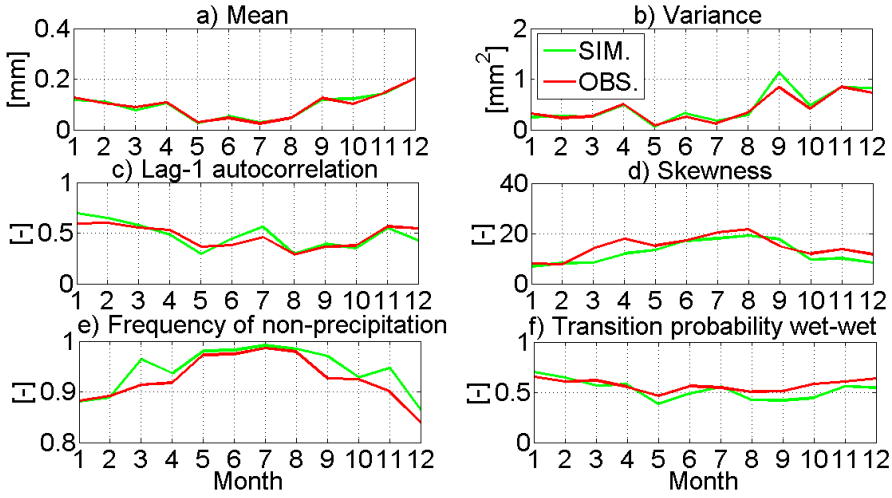

Figure 4.10. A comparison between observed (red) and simulated (green) monthly statistics of precipitation (mean, variance, lag-1 autocorrelation, skewness, frequency of non precipitation, transition probability wet-wet), for the aggregation period of 1 hour.

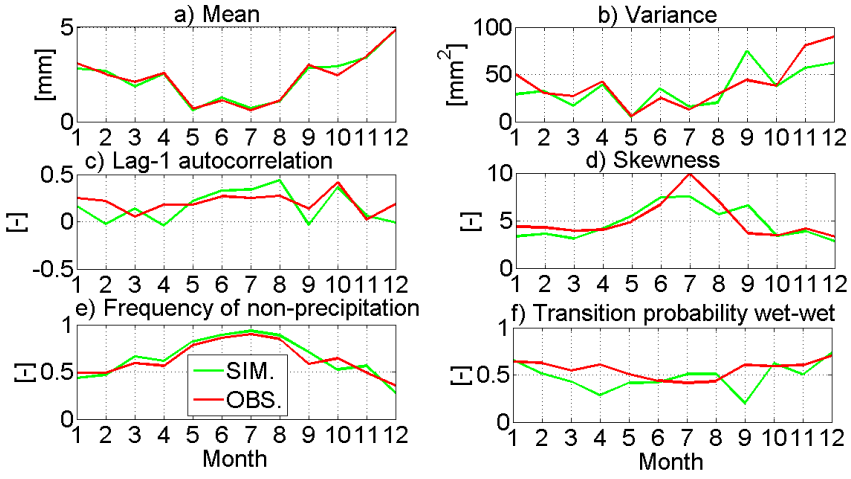

Figure 4.11. A comparison between observed (red) and simulated (green) monthly statistics of precipitation (mean, variance, lag-1 autocorrelation, skewness, frequency of non precipitation, transition probability wet-wet), for the aggregation period of 24 hours.

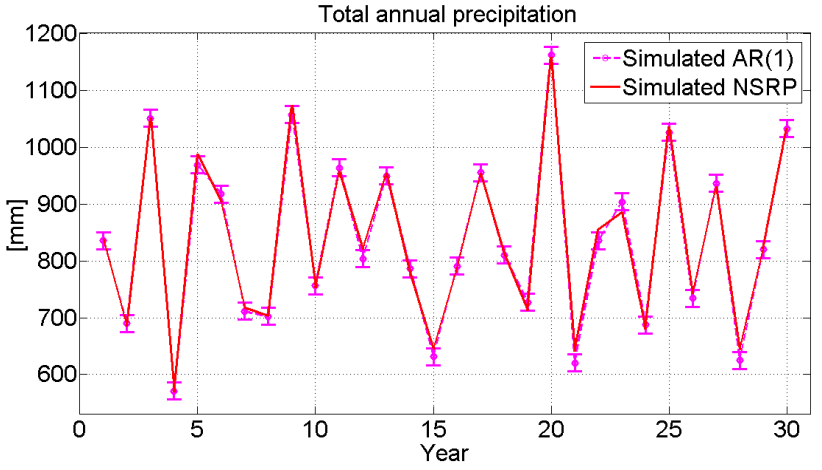

Figure 4.12. The annual precipitation simulated with the NSRP model (red line) after the external selection based on the AR(1) precipitation series (magenta dots) has been carried out. The vertical bars denote the p of the long-term average annual precipitation.

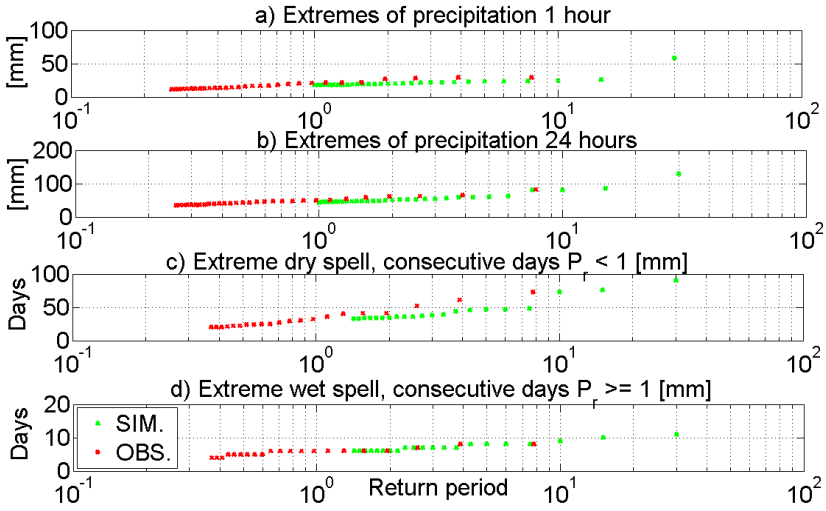

Figure 4.13. A comparison between the observed (red crosses) and simulated values of extreme precipitation (green crosses) at (a) 1-hour and (b) 24-hour aggregation periods; (c) extremes of dry and (d) wet spell durations. Dry/wet spell duration is the number of consecutive days with precipitation depth lower/larger than 1 mm.

In Figure 4.14 the observed and simulated average air temperature for every month, aggregation period of 1 h (a) and 24 h (b) are shown. In Figure 4.15 a comparison between the observed and simulated daily maximum (a) and minimum (b) air temperature for every month is shown.

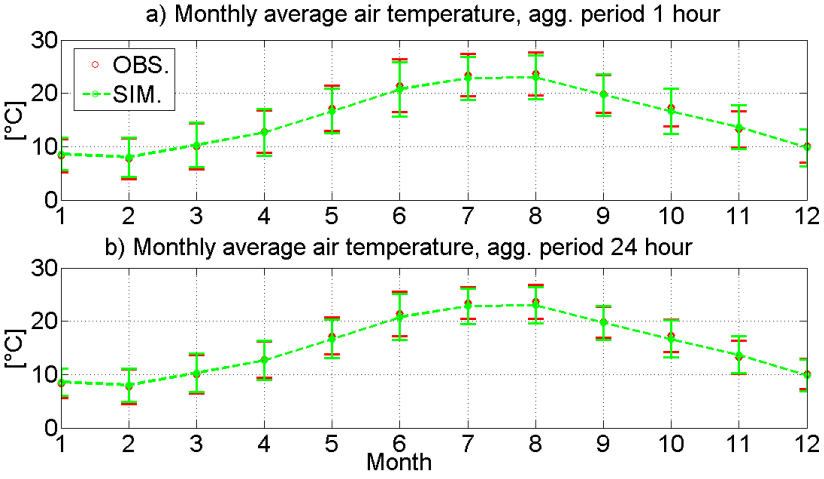

Figure 4.14. A comparison between the observed (red) and simulated (green) average air temperature for every month, aggregation period of 1 h (a) and 24 h (b). The vertical bars denote the standard deviations.

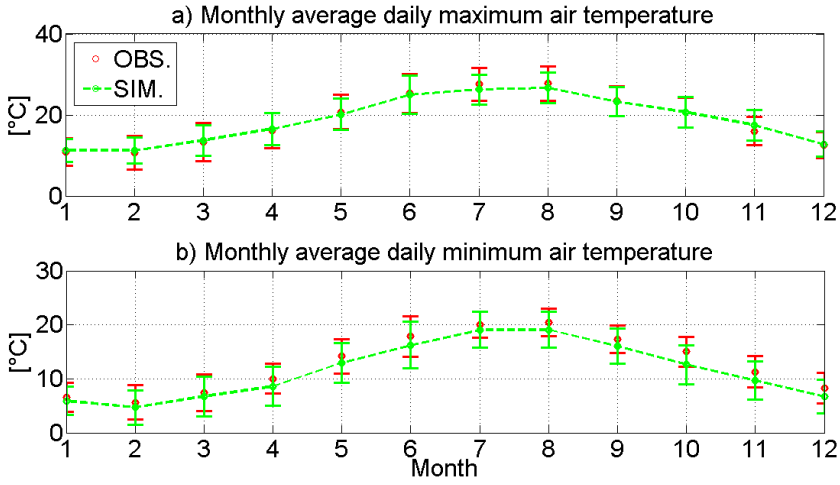

Figure 4.15. A comparison between the observed (red) and simulated (green) daily maximum (a) and minimum (b) air temperature for every month. The vertical bars denote the standard deviations.

In Figure 4.16 a comparison between the observed and simulated air temperature distribution (a) and average daily cycle (b) is shown. The triangles are the standard deviations for every day hour.

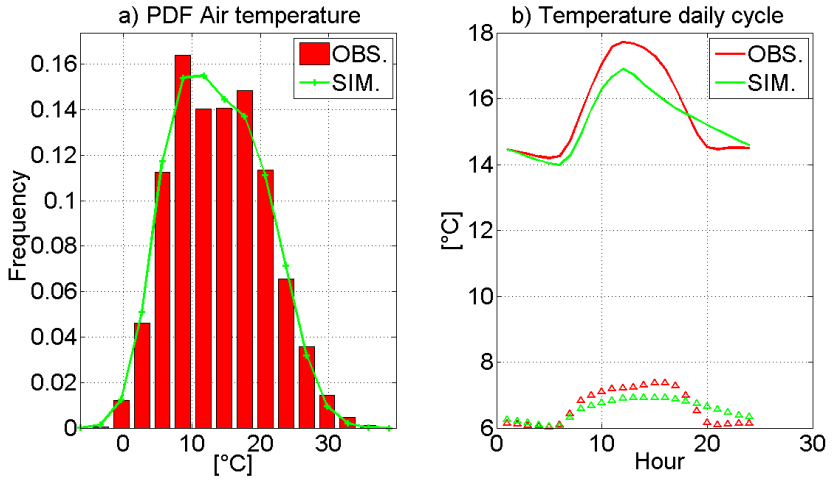

Figure 4.16. A comparison between the observed (red) and simulated (green) air temperature distribution (a) and average daily cycle (b). The triangles are the standard deviations for every day hour.

In Figure 4.17 a comparison between the observed and simulated mean monthly shortwave radiation is shown: a) Global radiation, b) Direct radiation radiation, c) Diffuse radiation. The vertical bars denote the standard deviations of the monthly values.

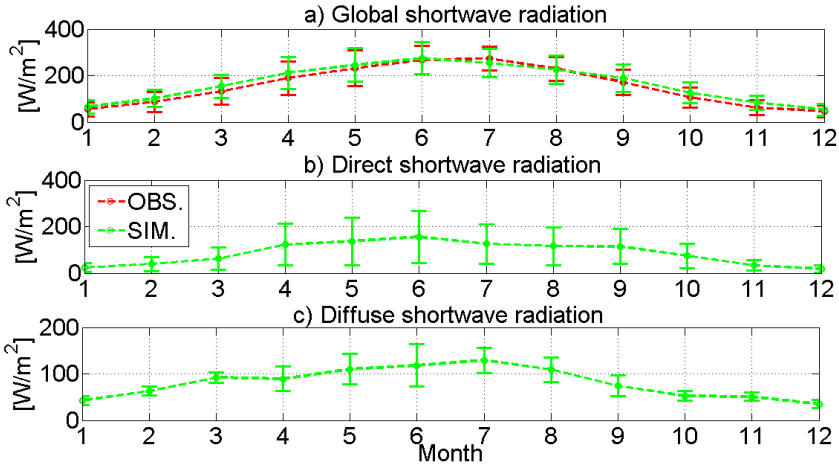

Figure 4.17. A comparison between the observed (red) and simulated (green) mean monthly shortwave radiation. (a) global radiation, (b) direct beam radiation, (c) diffuse radiation. The vertical bars denote the standard deviations of the monthly values.

In Figure 4.18 a comparison between the observed and simulated mean monthly vapor pressure for 1 h (a) and 24 h (b) aggregation time periods is shown.

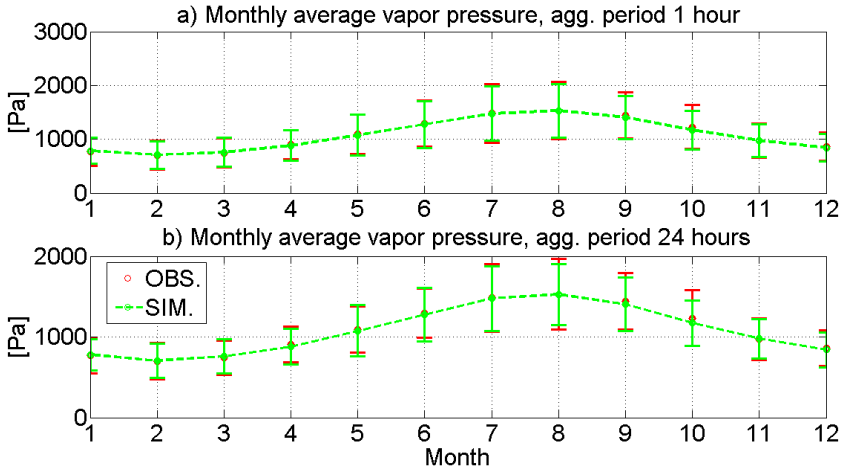

Figure 4.18. A comparison between the observed (red) and simulated (green) mean monthly vapor pressure for 1 h (a) and 24 h (b) aggregation time periods. The vertical bars denote the standard deviations of the monthly values.

In Figure 4.19 a comparison between the observed and simulated wind speed probability density function (a) and daily cycle of wind speed (b) are shown.

In Figure 4.20 a comparison between the observed and simulated monthly average relative humidity for 1 h (a) and 24 h (b) aggregation time periods is shown.

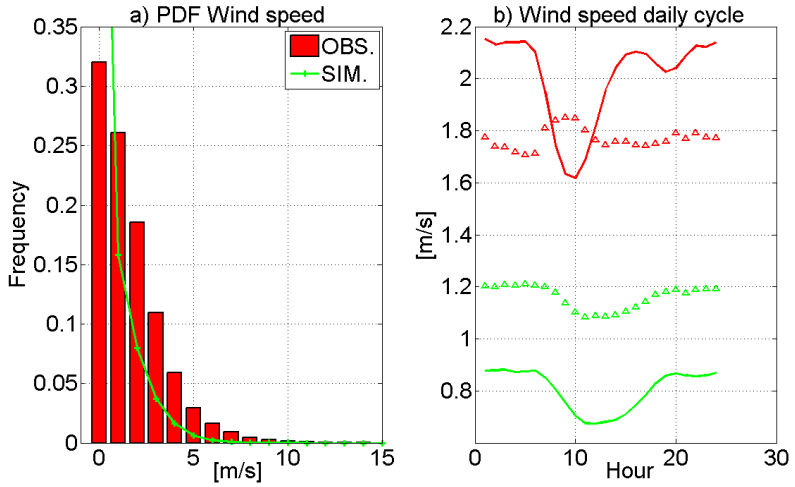

Figure 4.19. A comparison between the observed (red) and simulated (green) wind speed probability density function (a) and daily cycle of wind speed (b).

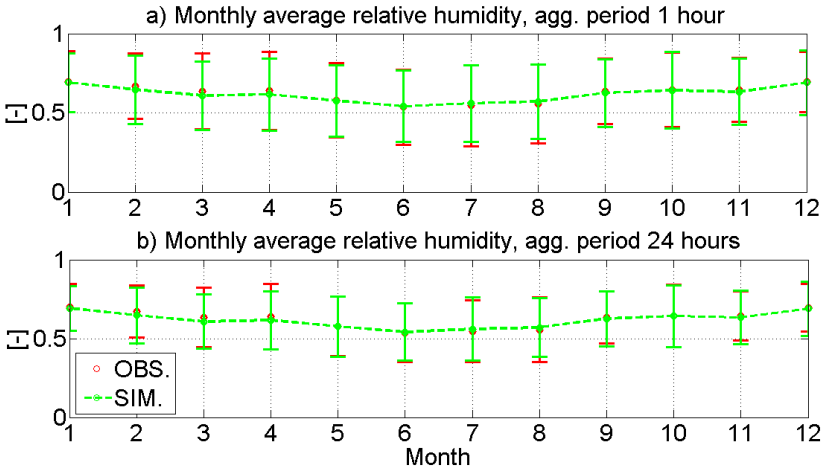

Figure 4.20. A comparison between the observed (red) and simulated (green) monthly average relative humidity for 1 h (a) and 24 h (b) aggregation time periods. The vertical bars denote the standard deviations.

In Figure 4.21 a comparison between the observed and simulated relative humidity daily cycle (a) and vapor pressure probability density function (b) are shown. The triangles in (a) represent the daily cycle of relative humidity standard deviation.

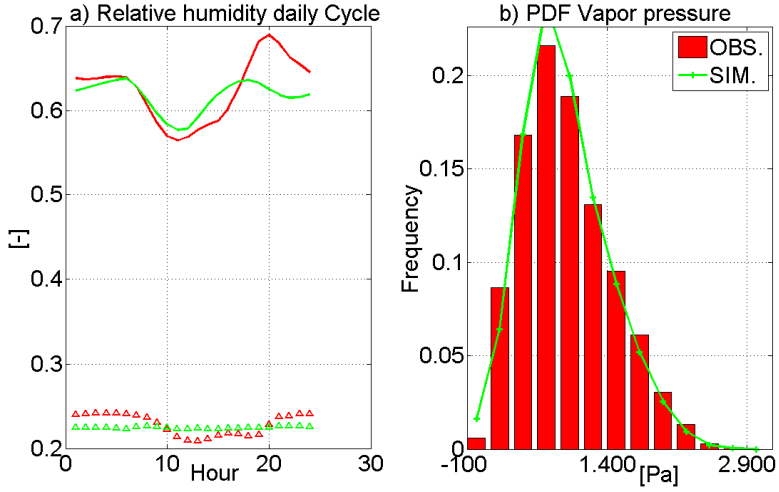

Figure 4.21. A comparison between the observed (red) and simulated (green) relative humidity daily cycle (a) and vapor pressure probability density function (b). The triangles in (a) represent the daily cycle of relative humidity standard deviation.

4.2.2.1.2. *Base run* weather forcings

In the *base run* storm generation, we used the *Poisson Rectangular Pulses (PRP)* model, with a one-parameter exponential distribution for time between storms (T_b) and storm durations (T_r); and a Gamma distribution for rainfall depth h conditioned on T_r (e.g., Ivanov et al., 2007). The storm intensity p, is calculated as: $p = h/T_r$. We have considered two rainfall seasons: *wet*, from the 1st of January to the 30th of April and from the 1st of October to the 31st of December, and *dry*, from the 1st of May to the 30th of September, following Pumo et al. (2008) findings, with seasonal precipitations denoted by P_w and P_d. The weather station data, from 2002 to 2011, are used to estimate the above mentioned rainfall model parameters (h, T_b, T_r) and to calculate the annual cycle of $T_{max\text{-}X}$ using the Penman-Monteith equation. Table 4.2, which compares all the rainfall statistics obtained from the San Pier Niceto Acquaurtedditi station weather data with those obtained with the *Poisson Rectangular Pulses* generator, confirms the good weather performances of the generator.

Table 4.2. Rainfall parameters in the San Pier Niceto station (2002-2011).

Parameter	Description	Observation	Modeled values
P	Mean annual precipitation [mm]	815.04	815
f_d	Dry season lenght [yr]	0.202	0.202
f_w	Wet season lenght [yr]	0.798	0.798
P_d	Dry season precipitation [mm]	164.8	166
P_w	Wet season precipitation [mm]	650.24	649
$T_{b,d}$	Dry season interstorm period [h]	94.15	95.3
$T_{b,w}$	Wet season interstorm period [h]	51.39	50.8
$T_{r,d}$	Dry season storm duration [h]	2.4	2.1
$T_{r,w}$	Wet season storm duration [h]	6.6	6.8
h_d	Mean storm depth dry season [mm]	4.22	4.25
h_w	Mean storm depth wet season [mm]	6.57	6.55
λ_d	Frequency of storm event dry season [d^{-1}]	0.255	0.252
λ_w	Frequency of storm event wet season [d^{-1}]	0.467	0.472

With regard to the evapotranspiration processes, CATGraSS uses prescribed annual cycle of the maximum transpiration $T_{max\text{-}X}$ for a flat topography as a function of day of year (DOY) based on a stationary cosine function for each PFT. The cosine function is fitted to mean daily values of $T_{max\text{-}X}$ calculated from the daily Penman Monteith equation. The fitted annual mean daily $\overline{T}^{F}_{\max -X}$ and the difference between the max and minimum points of the cosine curve Δ for each PFT are respectively 5.8 mm·d^{-1} and 4.7 mm·d^{-1} for oak, 4.9 mm·d^{-1} and 3.9 mm·d^{-1} for grass and 2.8 mm·d^{-1} and 1.8 mm·d^{-1} for Indian fig (Figure 4.22). In order to take into account the Indian fig behavior (see sections 4.1.3.2), its $T_{max\text{-}X}$ value was calculated using the modified Penman-Monteith equation (Allen et al, 2006), and multiplying the estimated value by a correction coefficient K_c equal to 0.35 following Consoli et al. (2013). Following this approach, the $ET_{a\text{-}X}$ curve of the Indian fig results in agreement with the observed data of Han and Felker (1997) and Consoli et al. (2013).

In order to illustrate the role of topography and incoming solar radiation on the potential evapotranspiration distribution, the mean $T_{max\text{-}X}$ for each vegetation type over the catchment is plotted (Figure 4.23). Annually, in the *S*-facing slope the $T_{max\text{-}X}$ is greater than in the *N*-facing slopes because it receives as much as twice the solar radiation received by *N*-facing slopes.

In order to reduce data requirements and keep the model simple, the bare soil evaporation, for a bare soil grid cell, E_b, is taken as a fraction (f_b) of the

maximum grass transpiration rate, $T_{max\text{-}G}$ (e.g., $E_b=f_b \cdot T_{max\text{-}G}$) (e.g., Mutziger et al., 2005; Istanbulluoglu et al., 2012, Zhou et al., 2013); the value of f_b is here set to 0.7 (Istanbulluoglu et al., 2012; Zhou et al., 2013).

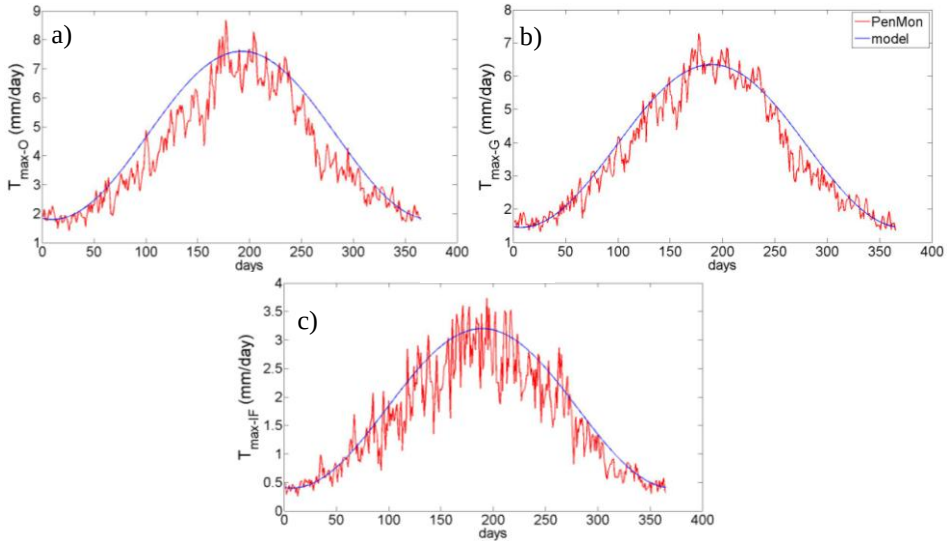

Figure 4.22. Calibration of $T_{max\text{-}X}$ annual curve: (a) oak, (b) grass, (c) Indian fig.

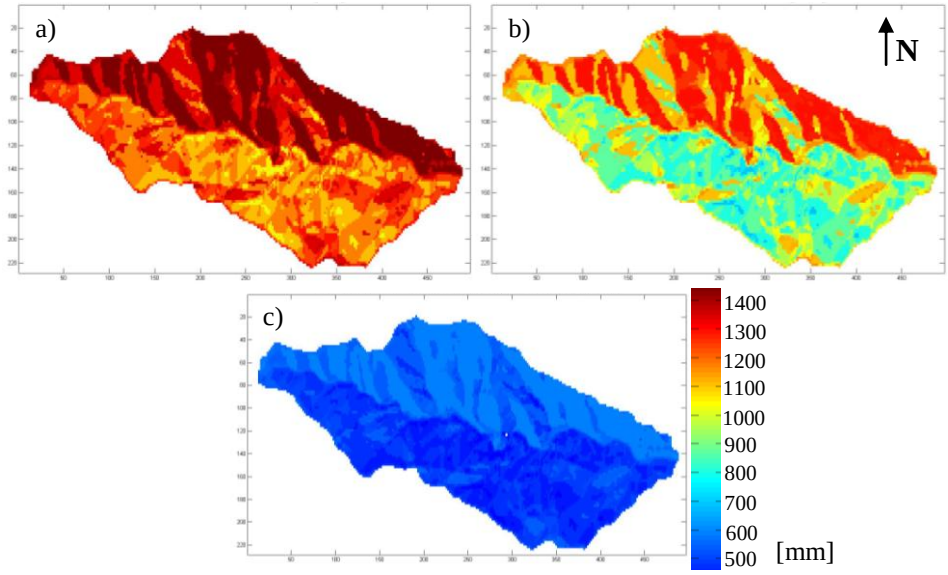

Figure 4.23. Mean annual $T_{max\text{-}X}$ over the basin for: oak (a), grass (b) and Indian fig (c).

4.2.2.1.3. *Future runs*, weather forcings

For generating the *future runs* weather we used realizations from a subset (twelve) of the GCMs used in the IPCC-4AR (Meehl et al., 2007). The selection of models is based on two criteria: data availability (availability of daily precipitation time series as the main constrain) and a relative independence among the models (different developing groups). The GCM realizations correspond to the A1B emission scenario (IPCC, 2000). The models used in this work are: *BCCR-BCM2.0, CCSM3, CGCM3.1 (T63), CNRM-CM3, CSIRO-Mk3.5, ECHAM5/MPI-OM, GFDL-CM2.1, GISS-ER, INGV-SXG, IPSL-CM4, MIROC3.2 (medres)* and *PCM.*

The stochastic downscaling is applied to the location of San Pier Niceto meteorological station, where the observed *SIAS* data are available from 2002 through 2011. This period thus represents the interval of the control scenario (*CTS*), for which both observations and climate model simulations can be used. The future climate scenario is based only on GCM projections for the period of 2045-2065, 2081-2100 (*FUT*). The downscaling procedure uses the GCMs outputs of the grid cell containing the study catchment.

An illustration of the relative performance of twelve *GCM*s in terms of monthly precipitation and temperature for the period 2045-2065 and 2081-2100 is provided in Figures 4.24-4.27. The time series of the mean monthly temperature (Figures 4.24, 4.26) and precipitation (Figures 4.25, 4.27) represent the Control scenario (*CTS*) (a), the Future scenario (*FUT*) (b), and the Factors of change (c).

The GCMs outputs exhibit a large spread, underlining inherent uncertainties in climate model predictions. This is particularly evident for precipitation where factors of change are substantially different among the models. Changes in air temperature are generally more coherent among climate models outputs (Figures 4.24, 4.26) and all of the factors of change are positive.

In a successive step, the posterior distributions of the factors of change (step 3 in Figure 3.7) are calculated for the analyzed statistics for each month using the Bayesian multi-model ensemble approach of Tebaldi et al. (2005).

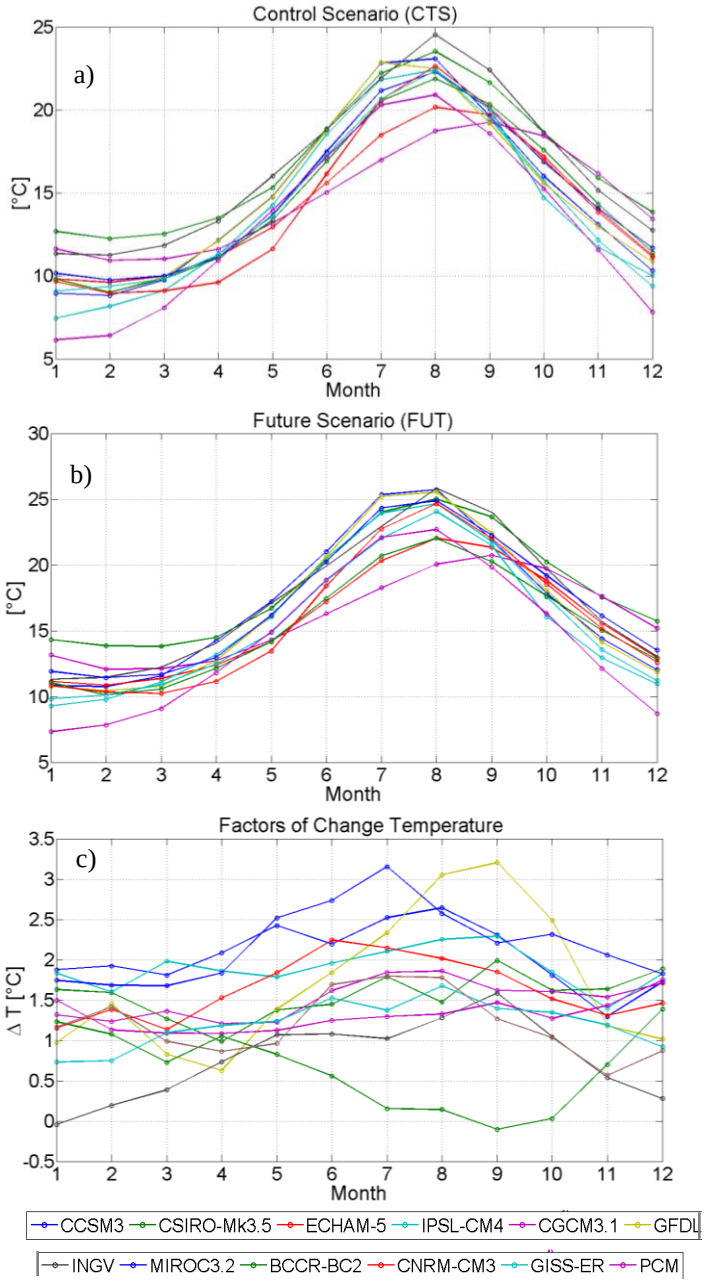

Figure 4.24. The time series of mean monthly temperature calculated from twelve GCMs: *CCSM3*, *CSIRO-Mk3.5*, *ECHAM-5*, *IPSL-CM4*, *CGCM3.1*, *GFDL*, *INGV*, *MIROC3.2*, *BCCR-BC2*, *CNRM-CM3*, *GISS-ER*, *PCM* for the location of San Pier Niceto. (a) Control scenario (*CTS*); (b) Future scenario (*FUT*), 2046–2065; (c) Factors of change for mean monthly temperature.

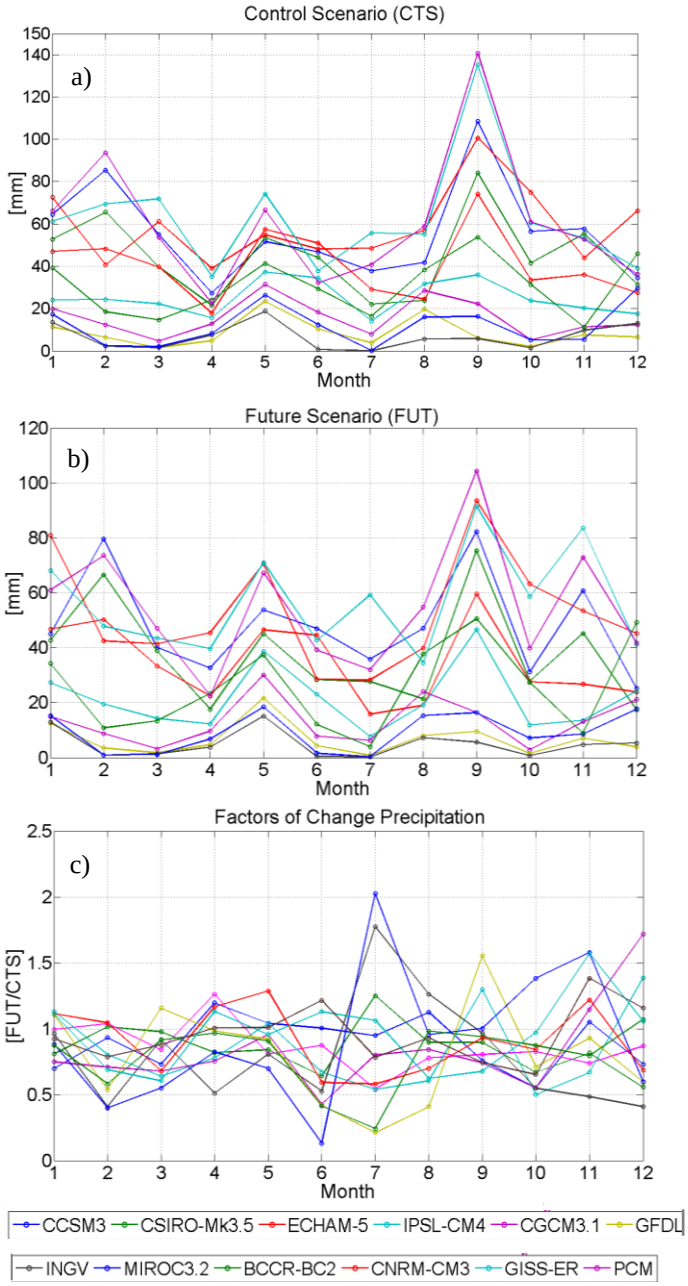

Figure 4.25. The time series of total monthly precipitation calculated from twelve GCMs: *CCSM3*, *CSIRO-Mk3.5*, *ECHAM-5*, *IPSL-CM4*, *CGCM3.1*, *GFDL*, *INGV*, *MIROC3.2*, *BCCR-BC2*, *CNRM-CM3*, *GISS-ER*, *PCM*. (a) Control scenario (*CTS*); (b) future scenario (*FUT*), 2046-2065; (c) Factors of change for monthly precipitation.

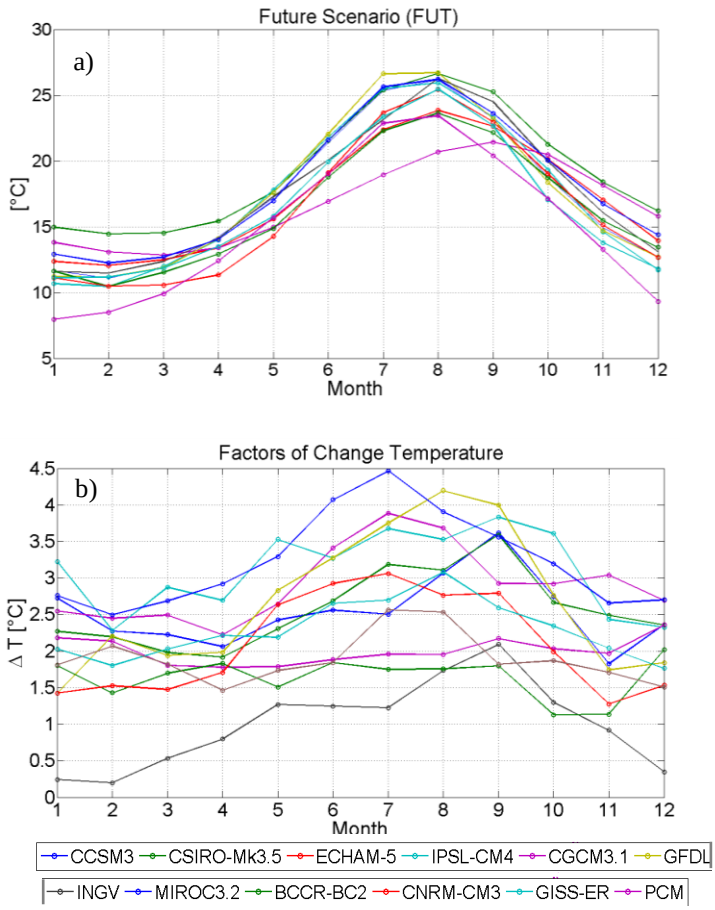

Figure 4.26. The time series of mean monthly temperature calculated from twelve GCMs: *CCSM3*, *CSIRO-Mk3.5*, *ECHAM-5*, *IPSL-CM4*, *CGCM3.1*, *GFDL*, *INGV*, *MIROC3.2*, *BCCR-BC2*, *CNRM-CM3*, *GISS-ER*, *PCM* for the location of San Pier Niceto. (a) Future scenario (*FUT*), 2081–2100; (b) Factors of change for mean monthly temperature.

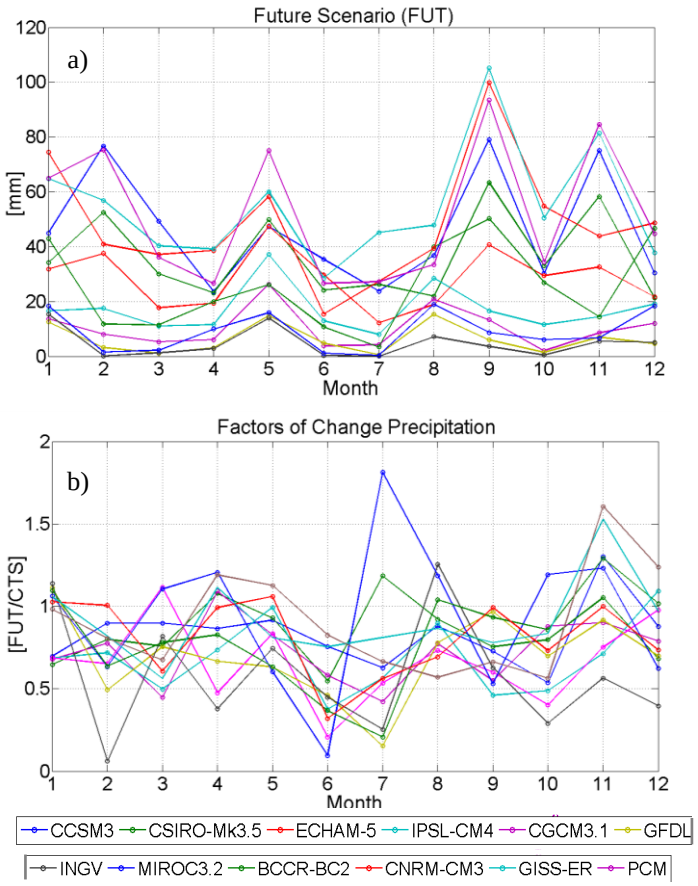

Figure 4.27. The time series of total monthly precipitation calculated from twelve GCMs: *CCSM3*, *CSIRO-Mk3.5*, *ECHAM-5*, *IPSL-CM4*, *CGCM3.1*, *GFDL*, *INGV*, *MIROC3.2*, *BCCR-BC2*, *CNRM-CM3*, *GISS-ER*, *PCM*. (a) future scenario (*FUT*), 2081-2100; (b) Factors of change for monthly precipitation.

For example, the Figure 4.28a illustrates the posterior probability density functions (*pdf*) of average temperature in March using simulations of the *CTS* and *FUT* scenarios for the period 2081-2100. The March temperature based on individual simulations by 12 models for the *CTS* and *FUT* is also shown (green and magenta dots, respectively). Figure 4.28b shows the posterior *pdf* of the additive factor of change, together with the factors of change predicted by the individual models. Figure 4.28c illustrates the probability density functions of the total precipitation in March for the *CTS* and *FUT* scenarios for the period 2081-2100. Figure 4.28d shows the *pdfs* of the product factor of change for the total precipitation in March as well as the factors of change predicted by the individual models. An illustration of the factors of change for the period 2081-2100, including the mean, and the 10-90 percentile intervals calculated for

several precipitation statistics at the aggregation period of 24 h is shown in Figure 4.29. As seen, the uncertainty present in the estimation of the factors of change for precipitation statistics is very high with a tendency to increase for higher order statistics. The uncertainty is also strongly related to seasonality, since in some months model predictions tend to provide a more accurate estimation than in others.

In this study only the medians of the probability distributions of *FOC* are used to re-estimate climate statistics for the central years (2055 and 2090) of the periods 2046-2065 and 2081-2100. *FOC*s for the central year (2006) of period of 2002 through 2011 are all equal to unity or zero, being 2002-2011 assumed as the control scenario period for which observations are available. *FOC*s for all of the other years in the period 2001-2100 were linearly interpolated between the downscaled years (2006, 2055 and 2090) using the same methodology presented by Burton et al. (2010) to obtain transient climate change scenarios (see also Fatichi et al., 2013). In this way one hundred sets of AWE-GEN parameters (one for each year) are estimated and can be used to generate meteorological time series of a given year. In Figure 4.30 a flowchart illustrating each step of the used methodology is shown. Due to the stochastic nature of AWE-GEN each year can be generated multiple, *n*, times. In this study we used *n* equal to fifty as a reasonable number of realizations which allows us to analyze the effect of natural climate variability without increasing excessively computational costs.

All this procedure provides fifty realizations of a 100-year hourly climate data between 2001-2100 which contain rainfall depths, and allow to calculate $T_{max\text{-}X}$ from the Penman-Monteith equation.

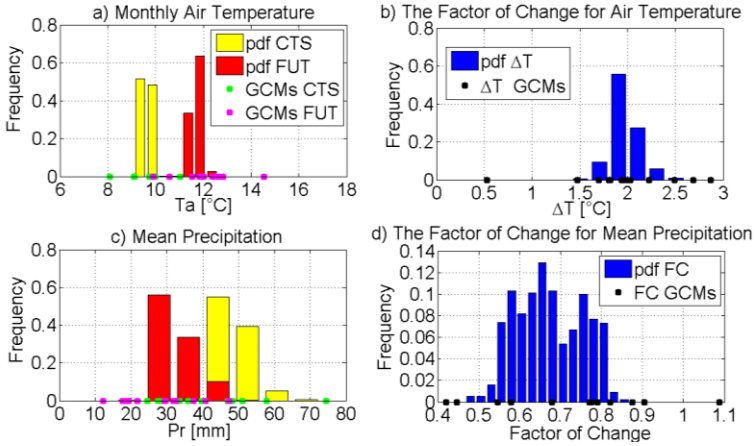

Figure 4.28. The posterior probability density functions (*PDF*) obtained from the multi-model ensemble for the location of San Pier Niceto (ME) 2081-2100, the month of March. (a) The *PDF* of mean March temperature for the *CTS* (yellow bars) and the FUT (red bars) scenarios. Also shown are the results from the individual models for the *CTS* (green dots) and *FUT* (magenta dots). (b) The *PDF* of the additive factor of change for air temperature, (blue bars) and predictions by the individual models (black dots). (c) The *PDF* of mean March precipitation for the *CTS* (yellow bars) and the *FUT* (red bars) scenarios. Also shown are the results from the individual models for the *CTS* (magenta dots) and *FUT* (green dots). (d) The *PDF* of the product factor of change for precipitation, (blue bars) and predictions by the individual models (black dots).

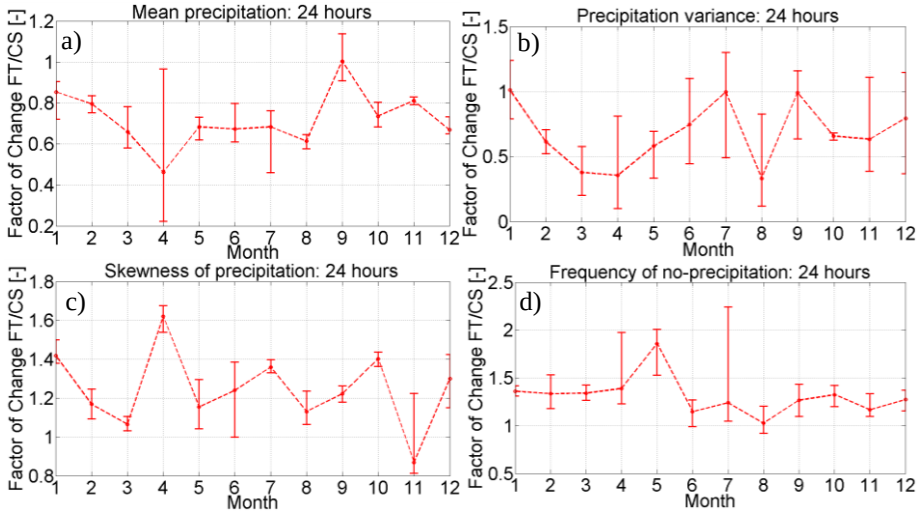

Figure 4.29. The factors of change estimated for different precipitation statistics at the aggregation interval of 24 h, 2081-2100. The mean and the 10-90 percentile intervals are computed from the posterior *PDF*s of these statistics. (a) Mean precipitation, (b) Variance of precipitation, (c) Skewness of precipitation, (d) Frequency of no-precipitation.

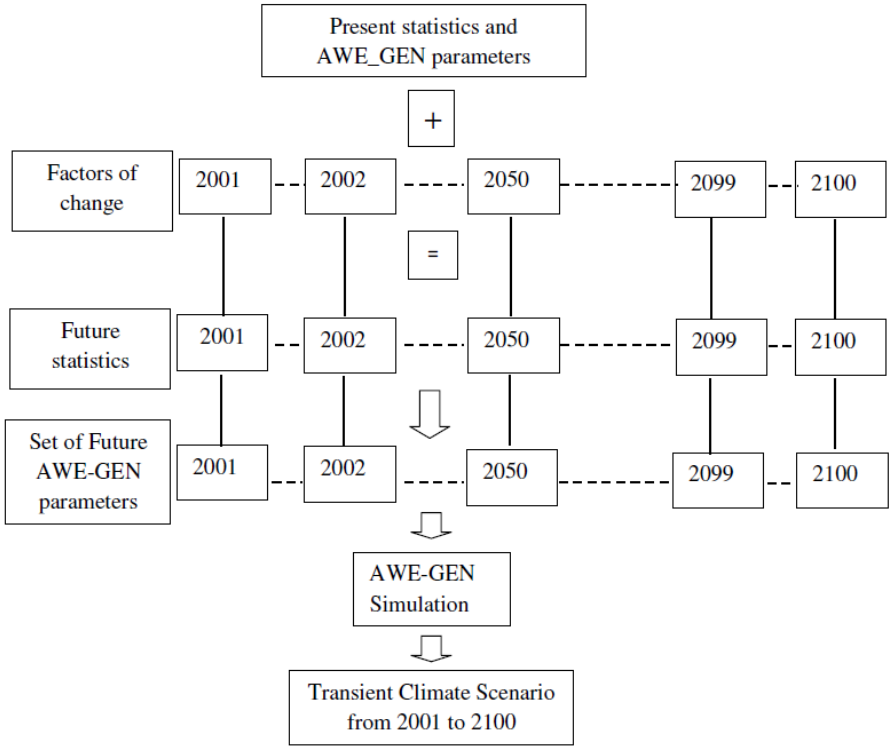

Figure 4.30. Flowchart illustrating each step of the AWE-GEN future transient climate methodology.

4.3. Results: base run

4.3.1. Model calibration

As previously said, the main purpose of the *base run* is to compare the model results with observed vegetation patterns (Figures 4.1, 4.2). As the basis of the model calibration, we compared the *current vegetation map* with the *base run* dominant vegetation (i.e., the vegetation type that has got the maximum occurrence of existence in the cell) spatial distribution. To generate this map, the model output from the last 3,000 years of the simulation has been used since it shows a relatively stable behavior while the first 2,000 years can be considered the spin-up period and removed. The *current vegetation map* has been obtained from a supervised classification (considering three vegetation classes), using the *Google Earth* aerial photo of the basin area together with field survey (Figure 4.31).

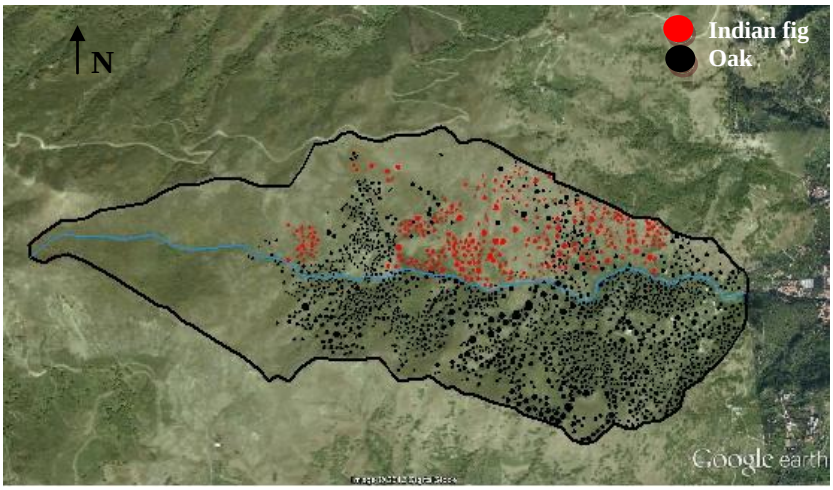

Figure 4.31. Edited Oak (black dots) and Indian fig (red dots) used for the basin calibration and the *Google Earth* aerial photo.

All the soil (modeled as a sandy-loam) and vegetation parameters used for simulating local water balance and plant dynamics (e.g., biomass production and loss) are listed in Tables 4.3-4.7. The parameters used to model soil water balance, *ET*, and local biomass dynamics are largely assigned according to typical published values in ecohydrology and land surface modeling literature (Tables 4.4, 4.5) presenting the source of each parameter as footnotes in the same Tables. We reserved only a limited number of parameters for calibration, including plant mortality and establishment parameters (Table 4.6), and plant decay coefficients which are calibrated against remote sensing-derived *Leaf Area Index* (*LAI*) within the ranges reported in other studies (discussed below).

In particular the decay coefficients for green biomass (k_{sg}), structural biomass (k_{ss}), dead biomass (k_{dd}), the maximum drought induced foliage loss (k_{sf}), the water use efficiency (*WUE*), the specific leaf are for green (c_g) and dead biomass (c_d) and the LAI_{max} are identified with calibration, using the ranges reported in the literature for semiarid ecosystems (e.g., Montaldo et al., 2005; Williams and Albertson, 2005; Ivanov et al., 2008a).

The MODIS (*Moderate-resolution Imaging Spectroradiometer*) data have been here used to calibrate the model as well as previously done with other ecohydrological models (i.e., Istanbulluoglu et al., 2012; Fatichi et al., 2012; Zhou et al., 2013). MODIS sensors, on the Terra and Aqua satellites, can provide valuable information to assess vegetation state at basin scales. The *LAI* is included in the products *MOD15A2* and *MYD15A2* (*NASA Land Processes Distributed Active Archive Center, LP DAAC*) and provided every 8 days at 1 km spatial resolution. Since three PFTs cover the basin area, we identified MODIS cells that have a relatively uniform cover of a given plant type (oak,

grass or Indian fig). The MODIS pixels selected to represent the *LAI* of trees are uniformly covered by oaks only and cover the north face of the basin and also areas outside the basin. The MODIS pixels selected to represent grass are located in the highest part of the basin and also contain areas that are outside the basin boundaries. The identification of MODIS pixels representative of the Indian fig Opuntia cover was not possible given the fact that Indian fig is typically mixed with the other two plant types and therefore it would have been impossible to separate the *LAI* from the different plants. Moreover, the algorithms used by MODIS to process reflectance data are not able to reproduce the spectral signature of succulent plants such as the Indian fig undermining the overall validity of MODIS data for this vegetation type.

The MODIS data for 12 years, from 2000 to 2012, are compared with *LAI* simulated by CATGraSS. In the calibration procedure, the lowest MODIS *LAI* values ($LAI<2$ for oak and $LAI<0.5$ for grass) are not considered because of their low signal-to-noise ratio. The decay coefficients k_{sg}, k_{ss}, k_{dd}, k_{sf}, the *WUE*, the c_g, the c_d, and the LAI_{max} have been manually adjusted within the literature parameter ranges so as to match the MODIS *LAI* data for oak and grass (Montaldo et al., 2005, 2008). The comparison between MODIS *LAI* and modeled *LAI* is shown in Figures 4.32a, b for oak and grass, respectively. The model shows consistency in estimating the onset of the growing and dormant seasons, and the *LAI* peak is estimated correctly in each years. The standard error of estimation *(SEE*), the Nash-Sutciffe efficiency (*NSE*) (Nash and Sutciffe, 1970), the coefficient of determination (R^2) and the coefficient of correlation (R) (for oak SEE=0.21, NSE=0.16, R^2=0.67, R=0.82 and for grass SEE=0.15, NSE=0.12, R^2=0.64, R=0.80) show good agreement between model predictions and remote sensing estimation. The model parameters for the Indian fig were obtained using for each parameter a value within a realistic range provided by scientific literature (Table 4.5) and imposing an evergreen behavior, and they provide a simulated *LAI* in agreement with other studies (Han and Felker, 1997; Inglese et al., 2009; Consoli et al., 2013).

The spatial patterns of plants obtained with CATGraSS are most sensitive to the mortality and establishments parameters reported in Table 4.6 (θ, P_{Mb}, $P_{\text{E-max}}$) which are obtained with a calibration as well. The conceptual design of the CA component of CATGraSS is very similar to that of van Wijk and Rodriguez-Iturbe (2002), which was used to simulate a semiarid Texas savanna. As such, we took the parameters used by van Wijk and Rodriguez-Iturbe (2002) and Zhou et al. (2013) as initial values, and calibrated CATGraSS through numerous simulations until the predicted vegetation patterns agreed with the *current vegetation map*.

Plant mortality is a key component of the vegetational model as it opens space for competition and can define the occupation density of a plant type in a given domain. Therefore, in calibrating the model with the *current vegetation map*, we started with the drought resistance threshold, θ, used for calculating the

probability of drought-induced plant mortality, P_{Md}. Since Indian fig is more drought resistant than oak and grass, we rank the PFTs as Indian fig, oak, and grass, e.g., from high to low drought resistant species, and calibrated the model by preserving this drought resistance ranking. In order to account for the fact that plant seedlings are in general more vulnerable to drought than mature plants, we assumed that all the seedlings are 20% less drought resistant than mature plants (Fenner, 1987; Zhou et al., 2013); this assumption is generally satisfied for both oak and Indian fig (Chew and Chew, 1965).

The background mortality probability ($P_{Mb\text{-}X}$) which represents the influence of local disturbances (e.g., diseases and grazing) has been fixed in a similar way to van Wijk and Rodrigues-Iturbe (2002) due to lack of observations. This parameter is assumed to take the same value for oaks and Indian fig, and a three-fold higher value for oaks and Indian fig seedlings using the same scheme adopted in Zhou et al. (2013).

The maximum probability of establishment parameter, $P_{E\text{-}max}$, has been also calibrated until the predicted plant patterns agreed with the vegetation cover map considering that grasses usually has a higher capability for colonization than trees (Jeltsch et al., 1996).

The inhibition factor, IN_G, was not used because in this case study there is not the allelopathy phenomenon. In fact the vegetation types that are in this area do not produce allelochemicals that affect the other vegetation types.

For the fire event we have assumed a probability of fire, P_F, (i.e., the inverse of return period, T_F) like to 0.05 (return period, T_F: 20 years; Casagrandi and Rinaldi, 1999) and the vulnerability to fire of each vegetation, $V_{F\text{-}X}$, is shown in Table 4.7 (plant seedlings are more vulnerable to fire than mature plants).

Table 4.3. Soil parameters used in the point water balance component (Laio et al., 2001).

Soil Type	Coefficient of the hydraulic conductivity power low	Saturated hydraulic conductivity	Porosity	Soil saturation degree at field capacity	Bare soil infiltration capacity
	β [-]	k_s [mm·d^{-1}]	N [-]	s_{fc} [-]	I_b [mm·d^{-1}]
Sandy loam	13.8	1.75	0.43	0.56	0.83

Table 4.4. Plant parameters used in the point water balance component.

Parameters	Description	Oak	Indian fig	Grass
Zv_{eg}	Vegetation height [m]	4 [1]	1.5 [2]	0.5 [3]
LAI_{max}	Maximum leaf area index [$m^2 \cdot m^{-2}$]	7.1 [8]	3 [7,8]	2.7 [8]
r_l	Stomatal resistance [$s \cdot m^{-1}$]	280 [3]	1000 [4]	100 [3]
α_s	shortwave albedo [-]	0.1 [1]	0.2 [4]	0.2 [3]
Z_r	Root depth [m]	1.5 [1]	0.1 [5]	0.3 [6]
I_{max}	Full canopy interception [mm]	2 [6]	1.5 [6]	1 [6]

Source: (1) Pumo et al. (2008); (2) Singh and Singh (2003) ; (3) Montaldo et al. (2013); (4) Acevedo (1983); (5) Snyman (2005); (6) Caylor et al. (2005); (7) Han and Felker (1997), Inglese et al. (2009), Consoli et al. (2013); (8) Calibration.

Table 4.5. Local plant dynamics component parameters.

Parameters	Description	Oak	Indian fig	Grass
WUE	Water Use Efficiency [$kg_{CO2} \cdot kg^{-1}_{H2O}$]	0.009 [1,8]	0.022 [2,8]	0.005 [1,8]
k_{sg}	Decay coefficient of green biomass [d^{-1}]	0.002 [3,8]	0.002 [3,8]	0.0025 [3,8]
k_{ss}	Decay coefficient of structural biomass [d^{-1}]	0.005 [4,8]	0.005 [3,8]	0.001 [3,8]
k_{dd}	Decay coefficient of dead biomass [d^{-1}]	0.05 [3,8]	0.07 [3,8]	0.15 [3,8]
k_{sf}	Maximum drought induced foliage loss rates [d^{-1}]	0.001 [8]	0.0005 [8]	0.005 [8]
c_g	Specific leaf area for green biomass [m^2 leaf $\cdot g^{-1}_{DM}$]	0.019 [3,8]	0.015 [3,8]	0.019 [3,8]
c_d	Specific leaf area for dead biomass [m^2 leaf $\cdot g^{-1}_{DM}$]	0.07 [4,8]	0.02 [3,8]	0.07 [4,8]
Td_{max}	Constant for dead biomass loss adjustment [mm $\cdot d^{-1}$]	10 [5]	10 [7]	10 [7]
s*	Saturation degree at stomata closure [-]	0.22 [6]	0.24 [6]	0.33 [6]
S_ω	Saturation degree at wilting point [-]	0.15 [6]	0.13 [6]	0.13 [6]
s_h	Saturation degree at soil hygroscopic [-]	0.1 [6]	0.1 [6]	0.1 [6]

Source: (1) Montaldo et al. (2013); (2) Nobel (1988), Nobel and Bobich (1995); (3) Montaldo et al. (2005); (4) Montaldo et al. (2008); (5) Istanbulluoglu et al. (2012); (6) Caylor et al. (2005); (7) Zhou et al. (2013); (8) Calibration.

Table 4.6. Model parameters for plant mortality and establishment.

Parameters	Description	Oak	Oak Seedling	Indian fig	Indian fig Seedling	Grass
θ_x	Drought-resistant threshold [-]	0.75[2]	0.6[2]	0.8[2]	0.64[2]	0.53[2]
P_{Mb-X}	Background mortality probability [-]	0.01[1]	0.03[1]	0.01[1]	0.03[1]	0.05[1]
$P_{E-X-max}$	Maximal establishment probability [-]	0.25[2]	N/A	0.25[2]	N/A	0.35[2]

Source: (1) Zhou et al. (2013), (2) Calibration.

Table 4.7. Fire parameters.

Parameters	Description	Oak	Oak Seedling	Indian fig	Indian fig Seedling	Grass
P_F	Probability of fire [yr^{-1}]			0.05 [1,3]		
T_F	Fire return period [yr]			20 [1,3]		
V_{F-X}	Vulnerability to fire [-]	0.06 [2,3]	0.2 [2,3]	0.1 [2,3]	0.2 [2,3]	0.8 [2,3]

Source: (1) Casagrandi and Rinaldi (1999), Le Houèrou (1974), Thomas (1991), (2) Accatino et al. (2010), (3) Calibration.

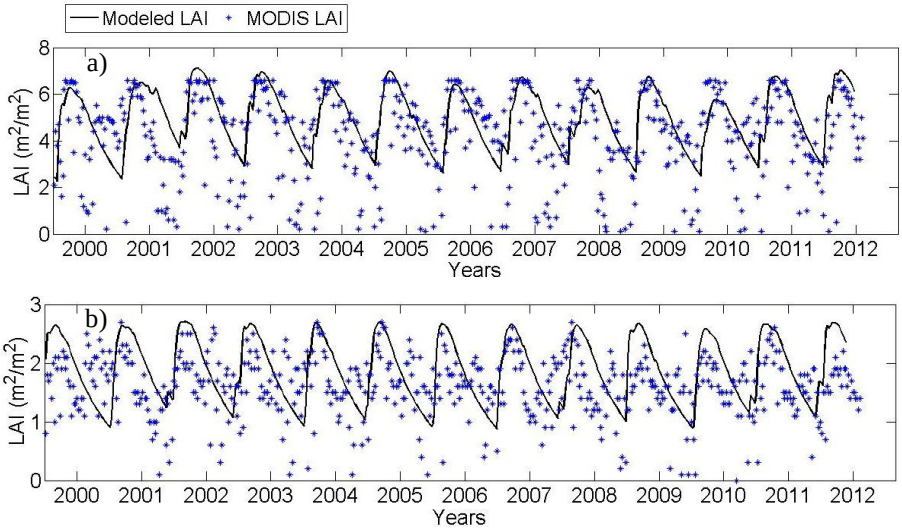

Figure 4.32. Calibration *LAI*: (a) oak, (b) grass.

4.3.2. Comparison between real and CATGraSS *base run* vegetation maps

In order to verify the goodness of the calibration, *current vegetation map* has been compared with the *base run* dominant vegetation distribution using the error Matrix (Cohen, 1960; Congalton, 1991; Foody, 2002). The error Matrix is a square matrix of size *r* (here equal to the number of the vegetation types). It expresses the number of vegetation cells assigned to a particular vegetation type (*base run* dominant vegetation map) related to the actual vegetation type as computed in the *current vegetation map*. The columns represent the actual data (*current vegetation map*) while the rows indicate the predictions (*base run* dominant vegetation map). The value x_{ij} (ij=1,2,3) denotes the number of pixel of *i-th* actual vegetation reproduced by the model as *j-th* vegetation. Pixels along main diagonal represent correct reproduction by the model. We calculated the Kappa coefficient, *K*, (Cohen, 1960) and the percentage corrected, *PC* (Foody, 2002):

$$K = \frac{N\sum_{i=1}^{3} x_{ii} - \sum_{i=1}^{3} x_{i+} \cdot x_{+i}}{N^2 - \sum_{i=1}^{3} x_{i+} \cdot x_{+i}} \tag{4.1}$$

$$PC = \frac{\sum_{i=1}^{3} x_{ii}}{N^2} \tag{4.2}$$

where x_{ii} is the number of corrected model reproduction for the *i-th* vegetation observation in row *i* and column *i*, x_{i+} and x_{+i} are the marginal totals of row *i* and column *i*, respectively, and *N* is the total number of observation (total number of vegetation cells in the basin). *K* and *PC* values provide an objective assessment of model simulation. For instance, Fleiss (1981) characterizes *K* exceeding 0.75 as excellent, 0.40 to 0.75 as fair to good, and below 0.40 as poor, while Thomlinson et al. (1999) characterize *PC* exceeding 0.85 as excellent. In our case, the performance indices *K* (equal to 0.77), and *PC* (equal to 0.87) shows that our model result, after calibration, matches reasonably well with the actual vegetation distribution.

4.3.3. Aspect influence on water stress

The role of topography on the vegetation spatial distribution can be illustrated by plotting the mean annual plant water stress as a function of slope and aspect by averaging 5,000 years of model outputs for each of the 40 *S-A* classes and considering only those with soil thickness equal to 3 m for simplicity (Figure 4.33). Among the three PFTs, the modeled mean annual water stress

(*WS*) follows the order, from high to low, grass (WS_G=0.62), oak (WS_T=0.54), and Indian fig (WS_{IF}=0.37) averaged across the slope-aspect domain (Figure 4.33). The role of morphology is more pronounced for oak and Indian fig than grass (Figure 4.33). Water stress for grasses shows a relatively small range, with higher (lower) values corresponding to steep *S*-facing (*N*-facing) slopes. In the north face the water stress is lower than in the south face because of the lower radiation and thus $ET_{max\text{-}X}$ (Figure 4.5). Lack of a considerable aspect influence on grass water stress suggests that grasses could grow opportunistically everywhere in the basin where bare soil, "space", is available. Water stress increases with slope angle dramatically on *S*-facing slopes for the other species. In the *E* and *S* facing slopes oak shows the greatest increase in water stress as slope steepens, while high water stress value of Indian fig is only confined to steep south facing slopes. In shallow to moderate slopes and for all aspects, oak shows more water stress than Indian fig. This greater water stress experienced by oak in the *E* and *S* facing could cause a slight chance for this specie to settle in this area, pushing it to establish on the *N*-facing while the grass and Indian fig mainly on the *S*-facing.

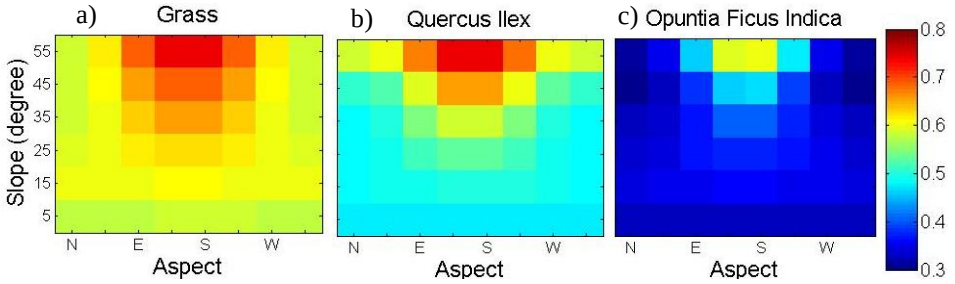

Figure 4.33. Mean annual water stress for grass (a), *Quercus Ilex* (b), and *Opuntia ficus-indica* (c) with different slope and aspect combinations.

4.3.4. Vegetation spatial patterns

Vegetation maps at three selected time steps, 1,000 years (lower tree population), 3,700 years (higher tree population), and 5,000 years, and the entire time series of vegetation cover percentages of the *base run* are presented in Figures 4.34a, b, c, e, respectively. In Figure 4.34d the map of the dominant vegetation cover, which is in agreement with field observations, is represented. Oak is dominant on the *N*-facing and coexist with grass. Indian fig coexists with grass and with a small oak clusters in *S*-facing slopes while in the steeper part of the basin whereas the soil is very shallow, the grass is dominant.

Cover percentages of the different species are dynamic, even under a stationary climate, and behave markedly different among species. The highly variable nature of grass fraction is typically driven by the inter-annual fluctuations in precipitation. Because grasses have an overall higher water stress

and lower drought resistance, they die rapidly during dry years, but also grow back quickly in the following wetter years, as their seeds are assumed to be available everywhere in space. In addition, the establishment and mortality of grass depend on the rainfall of a given year and therefore subjected to the same inter-annual variability of rainfall.

In contrast, the establishment of oak seedlings depends on the population of the parent plants in the area, which leads seedling establishment to depend significantly on the memory of the historical precipitation magnitudes. As a result, compared to grass vegetation, the areal coverage of oak shows a strong persistence over time. The India fig has got also a strong persistence over time due to its high resistance to the water stress. The coverage of oak is slightly more dynamic than that of Indian fig. In fact, the *lag-1* autocorrelation is 0.996 for oak, 0.994 for Indian fig and 0.813 for grass. Overall, with the selected model parameters, oak coverage exhibits persistence with multi-century trends.

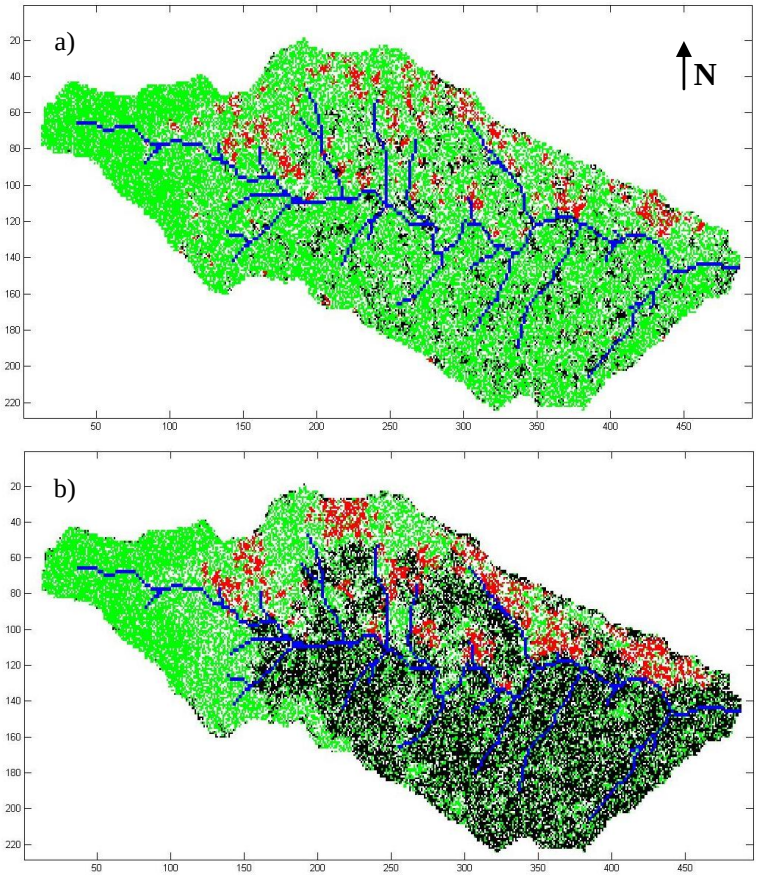

Figure 4.34. *Base run*: simulated plant distribution in the basin at years: (a) 1,000; (b) 3,700.

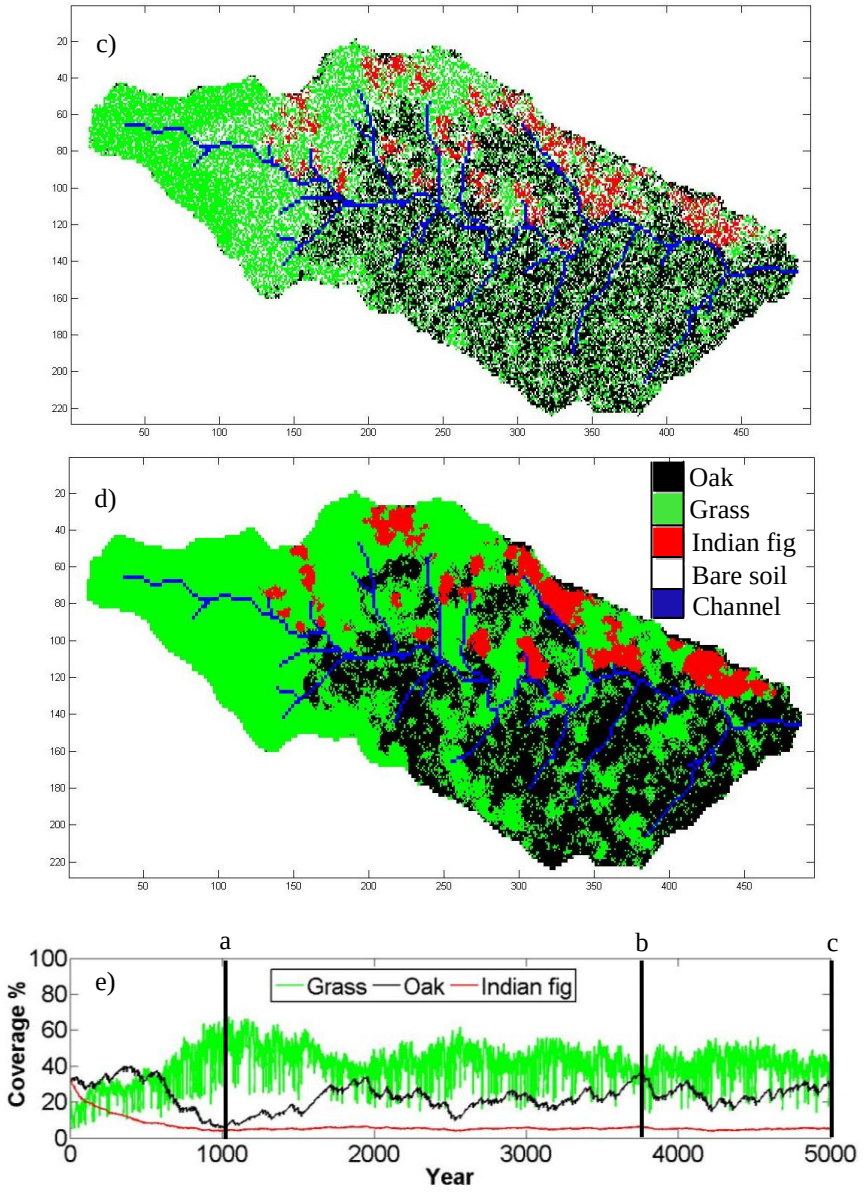

Figure 4.34. *Base run*: simulated plant distribution in the basin at years: (c) 5,000 and (d) dominant vegetation from 2,000 to 5,000, respectively; and (e) time series of percent coverage of PFTs in the modeled catchment.

Even though the plant distribution map provides an important indication of aspect control on plant patterns (Figures 4.34 c, d), the role of topography can be better viewed by illustrating, for the three species, the boxplots of annual percent

cover with respect to aspect (Figure 4.35 left panel), and the time probability of occurrence (*PO*) over the modeled domain (Figure 4.35 right panel) here defined as the number of years of existence of a specific species on a cell divided by the total duration of simulation, using the last 3,000 years of the simulation (see section 4.3.1).

From *N* to *S* aspects the modeled dominant plant type changes from oak to grass and Indian fig (Figures 4.35a, c, e). The range of the modeled cover percentages of oaks in a given aspect category captures the existing abundance in the field (Figure 4.35c). Grass shows a muted response to aspect (Figure 4.35a), which can be attributed to its relatively uniform water stress across the domain (Figure 4.33a). Conversely Indian fig shows a considerable variation of its percentage in function of the aspect (Figure 4.35b). It is in fact located only in the *S*, *S-E* and *E* aspects where it is actually observed in the basin.

We obtained the oak coverage for each aspect class from *current vegetation map* using spatial analysis techniques within *ESRI ArcGIS*. This presents an opportunity for a direct comparison of the model results with oak mapped from *current vegetation map*. In Figure 4.35c the red central line of the box-whisker plot is the median of the oak coverage for each aspect group obtained with the CATGraSS and the dotted black line represents the oak coverage derived from the *current vegetation map*. This comparison shows a good agreement of the oak coverage for each aspect group.

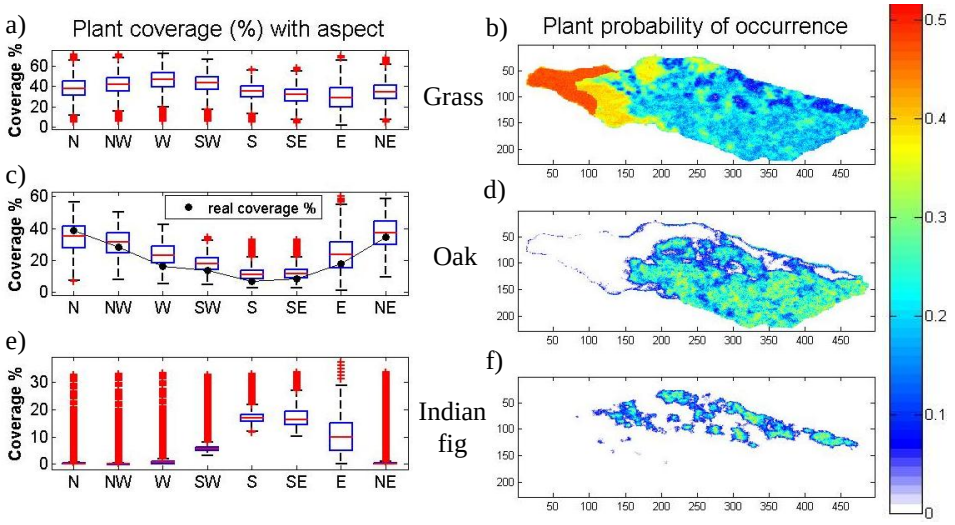

Figure 4.35. Model results for the *base run*: percent plant coverage with respect to aspect (left panel), and plant Probability of Occurrence, *PO* (right panel) for grass (a, b), oak (c, d) and Indian fig (e, f). In the box-whisker plots, the red central line is the median, the edges of the box are the 25th and 75th percentiles, the whiskers extend to the most extreme data points not considered outliers, and outliers are plotted as read squares. The dotted black line in (c) represents the oak coverage derived from the *aerial photo* of the basin editing the tree.

With regard to the *base run*, an attempt to analyze how the biodiversity changes during the 5,000 year simulation has been carried out using the Shannon index (*SHDI*, Shannon and Weaver, 1949):

$$SHDI = 1 - \sum_{i=1}^{N} p_i \cdot \ln p_i \tag{4.3}$$

where N is the number of vegetation type and p_i the proportional abundance of the i^{th} type. This index, ranges from 1 to infinity and it increases as the number of different vegetation types increases and the proportional distribution of area among vegetation types become more even. The *SHDI* for 5,000 years is shown in Figure 4.36. The minimum of biodiversity is reached after a 1,000 years when the grass is dominant and there are few trees and Indian figs (Figure 4.34a), while for the period between 2,000 and 5,000 years, *SHDI* remains fairly constant highlighting a general stability and stationarity of the ecosystem.

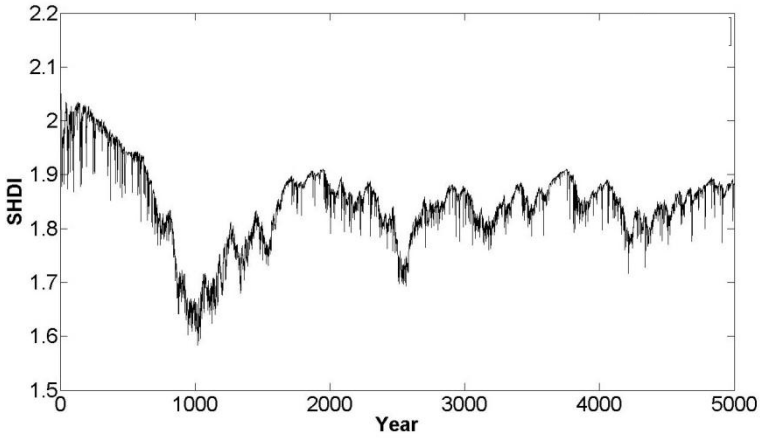

Figure 4.36. Shannon index of diversity, SHDI, for 5,000 years.

The model results presented above are not sensitive to the initial condition used for spatial plant distribution. The influence of initial vegetation pattern was tested by conducting ten numerical experiments with CATGraSS in which the model was started with a different random vegetation distribution, but with the same probability of assignments for all PFTs (33%). In the simulations we observed that the model forgets the initial condition within the first thousand year, during which aspect-driven vegetation organization emerges on the landscape.

4.3.5. Influence of PFTs size, soil thickness and topography in the vegetation spatial patterns

In this section a brief description of the influence of PFTs' size, soil thickness and topography on the vegetation spatial distribution has been carried out.

In order to analyze the influence of the PFTs' size in the vegetation patterns, we have run the model by using the identical rainfall, and the initial conditions and parameters of the *base run* for different PFTs' sizes: 2.5 m, 5 m and 10 m. In Figure 4.37 the dominant vegetation distribution for different PFTs' sizes, i.e., 2.5 m, 5 m and 10 m, is shown. Increasing the PFTs' size, from 2.5 m to 5 m to 10 m, the oak percentage increases (Table 4.8) and the grass percentage decreases. It can be explained considering that increasing the PFTs' size, the oak seed spread increases from 5 m (PFTs' size: 2.5 m) to 10 m (PFTs' size: 5 m) to 20 m (PFTs' size: 10 m) and the establishment ability of the oak increases. The seed spread of the Indian fig increases from 2.5 m (PFTs' size: 2.5 m) to 5 m (PFTs' size: 5 m) to 10 m (PFTs' size: 10 m) and, therefore, the establishment ability of the indian fig increases less than the establishment ability of the oak. The few changes of the vegetation percentage (i.e., Indian fig) could be also related to the stochastic component of the rainfall. In Figure 4.38 the time series of percent coverage of PFTs in the modeled catchment for different PFTs' sizes are shown. Using different PFTs' sizes, the variation of the cover fractions of each PFT in the years also changes.

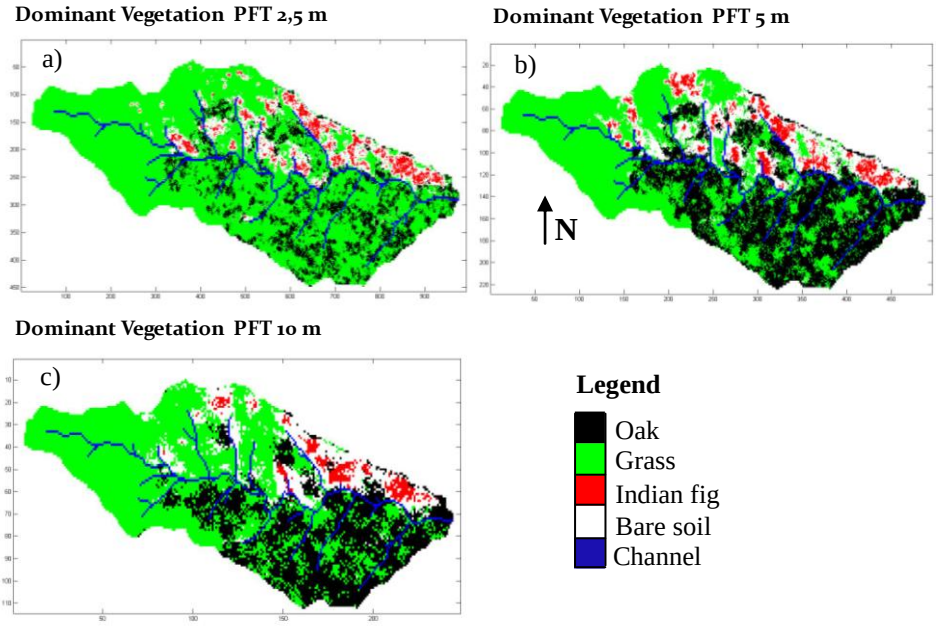

Figure 4.37. Dominant vegetation 2,000-5,000 years for different PFT size: (a) *PFT* 2.5 m, (b) PFT 5 m, (c) PFT 10 m.

Table 4.8. Mean vegetation voverage [%] (5,000 years), for different PFT size (2.5 m, 5 m, 10 m).

Mean Vegetation Coverage [%] 5,000 Years			
PFT Size	Oak	Indian fig	Grass
2.5 m	18.85	6.11	42.74
5 m	23.00	6.30	39.95
10 m	24.62	6.58	38.16

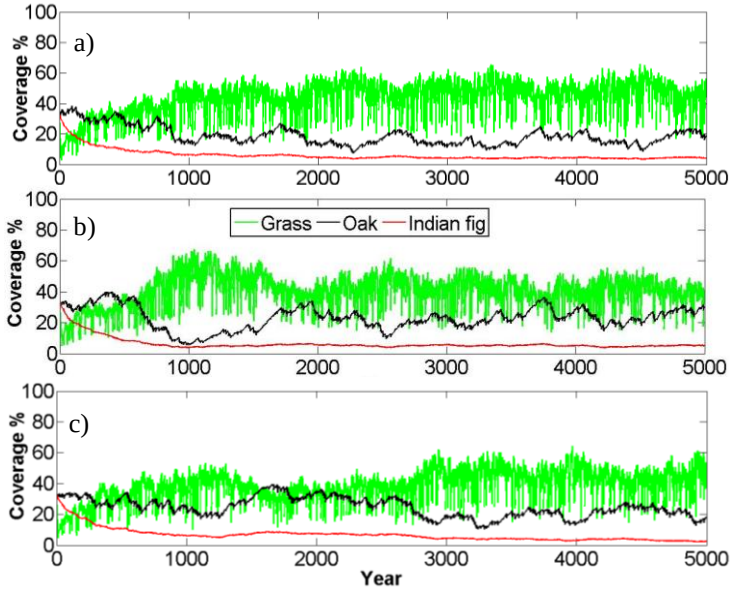

Figure 4.38. Time series of percent coverage of PFTs in the modeled catchment for different PFT sizes: (a) PFT 2.5 m, (b) PFT 5 m, (c) PFT 10 m.

CATGraSS was also run without soil depth limitation to examine the plant pattern in the absence of soil depth limitation. We have run the model by using the identical rainfall, and the initial conditions and parameters of the *base run.* The results in Figure 4.39 show that, in this case, since there is not soil thickness limitation, as elevation grows, oak and Indian fig are able to establish and grow also in the upstream area of the basin. These results underline that, for the Zafferia catchment, the vegetation distribution is tightly related to the spatial variability of the soil thickness in the basin.

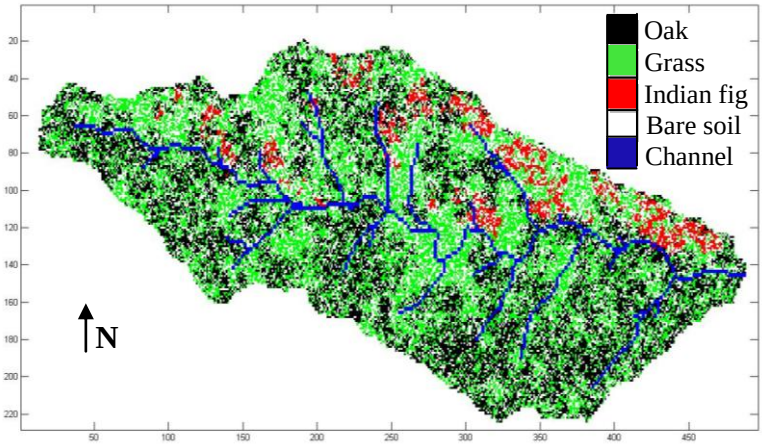

Figure 4.39. Simulation without soil depth limitation: vegetation distribution after 5,000 years in the modeled catchment.

In order to examine the influence of topography on the vegetation spatial patterns, CATGraSS was run on flat terrain (effect of topography) and with no soil depth limitation. We have run the model by removing the topography effect within the watershed boundaries and setting the elevations to the basin outlet elevation, using the identical rainfall sequencing, and the initial conditions and parameters of the *base run*. There is not the influence of the solar radiation and of the slope-aspect classes and the results in Figure 4.40 show that vegetation has got a random distribution. These results underline again that the vegetation distribution is tightly related to the topography of the basin.

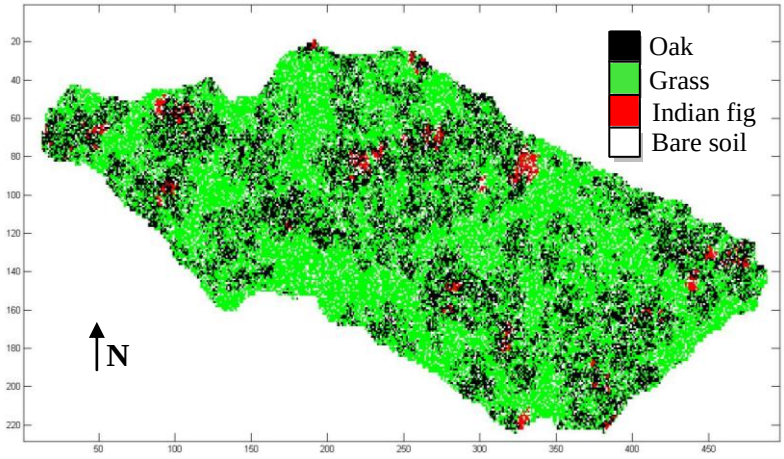

Figure 4.40. Flat surface simulation: vegetation distribution after 5,000 years in the modeled catchment.

Finally, in order to analyze the role of coexistence of the PFTs, simulations with single vegetation type in the basin for 5,000 years have been done (without effect of the soil thickness). In Figure 4.41 the time series of percent coverage of single vegetation type are shown. Looking at these results, we can state that using three vegetation types the observed pattern results from the competition. Without competition (single vegetation type) the single vegetation colonizes all the basin without a pattern. The percent plant coverage for each aspect class is almost the same (Figure 4.42).

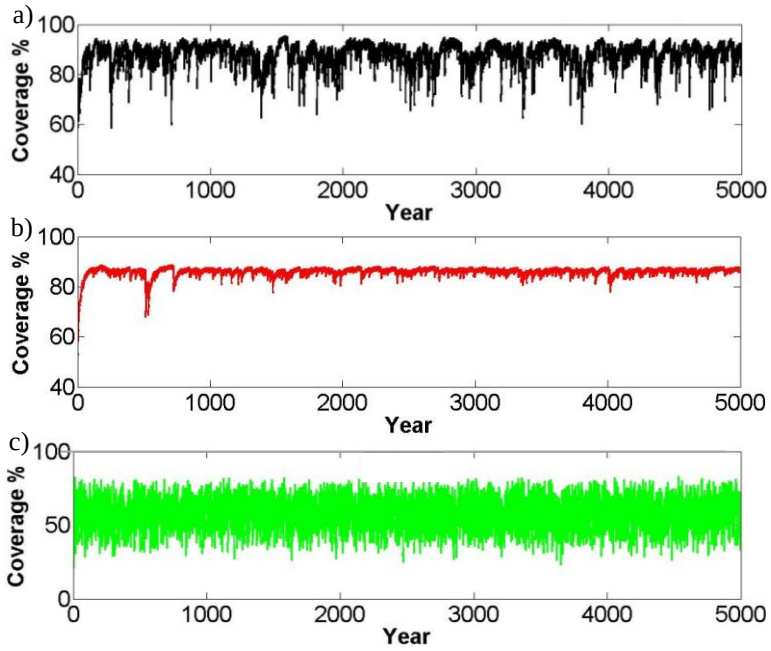

Figure 4.41. Time series of percent coverage of single vegetation type in the modeled catchment: (a) oak, (b) Indian fig, (c) grass.

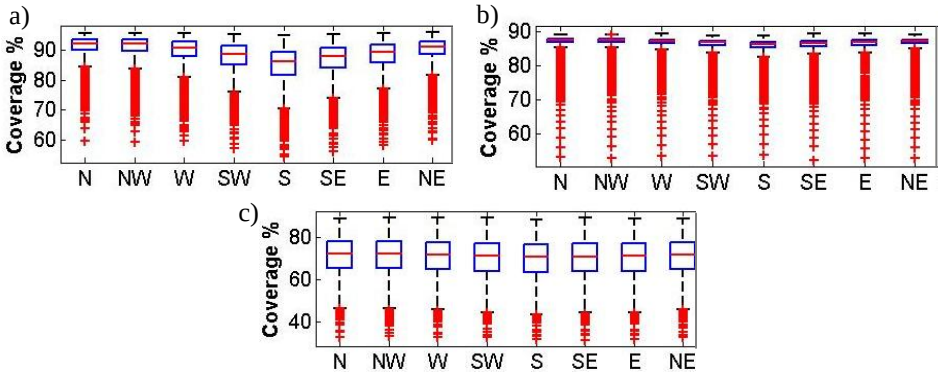

Figure 4.42. Percent plant coverage with respect to aspect for each vegetation: (a) oak, (b) Indian fig, (c) grass.

4.4. Result: *future run*, climate change analysis

4.4.1. Future scenarios

For the climate change analysis a transient climate scenario from 2001 to 2100 was generated as previously discussed (Section 4.2.2.1.3).

The annual cycles of observed temperature and precipitation along with the median predicted future temperature and precipitation for the period 2081-2100 are shown in Figure 4.43. As seen, the relative uncertainty for precipitation prediction is much higher than for air temperature. Results suggest a reduction of the annual precipitation and an increase of the annual temperature confirming the large scale predictions for the Mediterranean area (e.g., Giorgi and Lionello, 2008). Significant decreases of precipitation are predicted especially for March (26 mm), April (39 mm), November (22 mm), and December (45 mm). The maximum increase of temperature, 3° C, is predicted for the summer months, July and August, vice versa, the minimum temperature increase, 1.8° C, is predicted for April, November and December.

Using the re-parameterized AWE-GEN, we generated fifty realizations for the future climate, each consisting of hourly weather variables for 100 years. The median and the 5^{th} and 95^{th} percentiles of the fifty runs representing the stochastic variability in future annual precipitation and mean annual temperature are represented in Figure 4.44 and Figure 4.45, respectively. According to the median, the generated future climate scenarios are characterized by an annual precipitation reduction, from 815 mm to 576 mm (about 30% less in 100 years) and by a mean annual temperature increase, from 15.3° C to 18.1° C (+2.8° C in 100 years). The model uncertainty regarding precipitation prediction is much higher than that for air temperature.

Solar radiation, relative humidity and wind speed were also generated using AWE-GEN at hourly time scale. Changes of solar radiation, relative humidity and wind speed are not a direct consequence of the calculated factors of change, but are only due to the internal relationships used in the weather generator. For instance simulated changes in solar radiation are typically minor, as also confirmed by GCM outputs.

It is important to underline that the used stochastic downscaling do not contain any information about sources of uncertainty different from stochastic climate variability (e.g., future emission scenarios). Moreover, the uncertainty of climate change predictions due to different GCM realizations is only partially accounted for by the Bayesian weighing of the multi-model ensemble but not directly on the sampling of factors of change as done for instance in Fatichi et al. (2013). In order to derive the transient scenarios we were indeed forced to use only the median factors of change for all of the downscaled statistics.

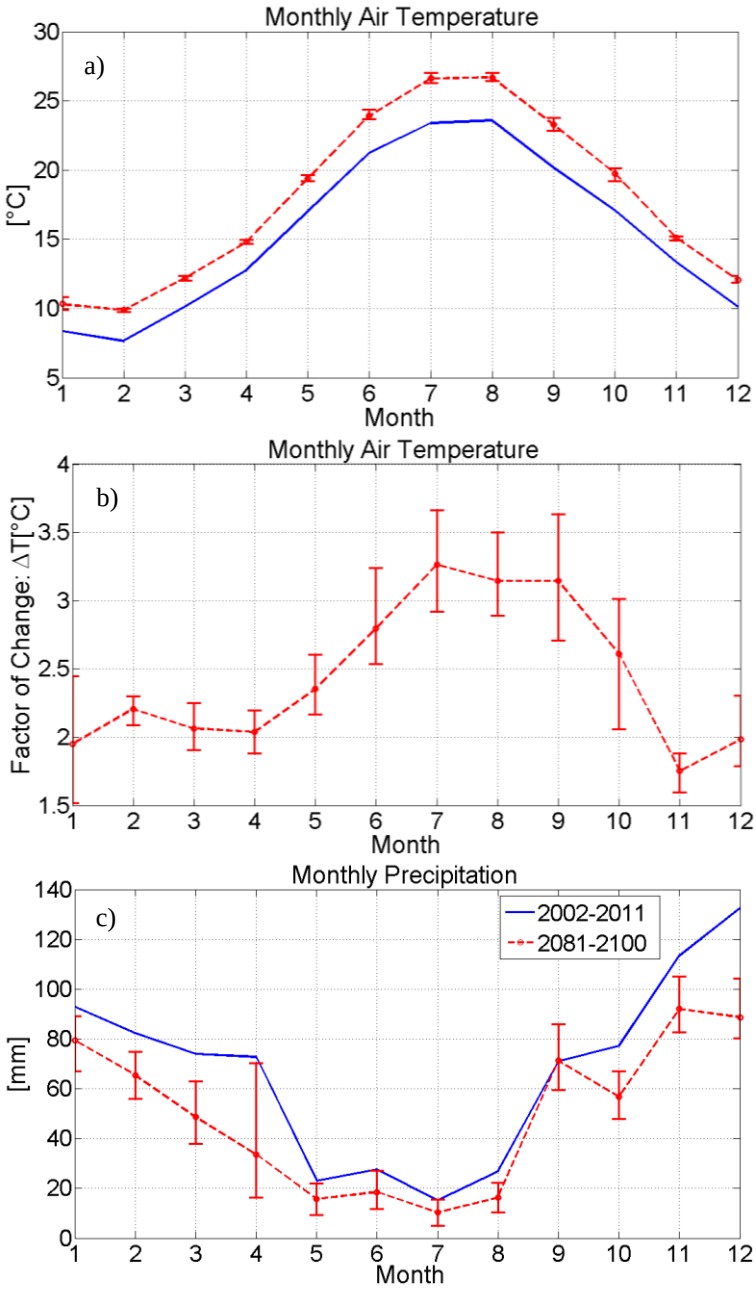

Figure 4.43. The effect of the factors of change on the annual cycles of monthly temperature and precipitation. The monthly temperature (a) and precipitation (c) for the period 2002-2011 (blue line) and for the period 2081-2100 (red dashed line) and the 10-90 percentile intervals (vertical bars); (b) the mean monthly temperature change (red dots) and the 10-90 percentile bounds (red vertical bars).

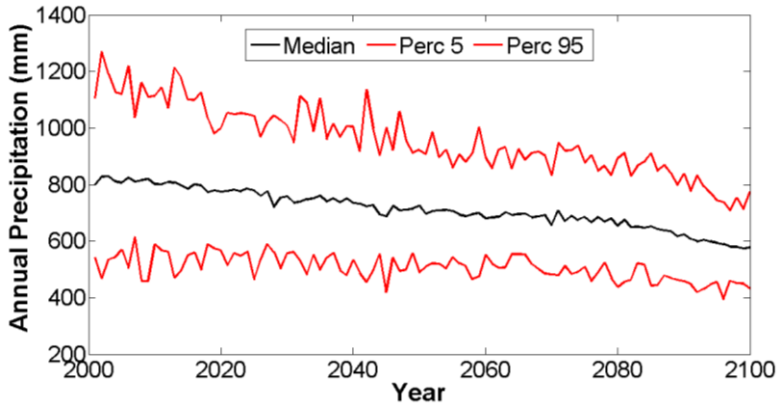

Figure 4.44. Annual precipitation (Median (black line), 5th percentile and 95th percentile (red lines)), 50 future runs.

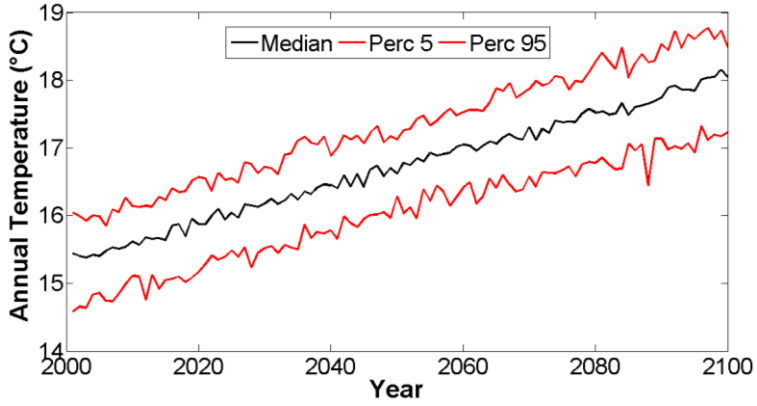

Figure 4.45. Mean annual temperature (Median (black line), 5th percentile and 95th percentile (red lines)), 50 future runs.

4.4.2. Effect of the future CO_2 concentration increase on vegetation

Climate change may also affect $T_{max\text{-}X}$ due to changes in air temperature, humidity, wind speed, and effects on cloudiness and atmospheric turbidity which, in turn, affect shortwave and longwave radiation. The increases in the concentration of CO_2 may also cause reductions in $T_{max\text{-}X}$ rates, due to the expected decrease of stomatal conductance which cause an increase in canopy resistance (Long et al., 2004, Moratiel et al., 2011; Fatichi and Leuzinger, 2013).

For grass the minimum canopy resistance r_c = 74.1 s·m^{-1} was derived by dividing the typical stomatal resistance r_s, equal to 100 s·m^{-1} (Table 4.4), for the

actively transpiring grass leaf surface, which was estimated as half of the LAI_{max} = 2.7 $m^2 \cdot m^{-2}$ as in Allen et al. (1998):

$$r_c = r_s/(0.5 \cdot LAI_{max}) \quad (4.4)$$

Assuming that the r_c = 74.1 $s \cdot m^{-1}$ applies under the current atmospheric CO_2 concentration, estimating a new r_c value for higher CO_2 concentrations could allow to estimate possible impacts of higher CO_2 concentrations on $T_{max\text{-}X}$. The current global CO_2 concentration is close to 400 ppm and it is projected to reach about 550 ppm by 2050 and 700 ppm by 2100 (IPCC, 2000).

Long et al. (2004) observed decreased stomata conductance by about 20% average for C_3 plants grown in elevated CO_2 concentration (about 550 ppm) in *FACE* (*Free-Air CO_2 Enrichment*) experiments, based on more than 200 independent measurements. Similar values were found in modeling studies (e.g., Fatichi and Leuzinger, 2013). Considering this 20% estimate as a reasonable estimate for the C_3 species, if the canopy resistance is 100 $s \cdot m^{-1}$, the stomatal resistance for grass should increase to r_s = 125 $s \cdot m^{-1}$. Using the same approach to calculate r_c in the evapotranspiration equation (Allen et al., 1998), the r_c for 550 ppm is calculated as:

$$r_c = r_s/(0.5 \cdot LAI_{max}) = 125 s \cdot m^{-1}/(0.5 \cdot 2.7 m^2 \cdot m^{-2}) = 92.6 s \cdot m^{-1} \quad (4.5)$$

assuming that the LAI_{max} will not change in the future. The approach was also applied to calculate r_c for oak and Indian fig.

Given the overall uncertainty of the CO_2 effects in reducing stomatal conductance especially in the long-term when plants might undergoes acclimation effects (Ainsworth and Long, 2005), the climate change simulations were carried out without and with the CO_2 concentration increase effect, using the following three *schemes*:

A. no decrease of stomatal conductance
B. linear decrease of stomatal conductance until 2100 (20% of decrease in 2050 and 40 % in 2100).
C. linear decrease of stomatal conductance until 2050 (20 % of decrease) and constant afterwards from 2051 to 2100.

The mean annual $T_{max\text{-}X}$ and $ET_{a\text{-}X}$ of each vegetation for the 2001-2010 and 2091-2100 periods and relative to the three above mentioned schemes are shown in Table 4.9 and 4.10 respectively. In the *scheme A*, e.g., without CO_2 effects on stomatal conductance, oak mean annual T_{max} will increase from 1383 mm in the period 2001-2010 to 1618 mm in the period 2091-2100 (+235 mm), the grass T_{max} will increase from 1175 mm to 1318 mm (+143 mm) and the Indian fig will increase from 571 to 657 mm (+86 mm). These increases are in the order of 11-15% for the different species.

In the *scheme B*, the oak T_{max} in the period 2091-2100 will be 1474 mm (+98 mm), the grass T_{max} will be 1269 mm (+97 mm) and the Indian fig T_{max} will be 585 mm (+20 mm). These increases are comprised between 3% for Indian fig

and 8% for grass. Therefore the CO_2 concentration increase can cause a considerable reduction of the $T_{max\text{-}X}$ increase.

Finally, if we considered the linear-constant decrease of the stomatal conductance (*scheme C*) the annual $T_{max\text{-}X}$ increase will be in the order of 6 to 10%.

The effect of the CO_2 increase is less marked for $ET_{a\text{-}X}$ due to the relatively dry nature of the analyzed climate. From 2001 to 2100, a reduction of the $ET_{a\text{-}X}$ due to the reduction of the precipitation can be observed. The oak mean annual $ET_{a\text{-}X}$ will be 431 mm (-19%) in the period 2091-2100 with the *scheme A*, 425 mm with the *scheme B* and 428 mm with the *scheme C* highlighting small differences and the dominant effect of precipitation changes. Similar small differences are observed for the two other species.

As consequence of the CO_2 increase and consequent stomatal closure, in the *scheme B* and *C*, we also considered a linear increase of the *WUE* for the three vegetation types from 2001 to 2100, in agreement with Wang et al. (2012) (Table 4.11). *WUE* has been estimated following Farquhar et al. (1989):

$$WUE = \frac{P_{air} C_{CO_2} (1-\alpha)}{\frac{g_v}{g_c}(e_i - e_a)} R_{c-a} \tag{4.6}$$

where P_{air} is the air pressure (KPa), C_{CO2} is the molar concentration of ambient CO_2 in the air (ppm), α is the ratio of intercellular to ambient CO_2 concentration (-), g_v and g_c are air diffusivities of water vapor and CO_2 respectively ($m^2 \cdot s^{-1}$), e_i and e_a are water vapor pressures inside the leaf and in the air respectively (KPa), $R_{c\text{-}a}$ is the ratio of mol weight of CO_2 to mol weight of air ($g_{CO2} \cdot g_{air}^{-1}$). We have considered C_{CO2} equal to 390 ppm in 2010 and 700 ppm in 2100 in accordance with the A1B emission scenario (IPCC, 2000).

Table 4.9. Mean annual $T_{max\text{-}X}$ for oak, grass and Indian fig in 2001-2010 and 2091-2100 period, for each scheme.

$T_{max\text{-}X}$ [mm]									
	Scheme A			Scheme B			Scheme C		
Years	Grass	Oak	Indian fig	Grass	Oak	Indian fig	Grass	Oak	Indian fig
2001-2010	1175	1383	571	1172	1376	565	1172	1376	565
2091-2100	1318	1618	657	1269	1474	585	1291	1537	604
increase	143	235	86	97	98	20	119	161	38
%	11	15	13	8	7	3	9	10	6

Table 4.10. Mean annual $ET_{a\text{-}X}$ for tree, grass and shrub in 2001-2010 and 2091-2100 period, for each scheme.

$ET_{a\text{-}X}$ [mm]									
	Scheme A			Scheme B			Scheme C		
Years	Grass	Oak	Indian fig	Grass	Oak	Indian fig	Grass	Oak	Indian fig
2001-2010	397	532	200	396	531	200	396	531	200
2091-2100	344	431	179	335	425	161	339	428	169

Table 4.11. Future *WUE* linear increment.

WUE $[Kg_{CO2} \cdot Kg^{-1}_{H2O}]$				
Years	CO_2 (ppm)	Oak	Grass	Indian fig
2010	390	0.009	0.005	0.02
2050	550	0.0103	0.0057	0.0228
2100	700	0.0111	0.0062	0.0243

4.4.3. Simulations of future scenarios

Fifty future simulations corresponding to fifty possible stochastic realizations of the 2001-2100 transient scenarios were simulated using CATGraSS for each scheme, for a total of one hundred and fifty transient simulations. Results are analyzed to identify the effect of the expected climate change on the vegetation distribution and on the biodiversity.

Changes of vegetation cover over time in the future climate scenarios for the 50 ensemble members of *scheme A* are shown in Figure 4.46, using the median, and the 5th and 95th percentile. The median trajectory highlights a decrease of oak (from 30.3% in 2001 to 20.7% in 2100) and Indian fig (from 5.3% in 2001 to 3.8% in 2100) and an increase of grass (from 40.9 % in 2001 to 54.8% in 2100). Looking at the 5th and 95th percentile of the fifty simulations in each year a large variability of grass cover can be observed (28.1-63.9%), oak shows a smaller variability (12.5-26.8%), and for the Indian fig the 5th and 95th are almost the same (3-4.3%).

For the same *scheme A*, the mean vegetation distribution for 2100 obtained considering the 50 runs of climate change still shows that aspect and slope will have an influence in the vegetation distribution but that grasses will be overall more dominant in the future scenario (Figure 4.47).

The estimated mean percentage of each vegetation type in 2001 and in 2100 according to the three schemes is shown in Table 4.12. In *scheme A*, in percentage there will be a 33% decrease for the oak, 28% for the Indian fig and a 26% increase for the grass. The effect of including a stomatal conductance

reduction effects due to the CO_2 concentration increase is illustrated in Figure 4.48 for the *scheme B* and in Figure 4.49 for *scheme C*. Comparing the three schemes, differences in the final results are very small as shown in Table 4.12. This aspect points out as the effect of the CO_2 concentration increase can be considered not important for the estimation of the future vegetation distribution in the Zafferia catchment because the overall $ET_{a\text{-}X}$ is very similar among the three schemes and dictated mostly by the available water resource (i.e., precipitation) (Table 4.10).

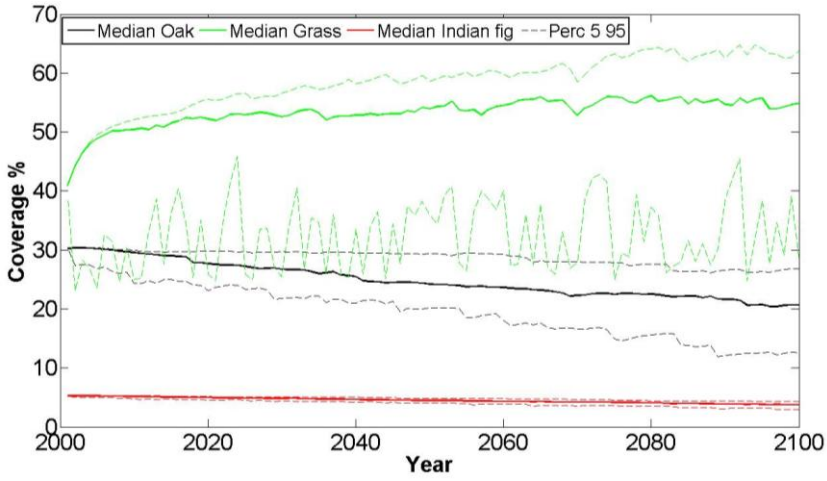

Figure 4.46. Vegetation coverage over time, 50 future runs, without CO_2 concentration increase (Median, 5th percentile and 95th percentile).

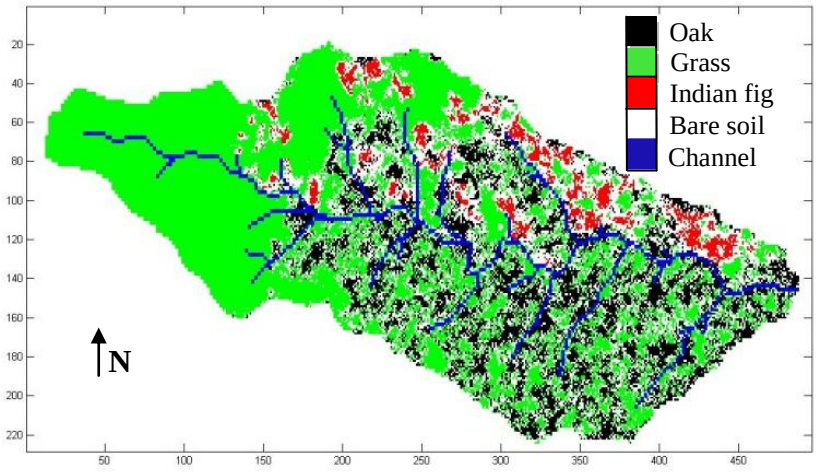

Figure 4.47. Final vegetation distribution (2100), mean 50 runs, without CO_2 concentration increase effect.

Table 4.12. Estimated mean percentage of each vegetation type in 2001 and in 2100.

Mean vegetation percentage [%] with climate change (50 runs)			
	Oak	Indian fig	Grass
Initial Vegetation	30.29	5.29	40.99
Scheme A	20.27	3.78	51.94
Scheme B	20.71	3.82	51.65
Scheme C	19.85	3.73	52.66

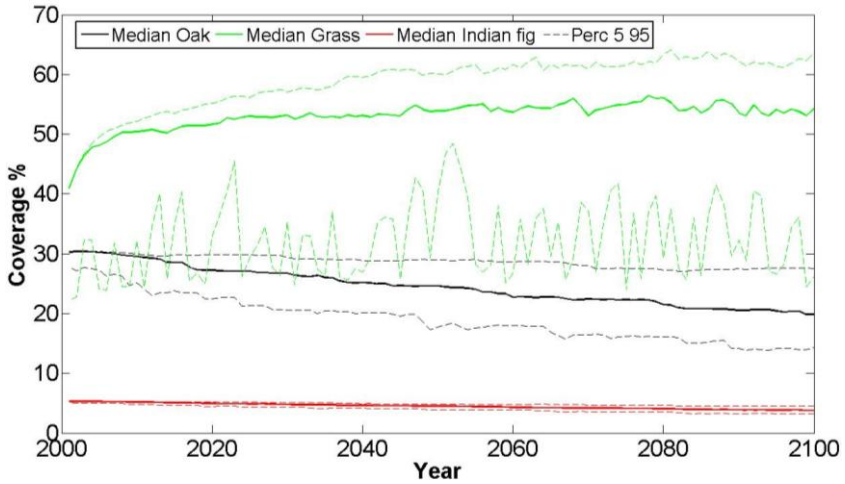

Figure 4.48. Vegetation coverage over time, 50 future runs, with linear decrease of stomatal conductance until 2100 (from 0 % to 40 %) (Median, 5th percentile and 95th percentile).

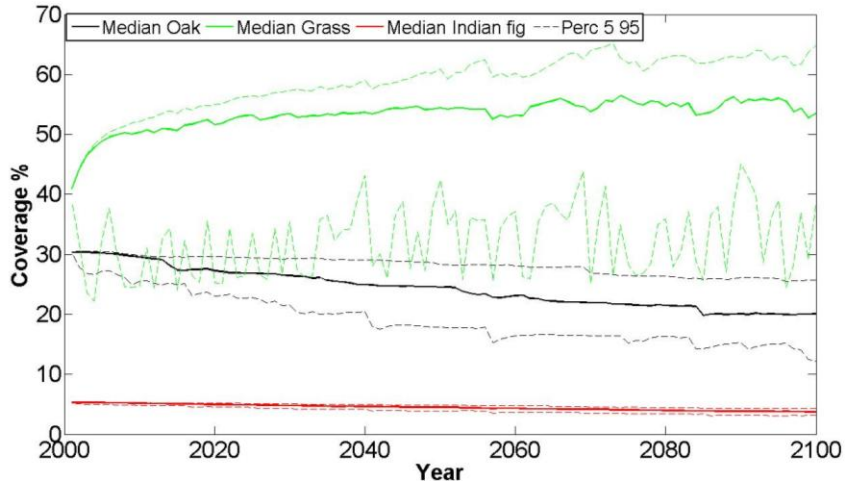

Figure 4.49. Vegetation coverage over time, 50 future runs, with linear decrease of stomatal conductance until 2050 (from 0 % to 20 %) and constant decrease from 2051 to 2100 (20 %) (Median, 5th percentile and 95th percentile).

Figure 4.50 shows the increase of the growing season length of the grasses with the climate change, in agreement with Walther et al. (2002).

In order to analyze how biodiversity change with the climate change in the *scheme A* we have used the already mentioned *SHDI* (Figure 4.51) and the Simpson index of biodiversity (*SIDI*) (Simpson, 1949) (Figure 4.52). While the *SHDI* is designed to emphasize the richness component of diversity, the *SIDI*, which ranges from 0 to1, emphasizes the evenness component and is defined as:

$$SIDI = 1 - \sum_{i=1}^{N} p_i \cdot p_i \tag{4.7}$$

where N is the number of vegetation type and p_i the proportional abundance of the i^{th} type. The median *SHDI* decreases from 1.88 in 2001 to 1.78 in 2100 (Figure 4.51). The median *SIDI* decreases from 0.74 in 2001 to 0.65 in 2100 (Figure 4.52). Therefore, the end of the century could be characterized by a reduction of the biodiversity, due to the grass expansion and reduction of oaks and Indian figs.

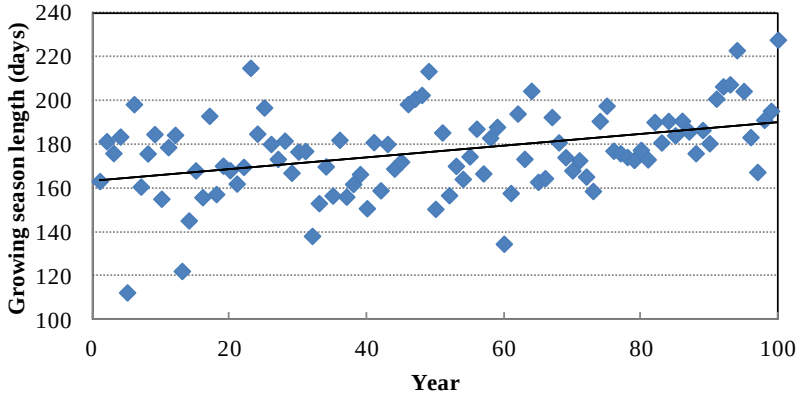

Figure 4.50. Growing season grass over the future years.

In order to identify the critical point in this evolving situation that may lead to a new and irreversible change (search of a tipping point), the model has been run, for another 800 years, starting from the mean final vegetation distribution of the 2100 (Figure 4.53). The climate forcing of this simulation has kept identical to the 2100 climate. The result of this simulation shows that a tipping point can occur after 300 years, and after 800 years most of the trees will disappear (oak percentage will be very low) (Figure 4.53a) and consequently the *SHDI* index will largely decrease (Figure 4.53b). In Figure 4.54 are shown: (a) vegetation distribution in 2100, (b) vegetation distribution in 2300, (c) vegetation distribution in 2500, that underline the strongly increasing of grass and reduction of oak in 400 years. These results indicate that the simulated vegetation

distribution is not in stable condition in the year 2100, and will eventually move from an ecotone environment (high-biodiversity) towards a grassland-dominated landscape (low-biodiversity) if climate change persists.

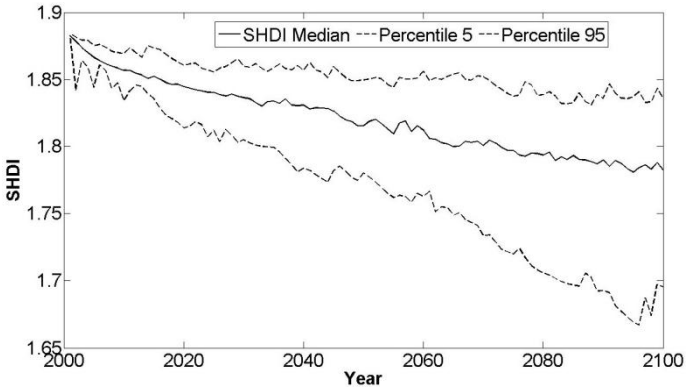

Figure 4.51. Shannon index of diversity, SHDI, 50 future runs (Median (black line), 5th percentile and 95th percentile (black dashed lines)).

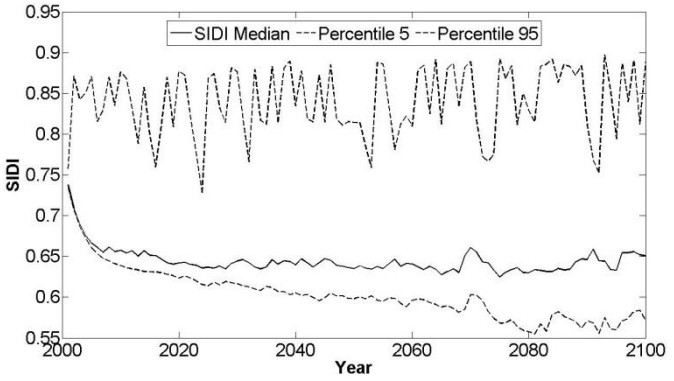

Figure 4.52. Simpson index, SIDI, 50 future runs (Median (black line), 5th percentile and 95th percentile (black dashed line)).

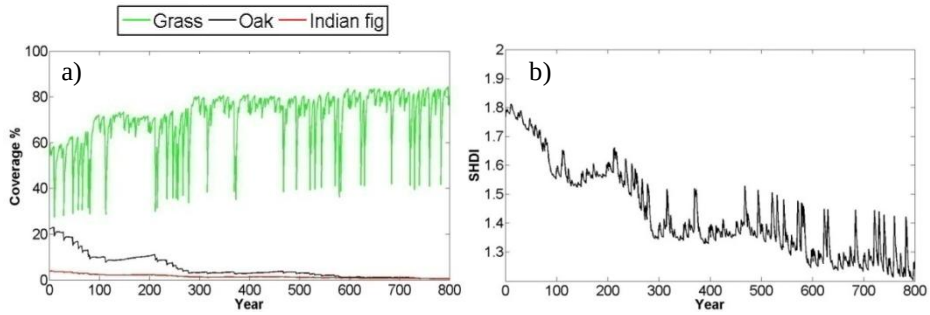

Figure 4.53. Tipping point analysis: (a) vegetation coverage over 800 years, (b) *SHDI* index.

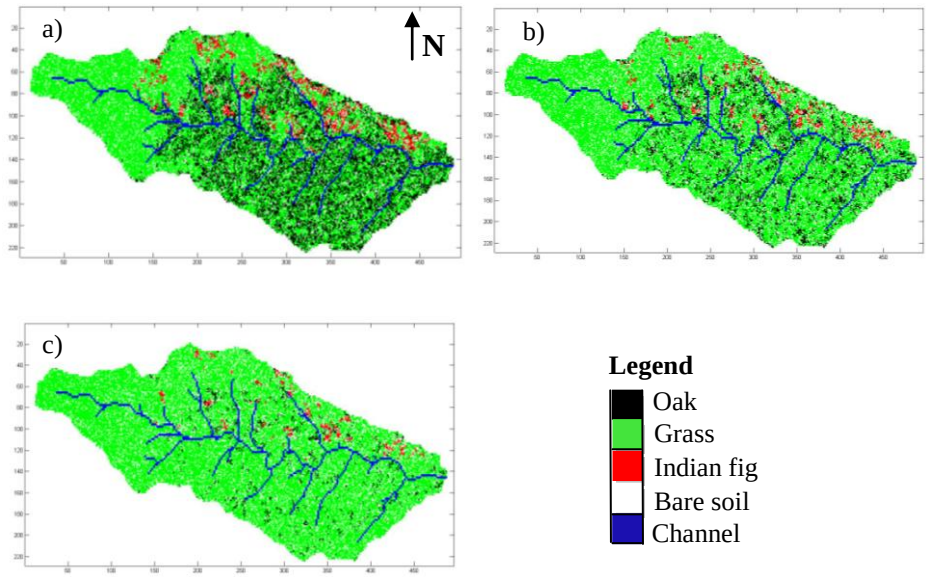

Figure 4.54. Tipping point analysis starting from 2100 to 2500 with constant climate of 2100: (a) vegetation distribution in 2100, (b) vegetation distribution in 2300, (c) vegetation distribution in 2500.

Chapter 5

Modeling the shrub and juniper encroachment in the american grasslands

Numerous studies have documented the expansion of woodlands and shrublands in the intermountain West America grasslands; however, few have compared the chronology of expansion for woodlands and shrubland across different geographic regions or determined the mix and extent of presettlement stands. We have studied this problem using, for the first time in literature, an ecohydrological CA model. We evaluated shrub and juniper establishment and encroachment for two grassland areas in Oregon and New Mexico, respectively.

Since 1870, the area occupied by western juniper has increased 125 to 625 percent in Oregon (Miller et al., 2008). The increase of trees was a result of infill into shrub-steppe communities with relatively open low density stands of trees and expansion of juniper into sagebrush-steppe communities that previously did not support trees. The majority of woodlands are still in the early to mid phases of stand closure, which means they often support an understory of shrubs and herbaceous vegetation. This has implications for future changes that will occur within these woodlands in the next 30 to 50 years. In the absence of disturbance or management, the majority of these landscapes will become closed woodlands resulting in the loss of understory plant species and greater costs for restoration (Miller et al., 2008). In this thesis juniper encroachment is studied inside the Ochoco National Forest, Crook County, in Oregon where a strongly western juniper encroachment started in 1870 (Miller et. al., 2005).

On the other side, since 1860, the encroachment of shrubs in North American deserts, has been particularly well documented for the Sonoran and Chihuahuan deserts (Buffington and Herbel, 1965; Archer et al., 1988). To this end, data from the *Sevilleta National Wildlife Refuge* (SNWR), located in the northern Chihuahuan desert, New Mexico, have been used. The creosote bush encroachment into native desert grassland of the SNWR is here studied.

This chapter provides in section 5.1 the case study of the shrub encroachment in SNWR and in section 5.2 the case study about the juniper encroachment in the Ochoco National Forest.

5.1. Case study: Sevilleta encroachment

5.1.1. Site description

In order to simulate the shrub encroachment, we selected a site in the SNWR (34°24' N, 106°59' W), located in the northern Chihuahuan desert of the Rio Grande Valley, approximately 80 km south of Albuquerque and 32 km north of Socorro, New Mexico (South-West of USA) (Figure 5.1). The Rio Salado flows through the refuge. The SNWR shows a dramatic encroachment front of creosote bush (*Larrea tridentata*) shrubs into native desert grassland (Figures 5.2, 5.3). Encroachment started in 1858 (Buffington and Herbel, 1965), 150 years ago (Van Auken, 2000).

More than 50 % of the annual precipitation falls during the North American Monsoon (MAP ~ 250 mm), and mean monthly temperatures ranges between 2.5° C in January and 25° C in July. Climatic data have been registered from *Deep Well Weather Station Site* (DWWSS) maintained by the *Sevilleta Long Term Ecological Research* (LTER), from 1990 to 2008.

Figure 5.1. Location of the Sevilleta National Wildlife Refuge, central New Mexico (Kurc and Small, 2004; 2007).

Figure 5.2. (a) Desert grassland, (b) shrubland (creosote bush), and (c) tree (juniper) in SNWR.

Figure 5.3. Grassland-shrubland transition zone in the northern Chihuahuan Desert (D'Odorico et al., 2010).

The study area location is shown in Figure 5.4 and it has got an area of 7.34 Km^2. The land cover map of the SNWR, overlain by the boundary of the study site and the DWWSS are shown in Figure 5.5. The study site is an alluvial fan deposit of the Sierra Ladrones formation (Green and Jones, 1997), sandy loam texture, overlain by a gravelly desert pavement, generally characterizes the soil type (Gutiérrez-Jurado et al., 2006).

A Sevilleta 10 m *Interferometric Synthetic Aperture Radar* (IFSAR) DEM (Figure 5.6a) (source: http://sev.lternet.edu/) is used for the modeling study (Gesch et al., 2002). This area is located in the elevation range of 1558 m to 1634 m a.s.l., the slope angle ranges from flat surfaces to as high as 45.9° on hillslopes, with an average of 3.9° (Figure 5.6b). The aspect map is also shown in Figure 5.6c.

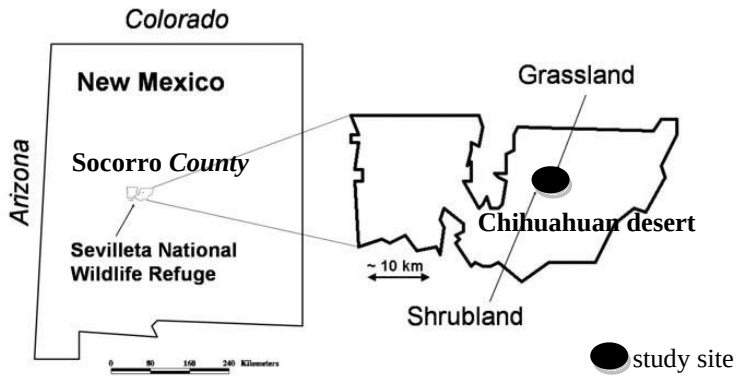

Figure 5.4. Location of the site in the SNWR.

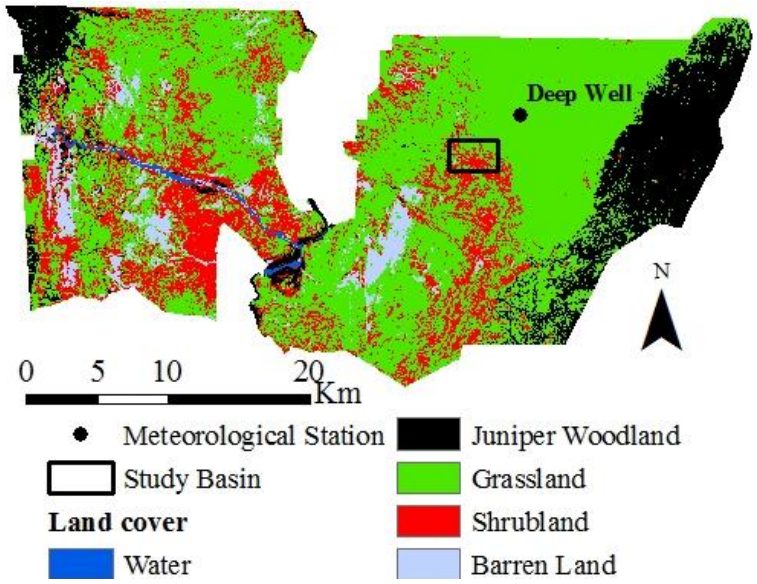

Figure 5.5. Study site in central New Mexico: the land cover map of the SNWR, overlain by the watershed boundary of the study site and the DWWSS.

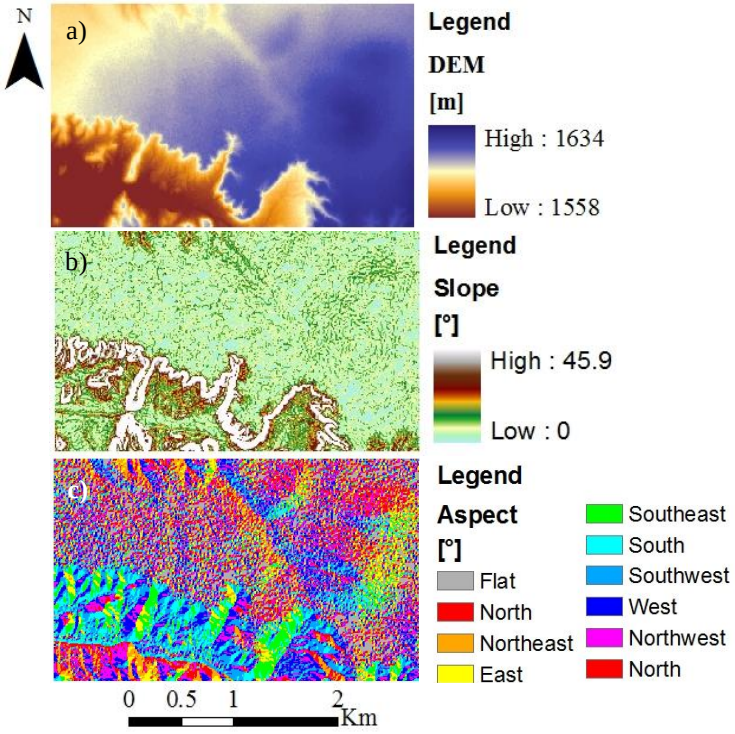

Figure 5.6. Topography of the site: (a) DEM, (b) slope, (c) aspect.

In Table 5.1 the general site characteristics for the study site are shown. The mean annual precipitation (MAP) is 242 mm, the mean annual temperature (MAT) is 13.3° C and the potential evapotranspiration (PET) is 747 mm.

Table 5.1. Site characteristics (Knapp et al., 2008b).

Site, state	Latitude/ longitude	Biome type (site code)	MAP/MAT (mm °C^{-1})	PET (mm)	Growing season length (days)	Dominant grassland species (photosynthetic pathway)	Dominant shrub species E = evergreen, D = deciduous, N = putative N-fixer
Sevilleta National Wildlife Refuge, NM	34.1/−106.9	Chihuahuan desert (CHI)	242/13.3	747	210	*Bouteloua eriopoda* (C_4) Black grama	*Larrea tridentata* (E) Creosote bush

5.1.2. Data

5.1.2.1. Vegetation distribution

The Sevilleta Refuge contains extensive semi-arid grassland dominated by C_4 perennial grasses: blue grama (*Bouteloua gracilis*), black grama (*Bouteloua eriopoda*), galleta (*Pleuraphis torr.*), poaceae (*Sporobolus spp.*), James' galleta (*Hilaria jamesii*) and muhley grass (*Muhlenbergia spp.*); they are located on relatively level topography along western edge of the Los Pinos Mountins. The shrub is creosote bush (*Larrea tridentata*) (see section 2.1) with a current coverage equal to 42%. Grass is deciduous and creosote bush is evergreen. The growing season length is equal to 210 days and the dominant vegetations are blue grama and creosote bush.

In Figure 5.7 the current vegetation distribution of the study area is shown in the SNWR *National Land Cover Database 2006* (NLCD, 2006) map having a 28.5 meters resolution (http://sev.lternet.edu/), while Figure 5.8 shows the Google map 2013 of the Sevilleta study site using the exact extent of Figure 5.7 (i.e., the two figures can be perfectly overlapped).

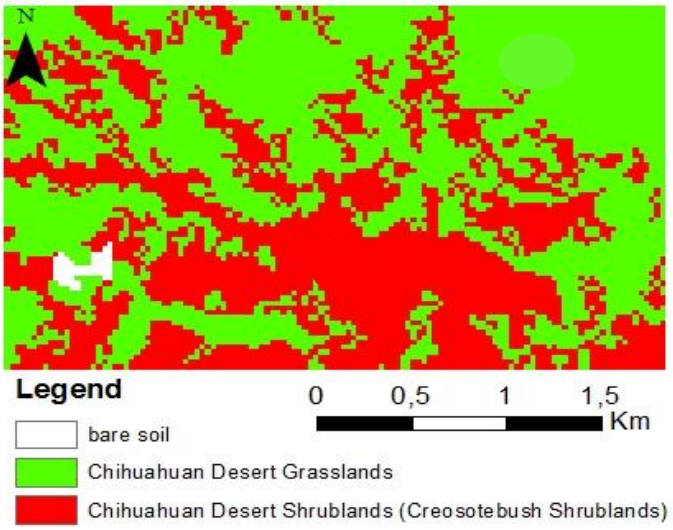

Figure 5.7. Vegetation distribution in the study site (NLCD, 2006).

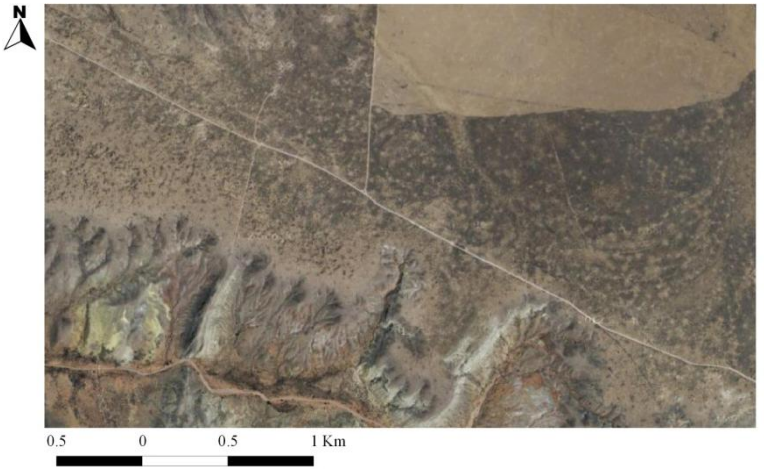

Figure 5.8. Google map of the Sevilleta study site (2013).

In order to compare the different vegetation pattern and coverage in the shrubland and in the grassland relative to this area, Kurc and Small (2004) collected data from the McKenzie flats area. They collected measurements from a grassland and a shrubland which are separated by 2 km. The grassland is nearly monospecific, dominated by black grama which covers about 60% of the ground surface (Figure 5.9a). The shrubland site is also monospecific, dominated by creosote bush which covers about 30% of the ground surface (Figure 5.9b).

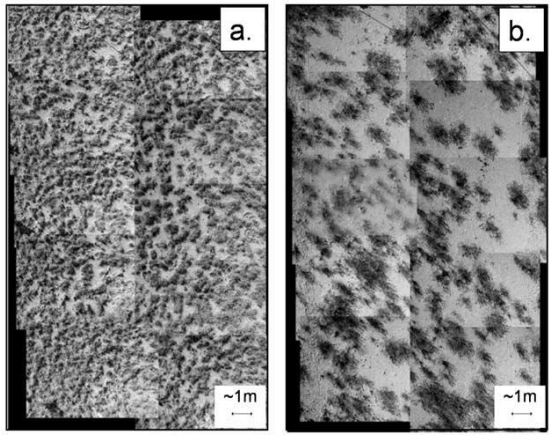

Figure 5.9. Overhead photo surveys of (a) grassland and (b) shrubland taken in January of 2002. The grassland has ~60% cover, and the shrubland has ~30% cover (Kurc and Small, 2004).

5.1.2.2. Historical precipitation, temperature and wind

In Figure 5.10 the historical annual precipitation in Socorro County, NM, from 1893 to 2008 is shown (source NOAA - *National Oceanic and Atmospheric Administration*); the MAP is equal to 239 mm (like Hall and Penner, 2013) (station elevation: 1398 m a.s.l.). The historical annual precipitation is in accordance with the historical annual precipitation measured by 8 stations in the Southeastern Arizona from 1898 to 1989 (Bahre and Shelton, 1993). In Figure 5.11 and 5.12 the wet and dry season annual precipitations are shown, respectively. Hall and Penner (2013) demonstrated that 12,800 years ago the temperature was about 2.4° C cooler and the precipitation over 100 mm than today. The greatest change was between 12,800 years ago and 3,300 years ago and in the last 150 years there was not climate change.

There was not climate change during the period 1893-2008. In fact, the Mann-Kendall (Mann, 1945; Kendall, 1962) test has been carried out with a significance level (α) equal to 0.01 for the annual precipitation data, for the wet and dry season precipitation data and results show the absence of a statistically significant trend in all the cases.

In Figure 5.13 the historical MAT in Socorro (1893-2008) is shown. The MAT is about 14° C. The Mann-Kendall test has been done with α equal to 0.01 for the mean annual temperature data and there is not a statistically significant trend at annual scale.

Moreover, even if the temperature and the precipitation are available, for this site there are missing data in forty-one years. The solar radiation, humidity, vapor pressure and wind speed are not measured by the station. Since these data

are missing, in order to have a better description of the site weather, the data of the DWWSS have been used.

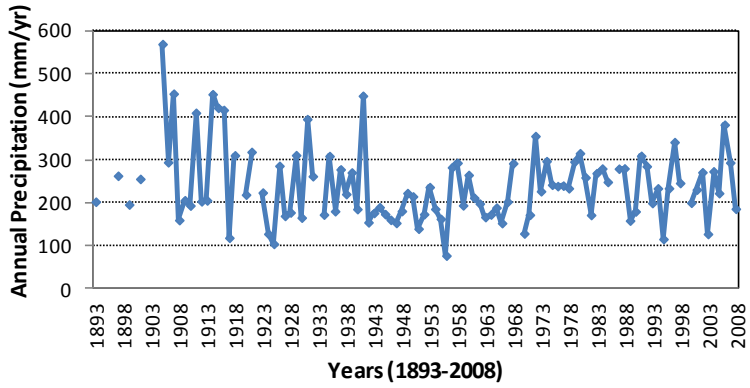

Figure 5.10. Historical annual precipitation in Socorro County.

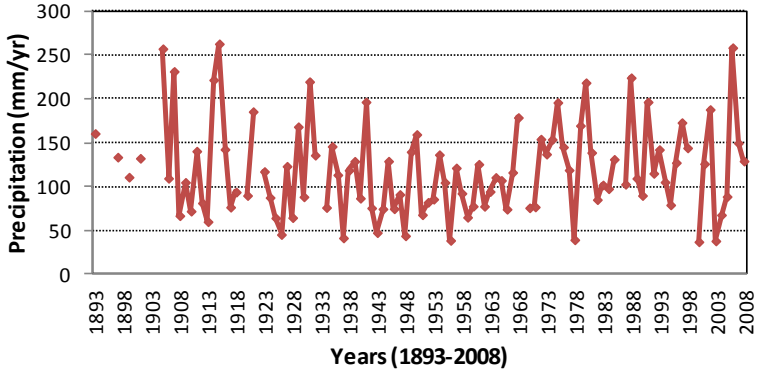

Figure 5.11. Historical annual precipitation in the wet season in Socorro County.

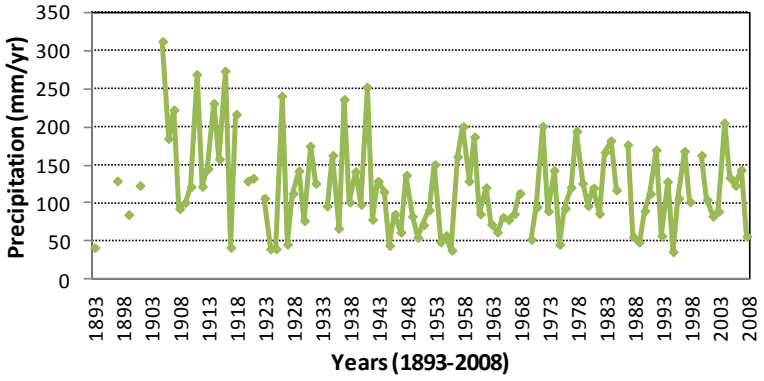

Figure 5.12. Historical annual precipitation in the dry season in Socorro County.

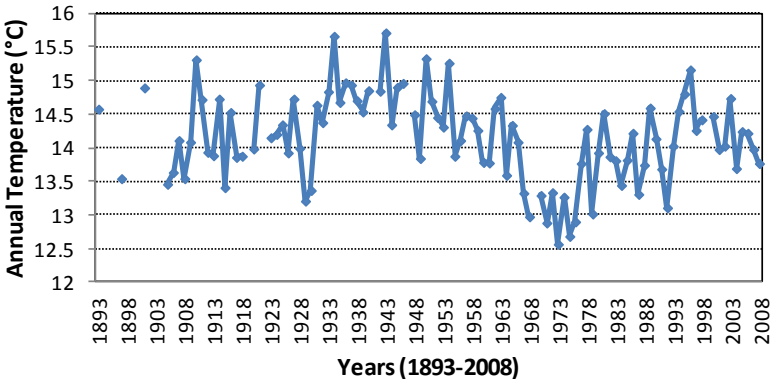

Figure 5.13. Historical MAT in Socorro County.

Assuming the absence of climate change in the past 150 years, nineteen years of the DWWSS data, from 1990 to 2008, for which all the weather variable data are available (i.e., hourly precipitation, temperature, wind speed, relative humidity, incoming shortwave solar radiation, vapor pressure, soil moisture potential, and soil temperature) have been used. The MAP is 246.4 mm with more than half of the precipitation falling during the monsoon season (July-September): high-intensity summer monsoon season during which approximately 50% of the MAP falls, and low-intensity winter rainfalls, controlled by broad-scale frontal systems (Gosz et al., 1995; Gutiérrez-Jurado et al., 2006). The wet season can be considered coincident with the monsoon season from July to September, 92 days, while the dry season is from October to June, 273 days. In Table 5.2 the observed rainfall parameters for the Deep Well weather station has shown.

Table 5.2. Observed rainfall parameters for the DWWSS (1990-2008).

Parameter	Description	Observations
P	Mean annual precipitation [mm]	249.1
P_d	Dry season precipitation [mm]	125.6
P_w	Wet season precipitation [mm]	123.5
$T_{b,d}$	Dry season interstorm period [h]	159.3
$T_{b,w}$	Wet season interstorm period [h]	84.1
$T_{r,d}$	Dry season storm duration [h]	2.1
$T_{r,w}$	Wet season storm duration [h]	2.5
h_d	Mean storm depth dry season [mm]	4.8
h_w	Mean storm depth wet season [mm]	3.1

In order to understand if the wind direction could have influenced the shrub encroachment direction, the wind direction data have been retrieved and analyzed. In particular, the wind direction predominant at the study site is from

southeast to northwest (source: http://www.eldoradocountyweather.com) as shown in Figure 5.14. While the red circle indicates the study area in New Mexico, the blue circle indicates the study site in Oregon (see section 5.2).

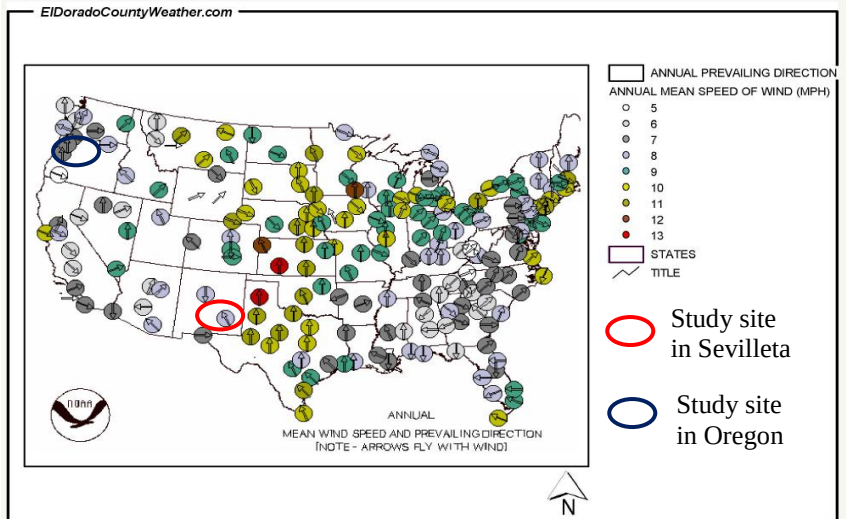

Figure 5.14. Wind speed direction in the USA (source: *Western Regional Climate Center*).

5.1.2.3. Future precipitation and temperature

The latest report on climate change of the Intergovernmental Panel on Climate Change (IPCC) (IPCC, 2013) shows, in the study area, a reduction of the monsoon precipitation of 20 mm and an increase of the temperature of 4° C.

Using a GCMs ensemble (eight GCMs: CCSM3, CSIRO-Mk3.5, ECHAM-5, IPSL-CM4, CGCM3.1, GFDL, INGV, MIROC3.2) and doing a stochastic downscaling, the medians of the future precipitation and temperature, for the period 2001-2100, were obtained with the AWE-GEN (Figures 5.15-5.17). The procedure was already described in section 4.2.2.1.3. In the period 2001-2010, the MAP is 104.5 mm in the wet season (July-September) and 149.15 mm in the dry season. In the period 2091-2100, the MAP is 88.97 mm in the wet season and 168.98 mm in the dry season (Figure 5.15a). For the future, the GCMs forecast a reduction of the Monson precipitation, from 104.5 mm to 88.97 mm, and an increase of the temperature of 4.2° C (Figure 5.15b).

The present and future precipitation and temperature for each month are shown in Figures 5.16a, c, respectively. The 10-90 percentile intervals inferred from monthly posterior distributions of the factor of change for the future scenario (FUT) are plotted along with the annual cycles of air temperature and precipitation. In the Monson season the precipitation will reduce, but it will increase in the dry season. The prediction of an increase of air temperature can

be regarded as very likely. The magnitude of this change is around 3-5° C. In Figure 5.16b the mean monthly temperature change (black dots) and the 10-90 percentile bounds (red vertical bars) are shown. The maximum monthly temperature increase will be in September, 5° C, and the minimum increase will be in February, 2.8° C. The uncertainty bounds for the air temperature changes are generally less than 2° C. Figure 5.16c shows the annual cycle of observed precipitation along with the mean predicted future precipitation that also includes the 10-90 percentile intervals. As seen the relative uncertainty for precipitation prediction is much higher than for air temperature. For instance, for the month of November the 10-90 percentile interval may indicate both a reduction and an increase in precipitation. Nonetheless, for most months the confidence about sign of the future change is much higher. Significant decreases are predicted for July, August and September, vice versa significant increase are predicted for January and February.

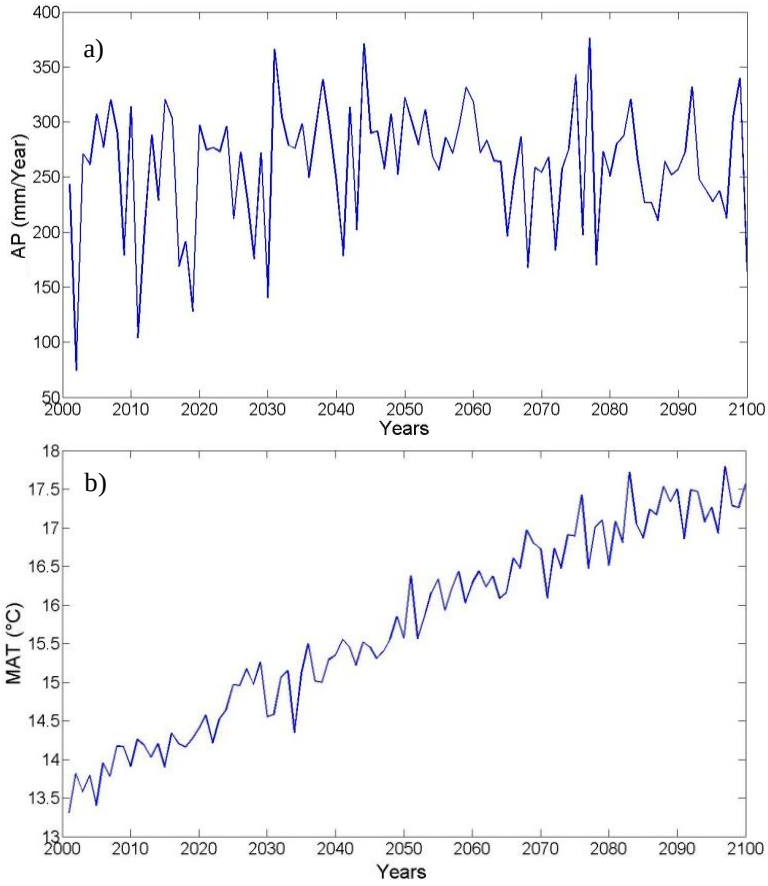

Figure 5.15. Downscaling GCMs: (a) future annual precipitation (AP); (b) future MAT.

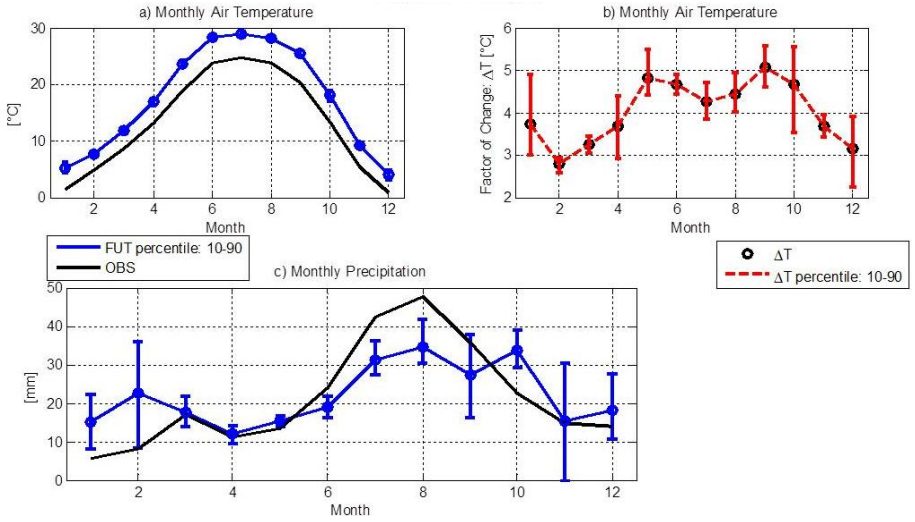

Figure 5.16. The effect of the factors of change on the annual cycles of monthly temperature and precipitation for the location of Sevilleta: (a) monthly air temperature, (b) factor of change MAT, (c) monthly precipitation (2081-2100).

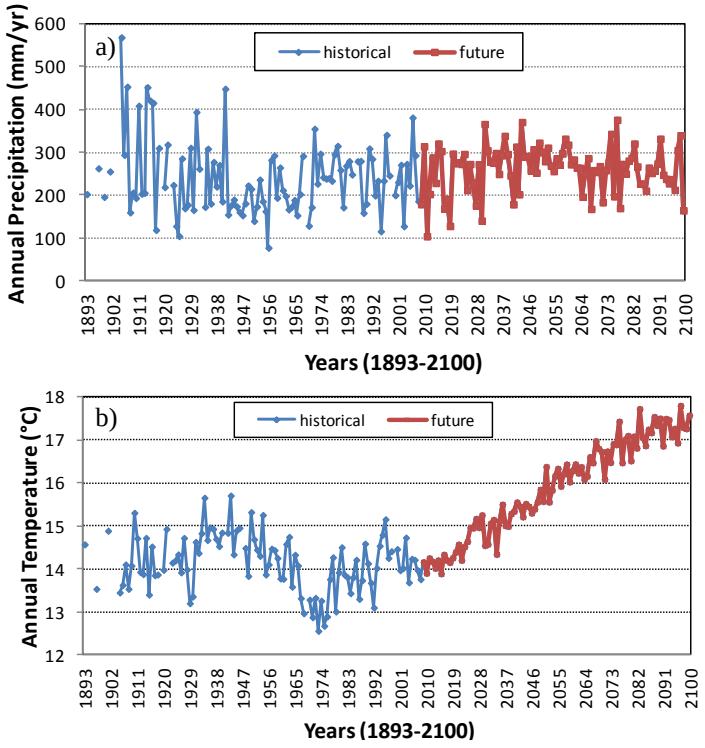

Figure 5.17. (a) Historical and future mean annual precipitation, and (b) temperature (1893-2100).

Comparing the historical and future precipitation (Figure 5.17a) and temperature (Figure 5.17b), the future MAP will be the same of the period 1960-2000, while the future temperature will increase. In 1903 the MAP is 569 mm and there is a reduction of MAP from 1903 to 1956 (77 mm); after this period the precipitation is almost stationary. In accordance with Seager et al. (2007) and http://www.nmdrought.state.nm.us/ClimateChangeImpact/completeREPORTfinal.pdf, in the past there was not a trend of temperature and precipitation change, vice versa in the future there could be a strong increase of the temperature and a reduction of the monsoon precipitation.

5.1.3. Model simulations

The verb encroach means: advance gradually causing damage. So by the selection of the verb used in the literature we know that a shrub line has moved during the time. It can be assumed that this movement is characterized by two time scales, long (5,000 years) and short (150 years). Most of the encroachment literature talks about the last 150 or more years. However shrubs have moved before from far south to north Mexico during a long term and slow processes in the last 4,000 or more years (e.g., Holmgren et al., 2007). In fact C_4 herbs and grasses persisted from late Pleistocene to the present, whereas many C_3 desert shrubs did not occupy the northern extent of their ranges until the last 4,000-5,000 years.

Our approach, ideally, builds potential cases of simulation scenarios and discusses the processes starting from that has been observed in the region:

a) *long time scale*: 5,000 years - under this scenario, we setup the model with equally distributed species (33% grass, shrub and bare soil), trying to obtain a stationary vegetation behavior coherent with the observed pattern. The simulation is run for 5,000 years, forced by statistically generated storms using a Poisson process and a cosine function to reproduce the annual cycle of the potential evapotranspiration.

b) *short time scale*: 150 years (from 1861 to 2010) - encroachment from ecotone boundary. This simulation is designed and carried out with the aim to reproduce the fast and recent encroachment phenomenon. Starting from 19 years of observed weather data of the DWWSS, 150 years of weather data have been obtained using the AWE-GEN and they have been used in input to the CATGraSS model for the encroachment simulation from 1861 to 2010, using as initial condition the final vegetation percentage obtained in the *long time scale* simulation.

5.1.3.1. Model set up

PFTs are defined at a 5m by 5m grid as described in section 4.2.1 for the Zafferia catchment.

The soil is modeled as sandy-loam and the parameters used in the model are shown in Table 5.3 assuming a spatially uniform soil thickness.

Site morphology has been classified into topographically similar slope-aspect (*S-A*) groups, considering a 6 degree increment for local slopes (5-47°) (8 slope classes) and a 30 degree increment for aspect (0-360°) (13 aspect classes) leading to 104 different combinations (*S-A* groups) in order to get and analyze the effect of the *Slope-Aspect* group on the vegetation distribution.

Table 5.3. Soil parameters used in the water balance component of the model.

Soil Texture	N [-]	s_{fc} [-]	I_{c-b} [mm·d^{-1}]	K_s [mm·d^{-1}]	B [-]
Sandy Loam[1]	0.43[2]	0.56[2]	0.83[3]	1.75[4]	4.9[2]

Source: (1) Soil Survey Staff (1994); (2) Laio et al. (2001); (3) calibrated based on Gutierrez-Jurado et al. (2006); (4) Bhark and Small (2003).

5.1.3.2. Weather forcings

5.1.3.2.1. Long time scale weather forcings

The model has been forced by daily rainfall and PET. The precipitation time series has been generated with a simplified stochastic Poisson process calibrated with the historical observed precipitation. The PET annual cycle has been obtained from a stationary cosine function fitted to mean daily values of PET calculated from the daily Penman-Monteith equation using the DWWSS data.

In storm generation, the *Poisson Rectangular Pulses* (PRP) model has been used, with a one-parameter exponential distribution for time between storms (T_b) and storm durations (T_r); and a Gamma distribution for rainfall depth h conditioned on T_r (e.g., Ivanov et al., 2007). The storm intensity p, is calculated as: $p=h/T_r$. The two rainfall seasons (wet and dry) have been considered, with seasonal precipitations denoted by P_w and P_d. For the wet season the parameters are (subscript w denotes the wet season):

$$T_{b,w}=3260\cdot(P_w\cdot 365/N_{d,w})^{0.59} \quad (5.1)$$

$$H_w=P_w\cdot(T_{b,w}/(N_{d,w}\cdot 24)) \quad (5.2)$$

$$R_{var,w}=7500\cdot((P_w/N_{d,w})\cdot 365)^{-0.6} \quad (5.3)$$

$$T_{r,w}=T_{b,w}/(R_{var,w}-1) \quad (5.4)$$

where $R_{var,w}$ is the rainfall variability and $N_{d,w}$ is the number of day of the wet season. The same equations are used for the dry season. These equations are obtained from calibration using DWWSS data (Istanbulluoglu and Bras et al, 2006). The rainfall parameters are shown in Table 5.2.

Daily maximum transpiration ($T_{max\text{-}X}$) is obtained from the cosine function fitting (3.40) to calculated $T_{max\text{-}X}$ for each PFT (3.36). $\overline{T}^{F}_{\max -X}$ ($\overline{T}^{F}_{\max -X}$=5.4901-0.0021·$P$), L_T equal to 0 days (peak T^{H}_{Cos-X} occurs when DOY is equal to N_d /2, consistent with the climate in the region), and Δ (Δ=0.858· $\overline{T}^{F}_{\max -X}$+2.8662) are obtained for each vegetation from calibration using DWWSS data (following Istanbulluoglu and Bras, 2006). As previously made in chapter 4, to reduce data requirements and keep the model simple, the bare soil T_{max}, E_b, is taken as a fraction (f_b) of the maximum grass transpiration rate, $T_{max\text{-}G}$ (e.g., E_b=f_b·$T_{max\text{-}G}$) (e.g., Mutziger et al., 2005; Istanbulluoglu et al., 2012; Zhou et al, 2013). The value of f_b is set to 0.7 like Istanbulluoglu et al. (2012) and Zhou et al. (2013).

5.1.3.2.2. Encroachment weather forcings

For the encroachment analysis, starting from 19 years of observed weather data (from 1990 to 2008) of the DWWSS, 150 years of weather, obtained using the AWE-GEN, have been used as input to the CATGraSS model for the encroachment simulation from 1861 to 2010. Since the CATGraSS model works at daily and interstorm time scale, the hourly precipitation data have been aggregated. The potential evapotranspiration has been calculated using the DWWSS data with the Penman-Monteith equation. Stationary precipitation (Figure 5.18) and temperature have been considered because, as previously mentioned, there was not a statistically significant variation of such variables in the past century (Figures 5.10, 5.13).

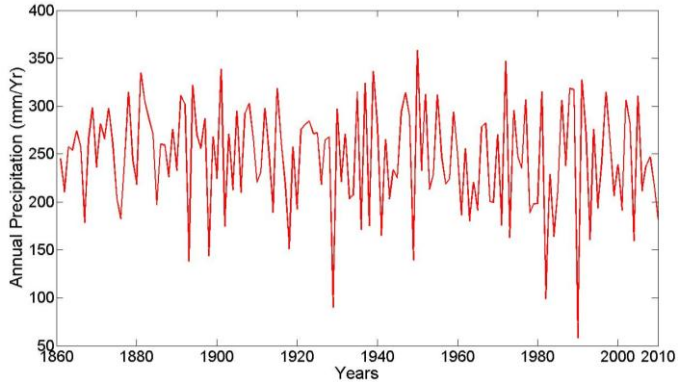

Figure 5.18. Annual precipitation for the period 1861-2010 obtained with the AWE-GEN using DWWSS data.

5.1.4. Long time scale: 5,000 years simulation

5.1.4.1. Model calibration

The model has been calibrated to reproduce the initial shrub percentage in the study area before encroachment in 1860 with a 5,000 years simulation without encroachment causes (fire return period, T_F, constant and equal to 10 years and no grazing effects).

Vegetation parameters here used for simulating local water balance and plant dynamics (e.g., biomass production and loss) come from the work of Zhou et al. (2013) and they are listed in Table 5.4.

Table 5.4. Plant parameters used to simulate soil moisture and vegetation dynamics.

Parameters	Description	Grass	Shrub
I_{max}	Full canopy interception [mm]	1.0[1]	1.5[1]
Z_r	Root depth [m]	0.3[2]	0.5[3]
Z_{veg}	Vegetation height [m]	0.3[4]	1.0[3]
r_l	Stomatal resistance [$s \cdot m^{-1}$]	130[4]	210[4]
s^*	Saturation degree at stomata closure [-]	0.33[1]	0.24[1]
s_w	Saturation degree at wilting point [-]	0.13[1]	0.13[1]
s_h	Saturation degree at soil hygroscopic [-]	0.10[5]	0.10[5]
LAI_{max}	Maximum leaf area index [$m^2 \cdot m^{-2}$]	2.0[4]	2.0[3]
R_{in}	Ratio of canopy-interspace infiltration capacity [-]	1.2[6]	2.0[11]
WUE	Water Use Efficiency [$kg_{CO2} kg^{-1}_{H2O}$]	0.01[7]	0.0025[8]
k_{sg}	Decay coefficient of green biomass [d^{-1}]	0.012[7]	0.002[9]
k_{ss}	Decay coefficient of structural biomass [d^{-1}]	0.01[7]	0.005[9]
k_{dd}	Decay coefficient of dead biomass [d^{-1}]	0.013[7]	0.013[13]
k_{sf}	Maximum drought induced foliage loss rates [d^{-1}]	0.02[10]	0.02[8]
c_g	Specific leaf area for green biomass [m^2 leaf $\cdot g^{-1}_{DM}$]	0.0047[7]	0.004[6]
c_d	Specific leaf area for dead biomass [m^2 leaf $\cdot g^{-1}_{DM}$]	0.009[7]	0.01[12]
α_s	Shortwave albedo [-]	0.12[1]	0.15[1]
GT, DT	Growth and dormancy thresholds [$mm \cdot d^{-1}$]	3.8, 6.8[7]	N/A
Td_{max}	Constant for dead biomass loss adjustment [$mm \cdot d^{-1}$]	10[7]	10[7]

Source: (1) Caylor et al. (2005); (2) Kurc and Small (2004); (3) Gutierrez-Jurado et al., (2006); (4) Guan and Wilson (2009); (5) Laio et al. (2001); (6) Bhark and Small (2003); (7) Istanbulluoglu et al. (2012); (8) Lajtha and Whitford (1989); (9) Montaldo et al. (2005); (10) Ivanov et al. (2008a); (11) Paul and Litvak (2009); (12) Williams and Albertson (2005); (13) Calibration.

The parameters in Table 5.4 are obtained by Zhou et al. (2013) from literature and from calibration and compared with the literature for given plant types in the field. For a more detailed description of the selection procedure of these parameters, interested readers are referred to Zhou et al. (2013). Table 5.5 reports parameters used for simulating plant establishment and mortality, mostly obtained from literature and calibration as described in the Zafferia study case (see section 4.3.1). Allelopathy (i.e., the allelochemicals produced by shrub which can influence the grasses growth) is incorporated in CATGraSS by using the inhibitory factor, IN_G. The IN_G was obtained from calibration: we have done different simulations considering first the absence of the inhibition factor (IN_G=1), and then increasing it to 2 (maximum inhibition), for a total of ten simulations. We obtained IN_G equal to 1.12.

For the fire event a probability of fire, P_F, (i.e., the reverse of return period, T_F) has been assumed equal to 0.1 (return period, T_F: 10 years in accordance with Casagrandi and Rinaldi, 1999) and the vulnerability to fire of each vegetation, $V_{F\text{-}X}$, is shown in Table 5.6 (plant seedlings are more vulnerable to fire than mature plants).

Table 5.5. Model parameters for modeling plant mortality and establishment.

Parameters	Description	Grass	Creosote bush	Shrub Seedling
θ_X	Drought-resistant threshold [-]	0.62[3]	0.80[3]	0.64[3]
$P_{Mb\text{-}X}$	Background mortality probability [-]	0.01[3]	0.01[3]	0.01[3]
$P_{E\text{-}X\text{-max}}$	Maximal establishment probability [-]	0.35[3]	0.2[3]	N/A
IN_X	Inhibitory factor [-]	1.12[3]	N/A	N/A
t_{max}	Maximum age [yr]	N/A	600[1]	18[2]

Source: (1) Bowers et al. (1995); (2) Chew and Chew (1965); (3) Calibration.

Table 5.6. Fire parameters.

Parameters	Description	Shrub	Shrub Seedling	Grass
P_F	Probability of fire [yr^{-1}]		0.1[1]	
T_F	Fire return period [yr]		10[1]	
$V_{F\text{-}X}$	Vulnerability to fire [-]	0.11 [2,3]	0.2 [2,3]	0.8 [2,3]

Source: (1) Parmenter (2006), Le Houèrou (1974), Thomas (1991), (2) Accatino et al. (2010), (3) Calibration.

In order to demonstrate the utility of the model in predicting local ecohydrologic dynamics of soil moisture (*s*), evapotranspiration (*ET*), and leaf area index (*LAI*), a limited model confirmation study is performed at the

DWWSS site by Zhou et al. (2013). The vegetation in the site is mainly grasses C_4, composed of black and blue grama (*Bouteloua gracilis*). Soil moisture is obtained from three different soil pits at 10 and 30 cm depths positioned nearby the DWWSS site, and averaged to represent the daily root-zone-average soil water content. *ET* is obtained from an adjacent Bowen ratio tower, which operated from 1996 (only partially) until the end of 1999. The weather variables measured at the DWWSS, Bowen ratio observations, and soil moisture measurements can be found on the web site http://sev.lternet.edu/data/sev-079.

The modeled *LAI* has been confirmed by using satellite-derived *LAI* from the MODIS. MODIS data became online in 2000 at a 1 km spatial resolution for every 8 days. The effect of local variability in MODIS *LAI* is eliminated by taking the mean value of a window of 3 by 3 MODIS grid cells.

CATGraSS is forced to run at a point using only grass vegetation type from 1996 to the end of 2008. Time series of daily rainfall, and modeled and observed relative soil moisture content (*s*), actual *ET* and MODIS-derived *LAI* (for 9 years, from 2000 to 2008) are presented in Figure 5.19. The modeled *s* shows good agreement with observations at three different pits for the 10 year-period between 1996 and 2006, reasonably capturing the timing and magnitude of soil moisture pulses and the slower rate of decays (Figure 5.19a). To better quantify the ability of CATGraSS in predicting soil moisture dynamics during the growing season, the modeled daily soil moisture was plotted against measured soil moisture (averaged over the three pits) in Figure 5.19b. The standard error of estimation (*SEE*) with respect to the one-to-one line and the Nash-Sutciffe efficiency (*NSE*) (Nash and Sutciffe, 1970) are reported in Figure 5.19b, showing good agreement between model predictions and field measurements. The model represents the observed seasonal behavior of *ET* with some skill (Figure 5.19c). The model shows a good agreement with observations in 1997, underestimates *ET* in the first half of 1998, and slightly overestimates *ET* during the peak of the rainy season in 1999. These discrepancies might result from the highly spatially variable nature of storms in the region, leading to differences in the rainfall received between the rain gage and the footprint of the Bowen ratio tower; or other errors in rainfall measurement, especially in 1998 when *ET* was measured in absence of rain. Because of these uncertainties we have not done a one-to-one comparison between the modeled and estimated evapotranspiration rates from the Bowen ratio tower.

The MODIS *LAI* consistently gives 0.1 in the winter and 0.2 in the spring before the growing season at this site, which could arguably be an artifact of the algorithm used for calculating *LAI* (Figure 5.19d). Therefore, as the basis of our model comparison, we focus on the periods when MODIS *LAI* is larger than 0.2. The model shows consistency in estimating the onset of the growing and dormant seasons except for 2003, the driest year in the simulations, while the peak *LAI* is overestimated in some years. In order to assess model capability, the modeled *LAI* is plotted against MODIS *LAI* (larger than 0.2) during the growing

seasons (Figure 5.19e). The result shows that CATGraSS can reasonably capture the local ecohydrological dynamics of grass.

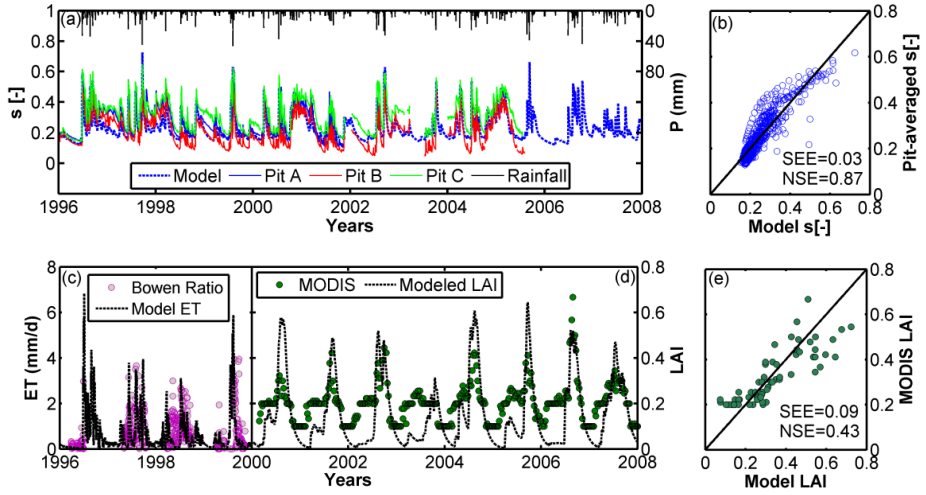

Figure 5.19. (a) Time series of observed precipitation, and depth-averaged relative soil moisture content (*s*) in the root zone obtained from model and observations at soil pits; (b) scatterplot of modeled against pit-averaged s during the growing season; (c) modeled and Bowen ratio-estimated evapotranspiration (*ET*); (d) modeled and MODIS-derived *LAI*; (e) scatterplot of modeled against MODIS-derived *LAI* during the growing season (Zhou et al., 2013).

5.1.4.2. Model simulation and results

As previously said, the model was initially run with a random vegetation distribution, characterized by the same probability of assignments for all PFTs and bare soil (33.3%). It is important to point out that the main goal of this *long time scale* simulation was to reproduce the initial condition of the fast encroachment occurred between 1860 and 2010, which corresponds to the vegetation distribution of 1860.

The shrub distribution in 1860 is not known in pattern and percentage; Knapp et al. (2008b) is one of the few works which talks about the shrub percentage in 1860, stating that "the shrub percentage was very low". In order to calibrate the model, a quantitative interpretation of Knapp et al. (2008) statement has been done by fixing shrub percentage equal to 2%.

The final vegetation distribution after 5,000 years and the time series of percent coverage of PFTs in the study site over the 5,000 years are shown in Figures 5.20a, b, respectively. The vegetation percentages in 1860 obtained at the end of the 5,000th year are: shrub 2 %, grass 78%, bare soil 20%.

After 5,000 years the shrubs are distributed following a sort of cluster pattern. The vegetation composition is not influenced by the topography because the study site is in a flat area.

While the shrub time series in Figure 5.20b decreases mainly from 2,000 to 5,000 years, the grass time series increases constantly from 0 to 5,000 years. The *lag-1* autocorrelation is equal to 0.78 for grass and to 0.997 for shrub. The highly variable nature of grass percentage, proved by a lower *lag-1* autocorrelation coefficient, is typically driven by the inter-annual fluctuations in precipitation. Because grasses have an overall higher water stress and lower drought resistance, they die rapidly during dry years, but also grow back quickly in the following wetter years, as their seeds are assumed to be available everywhere in space. In addition, the establishment and mortality of grass depend on the rainfall of a given year and therefore subjected to the same inter-annual variability of rainfall.

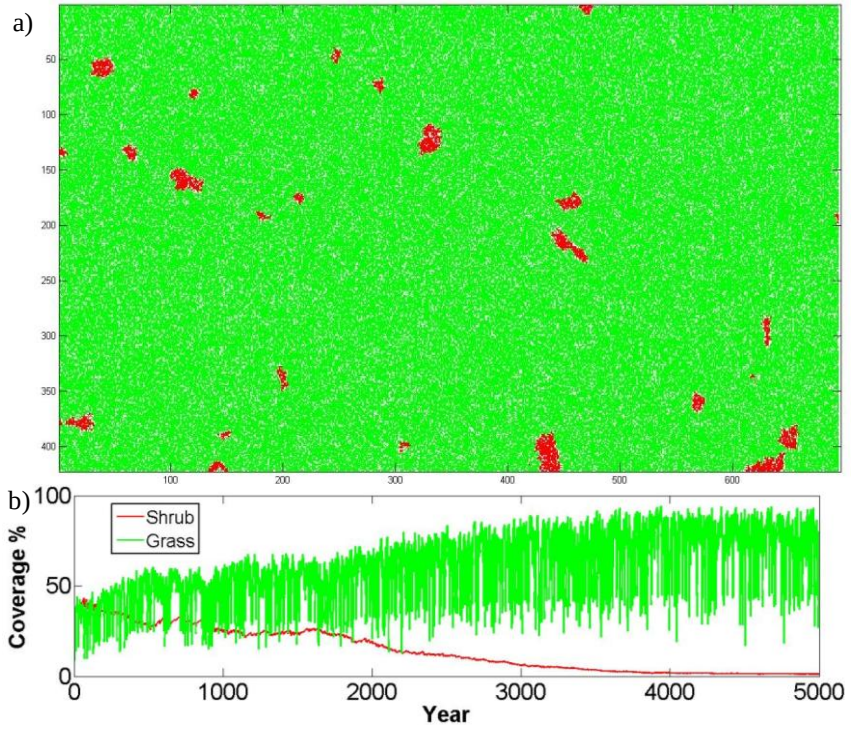

Figure 5.20. (a) Final vegetation distribution after 5,000 years of simulation, (b) time series of percent coverage of PFTs in the study site.

5.1.5. Short time scale: encroachment

While the information of shrub percentage can be considered as available in the work of Knapp et al. (2008), its initial spatial distribution in 1860 is unfortunately not known; for this reason three initial vegetation distribution hypothesis have been assumed in this work.

Three cases have been considered:

- *C1*. since Knapp et al. (2008b) stated that shrub line moved gradually from south to north, a particular spatial pattern of PFTs and bare soil, which respects vegetation percentage above mentioned, has been created in our work domain (extent: 422, 696 pixels): i.e., shrub percentage equal to 4% in the first 85 rows starting from the bottom, and a progressive reduction of this species from 4% to 0% moving upward (Figure 5.21);
- *C2*. the initial shrub distribution is obtained considering eight circular kernels and it is shown in Figure 5.22. From each kernel centre, moving from 0 to 100 pixels the shrub percentage is equal to 8%, from 100 to 300 pixels it is 4%, from 300 to 500 pixels it is 2%, from 500 to 700 pixels it is 1% and from 700 to 831 pixels it is 0% (shrub mean percentage equal to 2.4%);
- *C3*. the initial vegetation distribution is that obtained at the end of the *long time scale* simulation (i.e., 5000 years) and shown in Figure 5.20a.

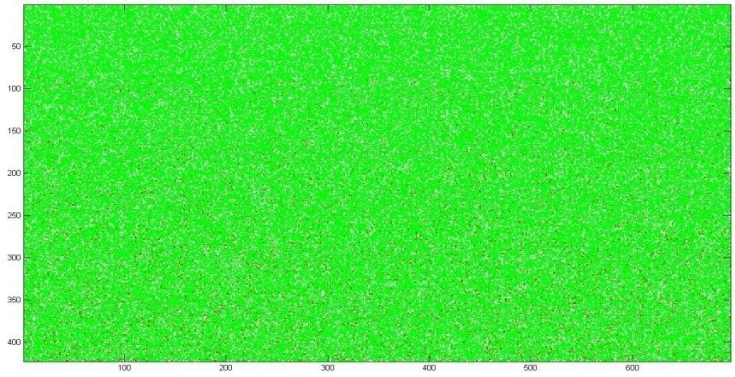

Figure 5.21. Initial vegetation distribution: shrub distribution gradual rectangular (*C1*).

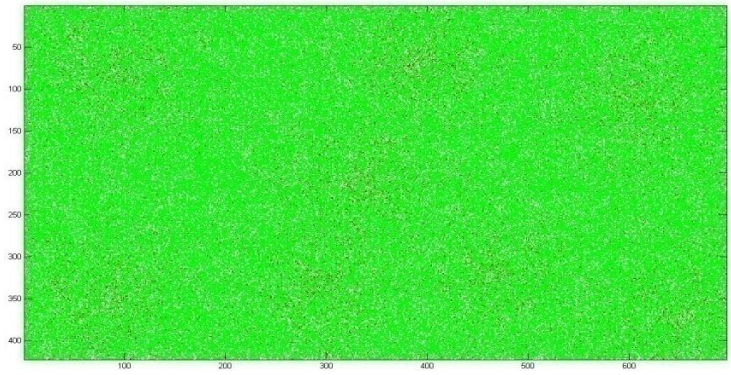

Figure 5.22. Initial vegetation distribution: shrub distribution obtained considering eight circular kernels (*C2*).

We will mainly discuss the results obtained starting from the *C1* because according to the literature sources (e.g., Knapp et al., 2008) the *C1* is the more realistic vegetation distribution in 1860. Therefore, the *C1* is used to calibrate the encroachment model in order to obtain the current shrub percentage, 42%, and the other cases (*C2*, *C3*) are simulated with the same parameters and they are used to analyze how change the final vegetation percentage starting from a different vegetation distribution.

5.1.5.1. Encroachment factors parameters used in the CATGraSS

The causes that have been considered for the shrub encroachment in this case study are summarized in Figure 5.23: the fire, the grazing increase, the seed dispersal caused by animals, the shrub-grass inhibition effect (i.e., allelopathy) and the plant type competition.

In order to obtain the value of these encroachment factors, we changed the model parameter values systematically assuming fixed ranges and doing multiple simulations, starting from *C1*. First, a *base simulation* (*BS*), i.e., the base simulation of 150 years (1861-2010) without encroachment factors [Zhou et al. (2013)'s parameters], has been carried out.

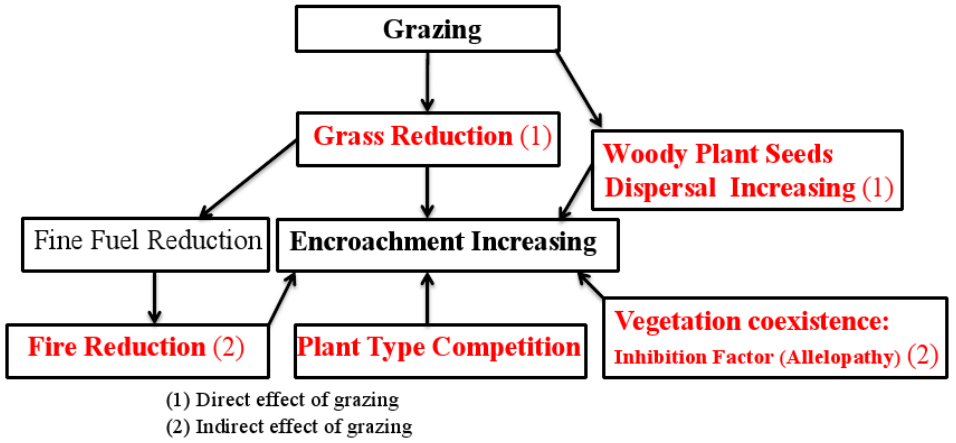

Figure 5.23. Conceptual model illustrating the causes of the encroachment.

White et al. (2006) and Parmenter (2008) stated that the fire return period, T_F, increased from 10 years in 1860 to 100 years in 2010 in the Sevilleta site. This increase is caused by the reduction of the fuel (grass) eaten by herbivores and it is one of the possible causes of the shrub increase because increasing the fire return period the shrub settle capacity increased. In fact, T_F equal to 10 years is able to maintain the semiarid grasslands of the pre-1900 and control shrub cover, while increasing the T_F the shrubs are not controlled and they are able to encroach the area. In CATGraSS we modeled the fire effect by considering a T_F

linear increasing from 10 years (in 1861) to 100 years (in 2010) according to Wright et al. (1980), Wright and Bailey (1982), White et al. (2006) and Parmenter (2008). The vulnerability to fire, $V_{F\text{-}X}$, has been setted equal to 0.8 for grass and to 0.11 for shrub (0.2 for young shrub, Burkhardt and Tisdale, 1976) after a sensitivity analysis carried out using Accatino et al. (2010) value ranges. This parameter varies from 0.02 if trees (or shrub) are very fire resistant, to 0.6 if trees are easily killed by fire in according to Casagrandi and Rinaldi (1999).

While in literature the fire model, that we used in the CATGraSS, has been previously studied and applied and values of its parameters are presented in different works, for grazing and seed dispersal there is not enough scientific literature useful to allow to us their choice. For this reason, for each single factor, different values have been first fixed trying to understand the effect of the choice of the single factor on the encroachment; then these factors have been combined, and among all the combinations, the one that provides the more acceptable reproduction of the current vegetation percentage has been selected.

Van Auken (2000; 2009) demonstrated that grazing increased from 1860 to 2010 causing a reduction of the grass and an increase of the shrub. In fact, in 1860 the grazing was introduced in this area and it progressively increased from 1860 to 2010. The grazing effect is only for grass. The animals eat only the herbaceous vegetation (herbivores) (Van Auken 2000; 2009). Grazing effect is obtained like Zhou et al. (2013), considering a constant background probability for disturbance factor, P_{Mb}, to be added to the annual probability of plant mortality, P_M (0.05 in Zhou et al., 2013). According to Van Auken (2000; 2009), the parameter has been obtained increasing it in the years to simulate the increase of the grazing effect. We do not know the initial and final P_{Mb} value, therefore, eight different grazing cases, that provide a linear increase of P_{Mb} from 1861 to 2010, have been assumed. In Table 5.7 the final shrub (*SH*) and grass (*G*) percentages for each P_{Mb} case are shown (e.g., case "0.01-0.05" means P_{Mb} equal to 0.01 in 1861 and P_{Mb} equal to 0.05 in 2010). In Figure 5.24 the final vegetation percentages in function of the P_{Mb} are shown. In the P_{Mb} axis, for each case the P_{Mb} value in 2010 is shown. As evident in Figure 5.24, the grazing alone could not cause the total shrub encroachment, since current shrub coverage is equal to 42%. In fact, with a P_{Mb} equal to 0.4 in 2010, the shrub increases from 0.65 to 13.10%. Obviously, values of P_{Mb} greater than 0.4 could cause a greater increase of the shrub percentage but they would be unrealistic values.

The grazing can not only cause the death of the plant in the cell (simulated using the P_{Mb}) but also reduce the percentage of the grass in the cell, i.e. reduction of the *LAI* in the cell (partial removing of grass biomass by cattle). In order to simulate this effect of biomass reduction (i.e., *LAI* reduction), the grass decay coefficient of green biomass, $K_{sg\text{-}G}$ has been increased from 1861 to 2010. This coefficient, that describes the decay (or senescence) of the plant in the time, has been assumed linearly increasing from 0.004 d^{-1} in 1860 to 0.012 d^{-1} in 2010, using the range of Montaldo et al. (2005) and the actual value used by Zhou et

al. (2013). In Figure 5.25 the modeled grass *LAI* for ten synthetic years in 1860 (lower $K_{sg\text{-}G}$) and in 2010 (higher $K_{sg\text{-}G}$) is shown.

Table 5.7. Final vegetation percentages in function of the grazing factor (P_{Mb}).

Grazing		
Encroachment Factor	Final Vegetation Percentage [%]	
$P_{Mb\ (-)}$	SH	G
BS	0.65	82.43
0.01-0.05	1.27	74.51
0.02-0.10	2.28	72.23
0.03-0.15	3.27	52.89
0.04-0.20	4.34	50.80
0.05-0.25	5.69	46.15
0.06-0.30	5.71	41.20
0.07-0.35	5.78	34.56
0.08-0.40	13.10	25.24

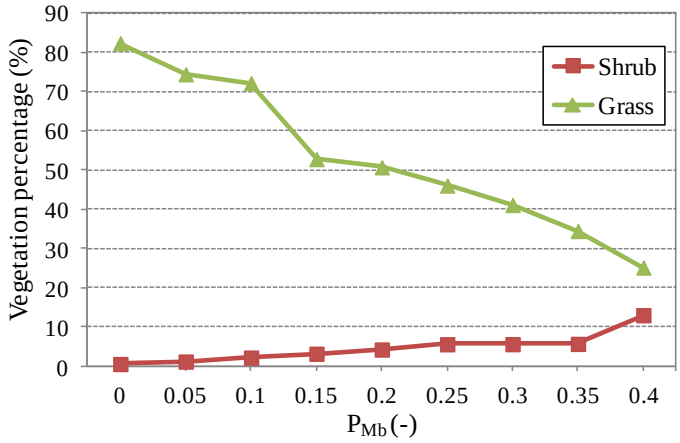

Figure 5.24. Final vegetation percentages in function of the grazing factor (P_{Mb}).

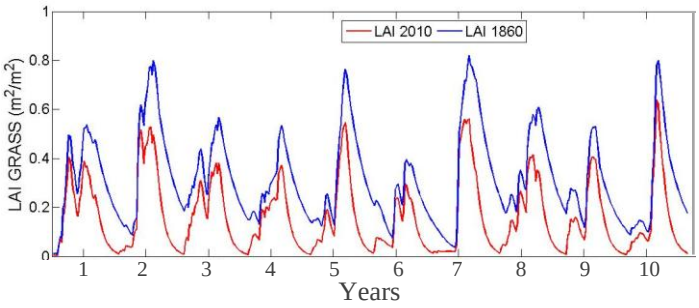

Figure 5.25. Modeled grass *LAI* increasing the $k_{sg\text{-}G}$ in 1860 and in 2010.

With regard to the seed spread, Van Auken (2000; 2009) stated that the introduction of the animals in the study area from 1860 caused the possibility that a seed can arrive in the bare soil from everywhere. In order to take into account this aspect within the model framework, the spread of seed probability, *SSP*, for the shrub has been introduced in the model and its value has been ranged from 0.001 to 0.02 for a total of seven values. In Table 5.8 the final vegetation percentages for different values of *SSP* factor are shown while Figure 5.26 shows the final vegetation percentages as function of the *SSP*. Also in this case, only the seed dispersal caused by animals could not cause the total shrub encroachment. In fact, with *SSP* equal to 0.02, the shrub increases from 0.65 to 18.05%. The decrease of the grass from *BS* to *SSP* equal to 0.001 and the subsequent increase from *SSP* equal to 0.001 to *SSP* equal to 0.002 could be linked to the highly variable nature of grass percentage as mentioned in section 5.1.4.2.

Table 5.8. Final vegetation percentages in function of the *SSP*.

Seed Dispersal caused by animals		
Encroachment Factor	Final Vegetation Percentage [%]	
SSP (-)	SH	G
BS	0.65	82.43
0.001	1.02	59.20
0.002	1.56	94.50
0.004	2.38	93.21
0.005	5.03	79.12
0.008	6.03	65.76
0.01	6.35	39.77
0.02	18.05	28.70

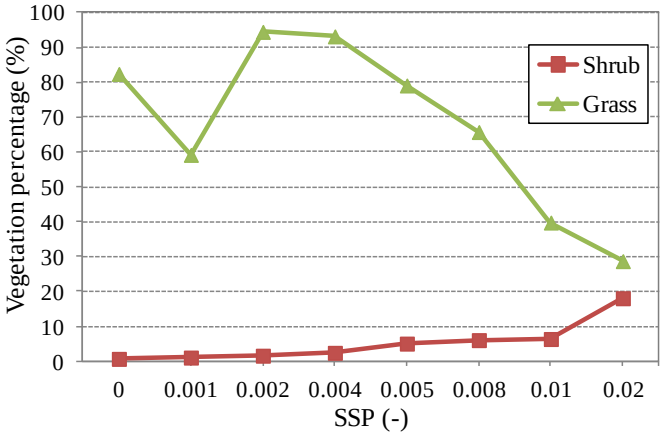

Figure 5.26. Final vegetation percentages in function of the *SSP*.

In order to take into account the wind direction influence on the vegetation pattern, the *wind direction factors WD'* and *WD''* have been introduced, as previously described in section 3.1.7.3. It is important to point out that wind is not an encroachment factor since in literature it was not mentioned as cause. The wind may cause a directionality of the seed dispersal that, in cascade, may influence the encroachment pattern. We assumed *WD'* ranging from 1.5 to 5 and *WD''* from 1 to 4 obtaining six different *WD'-WD''* combinations. In Table 5.9 the final vegetation percentages for each *WD'-WD''* combination are shown (e.g., case "1.5-1" means *WD'* and *WD''* equal to 1.5 and 1, respectively; the plant live index, φ_X, of the cells in the direction of the wind increases by 50% while the φ_X of the neighbor cells is unchanged). In Figure 5.27 the final vegetation percentages in function of the *WD'* are shown. Increasing the *WD'* to 5 (i.e., the greatest effect of the wind direction) the shrub increases from 0.65 to 5.02%, highlighting a non relevant effect of the wind direction. This behavior can be explained by the already high value of φ_{X_SH} due to the low water stress characterizing the shrub. Therefore, multiplying φ_{X_SH} for *WD*, the shrub establishment probability is not sensibly affected as it is limited by the maximal establishment probability value, $P_{E\text{-}X\text{-}\max}$, and then the *WD* increase causes a low shrub percentage increase. Therefore, we can affirm that the main effect of *WD* increase is to affect the directionality of the shrub establishment and encroachment, even if its role on encroachment velocity is low.

Table 5.9. Final vegetation percentages in function of the *WD* factor.

Wind		
Encroachment Factor	Final Vegetation Percentage [%]	
WD (-)	SH	G
BS	0.65	82.43
1.5-1	1.13	86.00
2-1.5	1.62	93.92
2.5-2	2.38	58.08
3-2.5	2.56	60.67
4-3	3.93	63.28
5-4	5.02	59.20

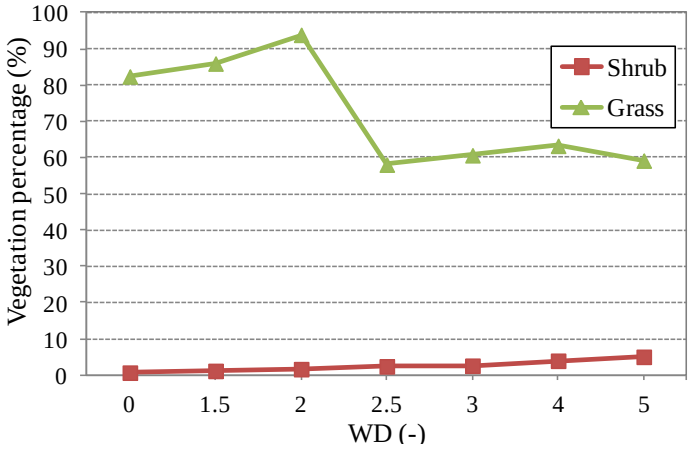

Figure 5.27. Final vegetation percentages in function of the *WD*.

Climate change has not been considered as encroachment cause in accordance with Bahre and Shelton (1993) and Van Auken (2000; 2009) and because in the past there was not a statistically significant trend of temperature and precipitation.

In order to define the combination of the above mentioned parameters which provides the actual vegetations percentages at 2010, a total of 1008 simulations have been carried out. This number derives from the combination of all the cases of each factor, considering also the *BS* simulation: 2 fire cases, 9 grazing cases, 8 seed dispersal cases, 7 wind cases. Among the 1008 combinations, that shown in Table 5.10 has been selected since it provides the current (i.e., 2010) vegetation percentages, even if it is important to point out that other simulations provided similar "acceptable" reproduction of the current vegetation percentages.

Table 5.10. Encroachment factor parameters used for each period.

Years	T_F [yr]	P_{Mb} [-]	$K_{sg\text{-}G}$ [d^{-1}]	SSP [-]	WD [-]
1861-1890	10	0.02	0.004		
1891-1920	32.5	0.04	0.006		
1921-1950	55	0.06	0.008	0.005	2-1.5
1951-1980	77.5	0.08	0.010		
1981-2010	100	0.10	0.012		

In Figure 5.28a the final vegetation distribution after the encroachment in case *C1*, using all the factors parameterized as shown in Table 5.10, is shown. The time series of percent coverage of PFTs in the study site over 150 years is shown in Figure 5.28b.

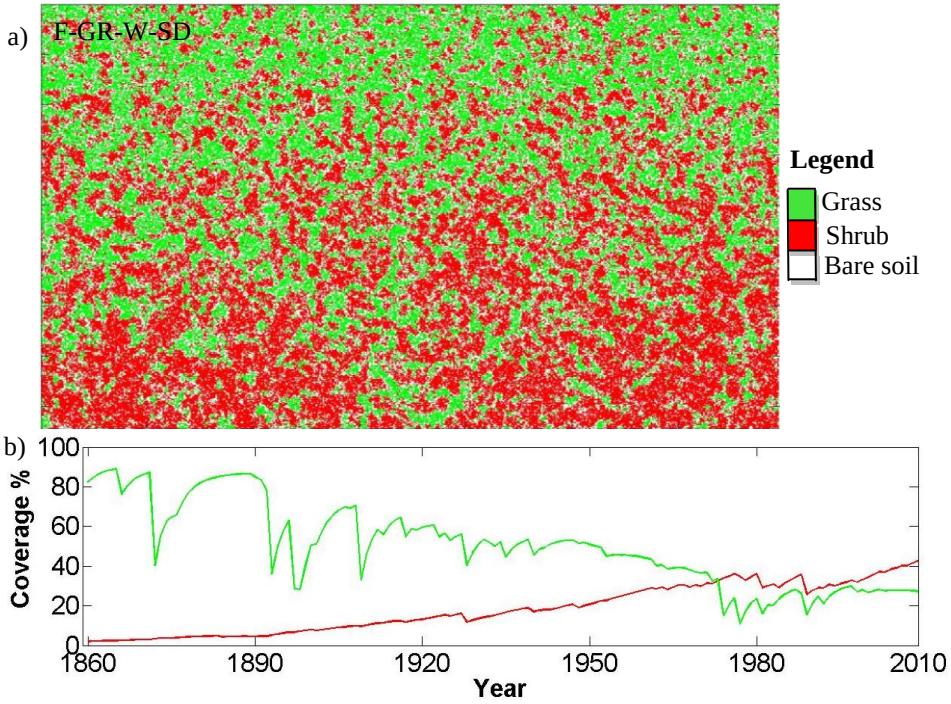

Figure 5.28. (a) Final vegetation distribution combining all the factors, *F-GR-W-SD*; (b) time series of percent coverage of PFTs in the study site, *C1*.

The model is able to simulate the encroachment, with an increasing of the shrub from 2% to 42.6% (grass 27.2% and bare soil 30.1%) like the current vegetation percentage in Figure 5.7 and, at the same time, simulating the shrub encroachment from south to north. The final vegetation pattern is very similar to that shown in Figure 5.7, therefore we can affirm that the model is able to

reproduce the final vegetation percentage and pattern. In Figure 5.28b, the shrub time series shows a low increase in the first 30 years (i.e., from 1960 to 1890), and a greater increase from 1930 to 1975 and from 1990 to 2010, vice versa from 1975 to 1990 the shrub percentage decreases. The grass time series shows a high variability as in the *long time scale* simulation. The *lag-1* autocorrelation is 0.913 for grass and 0.974 for shrub.

5.1.5.2. Results and discussion

5.1.5.2.1. Analysis of the influence of the single factors on the encroachment in the past 150 years

In order to understand the effect of each single factor on the encroachment phenomenon, a series of different simulations have been carried out assuming the presence of each factor separately and then different combination of such factors. These simulations have been compared with the *BS*, previously introduced. A multi-step strategy has been then used to explore what we learn with the model with respect to the contribution of different parameters that contribute to the observed vegetation change. We have combined fire return period (*F*), grazing (*GR*), wind direction (*W*) and seed dispersal caused by animals (*SD*): first using a single cause then combining these causes in pairs, three by three, and all the causes together for a total of 16 factors combinations. In Tables 5.11 the final vegetation percentages for each factors combination, starting from *C1*, is shown. For a fixed number of factors, the combinations that give the greatest shrub percentage increase are highlighted in italic.

Using only a cause, *F* has provided the greatest influence. Combining two factors, *F* and *SD* showed the greatest influence while combining three factors, the greatest influence is provided by *F*, *SD* and *GR*. The fire frequency reduction and the increased grazing intensity have the greatest influence on the encroachment. In fact, the fire causes the greatest increase of the shrub (from 0.65 to 10.32%) and the grazing causes the greatest reduction of grass (from 82.43 to 72.23%). The final vegetation distributions for each factors combination are shown in Figure 5.29.

Table 5.11. Final vegetation percentage for each factors combination (starting from *C1*).

Final Vegetation Percentage [%]					
Factors	SH	G	Factors	SH	G
BS	*0.65*	*82.43*	GR-W	2.65	64.28
F	*10.32*	*81.11*	GR-SD	8.24	64.40
GR	2.28	72.23	W-SD	5.99	87.51
W	1.62	93.92	F-GR-W	19.97	51.18
SD	5.03	79.12	*F-GR-SD*	*36.86*	*30.78*
F-GR	12.80	58.09	F-W-SD	27.89	57.24
F-W	12.20	78.92	GR-W-SD	13.71	57.56
F-SD	*25.53*	*61.79*	*F-GR-W-SD*	*42.67*	*27.20*

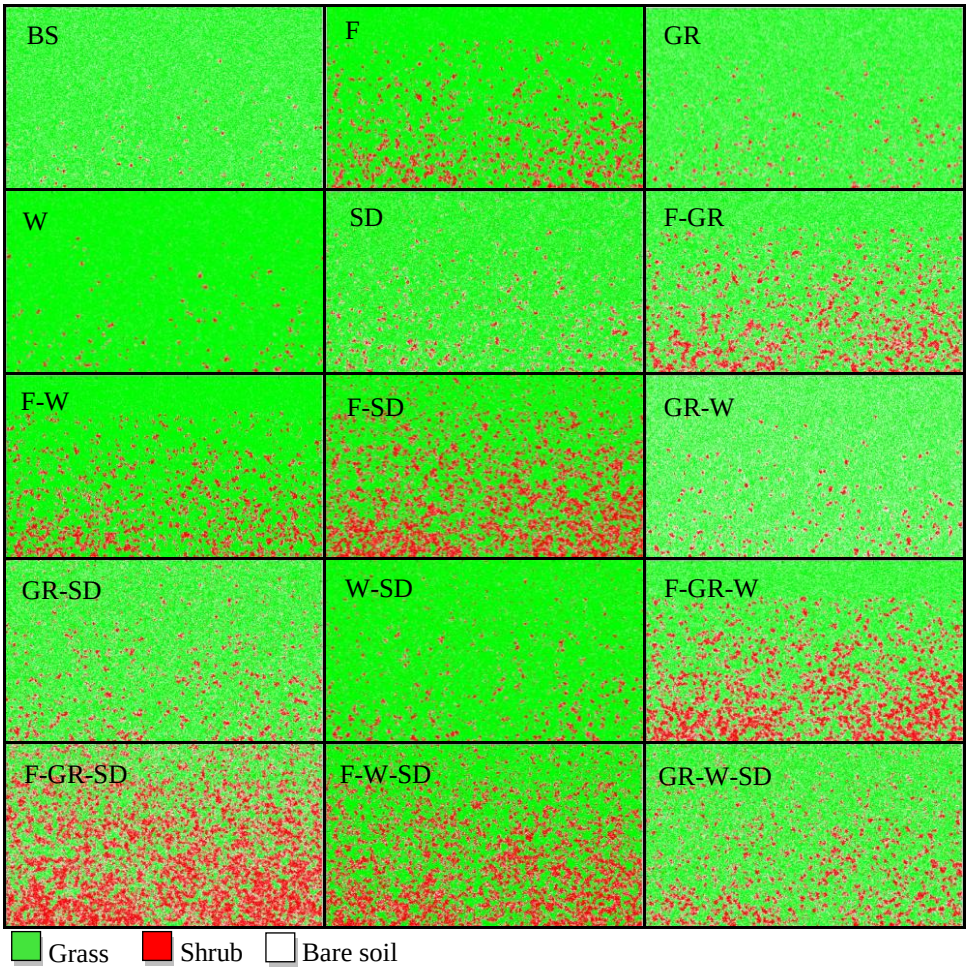

Figure 5.29. Final vegetation distribution for each factor combinations, *C1*.

In order to understand how the final vegetation percentages and its pattern may change starting from a different initial vegetation distribution, the cases *C2* and *C3* have been analyzed as well.

In Tables 5.12-5.13 the final vegetation percentage for each factors combination, starting from C*2*, C*3*, respectively, are shown.

Using only a cause in the *C2*, *F* has provided the greatest influence, while in the *C3*, *SD* has got the greatest influence because starting from a cluster distribution the seed dispersal caused by animals have a greater effect on the encroachment increase. In fact, in *C3* the shrub settlement process is strongly slowed down because the shrub is mainly present in the cluster and the mechanism of establishment (see section 3.1.6.1), based on the average value of the φ_X, provides a very modest progress, but inserting the ability to establish through seed dispersal caused by animals, the settlement increases because the

seed can establish everywhere. The *SD* in *C3* presents an influence more evident than that relative to *C1* and *C2*; these two latter cases, starting from a more uniform spatial pattern, are characterized by a settlement process faster than *C3* even if in essence of seed dispersal. Combining two factors, *F* and *SD* showed the greatest influence in all the cases while combining three factors, the greatest influence is provided by *F*, *SD* and *GR* in all the cases. The final vegetation distributions for each factors combination, for each case, are shown in Figures 5.30-5.31a, respectively, while Figures 5.30-5.31b shows the final vegetation distribution after the encroachment using all the factors for the C*2*, C*3*, respectively.

Therefore, the final vegetation patterns for *C2* and *C3* is different from *C1* because it is strongly influenced by the initial vegetation distribution. As previously seen in section 4.3.4, for the Zafferia case study, in the long *time scale* simulation, the model results are not sensitive to the initial condition used for spatial plant distribution because the model forgets the initial condition after the first thousand year, during which aspect-driven vegetation organization emerges on the landscape. Vice versa, when we *run short time* scale simulation the results are very sensitive to the initial condition and the model is not able to forget the initial condition. In fact, the establishment procedure (i.e., cellular automata component), is strongly influenced by the neighbors cells of the candidate cell, and therefore the initial vegetation distribution can limit or accelerate the establishment and also the final vegetation distribution.

Table 5.12. Final vegetation percentage for each factors combination (starting from *C2*).

Final Vegetation Percentage [%]					
Factors	SH	G	Factors	SH	G
BS	*1.49*	*75.29*	GR-W	5.05	49.41
F	*9.89*	*82.00*	GR-SD	7.09	65.94
GR	1.90	68.67	W-SD	5.18	89.27
W	1.74	93.42	F-GR-W	24.96	46.10
SD	4.80	41.03	*F-GR-SD*	*34.90*	*32.42*
F-GR	12.50	58.36	F-W-SD	34.01	51.69
F-W	12.48	76.25	GR-W-SD	12.72	58.59
F-SD	*16.27*	*72.45*	*F-GR-W-SD*	*40.72*	*29.05*

Table 5.13. Final vegetation percentage for each factors combination (starting from *C3*).

Final Vegetation Percentage [%]					
Factors	SH	G	Factors	SH	G
BS	*2.28*	*41.65*	GR-W	2.86	65.31
F	2.48	93.74	GR-SD	5.30	65.40
GR	2.58	71.68	W-SD	4.87	42.96
W	2.59	62.43	F-GR-W	3.42	72.44
SD	*4.67*	*86.21*	*F-GR-SD*	*14.23*	*36.41*
F-GR	2.84	72.77	F-W-SD	10.73	81.34
F-W	2.78	93.42	GR-W-SD	8.87	51.73
F-SD	*7.00*	*86.44*	*F-GR-W-SD*	*22.80*	*42.70*

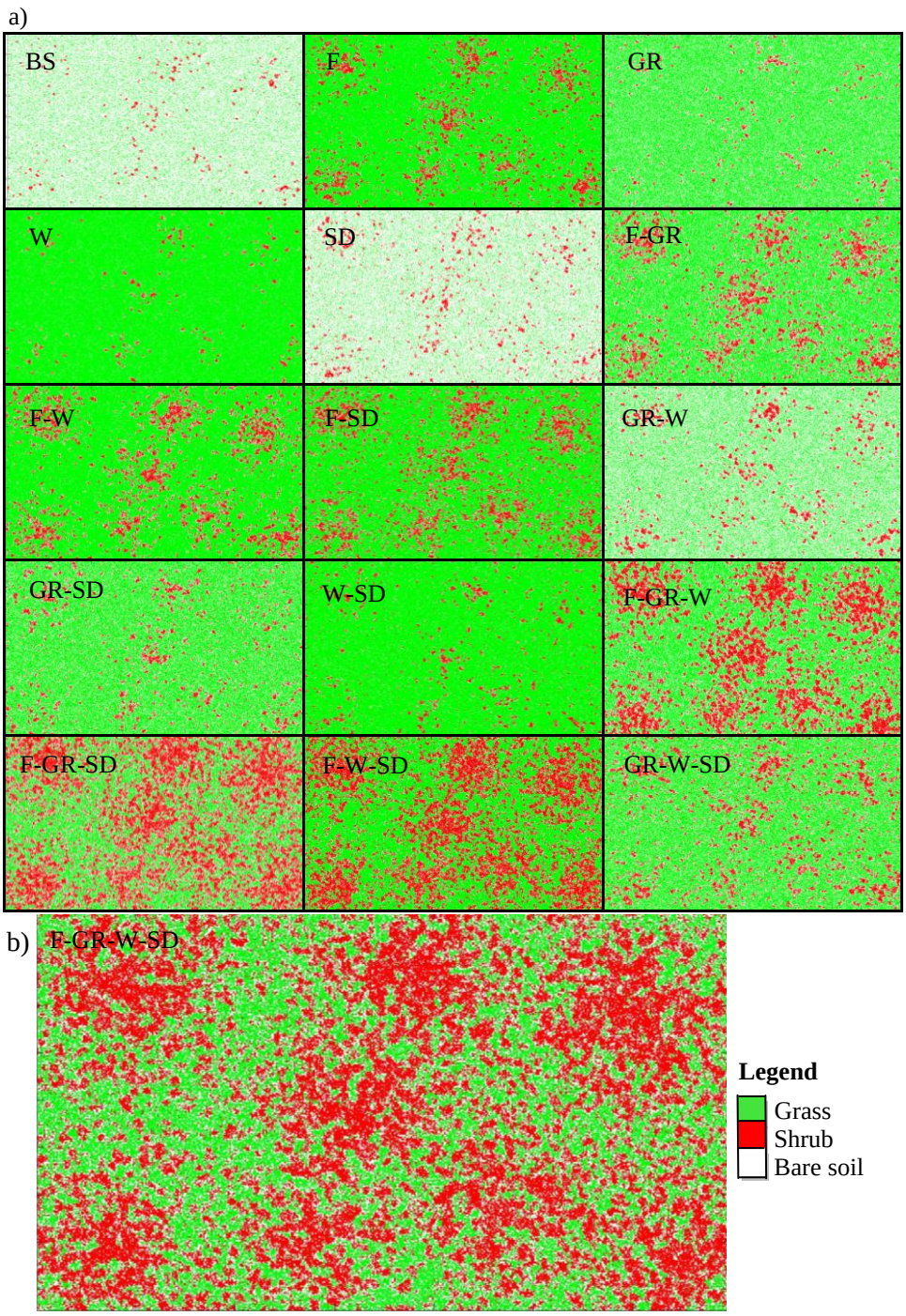

Figure 5.30. Final vegetation distribution for each factor combinations, *C2*.

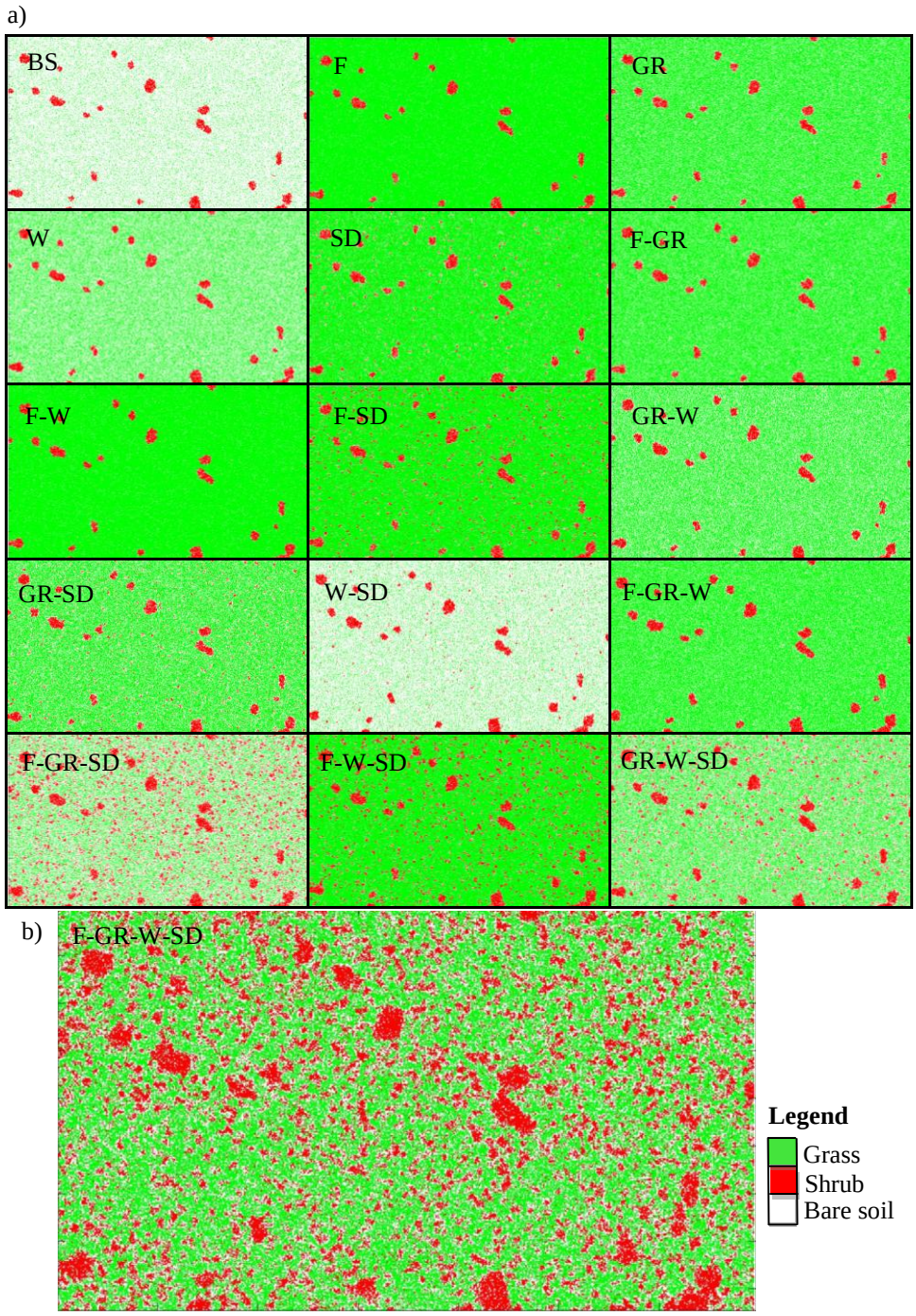

Figure 5.31. Final vegetation distribution for each factor combinations, *C3*.

Time series of percent coverage of PFTs in the study site over 150 years for C*2* and C*3* are shown in Figures 5.32-5.33, respectively. Combining all the factors, after 150 years (i.e., 2010), while in the *C2* shrub is 40.7%, grass is 29.1% and bare soil is 30.2%, in the *C3*, shrub is 22.8%, grass is 42.7% and bare soil is 34.5%. Then, starting from the vegetation distribution obtained in the *long time scale* simulation (*C3*), the final shrub percentage is lower than in the other cases (C*1*, C*2*); this could be due to the establishment procedure. In fact, in *C3* the shrub settlement process is strongly slowed down because the shrub is mainly present in the cluster and the mechanism of establishment (see section 3.1.6.1), based on the average value of the φ_X, provides a very modest progress.

In *C2* (Figure 5.32) the shrub time series shows a constant increase, and only from 1975 to 1990 the shrub percentage decreases. The grass time series shows a high variability as in the *C1*. The *lag-1* autocorrelation is 0.927 for grass and 0.973 for shrub. In *C3* (Figure 5.33), the shrub time series shows a low increase, and the grass time series shows a high variability. The *lag-1* autocorrelation is 0.8573 for grass and 0.967 for shrub. As previously seen in Figures 5.30 and 5.31, the shrub in *C2* has a greater increase than in *C3*. Comparing the Figures 5.28, 5.32 and 5.33 and the *lag-1* autocorrelation, while the grass in *C1* and *C2* show a greater persistence than in *C3*, the shrub has the same persistence in all the cases.

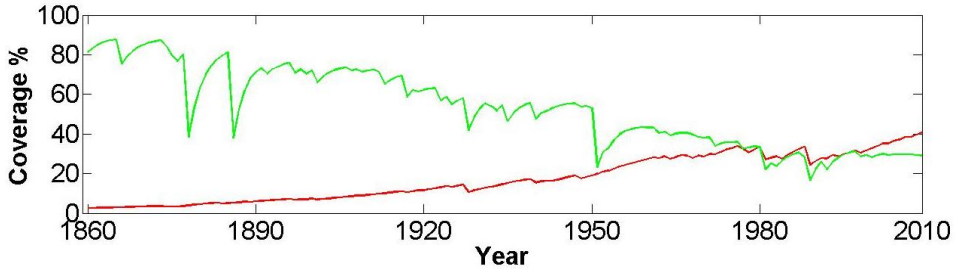

Figure 5.32. Time series of percent coverage of PFTs in the study site, *C2*.

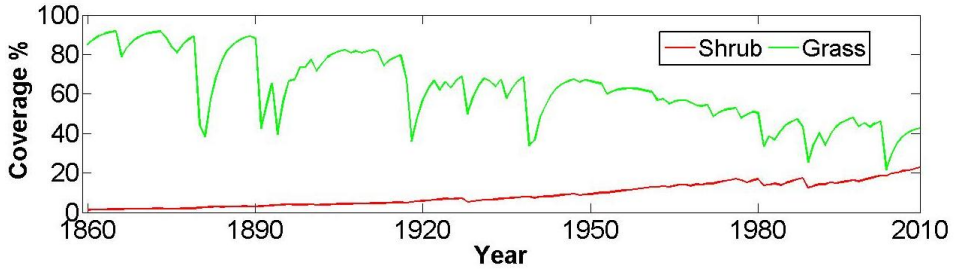

Figure 5.33. Time series of percent coverage of PFTs in the study site, *C3*.

5.1.5.2.2. Encroachment in the future and possible management strategies

Starting from the simulated vegetation distribution at 2010, we tried to figure out the possible vegetation pattern at 2100. Different scenarios named *S1* and *S2* have been assumed: absence of climate change (*S1*), presence of climate change (*S2*); moreover starting from the results of such scenarios, some management strategies have been depicted.

The future vegetation distributions at the end of 2100 adopting *S1* and *S2* scenarios have been obtained through simulations starting from the final vegetation distribution of *C1* (Figures 5.34 and 5.35, respectively). The fire return period has been considered constant and equal to 100 years like the actual condition, the grazing coefficient has been considered constant and equal to 0.10 while seed dispersal and wind effect are considered the same of the encroachment in the period 1861-2010 (i.e., parameters of the 1981-2010 period in Table 5.10).

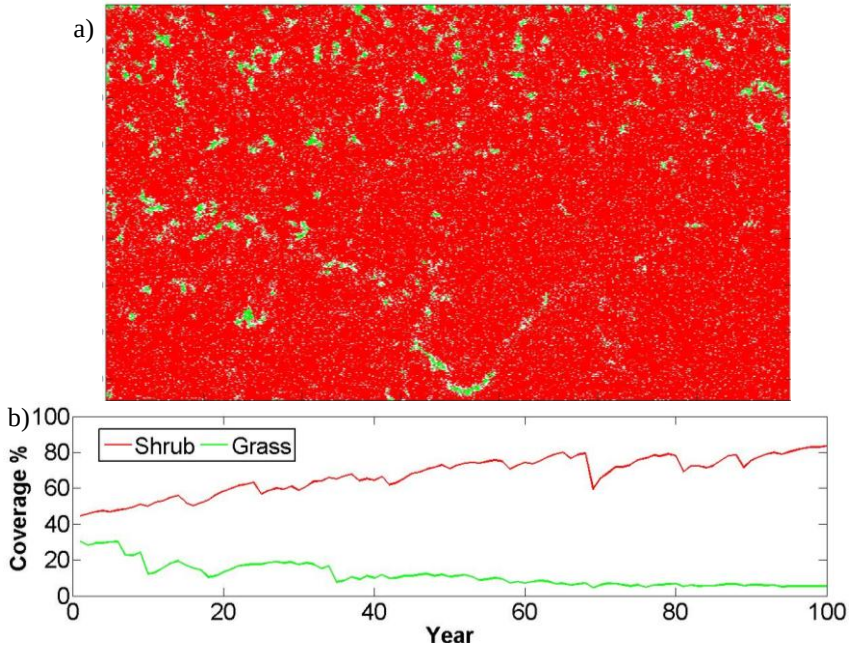

Figure 5.34. (a) Final vegetation encroachment in *S1*, in 2100; (b) future time series of percent coverage of PFTs in the study site, starting from *C1*.

The *S2* has been carried out considering the CO_2 concentration increase effect on the plant stomatal conductance and on the *WUE*. A linear decrease of stomatal conductance until 2100 (20% of decrease in 2050 and 40% in 2100) has been considered following that mentioned in section 4.4.2. A linear increase of the *WUE* has been also taken into account: grass *WUE* equal to 0.01 $kg_{CO_2} \cdot kg^{-1}_{H_2O}$

in 2010 and 0.0114 in 2100, shrub *WUE* equal to 0.0025 $kg_{CO_2} \cdot kg^{-1}_{H_2O}$ in 2010 and 0.0033 in 2100 (the values are obtained using the same procedure of the section 4.4.2).

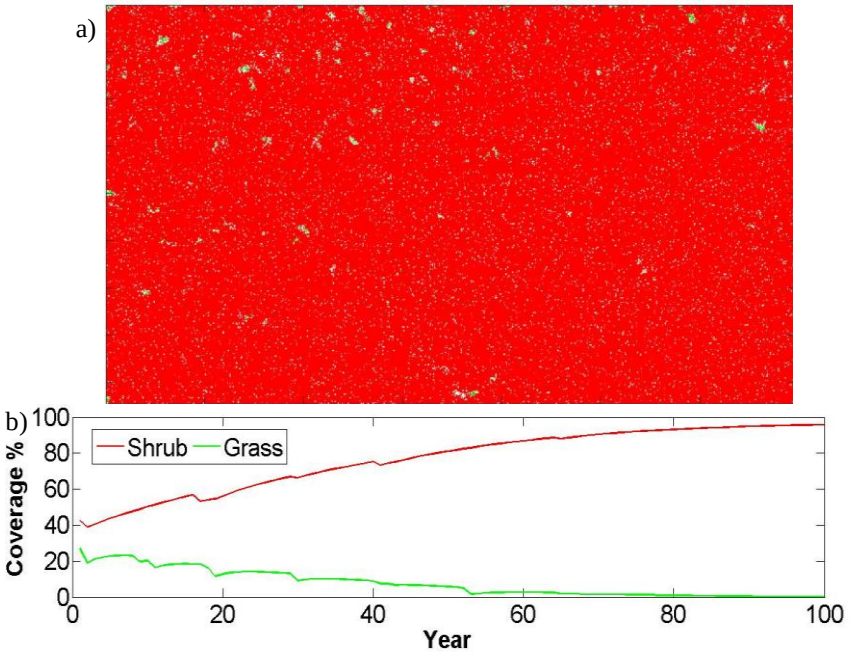

Figure 5.35. (a) Final vegetation encroachment in *S2*, in 2100; (b) future time series of percent coverage of PFTs in the study site, starting from *C1*.

The results of these simulations point out as the shrub increases from 42% to 90% without climate change (*S1*) and to 95.9% with the climate change (*S2*). The climate change, precipitation decrease and temperature increase, could then accelerate the encroachment and the shrub could settle in all the study area confirming the studies of Allen and Breshears (1998) and Van Auken (2009) which stated that the climate change could be another important cause of the future fast encroachment

Finally, in order to point out the best management practices to reduce encroachment in this area, for each one of the three cases *C1*, *C2* and *C3*, starting from the relative final vegetation distribution (Figures 5.28, 5.30, 5.31b), we have simulated the future encroachment, *S2* scenario (presence of climate change), assuming two different management practices in the area: the increasing of fire frequency (obtained fixing T_F equal to 10 years) and the removing of grazing (obtained fixing P_{Mb} equal to 0). In Figure 5.36-5.38 the final vegetation distribution in 2100, without management practices (T_F equal to 100 and P_{Mb} equal to 0.10) (Figures 5.36-5.38a, c) and with management practices (Figures 5.36-5.38b, d) are shown for each single case. It is important

to point out as, for the cases without management, the initial condition does not play any rule on the final shrub percentage (ranging from 93.7% to 95%). Moreover one can observe that the reduction of the fire return period and the removal of grazing are able to cause a great reduction of the future encroachment for the three cases. But, while in *C1* and *C2* the future shrub percentage is 95% considering grazing and fire return period equal to 100 years (Figures 5.36-5.37a) and 73% considering grazing removal and fire return period reduction (Figures 5.36-5.37b), in *C3* the reduction of shrub is more evident: from 93.77% in Figure 5.38a it reduces to 50.49% in Figure 5.38b. This can be simply explained with the different initial condition at 2010 for the three cases (*C1* and *C2* equal to about 40% and *C3* equal to 22%).

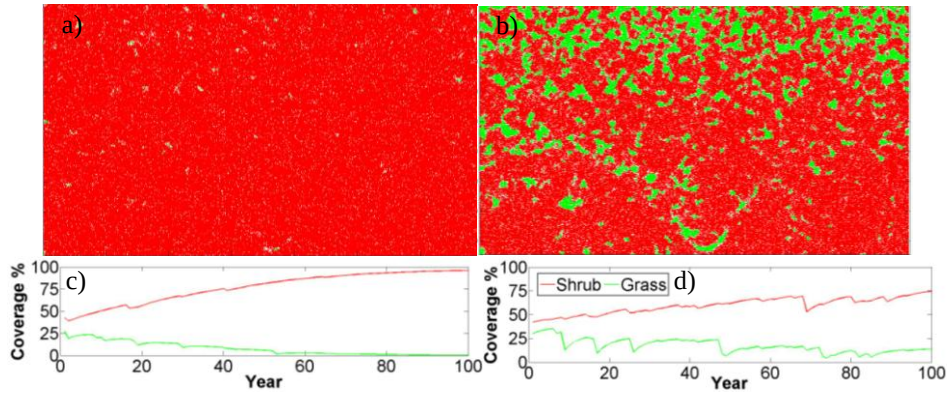

Figure 5.36. Final vegetation encroachment in 2100 and future time series of percent coverage of PFTs in the study site without management practices (a, c), and with management practices (b, d), starting from *C1*.

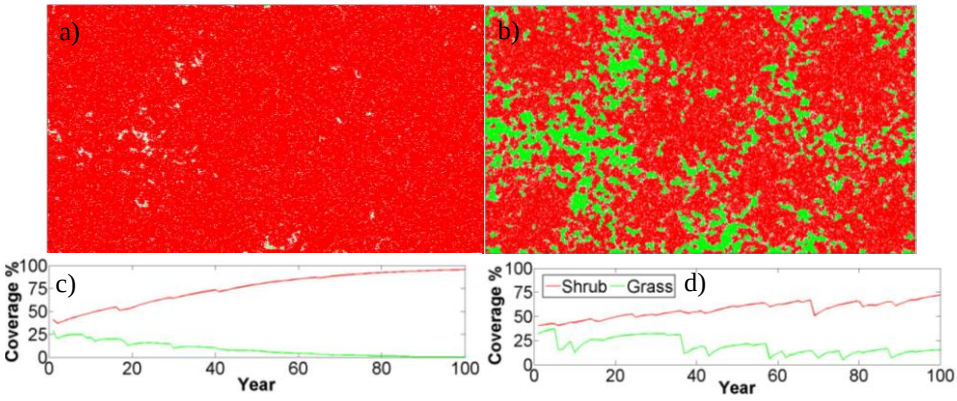

Figure 5.37. Final vegetation encroachment in 2100 and future time series of percent coverage of PFTs in the study site without management practices (a, c), and with management practices (b, d), starting from *C2*.

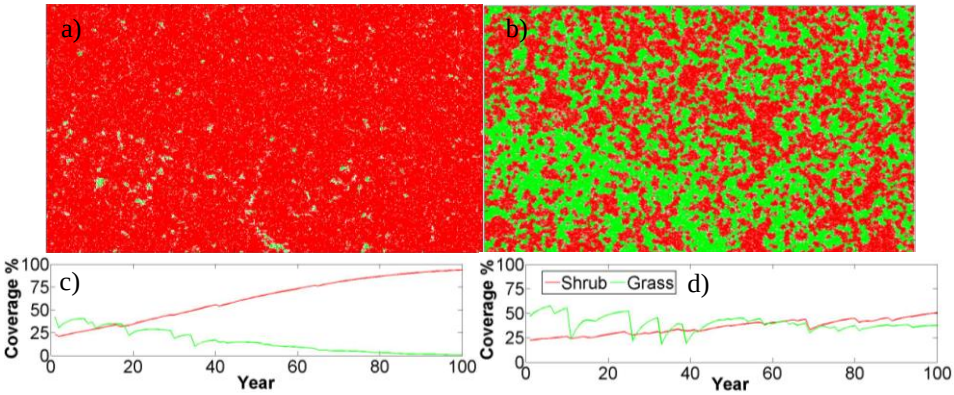

Figure 5.38. Final vegetation encroachment in 2100 and future time series of percent coverage of PFTs in the study site without management practices (a, c), and with management practices (b, d), starting from *C3*.

Therefore, the best treatments or control methods that can be introduced to reduce the future shrub encroachment in the study area are the fire return period decrease, triggering the fire intentionally and in a controlled way, and the decrease of the grazing, removing or limiting cattle and herbivores from the site, in accordance with Miller et al. (2005; 2007).

5.2. Case study: Oregon encroachment

As diffusely mentioned in chapter 2, strong evidences indicate that western juniper (*Juniperus Occidentalis*) has significantly expanded its range since the late 1800s by encroaching into landscapes once dominated by shrubs and herbaceous vegetation. As the juniper layer increases in dominance, the shrub and herb layer decline. The minimum time for the juniper overstory to begin suppressing the understory is 45-50 years and to approach stand closure 70-90 years on cool wet sites and 120-170 on dry warm sites.

Presettlement western juniper (before 1870) is estimated to account for only 10 percent or less of present day woodlands (Miller et al., 1999a; Johnson, 2005). Most woodlands have developed during the past 140 years. The chronologies, which describe the age composition and establishment of woodlands over time, show a rapid increase in establishment since the 1870's (Miller and Tausch, 2001; Soulé et al., 2004). As previously described in section 2.2.2.1, the juniper encroachment could be divided in three phases (Figure 5.39).

In Figure 2.20 (see chapter 2) and 5.40 two conceptual models illustrating the relationship between shrub canopy cover and juniper canopy cover during the three phases of woodland development in the western United States (Oregon, California, Idaho and Nevada) are shown. While in *phase I* junipers are present but shrubs and herbs are the dominant vegetations that influence ecological

processes on the site, in *phase II* junipers are codominant with shrubs and herbs and all three vegetation layers influence ecological processes on the site, finally, in *phase III* junipers are the dominant vegetation and the primary plant layer influencing ecological processes on the site.

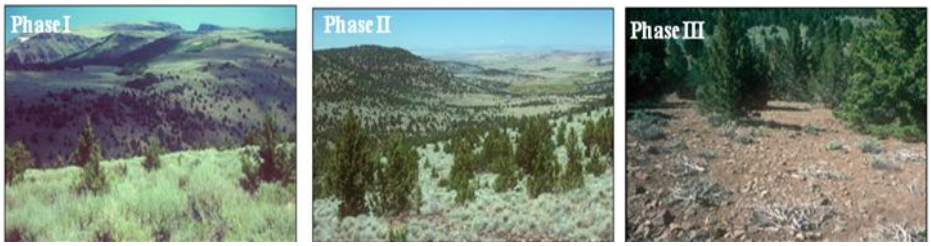

Figure 5.39. The three phases of woodland encroachment (Miller et al., 2005).

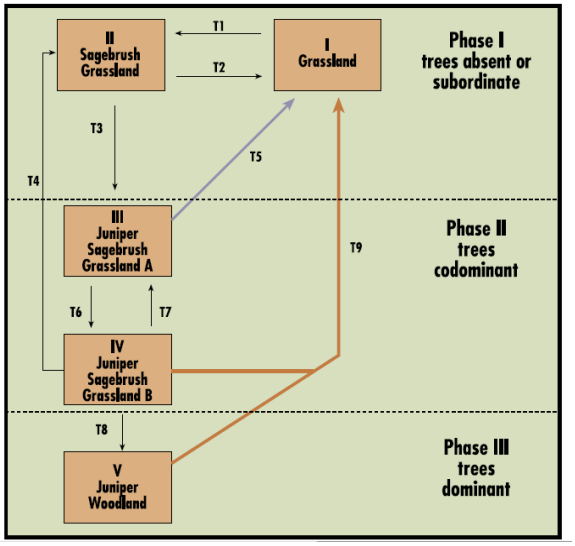

Figure 5.40. Encroachment phases (Miller et al., 2005).

5.2.1. Site description

Juniper encroachment is studied inside the Ochoco National Forest, Crook County, in Oregon where a strongly western juniper encroachment started in 1870 (Miller et al., 2005) (Figures 5.41, 5.42). In Figure 5.43 the position of the study site in the Google 2005 Map (Figure 5.43a), the boundary (Figure 5.43b) and the 3D view (Google Earth map, Figure 5.43c) are shown.

The Ochoco National Forest is located in Central Oregon in the United States, north-east of Prineville, location of the *National Forest Headquarters*. It encompasses 3,440 km^2 of rimrock, canyons, geologic oddities, dense pine

forests, and high desert terrain, as well as the headwaters of the North Fork of the Crooked River.

The study site has got an area of 11.86 Km^2. The Oregon 10 m DEM (source: http://library.uoregon.edu/map/gis_data/or_10mdemlist.htm) is used for the modeling study. This area is located in the elevation range of 1351 m to 1797 m a.s.l. (Figure 5.44a), the slope angle ranges from flat surfaces to as high as 50.7° on hillslopes (Figure 5.44b), with an average of 10.9°. The aspect map is also shown in Figure 5.44c. To illustrate the role of topography on incoming solar radiation, the mean daily clear-sky radiation over the study area is plotted (Figure 5.45). Annually, *S*-facing slope receives as much as twice the solar radiation received by *N*-facing slopes. The soil texture is sandy-loam (*Web Soil Survey* USDA).

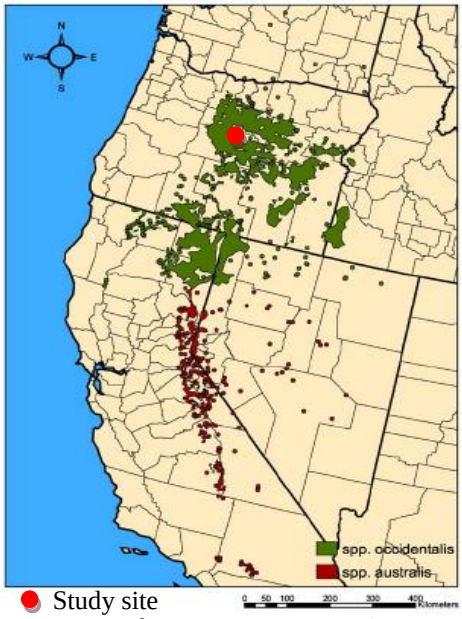

Figure 5.41. Distribution map of western juniper (*Juniperus occidentalis* var. *occidentalis*) and Sterra Juniper (*J.s occidentalis* var. *australis*) (derived from Griffin and Critchfield, 1972; Charlet, 1996; Gedney et al., 1999; and USGS 1:250,000 maps) and study area position.

Figure 5.42. Western juniper in the Keystone Ranch east of Prineville, Oregon, in Crook County on Ochoco Creek.

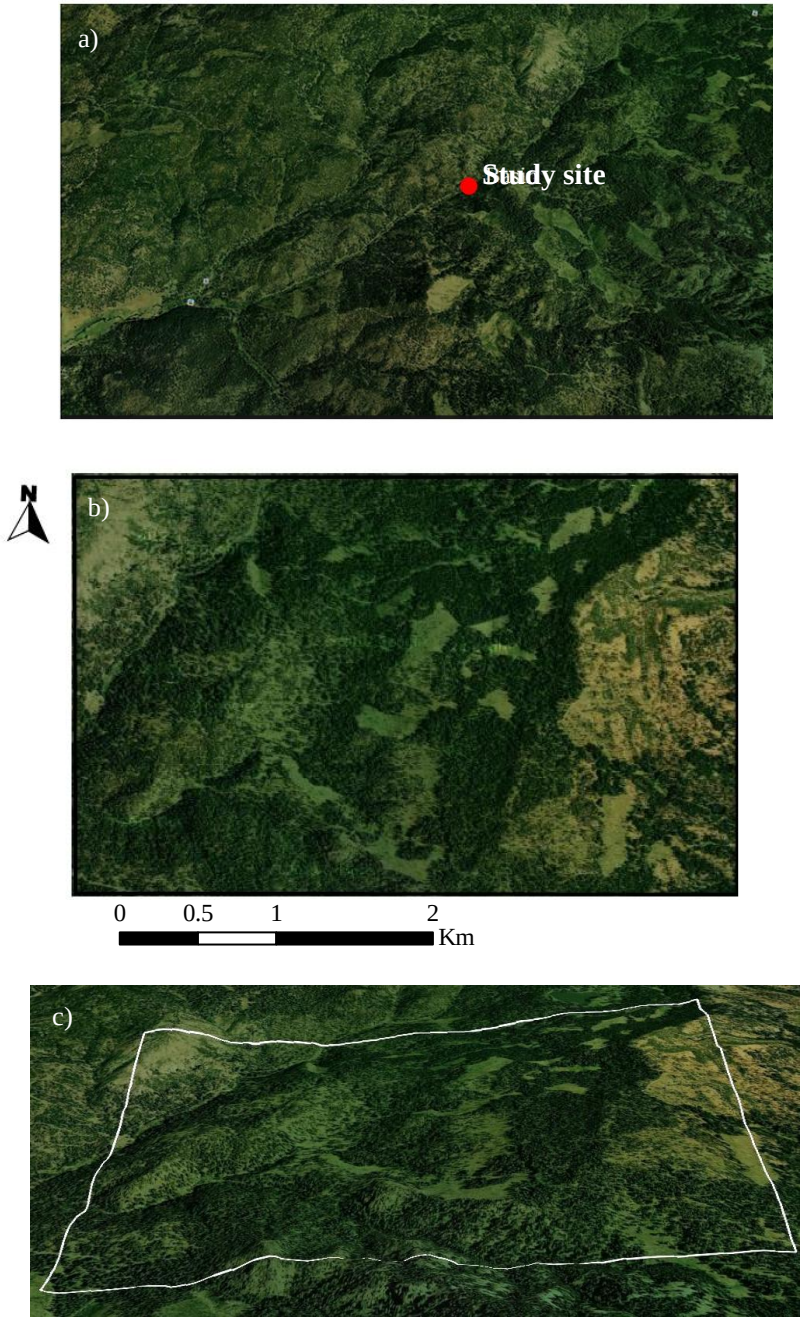

Figure 5.43. Study site: (a) position, (b) boundary, (c) 3D view.

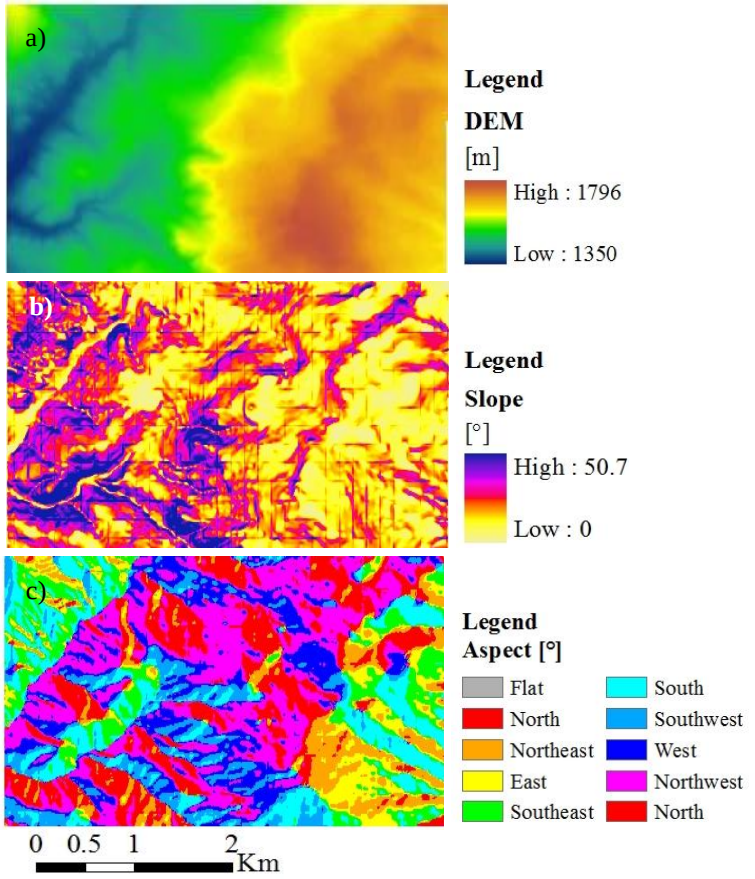

Figure 5.44. Topography of the site: (a) DEM, (b) slope, (c) aspect.

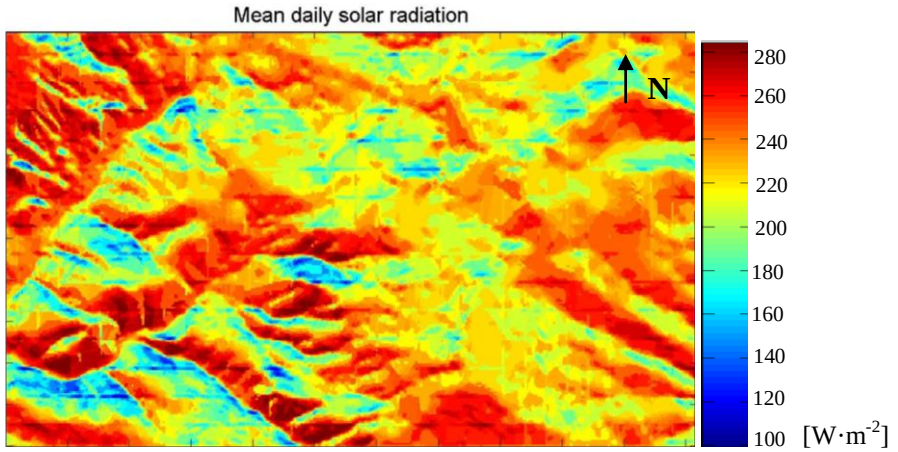

Figure 5.45. Simulated mean daily incoming clear-sky shortwave radiation over the study area over a year.

5.2.2. Data

5.2.2.1. Vegetation cover

The dominant plant types are: western juniper (tree), sagebush (shrub) and bunchgrass C_4 (grass). Grass is deciduous and western juniper and sagebush are evergreen. Western juniper is a long-lived species (the maximum age is 1000 years) and has got an elevation of 4-10 m (Miller et al., 2005) with a mean elevation equal to 7 m. Seed dispersal of western juniper occurs through gravity, overland flow, and animals. At least 12 different species of birds feed on the fruits and as a group are the most important disseminator's of western juniper seed (Miller et al., 2005).

In Figure 5.46a the actual vegetation distribution is shown using the *National Land Cover Database* (NLCD) 2006 map with 30 meters resolution (obtained from Landsat) (http://www.mrlc.gov/nlcd06_data.php): 86.5 % western juniper, 13% shrub, 0.5% grass. The database for this project was *Landsat TM data*, 2006 acquisition. *National Land Cover Database 2006* (NLCD2006) (published in Feb. 2010) is a 16-class land cover classification scheme that has been applied consistently across the conterminous United States at a spatial resolution of 30 meters. NLCD2006 is based primarily on the unsupervised classification of *Landsat Enhanced Thematic Mapper+* (ETM+) circa 2006 satellite data.

The Figure 5.46b overlays the Google 2005 map and the NLCD 2006 map: in the place where there is shrub in the NLCD map, there is bare soil/grass/shrub in the Google Map. In order to produce the NLCD map an unsupervised clustering algorithm has been used.

In Figure 5.47 the study area vegetation distribution, using the NLCD 2001 map overlying the Google map, is shown.

Summarizing, the most important problem related to the NLCD classification map are:

- some of the TM data sets are not temporally ideal. Leaves-off data sets are heavily relied upon for discriminating between hay/pasture and row crop, and also for discriminating between forest classes. The success of discriminating between these classes using leaves-off data sets hinges on the time of data acquisition. When hay/pasture areas are non-green, they are not easily distinguishable from other agricultural areas using remotely sensed data.
- The data sets used cover a range of years (2006), and changes that have taken place across the landscape over the time period may not have been captured.
- Wetlands classes are extremely difficult to extract from Landsat TM spectral information alone.
- Separation of grass and shrub is problematic. Areas observed on the ground to be shrub or grass are not always distinguishable spectrally.

In Figure 5.48 the *Google Earth* maps of 1994 (a), 2001 (b), 2003 (c), 2005 (d), 2011 (e), respectively, are shown. From these maps we can see the great encroachment in this area in 17 years, from 1994 to 2011. For the 1994 and 2001 only a few part of the site is covered by the *Google Earth* map (Figures 5.48a, b).

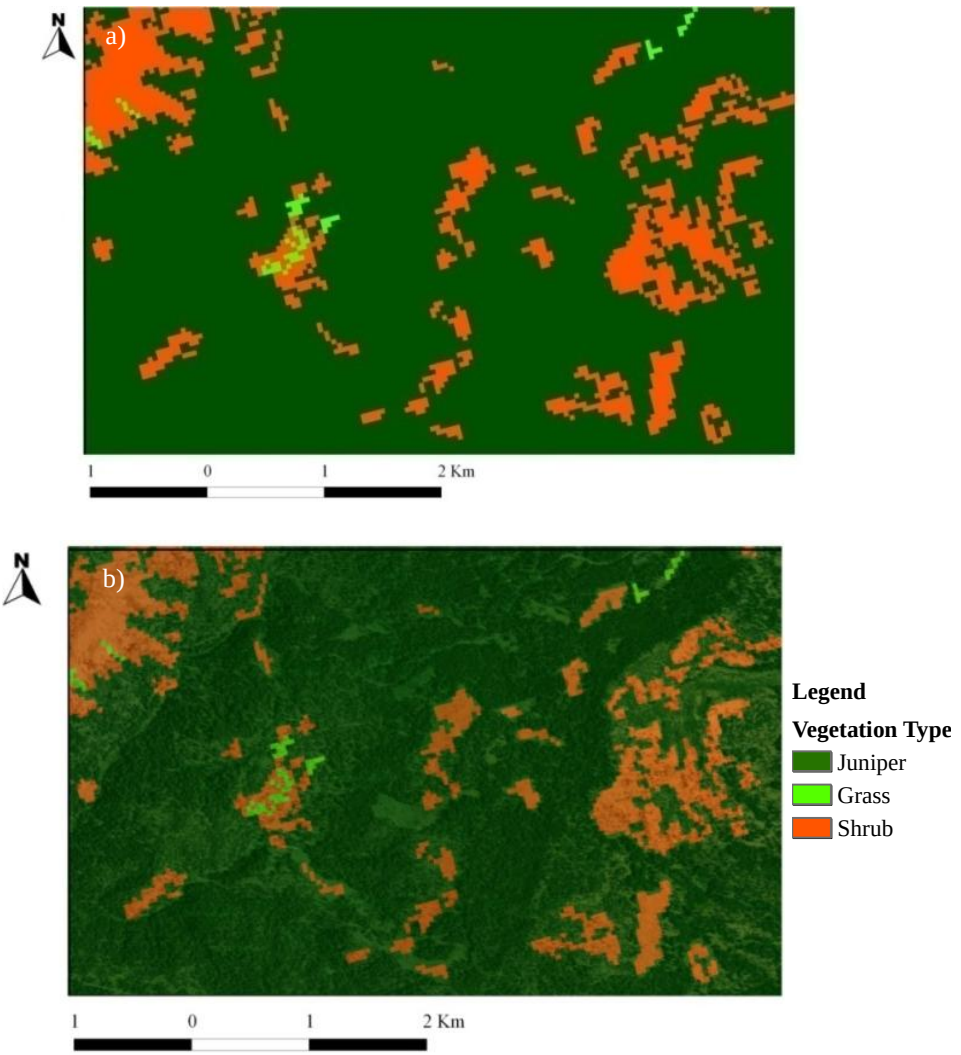

Figure 5.46. (a) Vegetation distribution NLCD 2006, (b) vegetation distribution NLCD 2006 overlying the Google map.

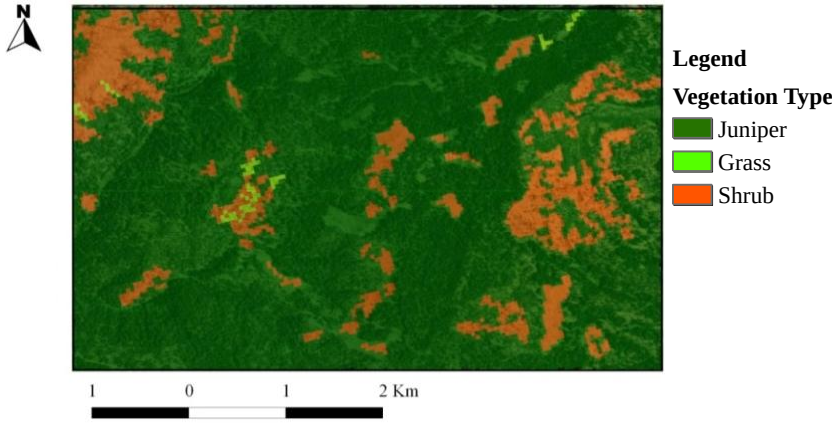

Figure 5.47. Vegetation distribution NLCD 2001 overlying the Google map.

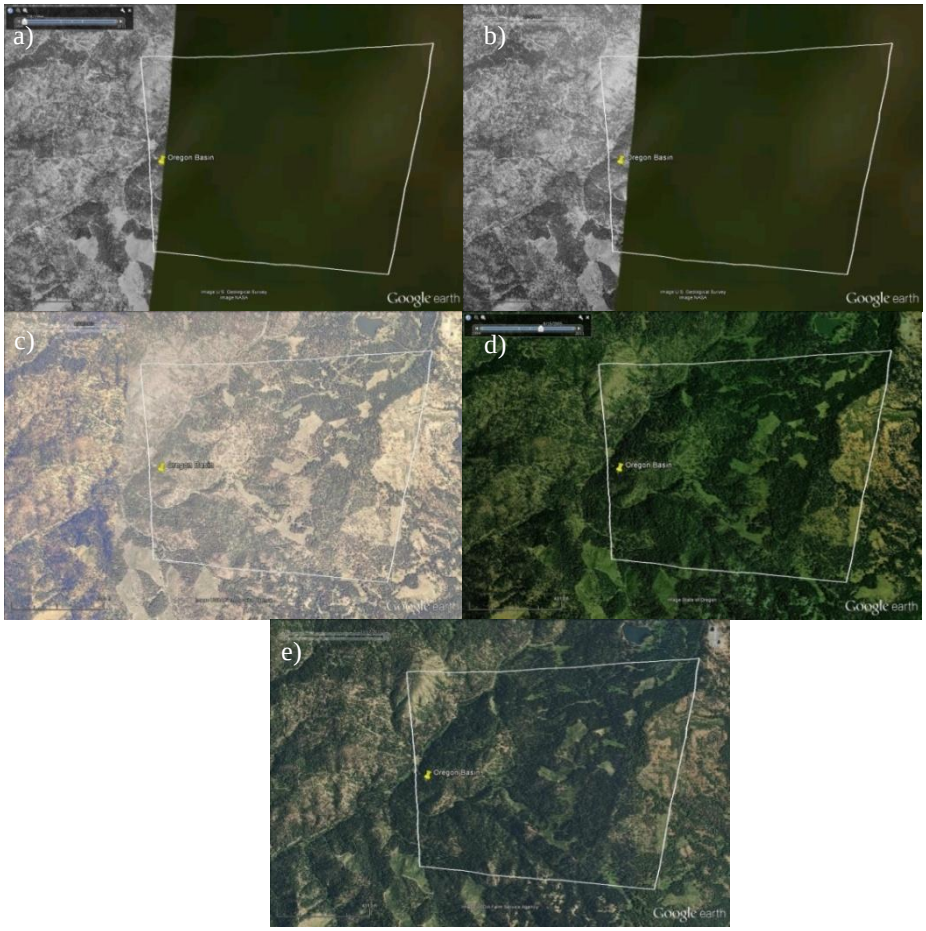

Figure 5.48. *Google Earth* maps of 1994 (a), 2001 (b), 2003 (c), 2005 (d), 2011 (e).

5.2.2.2. Precipitation

In Oregon there is a great spatial variation of the precipitation (Figure 5.49): from 130 mm to more than 2000 mm (source: http://www.nationalatlas.gov). Climate is characterized by cold nights throughout the year, particularly at higher elevations, and hot daytime summer temperatures.

Average annual precipitation ranges between 200 and 380 mm at lower elevations. In the Ochoco Mountains may reach 760 to 1000 mm at higher elevations. The highest monthly precipitation totals occur in the winter months, with a secondary maximum during the late spring and early summer. High intensity thunderstorms can contribute large proportions of local annual rainfall in the late spring and summer precipitation events. Summer temperatures are warm at lower elevations, but the growing season is relatively short (Nielsen-Pincus, 2008).

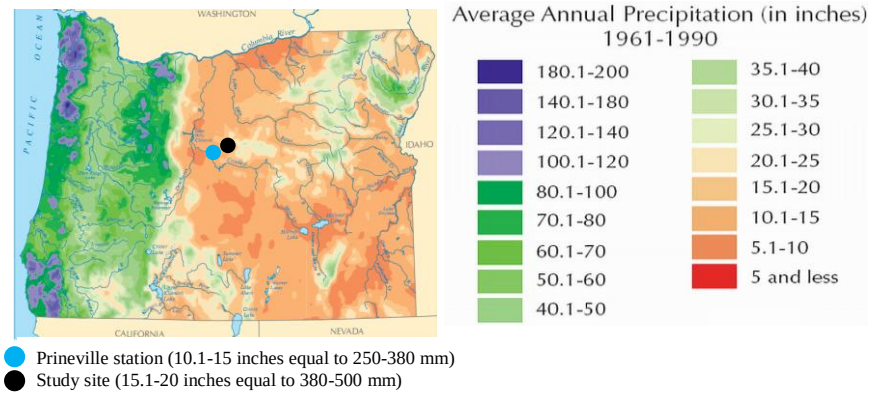

Figure 5.49. Oregon annual precipitation spatial distribution map (source: http://www.nationalatlas.gov).

In Figure 5.50 the historical precipitation (a) and temperature (b) measured in Prineville (OR) (44°30' N, 120°80' W, 888.5 m a.s.l.) from 1897 to 2012 are shown (source NOAA). Moreover, only the temperature and the precipitation are available and there are missing data in forty years. The solar radiation, humidity, vapor pressure and wind speed are not measured by the station. The MAP is about 246 mm and the mean annual temperature is 8.5° C. There was not climate change during the period 1897-2012. The Mann-Kendall test (Mann, 1945; Kendall, 1962) has been done with α equal 0.01 for the annual precipitation data, for the wet and dry season precipitation data and for the mean annual temperature and there is not statistically significant trend in all the cases.

The study site is located in the area in which the precipitation is between 380-500 mm. For this reason the data of the *Metolius* eddy-covariance station (AmeriFlux, sitename: *Metolius Intermediate Pine/US-Me2*; 44°45' N, 121°55'

W, 1353 m a.s.l.), for which all the weather variable data are available, have been selected (data availability from 01/01/2002 to 12/31/2012). The MAP is 462 mm (tipping bucket raingauge with 0.254 mm resolution). The original weather data time-resolution is half hour and we have aggregated the data at 1 hour resolution.

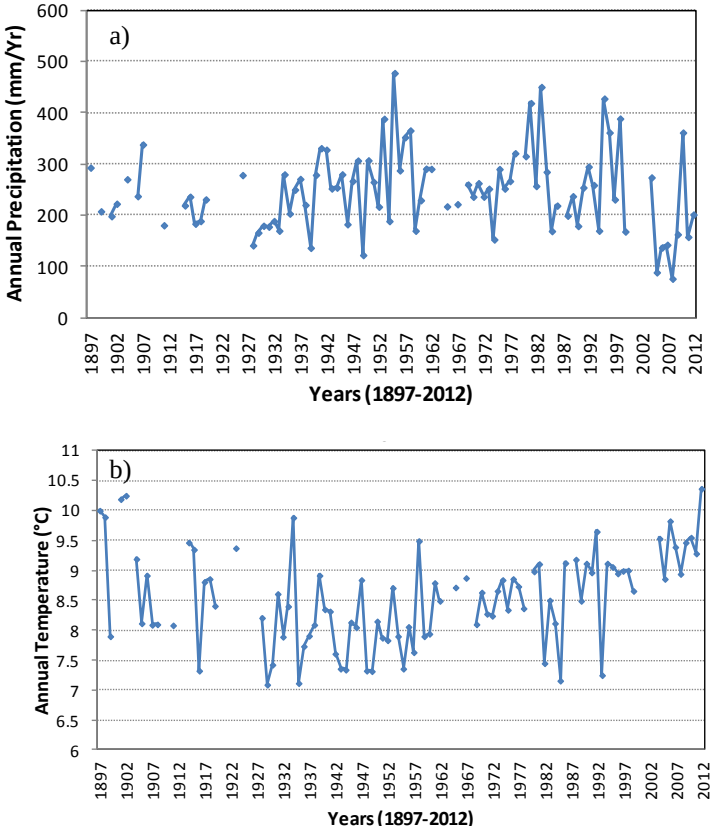

Figure 5.50. Historical annual precipitation (a), and MAT (b) measured by Prineville station.

5.2.3. Model simulations

The approach here used is the same assumed for the shrub encroachment (section 5.1.3), i.e., two different types of simulations have been carried out:

a) *long time scale*: 5,000 years - under this scenario, we setup the model with equally distributed species (33%), trying to obtain a stationary behavior coherent with the observed pattern. The simulation is run for 5,000 years, forced by statistically generated storms using a Poisson process and a cosine function to reproduce the annual cycle of the potential evapotranspiration.

b) *short time scale*: 140 years (from 1871 to 2010) - encroachment from ecotone boundary. This simulation is designed and carried out with the aim to reproduce the fast and recent encroachment phenomenon. Using eleven years of the *Metolius* station site data, 140 years of weather data with the AWE-GEN model have been obtained and the encroachment simulation has been done using hourly precipitation data and calculating the potential evapotranspiration with the Penman-Monteith equation.

5.2.3.1. Model set up

PFTs are defined at a 5m by 5m grid as described in the two previous case studies.

A spatially uniform soil thickness was assumed, while the soil (one soil type modeled as sandy-loam) parameters used in the model are shown in Table 5.14.

The site morphology has been classified into topographically similar slope-aspect (*S-A*) groups, considering a 6 degree increment for local slopes (5-53°) (9 slope classes) and a 30 degree increment for aspect (0-360°) (13 aspect classes) leading to 117 different combinations (*S-A* groups) in order to get and analyze the effect of the *Slope-Aspect* group on the vegetation distribution.

Table 5.14. Soil parameters used in the water balance component of the model. Source: Laio et al. (2001).

Soil Texture	n [-]	s_{fc} [-]	I_{c-b} [mm·d^{-1}]	K_s [mm·d^{-1}]	b [-]
Sandy Loam	0.43	0.56	0.83	1.75	4.9

5.2.3.2. Weather forcings

5.2.3.2.1. Long time scale weather forcings

The model has been forced by daily rainfall and potential evapotranspiration ($T_{max\text{-}X}$). The precipitation time series has been generated with a simplified stochastic Poisson process calibrated with the historical observed precipitation. The $T_{max\text{-}X}$ annual cycle has been obtained from a stationary cosine function fitted to mean daily values of $T_{max\text{-}X}$ calculated from the daily Penman-Monteith equation using the *Metolius* station data.

In storm generation, we have used the *Poisson Rectangular Pulses (PRP)* model, with a one-parameter exponential distribution for time between storms (T_b) and storm durations (T_r); and a Gamma distribution for rainfall depth h conditioned on T_r (e.g., Ivanov et al., 2007). The storm intensity p, is calculated as: $p=h/T_r$. Two rainfall seasons have been considered: wet season and dry season with seasonal precipitations denoted by P_w and P_d.

In Table 5.15, the observed and modeled rainfall parameters for the Poisson rectangular pulses method for the *Metolius* weather station (2002-2012) are

shown. N_{day} is the number of day of each season, f is the fraction of precipitation falling in each season, P is the mean annual precipitation for each season, λ is the frequency of storm event, T_b is the interstorm period, T_r is the storm duration, N_{storm} is the number of storm for each season, and α is the mean precipitation depth falling in each event.

Table 5.15. Comparison between observed data and storm generator outputs.

Observed Data								
Season	N_{day}	f	P [mm·yr^{-1}]	λ [d^{-1}]	T_b [h]	T_r [h]	N storm	α [mm]
wet	273	0.907	419.5	0.227	105.7	6.17	62	6.8
dry	92	0.093	43.0	0.130	184.0	1.96	12	3.6

Output Model						
Season	P [mm·yr^{-1}]	λ [d^{-1}]	T_b [h]	T_r [h]	N storm	α [mm]
wet	420	0.224	107.1	6.07	63	6.7
dry	44	0.131	182.9	2.01	13	3.4

According with Miller et al. (2005), the wet season is considered as ranging from October to June, 273 days, while the dry season ranges from July to September, 92 days.

Daily maximum transpiration is obtained from the cosine function fitting (3.40) to calculated $T_{max\text{-}X}$ for each PFT (3.36). $\overline{T}^{F}_{\max-X}$ (juniper: 3.3 mm·d^{-1}; grass: 3.2 mm·d^{-1}; shrub: 2.4 mm·d^{-1}), L_T equal to 30 days (peak T^{H}_{Cos-X} occurs when DOY is greater than $N_d/2$, consistent with the climate in the region), and Δ (juniper: 6.3 mm·d^{-1}; grass: 6 mm·d^{-1}; shrub: 4.6 mm·d^{-1}) are obtained for each vegetation calibrating the cosine function with the T_{max} obtained from observed data using the Penman-Monteith equation (Figure 5.51). To reduce data requirements and keep the model simple, the bare soil T_{max}, E_b, is calculated as described in section 5.1.3.2.1.

In order to illustrate the role of topography and incoming solar radiation on the potential evapotranspiration distribution, the mean $T_{max\text{-}X}$ for each vegetation type over the study area is plotted in Figure 5.52. Annually, in the *S*-facing slope the $T_{max\text{-}X}$ is greater than in the *N*-facing slopes because it receives as much as twice the solar radiation received by *N*-facing slopes.

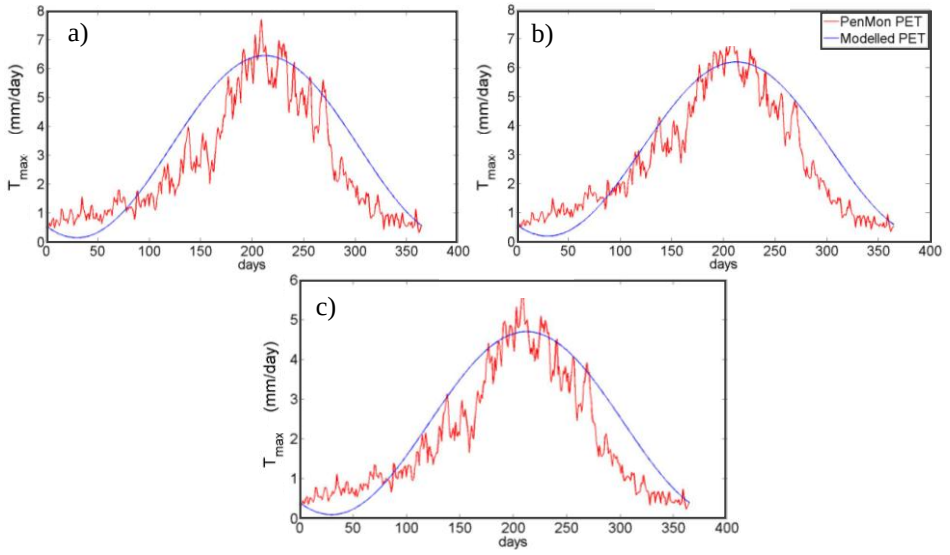

Figure 5.51. Calibration of $T_{max\text{-}X}$ annual curve: (a) juniper, (b) grass, (c) shrub.

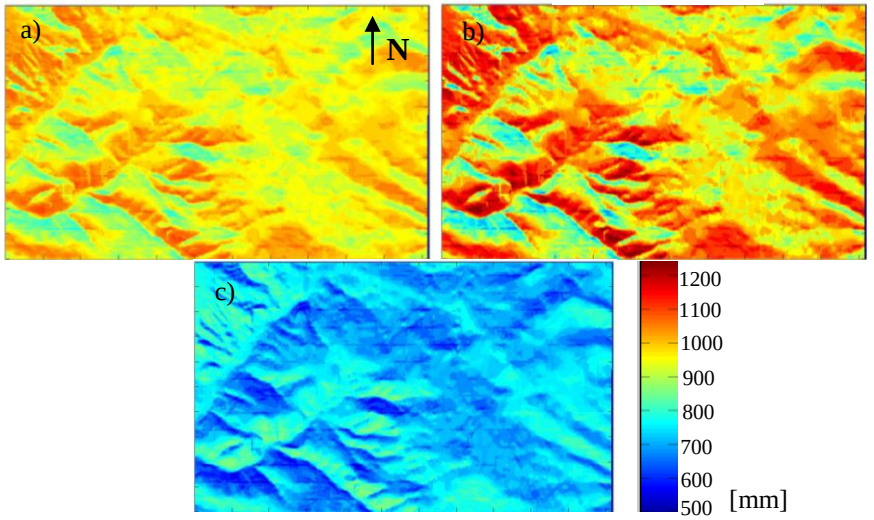

Figure 5.52. Mean annual $T_{max\text{-}X}$ over the study area for: juniper (a), grass (b) and shrub (c).

5.2.3.2.2. Encroachment weather forcings

For the encroachment analysis, using eleven years of the *Metolius* station site data, 140 years of weather data with the AWE-GEN model have been generated (Figure 5.53) and the encroachment simulation has been done using hourly precipitation data and calculating the potential evapotranspiration with the

Penman-Monteith equation. Since the CATGraSS model works at daily and interstorm time scale, the hourly data have been aggregated.

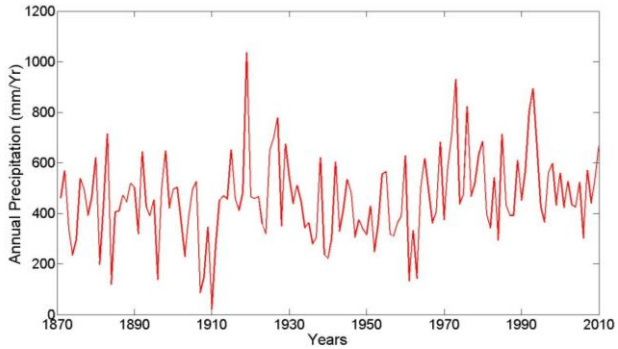

Figure 5.53. Annual precipitation for the period 1871-2010 obtained with the AWE-GEN using *Metolius* station site data.

For the encroachment from 1871 to 2010, stationary precipitation and temperature have been considered because there was not a statistically significant variation of such variables in the past century.

5.2.4. Long time scale: 5,000 years simulation

5.2.4.1. Model calibration

The model has been calibrated to reproduce the initial vegetation percentage in the study area before encroachment in 1870 with a 5,000 years simulation without encroachment causes (fire return period, T_F, constant and equal to 10 years and no grazing effects).

The initial condition (juniper, shrub and grass percentage before encroachment) and the final vegetation percentage (after encroachment) have been set using two different data sources:

- Miller et al. (2000; 2005): there is a qualitative description of vegetation percentage dynamics in the Miller's papers, but it is relative to an area (Oregon, California, Idaho, Nevada) wider than our plot and, for this reason, the percentages could be misleading (Figure 2.20);
- NLCD map (2006) of the study area (Figure 5.46); in this map the separation of grass and shrub is problematic. Areas observed on the ground as shrubs or grasses are not always distinguishable spectrally, as previously said in section 5.2.2.1. Moreover, there is not the availability of a vegetation map of our study area relative to 1870.

In Table 5.16, the past and current vegetation percentages obtained from the two sources are shown. In particular, the final juniper percentage is 46% in Miller et al. (2005) (Figure 2.20) and 86.5% in the NLCD map (Figure 5.46).

Table 5.16. Vegetation percentage in Miller et al. (2000; 2005) and NLCD map.

Vegetation percentage [%]						
Vegetation	Miller et al. (2000)		Miller et al. (2005)		NLCD Map (2006)	
	1870	Current	1870	Current	1870	Current
Juniper	0-10	40-50	0	46	-	86.5
Shrub	20-30	4-5	28.5	0.5	-	13
Grass	-		-	-	-	0.5

Since the different data sources lead to apparently contradictory classification, one hypothesis has been assumed for this work: NLCD map is related to our study area at 2006, therefore we assumed it as the true current vegetation distribution map in 2010 while we assumed that the vegetation dynamics followed Miller et al. (2005) (even if valid for a larger area). Estimating the percentage increase from Figure 2.20 (juniper increase from 5% to 46% corresponds to a relative increase of 820%; shrub decrease from 28.5% to 4.5% corresponds to a relative decrease of 84%) and applying this value to obtain the initial condition which leads to 86.5% for juniper and 13.5% for shrub-grass (NLCD vegetation percentage), the initial vegetation percentage in 1870 is equal to 11% for juniper and 76% for shrub-grass.

Vegetation parameters used for simulating local water balance and plant dynamics (e.g., biomass production and loss) are listed in Table 5.17. The parameters in Table 5.17 are obtained from literature and from calibration in the *long time scale* simulation and compared with the literature for given plant types in the field. Table 5.18 reports parameters used for simulating plant establishment and mortality, mostly obtained from literature and calibration in the *long time scale* simulation as described in the Zafferia study case (see section 4.3.1). Parameters reported in Table 5.17 are obtained from calibration of the model *LAI* to reproduce the observed vegetation patterns in the study area.

We used the time series of MODIS *LAI* to calibrate the model simulated *LAI*. Since three different PFTs cover the study area, we identified MODIS cells that have a relatively uniform cover of a given plant type (juniper and shrub). As shown in Figure 5.54 the MODIS pixel selected to represent the *LAI* of juniper is uniformly covered by junipers only and it is inside the study site, the MODIS pixel selected to represent shrub is located in the eastern part of the study site and it is covered uniformly by shrubs. The identification of MODIS pixels representative of the grass cover was not possible given the fact that grass is mixed with the other two plant types and therefore it would have been impossible to separate the *LAI* from the different plants.

As previously made for the other case studies, the MODIS data for 10 years, from 2003 to 2012, are compared with simulations of *LAI* provided by CATGraSS (Figures 5.55, 5.56). In the calibration procedure the decay coefficients for green biomass (k_{sg}), structural biomass (k_{ss}), dead biomass (k_{dd}), the maximum drought induced foliage loss (k_{sf}), the water use efficiency (*WUE*),

the specific leaf are for green (c_g) and dead biomass (c_d), and the LAI_{max} have been manually adjusted to match the MODIS *LAI* data for juniper and shrub controlling, at the same time, that such parameters were within literature parameter ranges (Montaldo et al., 2005, 2008).

The comparison between MODIS *LAI* and modeled *LAI* is shown in Figures 5.55 and 5.56 for juniper and shrub, respectively. The model shows consistency in estimating the onset of the growing and dormant seasons, and the *LAI* peak is estimated correctly in each years. For the grass, the same parameters of Zhou et al. (2013) has been used (Table 5.17). The Nash-Sutcliffe efficiency (*NSE*) (Nash and Sutcliffe, 1970) and the coefficient of determination (R^2) (for juniper *NSE*=0.63, R^2=0.87, and for shrub *NSE*=0.45, R^2=0.69) show an agreement between model predictions and remote sensing estimation, ranging from acceptable to good.

Table 5.17. Plant parameters used to simulate soil moisture and vegetation dynamics.

Parameters	Description	Grass	Western juniper	Creosote bush
I_{max}	Full canopy interception [mm]	1.0[1]	2.0[1]	1.5[1]
Z_r	Root depth [m]	0.3[2]	1.3[3]	0.5[3]
Z_{veq}	Vegetation height [m]	0.3[4]	7.0[9]	1.0[3]
r_l	Stomatal resistance [$s \cdot m^{-1}$]	130[4]	270[1]	210[4]
s^*	Saturation degree at stomata closure	0.33[1]	0.22[1]	0.24[1]
s_w	Saturation degree at wilting point [-]	0.13[1]	0.15[1]	0.13[1]
s_h	Saturation degree at soil hygroscopic	0.10[5]	0.10[5]	0.10[5]
LAI_{max}	Maximum LAI [$m^2 \cdot m^{-2}$]	2.0[4]	4.0[14]	2.9[3]
R_{in}	Ratio of canopy-interspace infiltration capacity [-]	1.2[6]	2.0[3]	2.0[10]
WUE	Water Use Efficiency [$kg_{CO2} kg^{-1}_{H2O}$]	0.01[7]	0.006[11]	0.004[11]
k_{sg}	Decay coef. green biomass [d^{-1}]	0.012[7]	0.01[11]	0.007[11]
k_{ss}	Decay coefficient of structural biomass [d^{-1}]	0.01[7]	0.009[11]	0.001[11]
k_{dd}	Decay coef. of dead biomass [d^{-1}]	0.013[7]	0.05[11]	0.08[11]
k_{sf}	Maximum drought induced foliage loss rates [d^{-1}]	0.02[8]	0.001[11]	0.02[11]
c_g	Specific leaf area for green biomass [m^2 leaf $\cdot g^{-1}_{DM}$]	0.0047[7]	0.015[11]	0.019[11]
c_d	Specific leaf area for dead biomass [m^2 leaf $\cdot g^{-1}_{DM}$]	0.009[7]	0.03[11]	0.025[11]
α_s	Shortwave albedo [-]	0.12[1]	0.1[1]	0.15[1]
GT, *DT*	Growth and dormancy thresholds [$mm \cdot d^{-1}$]	3, 4[11]	N/A	N/A
Td_{max}	Constant for dead biomass loss adjustment [$mm \cdot d^{-1}$]	10[7]	10[7]	10[7]

Source: (1) Caylor et al. (2005); (2) Kurc and Small (2004); (3) Gutierrez-Jurado et al., (2006); (4) Guan and Wilson (2009); (5) Laio et al. (2001); (6) Bhark and Small (2003); (7) Istanbulluoglu et al. (2012); (8) Ivanov et al. (2008a); (9) Miller et al. (2005); (10) Paul and Litvak (2009); (11) Calibration.

Allelopathy is incorporated in CATGraSS by using the inhibitory factor, IN_G. The IN_G was obtained from calibration: we have done different simulations considering first the absence of the inhibition factor (IN_G=1), and then increasing it to 2 (maximum inhibition), for a total of ten simulations. We obtained IN_G equal to 1.92 (Table 5.18).

For the fire event we have assumed a probability of fire, P_F, (i.e., the reverse of return period, T_F) like to 0.1 (return period, T_F: 10 years; Casagrandi and Rinaldi, 1999) while the vulnerability to fire of each vegetation, $V_{F\text{-}X}$, is shown in Table 5.19.

Table 5.18. Model parameters for modeling plant mortality and establishment.

Parameters	Description	Grass	Creosote bush	Shrub Seedling	Western juniper	Juniper Seedling
θ_X	Drought resistant threshold [-]	0.57[5]	0.9[5]	0.8[5]	0.72[5]	0.57[5]
$P_{Mb\text{-}X}$	Background mortality probability [-]	0.01[5]	0.01[5]	0.01[5]	0.01[5]	0.01[5]
$P_{E\text{-}X\text{-}max}$	Maximal establishment probability [-]	0.4[5]	0.3[5]	N/A	0.2[5]	N/A
IN_X	Inhibitory factor [-]	1.92[5]	N/A	N/A	N/A	N/A
t_{max}	Maximum age [yr]	N/A	600[1]	18[2]	1000[3]	20[4]

Source: (1) Bowers et al. (1995); (2) Chew and Chew (1965); (3) Miller et al. (2005); (4) Schott and Pieper (1986); (5) Calibration.

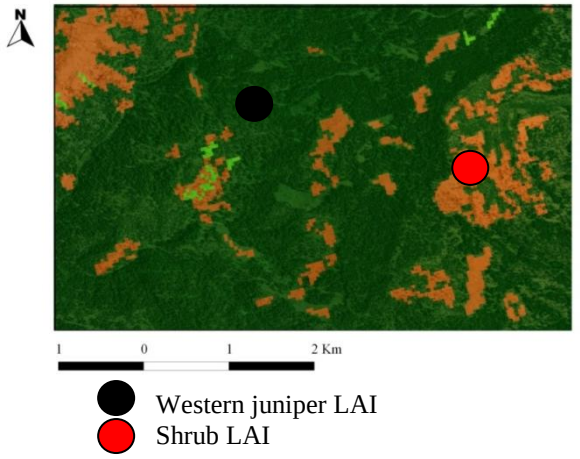

Figure 5.54. Vegetation map and MODIS *LAI* pixels used to evaluate the juniper and shrub LAI.

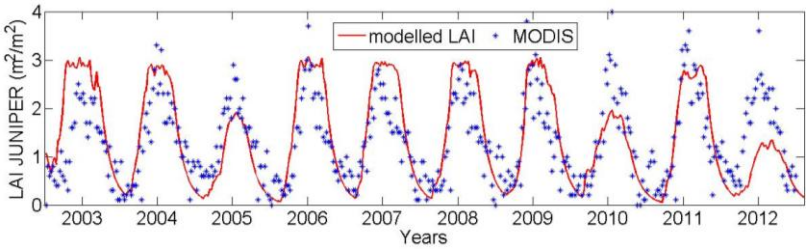

Figure 5.55. Comparison between western juniper MODIS *LAI* and modeled *LAI*, period 2003-2012.

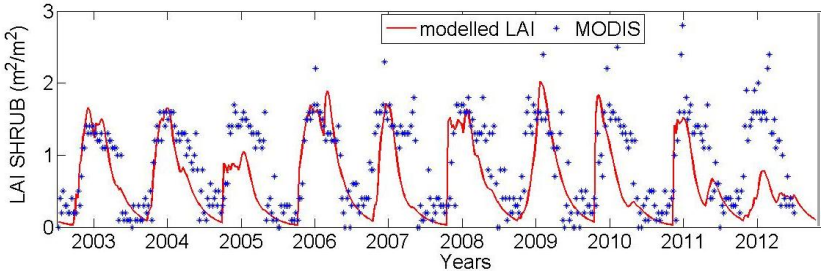

Figure 5.56. Comparison between shrub MODIS *LAI* and modeled *LAI*, period 2003-2012.

Table 5.19. Fire parameters.

Parameters	Juniper	Juniper seedling	Shrub	Shrub seedling	Grass
Probability of fire P_F [yr^{-1}]			0.1 [1]		
Fire return period T_F [yr]			10 [1]		
Vulnerability to fire $V_{F\text{-}X}$ [-]	0.08 [2,3]	0.2 [2,3]	0.1 [2,3]	0.2 [2,3]	0.8 [2,3]

Source: (1) Miller et al. (2006), Le Houèrou (1974), Thomas (1991), (2) Accatino et al. (2010), (3) Calibration.

In Figure 5.57, the actual evapotranspiration (ET_a) measured by the *Metolius* eddy covariance station has been compared with the ET_a obtained by the model. The mean ET_a is 296 mm, while the modeled mean ET_a is 290 mm. The calibrated model is able to reproduce the ET_a.

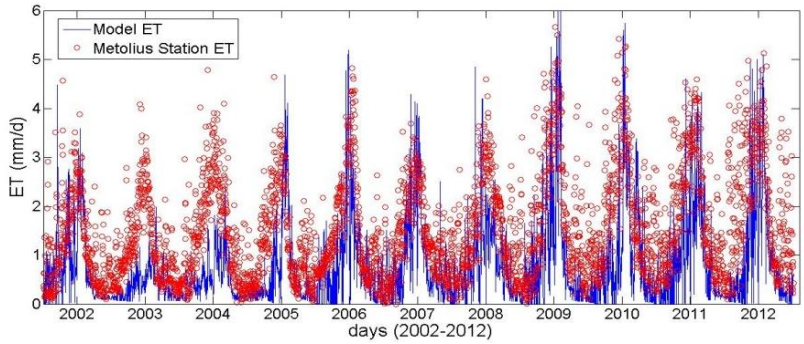

Figure 5.57. Real evapotranspiration: *Metolius* eddy covariance station.

5.2.4.2. Model simulation and results

The model has been calibrated to reproduce the initial vegetation percentage in the study area before encroachment in 1870 using a 5,000 years simulation without encroachment causes. The model was initially run with a random vegetation distribution, characterized by the same probability of assignments for all PFTs and bare soil (33.3%) as in the previous case studies.

The vegetation percentage in 1870, obtained at the end of the 5,000th year, is composed by juniper 11%, shrub 28%, grass 48% (shrub-grass 76%), bare soil 18.5% (Figure 5.58). These values are in accordance with Miller et al. (2005; 2007), Table 5.16 and Figure 2.20, for which in 1870 shrub percentage was between 20 and 30, juniper percentage between 0 and 10 and grass-bare soil percentage between 60 and 70. The final vegetation distribution after 5,000 years of simulation and the time series of percent coverage of PFTs in the study site are shown in Figures 5.58a and 5.58b, respectively.

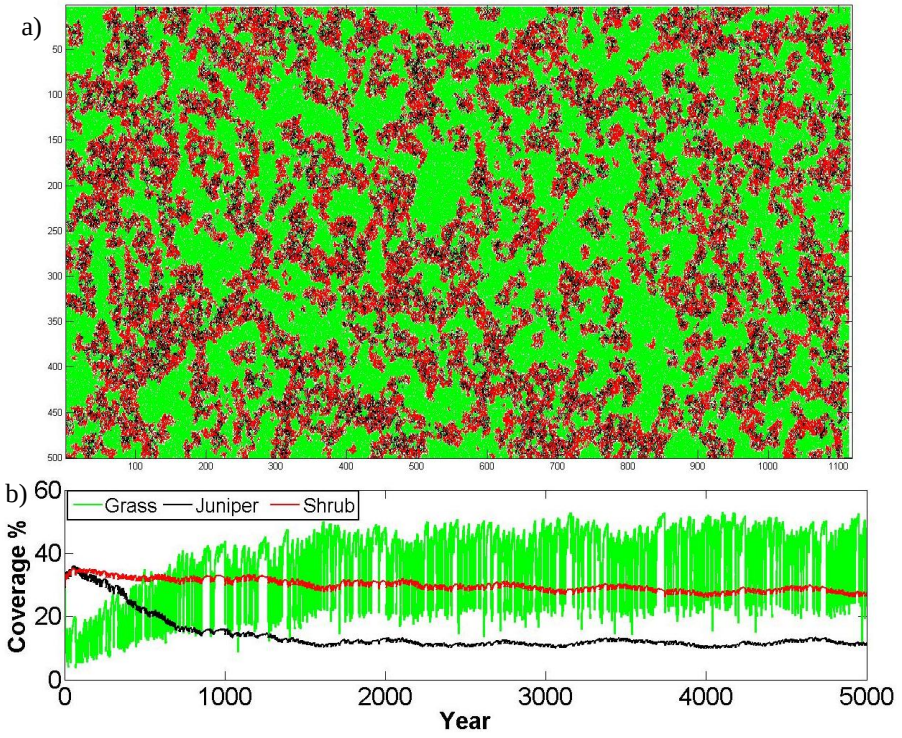

Figure 5.58. (a) Final vegetation distribution after 5,000 years of simulation, (b) time series of percent coverage of PFTs in the study site.

After 5,000 years the shrubs are distributed following cluster, but the vegetation composition is not influenced by the topography. While the shrub

time series in Figure 5.58b is mainly stationary, the juniper time series decrease mainly from 0 to 1,000 years and it is mainly constant from 1,000 to 5,000 years. The grass time series increase mainly from 0 to 1,000 years. The highly variable nature of grass percentage is typically driven by the inter-annual fluctuations in precipitation. Because grasses have an overall higher water stress and lower drought resistance, they die rapidly during dry years, but also grow back quickly in the following wetter years, as their seeds are assumed to be available everywhere in space. In addition, the establishment and mortality of grass depend on the rainfall of a given year and therefore subjected to the same inter-annual variability of rainfall. The *lag-1* autocorrelation is 0.801 for grass, 0.997 for juniper and 0.979 for shrub.

5.2.5. Short time scale: encroachment

After that the initial vegetation percentage in the study area in 1870 (i.e., before encroachment) has been reproduced, the CATGraSS has been run to reproduce the juniper encroachment occurred in the last 140 years (from 1871 to 2010).

5.2.5.1. Encroachment factors parameters used in the CATGraSS

The causes that have been considered for the juniper encroachment in this case study are (Figure 5.23): the fire, the grazing, the seed dispersal caused by animals, the shrub-grass inhibition effect (i.e., allelopathy) and the plant type competition.

In CATGraSS we modeled the fire effect by considering a T_F linear increasing from 10 years (in 1871) to 100 years (in 2010) according to Figure 5.59 (Miller et al., 2007). In Figure 5.59 the relationship between fire return period and the percent composition of grasses, shrubs and junipers in this area is shown. Setting the initial (1871) and final (2010) shrub percentage (22% and 4.5%, respectively), using the curve related to the shrub in Figure 5.59, the initial and final fire return period have been obtained: 10 and 100 years, respectively. The vulnerability to fire, $V_{F\text{-}X}$, has been setted equal to 0.8 for grass, 0.08 for juniper (0.2 for young juniper) and 0.10 for shrub (0.2 for young shrub, Burkhardt and Tisdale, 1976) after a sensitivity analysis carried out using Accatino et al. (2010) value ranges. This parameter varies from 0.02 if junipers (or shrubs) are very fire resistant, to 0.6 if junipers are easily killed by fire according to Casagrandi and Rinaldi (1999).

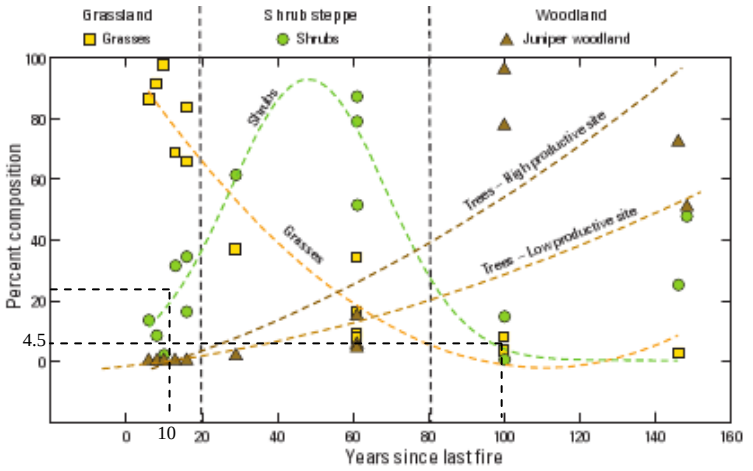

Figure 5.59. Relationship of time since fire and the percent composition of grasses, shrubs and junipers (Miller et al., 2007).

A previously said in section 5.1.5.1, while in literature the fire model, that we used in the CATGraSS, has been previously studied and applied and values of its parameters are presented in different works, for grazing and seed dispersal there is not enough scientific literature useful to allow to us their choice. For this reason, for each single factor, different values have been first fixed trying to understand the effect of the choice of the single factor on the encroachment; then these factors have been combined, and among all the combinations, the one that provide the more acceptable reproduction of the current vegetation percentage has been selected. First, the *base simulation*, *BS*, i.e., the base simulation of 140 years (1871-2010) without encroachment factors has been done.

The grazing effect is for grass and shrub and not for juniper. Grazing effect has been obtained following the approach of previous case studies. The parameter P_{Mb} has been obtained increasing it in the years to simulate the increase of the grazing effect (Van Auken, 2000; 2009). Eight different grazing cases, that provide a linear increase of P_{Mb} from 1871 to 2010, have been assumed. In Table 5.20 the final shrub (*SH*), grass (*G*) and juniper (*T*) percentages for each P_{Mb} case are shown (e.g., case "0.01-0.05" means P_{Mb} equal to 0.01 in 1871 and P_{Mb} equal to 0.05 in 2010). In Figure 5.60 the final vegetation percentages in function of the P_{Mb} are shown. In the P_{Mb} axis, for each case the P_{Mb} value in 2010 is shown. Only the grazing could not cause the total juniper encroachment, i.e., current juniper coverage equal to 86.5%. But, with the 40% of P_M related to the grazing in 2010, the juniper increases from 12.80 to 69.04%, which means a consistent increase.

Table 5.20. Final vegetation percentages in function of the grazing factor (P_{Mb}).

Grazing			
Encroachment Factor	Final Vegetation Percentage [%]		
$P_{Mb\,(-)}$	SH	G	T
BS	30.60	46.50	12.80
0.01-0.05	24.06	27.99	34.62
0.02-0.10	4.39	21.48	50.60
0.03-0.15	0.80	25.13	57.92
0.04-0.20	0.08	19.25	61.00
0.05-0.25	0.01	16.08	64.11
0.06-0.30	0.00	9.08	66.09
0.07-0.35	0.00	9.75	68.25
0.08-0.40	0.00	6.50	69.04

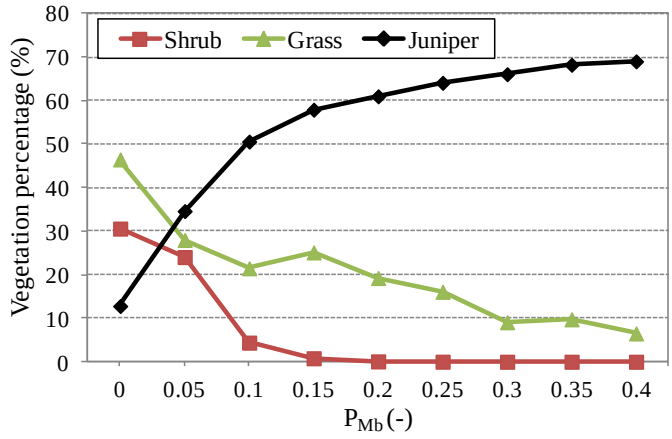

Figure 5.60. Final vegetation percentages in function of the grazing factor (P_{Mb}).

As previously made in section 5.1.5.1, the grass decay coefficient of green biomass, $K_{sg\text{-}G}$ has been increased from 1871 to 2010 to simulate the grass biomass reduction caused by cattle (i.e., *LAI* reduction). This coefficient has been assumed linearly increasing from 0.004 d^{-1} in 1870 to 0.012 d^{-1} in 2010, using the range of Montaldo et al. (2005) and the actual value used by Zhou et al. (2013).

Dispersal of seeds of woody plants by domestic animals had increased the encroachment (Van Auken, 2000; 2009). The spread of seed probability for the juniper, *SSP*, has been introduced in the model and its value has been ranged from 0.001 to 0.02 for a total of seven values. In Table 5.21 the final vegetation percentages for different values of *SSP* factor are shown. In Figure 5.61 the final vegetation percentages in function of the *SSP* are shown. Also in this case, only the seed dispersal caused by animals could not cause the total juniper

encroachment. In fact, with *SSP* equal to 0.2, the juniper increases from 12.80 to 31.82% with a relative growth of more than 120%.

Table 5.21. Final vegetation percentages in function of the *SSP*.

Seed Dispersal			
Encroachment Factor	Final Vegetation Percentage [%]		
SSP (-)	SH	G	T
BS	30.60	46.50	12.80
0.01	45.45	27.59	22.22
0.02	45.23	27.11	22.53
0.04	44.05	28.73	22.68
0.05	44.36	21.90	28.42
0.08	44.35	20.77	29.68
0.1	44.44	15.93	30.30
0.2	42.45	21.64	31.82

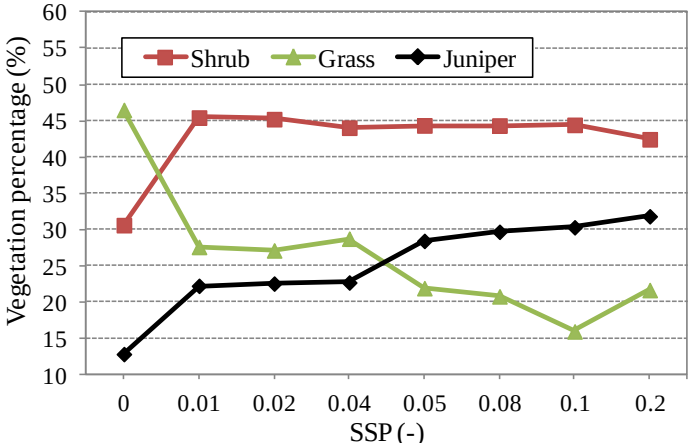

Figure 5.61. Final vegetation percentages in function of the *SSP*.

As mentioned in section 5.1.5.1, in order to take into account the wind direction influence on the shrub encroachment direction and on the vegetation pattern direction, the *wind direction factors WD'* and *WD''* have been introduced. They are not encroachment factors. In fact, the wind may cause a directionality of the seed dispersal. In the study area the wind speed direction predominant is from southeast to northwest (Figure 5.14). We assumed *WD'* ranging from 1.5 to 5 and *WD''* from 1 to 4. Six different *WD'-WD''* combinations have been obtained. In Table 5.22 the final vegetation percentages for each *WD'-WD''* combination are shown (e.g., case "1.5-1" means *WD'* and *WD''* equal to 1.5 and 1, respectively), while Figure 5.62 shows the final

vegetation percentages in function of the *WD*. In the *WD* axis, for each case the *WD'* value is shown. Increasing the *WD'* to 5 (i.e., the greatest effect of the wind direction) the juniper increases from 12.80 to 42.66%, which means a great effect of the wind direction. If one compares the effect of the wind direction on the juniper encroachment with that related to the shrub encroachment (Figure 5.27), it can be observed a greater increase of the juniper percentage and then a greater effect of the wind direction. In fact, the juniper plant live index, φ_T, is, in average, smaller than the φ_{SH} because its water stress is greater than the shrub water stress, then when it is multiplied for the *WD*, the probability of establishment has a greater increase leading to a faster encroachment.

Table 5.22. Final vegetation percentages in function of the *WD* factor.

Wind			
Encroachment Factor	Final Vegetation Percentage [%]		
WD (-)	SH	G	T
BS	30.60	46.50	12.80
1.5-1	44.96	21.87	22.18
2-1.5	43.56	18.70	25.11
2.5-2	42.60	15.14	37.54
3-2.5	41.46	13.62	40.26
4-3	38.93	10.57	41.93
5-4	37.54	13.03	42.66

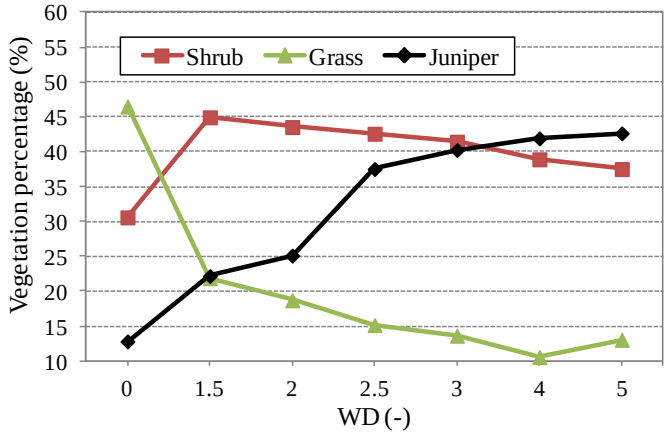

Figure 5.62. Final vegetation percentages in function of the *WD* factor.

Climate change has not been considered as encroachment cause in accordance with Bahre and Shelton (1993) and Van Auken (2000; 2009) and because in the past there was not a statistically significant trend of temperature and precipitation.

As made for the shrub encroachment case in Sevilleta, in order to define the combination of the above mentioned parameters which provides the actual vegetations percentages at 2010, a total of 1008 simulations have been carried out. This number derives from the combination of all the cases of each factor, considering also the *BS* simulation: 2 fire cases, 9 grazing cases, 8 seed dispersal cases, 7 wind cases. Among the 1008 combinations, the one selected by us that causes the increase of the juniper to 86.5% (i.e., current percentage) is summarized in Table 5.23, even if it is important to point out that other simulations provided similar "acceptable" reproduction of the actual vegetation percentage.

Table 5.23. Encroachment factor parameters used for each period.

Years	T_F [yr]	P_{Mb} [-]	$K_{sg\text{-}G}$ [d^{-1}]	SSP [-]	WD [-]
1871-1898	10	0.02	0.004		
1898-1926	32.5	0.04	0.006		
1926-1954	55	0.06	0.008	0.04	1.5-2
1954-1982	77.5	0.08	0.010		
1982-2010	100	0.10	0.012		

In Figure 5.63 the final vegetation distribution after the juniper encroachment (a), using all the factors parameterized as shown in Table 5.23, and the time series of percent coverage of PFTs in the study area (b) are shown. The juniper time series shows a constant increase during the 140 years, only from 1900 to 1910 it shows a decrease. The shrub percentage is mainly constant until 1920, and it decreases from 1920 to 2010. The grass time series shows a high variability as in the *long time scale* simulation. The *lag-1* autocorrelation is 0.842 for grass, 0.981 for juniper and 0.985 for shrub.

The western juniper settles all the study area and the shrub disappears in the study area (according to Figure 2.20, Miller et al., 2005). There is not vegetation pattern because all the area is established by juniper. The final vegetation percentage is: juniper 86.5 %, grass 8.7% and shrub 2.3% and it is in accordance with the real vegetation percentage in Figure 5.46, with Miller et al. (2000; 2005) and Tausch and West (1995). These results are also in accordance with Figure 5.64 (Johnson and Miller, 2006) that shows a conceptual model with estimated time periods from initial juniper establishment to minimum stocking adequate for *phase III*, and estimated maximum potential for relative abundance and cover for stands developing on sites from high to low productivity. In 140 years, the western juniper percentage increase from 5% to 46% with a relative increase of 820% like our simulation.

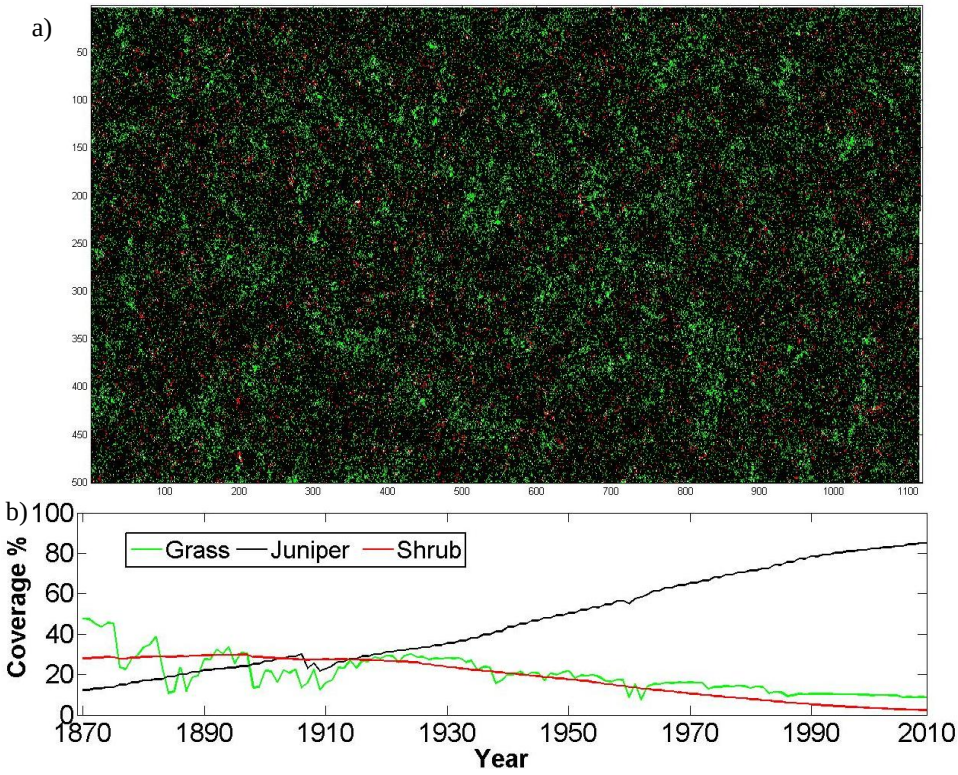

Figure 5.63. (a) Final vegetation distribution after 140 years of encroachment simulation, (b) time series of percent coverage of *PFT*s in the study site.

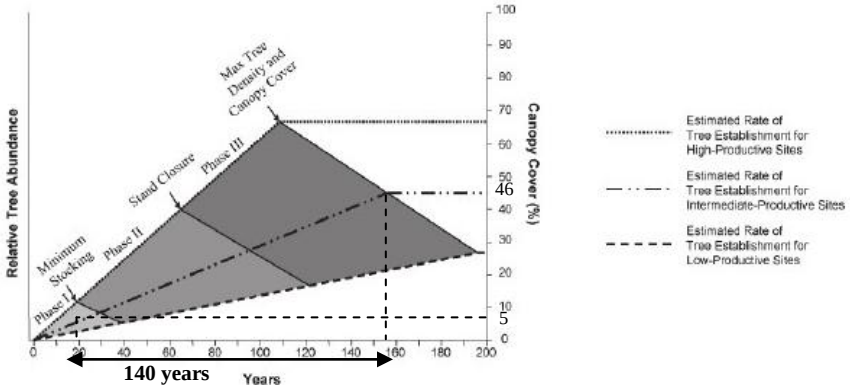

Figure 5.64. Conceptual model with estimated time periods from initial juniper establishment to minimum stocking adequate for *phase III*, and estimated maximum potential for relative abundance and cover for stands developing on sites from high to low productivity (Johnson and Miller, 2006).

5.2.5.2. Results and discussion: analysis of the influence of the single factors on the encroachment in the past 140 years

In order to understand the effect of each single factor on the encroachment phenomenon, a series of different simulations have been carried out assuming the presence of each factor separately and then different combination of such factors. These simulations have been compared with the *BS*, previously introduced. A multi-step strategy has been then used to explore what we learn with the model with respect to the contribution of different parameters that contribute to the observed vegetation change. We have combined fire return period (*F*), grazing (*GR*), wind direction (*W*) and seed dispersal caused by animals (*SD*): first using a single cause then combining the causes in pairs, three by three, and all the causes together for a total of 16 factors combinations. In Table 5.24 the final vegetation percentages for each factors combination are shown. For a fixed number of factors, the combinations that provide the greatest juniper percentage increase are highlighted in italic.

Table 5.24. Final vegetation percentage for each factors combination.

Final Vegetation Percentage [%]							
Factors	SH	G	T	Factors	SH	G	T
BS	*30.60*	*46.50*	*12.80*	GR-W	3.90	27.00	55.53
F	40.17	9.71	35.33	GR-SD	4.36	28.69	53.59
GR	*4.39*	*21.48*	*50.60*	W-SD	42.24	27.35	26.02
W	43.56	18.70	25.11	F-GR-W	2.59	11.66	79.61
SD	44.05	28.73	22.68	*F-GR-SD*	*2.67*	*11.03*	*81.33*
F-GR	*2.95*	*10.89*	*77.45*	F-W-SD	36.80	19.31	40.73
F-W	38.92	14.22	39.55	GR-W-SD	3.91	26.93	56.94
F-SD	37.56	19.79	39.29	*F-GR-W-SD*	*2.32*	*8.71*	*86.50*

The fire frequency reduction and the increased grazing intensity have the greatest influence on the encroachment. In fact, the grazing causes the greatest increase of the juniper, from 12.80 to 50.60%, and the fire causes an increase of the juniper from 12.80 to 35.33%. Using only a cause, *GR* has provided the greatest influence. Combining two factors, *F* and *GR* showed the greatest influence (juniper increases from 12.80 to 77.45%, almost the target percentage) while combining three factors, the greatest influence is provided by *F*, *GR* and *SD* (juniper increases from 12.80 to 81.33%).

The time series of percent coverage of PFTs in the study site over 140 years for each factors combination are shown in Figure 5.65. In the *BS* simulation there is not the increase of the juniper, and the shrub and juniper percentages are almost stationary. Using all the encroachment factors, the juniper time series increase faster increasing the number of factors.

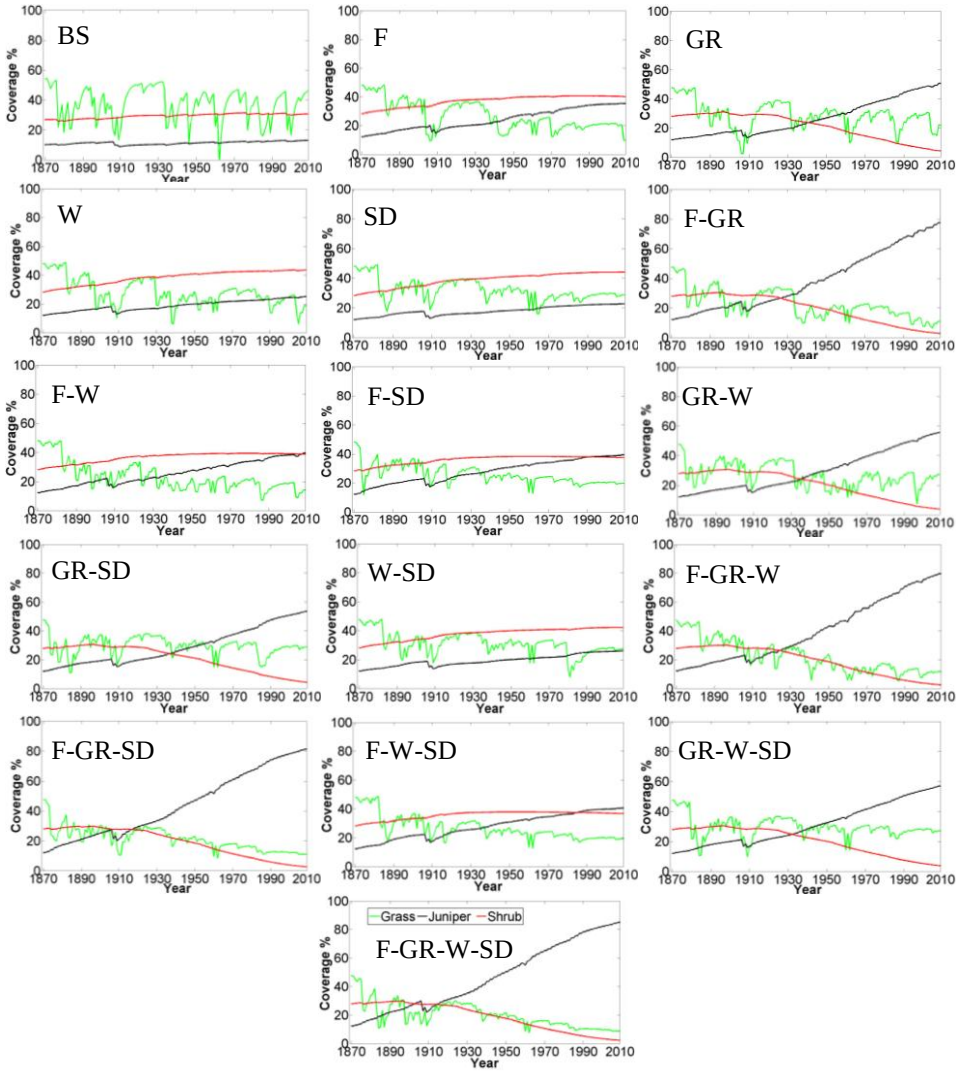

Figure 5.65. The time series of percent coverage of PFTs in the study site over 140 years for each factor combinations.

The latest report on the future climate change of the IPCC (IPCC, 2013) shows, in the study area, a reduction of precipitation of 120 mm and an increase of the temperature of 3° C. Considering the results obtained in Sevilleta (i.e., the climate change, precipitation decrease and temperature increase, accelerates the encroachment), for the future encroachment, as the juniper has already invaded the whole study site in 2010, it could persist in this area and also increase from 86.5% to 100%. Therefore, we consider not necessary to analyze what could happen in the future doing future encroachment simulation as done for the shrub encroachment in Sevilleta.

Conclusions

Natural ecosystems are complex structures whose peculiarities and properties depend on three fundamental factors, interacting in space and time with each other: climate, soil and vegetation. Predicting how ecosystems could respond to forecasted environmental and climatic changes and evaluating the consequences of this response are the major challenges in ecohydrology today.

Vegetation pattern and dynamics are inseparably linked to initial conditions of site characteristics (i.e., topography) and species availability. In fact, vegetation has been observed to exhibit a degree of spatial organization in a number of ecosystems in space and time. The emergence of these organization patterns is attributable to a range of spatial process such as local interactions between species, localized dispersal abilities and disturbance regime. Moreover, space and time dynamics of ecosystems are tightly related to fluctuations in the climate and to the competition strategies of individual plants for different resources. The climatic regime influence species' distributions, often through species-specific physiological thresholds of temperature and soil water potential tolerance. Divergent responses or susceptibilities of individual species to climate change may modify their interactions with others species at the same or adjacent trophic levels as long-term data on both terrestrial and marine organisms indicate.

However, understanding the impact of climatic disturbances, topography and soil variability on vegetation in space and time requires dynamic vegetation modeling across the landscapes. In this context, in thesis we have modeled the past and future dynamic of the vegetation patterns using and improving an existent ecohydrological Cellular Automata Model. We have studied three case studies: the variation of the vegetation pattern in a Mediterranean basin subsequent to likely climate change, and the shrub and juniper encroachment in the western north America grasslands.

Despite the potential important role of topography on water, nutrient, and energy distribution, few studies have related topographic controls on the dynamics and patterns of plant co-existence. Especially in semiarid systems, topography mediates patterns of soil moisture that affects plant productivity, and could lead to specific vegetation patterns in certain hillslopes with specific aspects and morphologies. The first case study can be considered as the first application of a CA model with future climate scenarios to examine ecotone boundaries, composition of vegetation within each ecotone and their dynamics.

The *Cellular Automata Tree-Grass-Shrub Simulator* (CATGraSS) has been here further developed and used for modeling the long-term spatial dynamics of oaks, grass, and Indian fig species typical of mediterranean ecotone in the current and future climates. In the model, the incoming shortwave radiation and maximum evapotranspiration were treated spatially-explicitly on the terrain using a DEM. A fine-scale gridded domain is used to represent vegetation type. Each cell can hold a single plant type or remain empty. Plant competition is modeled explicitly by keeping track of mortality and establishment of plants, both calculated probabilistically based on soil moisture stress. Forced by a stochastic representation of the current climate, the calibrated model run on catchment in Sicily, Italy, where north-facing slopes are characterized by oaks, and south-facing slopes exhibit plant coexistence, composed of Indian figs and grasses. Spatially explicit treatment of solar radiation, and a lower limit to soil moisture storage imposed by bedrock depth lead to spatial organization in evapotranspiration and soil moisture that control the current vegetation pattern which has been predicted by the model reasonably well. CATGraSS results underscore the importance of topography and soil thickness in determining vegetation composition over complex terrain in semiarid Mediterranean climates.

Climate change scenarios for the analyzed catchment in Sicily showed that the median projected climate change in this region could be characterized by an increase of the mean annual air temperature, equal to about 2.8° C in 100 years, and a reduction of the annual precipitation, equal to 30% in 100 years.

A considerable sensitivity of the vegetation spatial distribution to variation of rainfall and temperature was simulated. In particular, the numerical results suggest that the observed vegetation pattern is tightly link to the current climate. The changes in the future precipitation could lead to a reorganization of the plant composition based mainly on the topography, characterized by loss of oaks and expansion of grass. Reduction of precipitation will increase the water stress of all the vegetation types. While grass dies rapidly, it also grows back quickly, as its seeds are assumed to be available everywhere in space, therefore grass cover fraction tends to increase quickly with time in a drier climate. This study highlights, arguably for one of the first times at this scale, the importance of simulating local plant competition and interactions and the role of climate variability in determining impacts on vegetation diversity. Simulations including or not the effects on stomatal closure induced by elevated CO_2 concentration are rather similar suggesting that CO_2 effects are unlikely to counteract the climate change effects in meteorological variables in this specific catchment and scenario (-30% in mean precipitation) because reduction in water availability has the greatest influence on actual evapotranspiration and plant performance.

Spatio-temporal vegetation dynamics can be also discussed for studying the shrub and tree encroachment phenomenon that is one of the most prevalent contemporary shrubs and trees cover increase and land-cover changes into

grasslands. Causes of increased woody plant abundance may vary in different grasslands, and some likely factors include increased grazing intensity, the fire return period increase, alterations in local land management practices, and rising atmospheric CO_2 concentrations. Because grassland and savanna ecosystems account for 30-35% of global terrestrial net primary production, any change in patterns or controls of carbon inputs and storage due to increase woody vegetation in grasslands will have important implications for regional and global nutrient cycles. In addition, woody plant expansion often decreases herbaceous species diversity. The fire plays the major role in determining the coexistence and balance of grasses and woody plant species in grasslands. Frequent fires (every year or two) are sufficient to limit the cover and spread and woody plants, while fire exclusion can lead to shrub dominance or complete conversion to woodlands in as little as a few decades.

Therefore, in order to reproduce this phenomenon, creosote bush and western juniper encroachments in the *Sevilleta National Wildlife Refuge* (SNWR), New Mexico, and in the Ochoco National Forest, Oregon, have been simulated with the CATGraSS, respectively, in the second and third case study.

A fire cellular automata component has been introduced in the CATGraSS in order to simulate the fire effect. For each plant type, the probability of be ignited and killed by fire is a function of the fuel availability and of the vulnerability to fire. CATGraSS is also improved with a grazing and seed dispersal function, and its plant establishment algorithm is modified. The causes, here considered for the encroachment in these case studies, are: the fire return period increase, the grazing increase, the seed dispersal caused by animals and the plant type competition.

In the SNWR, the model is able to simulate the encroachment, simulating an increasing of the shrub from 2% to 42% (i.e., current vegetation percentage) highlighting among the most influent factors the reduced fire frequency that causes the greatest increase of shrub, and the increased grazing intensity that causes the greatest reduction of grass, in accordance with Van Auken (2000; 2009). The model is sensitive to the initial conditions. When a South to North gradient is considered in the initial distribution of shrubs, shrub expanded in the domain faster.

Simulating the future vegetation distribution in 2100 with climate change, the shrub increases from 42% to 95.9%. The future climate change, characterized by a reduction of precipitation and an increase of temperature, will accelerate the encroachment and the shrub will settle in all the study area. Therefore, it can be also considered an important cause of the shrub encroachment increase.

In the Ochoco National Forest, the western juniper could encroach all the study area and the shrub and grass could disappear. The most influent factors are the reduced fire frequency and the increased grazing intensity. The model could be used for the assessment of the encroachment in the future decades in the study area.

While in Sevilleta the shrub encroached the study site grassland, in Oregon the juniper (i.e., tree) encroached the shrubland-grassland area. Therefore, in the first case the shrub is the species that encroaches the area, in the second case it is the species invaded and dominated by the juniper. It can be obviously related to environmental and climatic conditions that favor the invasion of a species respect to another. Comparing the encroachment in Sevilleta and in Oregon the most important differences are the more complexity of the Oregon juniper encroachment linked to the presence of other two vegetation types (grass and shrub) and the effect of the grazing obtained by the model greater in the Oregon juniper encroachment than in the shrub encroachment.

For the future management and encroachment control, the reduction of the fire return period and the grazing removal or limitation could be the best actions in order to reduce and control the encroachment.

Overally the CATGraSS has reproduced reasonably well the influence of the topography on the vegetation pattern distributions, and the encroachment phenomena. Therefore, the research here presented, thus, has given an important contribution in the field of vegetation pattern evaluation, providing a starting point for further improvements, developments and applications.

In conclusion, the CATGraSS can be considered a good ecohydrological CA model able to reproduce the spatio-temporal vegetation dynamics, even if the difficulties to calibrate it because of the high number of parameters. The encroachment phenomenon has been very difficult to reproduce and simulate; in fact, it is the first time in literature that an ecohydrological model is used to reproduce this phenomenon and there was not enough scientific literature useful to allow us the encroachment factors parameters choice.

Moreover, it is important to underline that there are large uncertainties in the future climate estimation related to the GCMs. The GCMs outputs exhibit a large spread, underlining inherent uncertainties in climate model predictions. In fact, GCMs have two important drawbacks: the spatial resolution, that is too coarse to be used directly in local studies, and the temporal resolution (GCMs realizations are only available at the daily or larger aggregation intervals). But the GCMs are the only tools available which allow us to estimate the future climate.

Further efforts could be made in the future, in order to improve the model. A future research development could interest the study of the effect of the morphology on the Oregon juniper encroachment. The fire return period change and the grazing have been implemented in the model separately. But, following the literature works they are strongly linked: the fire return period increases because the grazing increases reducing the fine fuel available for the fire. Therefore, a future improvement of the CATGraSS model could be connect these two variables, and determine the change in the fire return period as function of the grazing variation. Another improvement of the work could be study the effect of the vegetation distribution and pattern change on the soil

erosion. In fact, the rapid vegetation change could lead to an increase in the soil erosion rates and subsequent changes in the biogeochemical processes. The model could be improved with a geomorphic component to analyze the effect of the vegetation pattern and of the vegetation dynamics on the erosion at catchment scale. Hillslope and channel erosion processes can coupled with vegetation-hydrology dynamics, making it possible to study the impact of vegetation on hydrologic and geomorphic processes and how the latter processes affect vegetation.

Bibliography

Accatino, F., De Michele, C., Vezzoli, R., Donzelli, D., Scholes, R.J. (2010). Tree-grass co-existence in savanna: Interactions of rain and fire. *Journal of Theoretical Biology, 267, 235-242.*

Acevedo, E., Badilla, I., Nobel, P.S. (1983). Water Relations, Diurnal Acidity Changes, and Productivity of a Cultivated Cactus, Opuntia ficus-indica. *Plant Physiol., 72, 775-780.*

Adams, A.W. (1975). A brief history of juniper and shrub populations in southern Oregon. *Oregon State Wildlife Commission Research Division. Wildlife Research Report No. 6, Corvallis, OR.*

Ainsworth, E.A., and Long, S.P. (2004). What have we learned from 15 years of free-air CO_2 enrichment (FACE)? A meta-analytic review of the responses of photosynthesis, canopy properties and plant production to rising CO_2. *New Phytologist, 165 (2): 351-372. doi:10.1111/j.1469-8137.2004.01224.x.*

Albertson, F.W., and Tomanek, G.W. (1965). Vegetation changes during a 30 year period in grassland communities near Hays, Kansas. *Ecology, 46, 714-20.*

Allen, C.D., and Breshears, D.D. (1998). Drought-induced shift of a forest-woodland ecotone: Rapid landscape response to climate variation. *Proc. Natl. Acad. Sci. USA, Vol. 95, pp. 14839-14842, December 1998.*

Allen, C.D., Betancourt, J., Swetnam, T. (2002). Range expansion of woody plants on the Colorado Plateau. *In: Grahame, J.D., Sisk, T.D. (Eds.). http://www.cpluhna.nau.ed/.*

Allen, R.G., Pereira, L.S., Raes, D., Smith, M. (1998). Crops evapotranspiration: Guidelines for computing crop water requirements. *Irrigations and Drainage. Paper 56, FAO, Rome, 300 pp.*

Allen, R. G., Trezza, R., Tasumi, M. (2006a). Analytical integrated functions for daily solar radiation on slopes. *Agric. For. Meteorol., 139, 55-73.*

Allen, R. G., Pruitt, W.O., Wright, J.L., Howell, T.A., Ventura, F., Snyder, R., Itenfisu, D., Steduto, P., Berengena, J., Yrisarry, J.B., Smith, M, Pereira, L.S., Raes, D., Perrier, A., Alves, I., Walter, I., Elliott, R. (2006b). "A recommendation on standardized surface resistance for hourly calculation of reference ET_0 by the FAO56 Penman-Monteith method." *Agric. Water Manage., 81(1-2), 1-22.*

Allen, M. F., Allen, E. B., Lansing, J. L., Pregitzer, K. S., Hendrick, R. L., Ruess, R. W., Collins, S. L. (2010). Responses to chronic N fertilization of ectomycorrhizal piñon but not arbuscular mycorrhizal juniper in a piñon-juniper woodland. *J. of Arid. Environ., 74, 1170-1176.*

Andrade, J.L., Cervera, J.C., Graham, E.A. (2009). Microenvironments, water relations, and productivity of CAM plants. *Pages 95-120 in De la Barrera E, Smith W, eds. Perspectives in Biophysical Plant Ecophysiology: A Tribute to Park S. Nobel. UNAM.*

Antevs, E. (1938). Rainfall and tree growth in the Great Basin. *Carnegie Institution of Washington Publication 469, Washington, D.C. and American Geographical Society, Special Publication No. 21, New York, NY.*

Archer, S., Scifres, C., Bassham, C.R., Maggio, R. (1988). Autogenic succession in a subtropical savanna: Conversion of grassland to thorn woodland. *Ecological Monographs, 58, 111-27.*

Archer, S. (1994). Woodly plant encroachment into southwestern grasslands and savannas: rates, patterns and proximate causes. *Ecological Implications of Livestock Herbivor in the West, pp 13-69. Denver: Soc. Range Manage.*

Archer, S. (1995). Harry Stobbs Memorial Lecture, 1993. Herbivoe mediation of grass-woody plant interactions. *Tropical Grasslands, vol. 29, 218-235.*

Armesto, J.J., and Martınez, J.A. (1978). Relations between vegetation structure and slope aspect in the Mediterranean region of Chile. *J. Ecol., 66:881-889. doi:10.2307/2259301.*

Arora, V. K. (2002). Modeling vegetation as a dynamic component in soil-vegetation-atmosphere transfer schemes and hydrological models. *Rev. Geophy., 40, doi:10.1029/2001RG000103.*

Arora, V.K., and Boer, G.J. (2005). A parameterization of leaf phenology for the terrestrial ecosystem component of climate models. *Global Change Biol., 11(1), 39-59.*

Arora, V. K., and Boer, G. J. (2006). Simulating Competition and Coexistence between Plant Functional Types in a Dynamic Vegetation Model. *Earth Interactions, 10(10), 1-30.*

ASCE EWRI (2005). The ASCE Standardized Reference Evapotranspiration Equation. Environmental and Water Resources Institute (EWRI) of the American Society of Civil Engineers Task Committee on Standardization of Reference Evapotranspiration Calculation. *ASCE, Washington, DC, p. 190.*

Asner, G.P., Archer, S., Hughes, R.F., Ansley, R.J., Wessman, C.A. (2003). Net changes in regional woody vegetation cover and carbon storage in Texas Drylands, 1937-1999. *Global Change Biology, 9, 316-335.*

Austin, M.P. (1981). Permanent quadrats: An interface for theory and practice. *Vegetation, 46, 1-10.*

Azuma, K.L., Hiserote, B.A., Dunham, P. A. (2004). The western juniper resource of eastern Oregon. *USFS GTR.*

Bachelet, D., Neilson, R.P., Lenihan, J.M., Drapek, R.J. (2001). Climate Change Effects on Vegetation Distribution and Carbon Budget in the United States. *Ecosystems, 4: 164-185. doi: 10.1007/s10021-001-0002-7.*

Bae, D-H, Jung, I.W., Chang, H. (2008). Potential changes in Korean water resources estimated by high-resolution climate simulation. *Climate Res., 35:213-226, doi:10.3354/cr00704.*

Bahre, C.J., and Shelton, M.L. (1993). Historic vegetation change, mesquite increases, and climate in southeastern Arizona. *Journal of Biogeography, 20, 489-504.*

Bahre, C.J. (1995). Human impacts on the grasslands of southeastern Arizona. In: The Desert Grassland. *Tucson: Univ. Ariz. Press, 110, pp 230-264.*

Bakkenes, M., Alkemade, J. R. M., Ihle, F., Leemans, R., Latour, J. B. (2002). Assessing effects of forecasted climate change on the diversity and distribution of European higher plants for 2050. *Global Change Biology, 8, 390-407.*

Band, L.E., Patterson, P., Nemani, R., Running, S.W. (1993). Forest ecosystem processes at the watershed scale - Incorporating hillslope hydrology. *Agric. For. Meteorol., 63(1-2), 93-126.*

Barbera, G. (1984). Ricerche sull'irrigazione del Ficodindia (in Italian). *Frutticoltura 46, 49-55.*

Bates, B.C., Kundzewicz, Z.W., Wu, S., Palutikof, J.P. (2008). Climate change and water. Technical paper. *Intergovernmental Panel on Climate Change, IPCC Secretariat, Geneva.*

Bavay, M., Lehning, M., Jonas, T., Lowe, H. (2009). Simulations of future snow cover and discharge in Alpine headwater catchments. *Hydrol. Process., 23:95-108, doi:10.1002/hyp.7195.*

Beaty, R.M., and Taylor, A.H. (2001). Spatial and temporal variation of fire regimes in a mixed conifer landscape, Southern Cascades, California, USA. *J. Biogeogr., 28:955-966. doi:10.1046/ j.1365-2699.2001.00591.x.*

Bedwell, S.F. (1973). Fort Rock Basin prehistory and environment. *University of Oregon Books, Eugene, OR.*

Ben Wu, X., and Archer, S.R. (2005). Scale-dependent influence of topography-based hydrologic features on patterns of woody plant encroachment in savanna landscape. *Landscape Ecology, 20:733-742.*

Betancourt, J. (1987). Paleoecology of pinyon juniper woodlands: summary. *Pages 129–139 In R.L. Everett (compiler). Proceedings: Piñon-juniper Conference. USDA Forest Service General Technical Bulletin Report INT-215.*

Bhark, E. W., and Small, E. E. (2003). Association between plant canopies and the spatial patterns of infiltration in shrubland and grassland of the Chihuahuan desert, New Mexico. *Ecosystems, 6, 185-196.*

Boisvenue, C. and Running, S.W. (2006). Impacts of climate change on natural forest productivity - evidence since the middle of the 20th century. *Global Change Biology, 12: 862-882.*

Bolsinger, C.L., and Berger, J.L. (1975). The timber resources of the Blue Mountain area, Oregon. *Resour. Bull. PNW-57. Portland, OR. U.S. Department of Agriculture, Forest Service, Pacific Northwest Forest and Range Experiment Station. 62 pp.*

Bonan, G. B., Levis, S., Sitch, S., Vertenstein, M., Oleson, K. W. (2003). A dynamic global vegetation model for use with climate models: concepts and description of simulated vegetation dynamics. *Global Change Biology, 9, 1543-1566.*

Bornkamm, R. (1988). Mechanisms of succession on follow land. *Vegetation, 77, 95-101.*

Botkin, D.B. (1992). The Ecology of Forests: Theory and Evidence. *Oxford Univ. Press, New York.*

Bouraoui, F., Vachaud, G., Li, L.Z.X., Treut, H.L., Chen, T. (1999). Evaluation of the impact of climate changes on water storage and groundwater recharge at the watershed scale. *Climate Dynam., 15:153-61.*

Bovard B.D., Curtis P.S., Vogel C.S., Su H-B., Schmid H.P. (2005). Environmental controls on sap flow in a northern hardwood forest. *Tree Physiol., 25:31-8.*

Bowers, J. E., Webb, R. H., Rondeau, R. J. (1995). Longevity, recruitment and mortality of desert plants in Grand Canyon, USA. *J. of Veget. Sci., 6, 551-564.*

Bras, R. L. (1990). Hydrology, An Introduction to Hydrologic Science. *1st ed., Addison-Wesley Publishing Company, U.S.*

Brolsma, R. J., and Bierkens, M. F. P. (2007). Groundwater-soil water-vegetation dynamics in a temperate forest ecosystem along a slope. *Water Resour. Res., 43: W01414. DOI:10.1029/ 2005WR004696.*

Brown, J.H., Valone, T.J., Curtin, C.G. (1997). Reorganization of an arid ecosystem in response to recent climate change. *Proc. Natl Acad. Sci. USA, 94, 9729-9733.*

Browning, D.M., Archer, S.R., Asner, G.P., McClaran, M.P., Wessman, C.A. (2008). Woody Plants in grasslands: Post-Encroachment stand dynamics. *Ecological Applications, 18(4), pp. 928-944.*

Bruijnzeel, L.A., and Veneklaas, E.J. (1998). Climatic conditions and tropical montane forest productivity: the fog has not lifted yet. *Ecology, 79:3-9.*

Buffington, L.C., and Herbel, H. (1965). Vegetational Changes on a semidesert grassland range from 1858 to 1963. *Ecological Monographs, vol. 35, No. 2, pp.139-164.*

Bunting, S.C., Kingery, J.L., Stand, E. (1999). Effects of succession on species richness of the western juniper woodland/sagebrush steppe mosaic. *Pages 76-81. In S.B. Monsen, S. Richards, R.J. Tausch, R.F. Miller, and C. Goodrich*

(compilers). Proceedings Ecology and Management of piñon-juniper communities within the Interior West. USDA Forest Service, RMRS-P-9.

Burkhardt, J.W., and Tisdale, E.W. (1976). Causes of juniper invasion in southwestern Idaho. *Ecology, 57:472-484.*

Burlando, P, and Rosso, R. (2002). Effects of transient climate change on basin hydrology. Precipitation scenarios for the Arno river, central Italy. *Hydrol. Process, 16:1151-75*.

Burton, A., Kilsby, C.G., Fowler, H.J., Cowpertwait, P.S.P., O'Connell, P. (2008). RainSim: a spatial–temporal stochastic rainfall modelling system. *Environ Model Software, 23:1356-69, doi:10.1016/j.envsoft.2008.04.003.*

Burton, A., Fowler, H.L., Blenkinsop, S., Kilsby, C.G. (2010). Downscaling transient climate change using a Neyman-Scott Rectangular Pulses stochastic rainfall model. *J. Hydrol., 381:18-32, doi: 10.1016/j.jhydrol.2009.10.031*.

Busing, R.T. (1991). A spatial model of forest dynamics. *Vegetatio, 92, 167-79.*

Cannarozzo, M., Noto, L.V., Viola, F. (2006). Spatial distribution of rainfall trends in Sicily (1921–2000). *Physics and Chemistry of the earth, vol. 31(8); p. 1201-1211, ISSN: 1474-7065, doi: 10.1016/j.pce.2006.03.022.*

Cantlon, J.E. (1953). Vegetation and microclimate on north and south slopes of Cashetunk Mountain, New Jersey. *Ecological Monographs, 23,241-270.*

Casagrandi, R., and Rinaldi, S. (1999). A minimal Model for Forest Fire Regimes. *The American naturalist, vol. 153, no. 5.*

Caylor, K.K., Scanlon, T.M., Rodríguez-Iturbe, I. (2004). Feasible optimality of vegetation patterns in river basin. *Geophys. Res. Lett., 31, L13502.*

Caylor, K. K., Manfreda, S., Rodriguez-Iturbe, I. (2005). On the coupled geomorphological and ecohydrological organization of river basins. *Adv. Water Resour., 28(1), 69-86*.

Caylor, K. K., Scanlon, T. M., Rodriguez-Iturbe, I. (2009). Ecohydrological optimization of pattern and processes in water-limited ecosystems: A trade-off-based hypothesis. *Water Resour. Res. 45, W08407, doi:10.1029/2008WR007230.*

Cayrol, P., Chehbouni, A., Kergoat, L., Dedieu, G., Mordelet, P., Nouvellon, Y. (2000). Grassland modeling and monitoring with SPOT-4 VEGETATION instrument during the 1997-1999 SALSA experiment. *Agric. For. Meteorol, 105 (2000), 91-115.*

Chahine, M.T. (1992). The hydrological cycle and its influence on climate. *Nature, 359, 373-380.*

Chew, R. M., and Chew, A. E. (1965). The Primary Productivity of a Desert-Shrub (Larrea tridentata) Community. *Ecol. Monogr., 35(4), 355-375.*

Christensen, N.S., Wood, A.W., Voisin, N., Lettenmaier, D.P., Palmer, R.N. (2004). Effects of climate change on the hydrology and water resources of the Colorado river basin. *Climatic Change, 62:337-63*.

Clark, D.B., Palmer, M.W., Clark, D.A. (1999). Edaphic factors and the landscape-scale distributions of tropical rain forest trees. *Ecology, 80:2662-2675.*

Clements, F.E. (1904). The development and structure of vegetation. *Botanical Survey of Nebraska 7. Studies in Vegetation of the State, Lincoln, Nebraska.*

Clements, F.E. (1916). Plant Succession. *Carniage Institute Washington Publication 242, Washington, D.C.*

Clements, F. E. (1934). The relict method in dynamic ecology. *J. Ecol., 22: 39-68.*

Cohen, J. (1960). A coefficient of agreement for nominal scales. *Educ. Psychol. Measurement, 20(1):37-46.*

Cohen, S.J. (1990). Bringing the global warming issue close to home: The challenge of regional impact studies. *Bulletin of the American Meteorological Society, 71: 520-526.*

Cole, K.L. (1983). Late Pleistocene vegetation of Kings Canyon, Sierra Nevada, California. *Quaternary Research, 19:117-129.*

Congalton, R. G. (1991). A review of assessing the accuracy of classifications of remotely sensed data. *Remote Sensing of Environment, 37, 35-46.*

Connell, J.H., and Slatyer, R.O. (1977). Mechanisms of succession in natural communities and their roles in community stability and organization. *Amer. Nat., 111, 1119-44.*

Connell, J.H. (1978). Diversity in tropical rain forests and coral reefs. *Science, 199, 1302-10.*

Consoli, S., Inglese, G., Inglese, P. (2013). Determination of Evapotranspiration and Annual Biomass Productivity of a Cactus Pear (Opuntia ficus-indica L. (Mill.) Orchard) in a Semi-arid Environment. *Journal of Irrigation and Drainage Engineering, 139:680-690. doi:10.1061/(ASCE)IR.1943-4774.0000589.*

Coop, J.D., and Givnish, T.J. (2007). Spatial and temporal patterns of recent forest encroachment in montane grasslands of the Valles Caldera, New Mexico, USA. *Journal of Biogeography, 34, 914-927.*

Coppedge, B.R., Engle, D.M., Masters, R.E., Gregory, M.S. (2001). Avian response to landscape change in fragmented southern Great Plains grasslands. *Ecological Applications, 11:47-59.*

Couteron, P., and Lejeune, O. (2001). Periodic spotted patterns in semi-arid vegetation explained by a propagation-inhibition model. *J. of Ecol., 89, 616-628.*

Cowles, H.C. (1901). The physiographic ecology of Chicago and vicinity. *Bot. Gazette, 31, 73-108.*

Cowlin, R.W., Briegleb, P.A., Moravets, F.L. (1942). Forest resources of the ponderosa pine region of Washington and Oregon. *Misc. Publ. 490. Washington, DC: U.S. Department of Agriculture, Forest Service. 99 p.*

Cowpertwait, P.S.P. (1991). Further developments of the Neyman–Scott clustered point process for modeling rainfall. *Water Resour. Res.,27:1431-8.*

Cowpertwait, P.S.P. (1994). A generalized point process model for rainfall. *Proc. Roy. Soc. Lond. Ser. A., 447:23-7.*

Cowpertwait, P.S.P., O'Connell, P., Metcalfe, A., Mawdsley, J. (1996). Stochastic point process modelling of rainfall: I. Single-site fitting and validation. *J. Hydrol., 175:17-46.*

Cowpertwait, P.S.P. (1998). A Poisson-cluster model of rainfall: high order moments and extreme values. *Proc. Roy. Soc. Lond. Ser. A., 454:885-98.*

Cowpertwait, P.S.P., Kilsby, C., O'Connell, P. (2002). A space-time Neyman-Scott model of rainfall: empirical analysis of extremes. *Water Resour. Res., 38(8):1-14.*

Cowpertwait, P.S.P. (2004). Mixed rectangular pulses models of rainfall. *Hydrol. Earth Syst. Sci., 8:993-1000.*

Cowpertwait, P.S.P. (2006). A spatial-temporal point process model of rainfall for the Thames catchment. *J. Hydrol., 330:586-95.*

Cowpertwait, P.S.P., Isham, V., Onof, C. (2007). Point process models of rainfall: developments for fine scale structure. *Proc. Roy. Soc. Lond. Ser. A., 463(2086):2569-87.*

Cramer, W., Bondeau, A., Woodward, F. I., Prentice, I. C., Betts, R. A., Brovkin, V., Cox, P. M., Fisher, V., Foley, J. A., Friend, A. D., Kucharik, C., Lomas, M. R., Ramankutty, N., Sitch, S., Smith, B., White, A., Young-Molling, C. (2001). Global response of terrestrial ecosystem structure and function to CO_2 and climate change: results from six dynamic global vegetation models. *Global Change Biology, 7, 357-373.*

Crawley, M.J. (1997). Plant-herbivore dynamics. *In Plant Ecology, ed. MJ Crawley, pp. 401-474. Oxford: Blackwell Sci.*

Curtis, D.C., and Eagleson, P.S. (1982). Constrained stochastic climate simulation. *Technical report 274, Mass. Inst. of Technol., Dep. of Civ. and Environ. Eng. Ralph M. Parsons Lab., Cambridge, Mass, USA.*

D'Odorico, P., Laio, F., Ridolfi, L., Lerdau, M.T. (2008). Biodiversity enhancement induced by environmental noise. *J. Theor. Biol., 255, 332–337.*

Daubenmire, R. (1968). Plant communities. *Harper and Row, New York.*

Davis, J.O. (1982). Bits and pieces: the last 35,000 years in the Lahontan area. *Pages 53-75. In Society of American Archeology Paper 2.*

De Kock, G.C. (1980). Drought-resistant fodder shrub crops in South Africa. In: Le Houèrou, H.N. (Ed.), Browse in Africa: the current state of knowledge. *International Livestock Centre for Africa, Addis-Ababa, pp. 339-410.*

Deaves, D.M. and Lines, I.G. (1997). On the fitting of low mean windspeed data to the Weibull distribution. *J Wind Eng Indus Aerodynam, 66:169-78.*

Deser, C., Phillips, A., Bourdette, V., Teng, H. (2012). Uncertainty in climate change projections: the role of internal variability. *Climate Dynam., 38: 527-546. Doi:10.1007/s00382-010-0977-x.*

Di Piazza, A., Lo Conti, F., Noto, L.V., Viola, F., La Loggia, G. (2011). Comparative analysis of different techniques for spatial interpolation of rainfall data to create a serially complete monthly time series of precipitation for Sicily, Italy. *International Journal of Applied Earth Observation and Geoinformation, 13(3), 396-408, doi: 10.1016/j.jag.2011.01.005*.

Dickinson, R.E., and Kennedy, P. (1992). Impacts on regional climate of Amazon deforestation. *Geophys. Res. Lett., 19, 1947-1950.*

Dickinson, R.E. (2000). How coupling of the atmosphere to ocean and land helps determine the timescales of interannual variability of climate. *J. Geophys. Res., 105(D15), 20,115-20,119.*

Dick-Peddie, W.A. (1993). New Mexico vegetation, past, present, and future. *University of New Mexico Press, Albuquerque, NM, 244*.

Dietrich, W. E., and Perron, J. T. (2006). The search for a topographic signature of life. *Nature, 439(7075), 411-418.*

Dingman, S. L., (2002). Physical Hydrology, 2nd Ed. *Upper Saddle River, New Jersey, Prentice Hall.*

Dirnbock, T., Hobbs, R.J., Lambeck, R.J., Caccetta, P.A. (2002). Vegetation distribution in relation to topographically driven processes in southwestern Australia. *Appl. Vegetat. Sci., 5(1), 147-158.*

D'Odorico, P., Ridolfi, L., Porporato, A., Rodriguez-Iturbe, I. (2000). Preferential states of seasonal soil moisture: The impact of climatic fluctuations. *Water Resour. Res., 36(8), 2209-2220.*

D'Odorico, P., Fuentes, J.D., Pockman, W.T., Collins, S.L., He, Y., Medeiros, J.S., Dewekker, S., Litvak, M.E. (2010). Positive feedback between microclimate and shrub encroachment in the northern Chihuahuan desert. *Ecosphere, vol. 1(6), article 17.*

Drake, B. G., Gonzàlez-Meler, M.A., Long, S.P. (1997). More efficient plants: A consequence of rising atmospheric CO_2? *Ann. Rev. Plant. Physiol. Plant Mol. Biol., 48, 609-639.*

Dubayah, R., and Loechel, S. (1997). Modeling topographic solar radiation using GOES data. *J. Appl. Meteorol., 36:141-54.*

Duffie, J.A., and Beckman, W.A. (1980). Solar Engineering of Thermal Process. *1st ed. John Wiley and Sons, NY.*

Duffy, J.E., and Stachowicz, J.J. (2006). Why biodiversity is important to oceanography, potential roles of genetic, species, and trophic diversity in pelagic ecosystem processes. *Mar. Ecol. Progr. Ser., 311, 179-189.*

Dunne, J. A., Harte, J., Taylor, K. J. (2003). Subalpine meadow flowering phenology responses to climate change: Integrating experimental and gradient methods. *Ecol. Monogr., 73, 69-86.*

Dyck, S. (1983). Overview on the Present Status of the Concepts of Water Balance Model. *IAHS Publ. 148. Wallingford, 3-19.*

Dymond, C.C., and Johnson, E.A. (2002). Mapping vegetation spatial patterns from modeled water, temperature and solar radiation gradients. *ISPRS Journal of Photogrammetry and Remote Sensing 57 (1-2), 69-85.*

Eagleson, P.S. (1978). Climate, soil, and vegetation 1. Introduction to water balance dynamics. *Water Resources Research, 14* (5), 705-712.

Eagleson, P.S. (1982). Ecological optimality in water-limited natural soil vegetation systems, 1, Theory and hypothesis. *Water Resour. Res., 18(2), 325-340.*

Eagleson, P.S. (2002). Ecohydrology: Darwinian Expression of Vegetation Form and Function. *Cambridge University Press, Cambridge, U.K.*

Eamus, D. (1991). The interaction of rising CO_2 and temperatures with water use efficiency. *Plant, Cell & Environment, 14(8): 843-852.*

Emmerich, W.E. (2003). Carbon dioxide fluxes in a semiarid environment with high carbonate soils. *Agric. For. Meteorol., 116,91-102.*

Entekhabi, D., Rodriguez-Iturbe., I., Eagleson, P.S. (1989). Probabilistic representation of the temporal rainfall process by a modified Neyman-Scott rectangular pulses model: parameter estimation and validation. *Water Resour Res, 25(2):295-302.*

Erdman, J.A. (1970). Piñon-juniper succession after naturalfires on residual soils of Mesa Verde, Colorado. *Brigham Young University Science Bulletin Biology Series Vol. 11 No. 2.*

Escudero, A., Albert, M. J., Pita, A. J. M., Perez-Garcia, F. (2000). Inhibitory effects of Artemisia herba-alba on the germination of the gypsophyte Helianthemum squamatum. *Plant Eco., 148, 71-80.*

Farquhar, G.D., Ehleringer, J.R., Hubick, K.T. (1989). Carbon Isotope discrimination and photosynthesis. *Annual Review of Plant Physiology and Plant Molecular Biology, 40: 503-537.*

Farrenkopf, T.O. (1982). Forest statistics for eastern Oregon, 1977. *Resour. Bull. PNW-94. Portland, OR: U.S. Department of Agriculture, Forest Service, Pacific Northwest Forest and Range Experiment Station. 28 p.*

Fatichi, S. (2010). The modeling of hydrological cycle and its interaction with vegetation in the framework of climate change. *PhD thesis, University of Firenze, Italy, and T.U. Braunschweig, Germany.*

Fatichi, S., Ivanov, V.Y., Caporali, E. (2011). Simulation of future climate scenarios with a weather generator. *Adv. Water Resources, 34(4), 448-467.*

Fatichi, S., Ivanov, V.Y., Caporali, E. (2012). A mechanistic ecohydrological model to investigate complex interactions in cold and warm water-controlled environments: 1. Theoretical framework and plot-scale analysis. *Journal of Advances in Modeling Earth Systems, 4, M05002, doi:10.1029/2011MS000086.*

Fatichi, S., and Leuzinger, S. (2013). Reconciling observations with modeling: the fate of water and carbon allocation in a mature deciduous forest exposed

to elevated CO_2. *Agricultural and Forest Meteorology, 174/175, 144-157 doi:10.1016/j.agrformet.2013.02.005*.

Fatichi, S., Ivanov, V.Y., Caporali, E. (2013). Assessment of a stochastic downscaling methodology in generating an ensemble of hourly future climate time series. *Climate Dynamics, Volume 40, Issue 7-8, pp 1841-1861. Doi: 10.1007/s00382-012-1627-2.*

Fenner, M. (1987). Seedlings. *New Phytol. 106, 35-47.*

Fernandez-Illescas, C. P., and Rodriguez-Iturbe, I. (2004). The impact of interannual rainfall variability on the spatial and temporal patterns of vegetation in a water-limited ecosystem. *Adv. Water Resour., 27, 83-95*.

Fiering, M.B., and Jackson, B.B. (1971). Synthetic hydrology. *Water resources monograph, American Geophysics Union.*

Fleiss, J.L. (1981). Statistical methods for rates and proportions (2nd ed.). *New York: John Wiley. ISBN 0-471-26370-2.*

Flores-Cervantes, J.H., Istanbulluoglu, E., Vivoni, E.R., Bras, R.L. (2013). Patterns and organization of vegetation productivity along topographic gradients in two semiarid semiarid sites in Southwestern United States. *Ecohydrology, doi: 10.1002/eco.1333.*

Florinsky, I. V., and Kuryakova, G. A. (1996). Influence of topography on some vegetation cover properties. *Catena, 27(2), 123-141.*

Foley, J.A., Levis, S., Costa, M.H., Cramer, W., Pollard D. (2000). Incorporating dynamic vegetation cover within Global Climate Models. *Ecological Applications, 10 (6), 1620-1632.*

Foody, G. M. (2002). Status of land cover classification accuracy assessment. *Remote Sensing of Environment, 80, 185-201*.

Forman, R.T.T., and Godron, M. (1986). Landscape Ecology. *Wiley, New York.*

Forzieri, G., Castelli, F., Vivoni, E. R. (2011). Vegetation dynamics within the North American monsoon region. *J. of Climate., 24(6): 1763-1783*.

Fowler, N.L. (1986). The role of competition in plant communities in arid and semiarid regions. *Annu. Rev. Ecol. Syst., 17: 89-110.*

Franklin, J. (1998). Predicting the distribution of shrub species in southern California from climate and terrain-derived variables. *J. Vegetat. Sci., 9(5), 733-748.*

Franklin, J., McCullough, P., Gray, C. (2000). Terrain variables used for predictive mapping of vegetation communities in Southern California. *In: Wilson JP, Gallant JC (eds) Terrain analysis: principles and applications. Wiley, New York, pp 331-354.*

Franz, T.E., Caylor, K.K., King, E.G., Nordbotten, J.M., Celia, M.A., Rodriguez-Iturbe, I. (2012). An ecohydrological approach to predicting hillslope-scale vegetation patterns in dryland ecosystems. *Water Resources Research, vol. 48, W01515, doi: 10.1029/2011WR010524.*

Freidenreich, S.M., and Ramaswamy, V. (1999). A new multiple-band solar radiative parameterization for general circulation models. *J. Geophys. Res., 104(D24):31389-409.*

Friend, A. D. (1997). PGEN: an integrated model of leaf photosynthesis, transpiration, and conductance. *Ecol. Model., 77:233-55.*

Fritts, H.C., and Wu, X. (1986). A comparison between response-function analysis and other regression techniques. *Tree-ring Bulletin, 46:31-46.*

Frost, P.G.H., and Robertson, F. (1987). The ecological effect of fire in savannas. *Determinants of Tropical Savannas (ed. Walker, B.K.), pp. 93-140. ICSU Press, Miami.*

Gallardo-Cruz, J.A., Pèrez-Garcìa, E.A., Meave, J.A. (2009). B-Diversity and vegetation structure as influenced by slope aspect and altitude in a seasonally dry tropical landscape. *Landscape Ecol., 24:473-482, DOI 10.1007/s10980-009-9332-1*.

Gardner, M. (1970). Mathematical Games – The fantastic combinations of John Conway's new solitaire game "life". *Scientific American 223. pp. 120-123. ISBN 0-89454-001-7.*

Gedney, D.R., Bassett, P.M., Mei, M.A. (1989). Timber resource statistics for all forest land, except National Forests, in eastern Oregon. *Resour. Bull. PNW-164. Portland, OR: U.S. Department of Agriculture, Forest Service, Pacific Northwest Research Station. 25 p.*

Gedney, D.R., Azuma, D.L., Bolsinger, C.L., McKay, N. (1999). Western juniper in eastern Oregon. *U.S. Forest Service General Technical Report NW-GTR-464.*

Gesch, D., Oimoen, M., Greenlee, S., Nelson, C., Steuck, M., Tyler, D., (2002). The National Elevation Dataset. *Photogrammetric Engineering and Remote Sensing, 68(1), 5-11.*

Ghil, M., and Vautgard, R. (1991). Interdecadal oscillations and the warming trend in global temperature time series. *Nature, 350:324-327.*

Giorgi, F., and Lionello, P. (2008). Climate change projections for the Mediterranean region. *Global and Planetary Change 63 (2008) 90-104.*

Gitay, H., Suàrez, A., Watson, R. (2005). Climate change and biodiversity. *Intergovernmental Panel on Climate Change.*

Glenn-Lewin, D.C., Peet, R.K., Veblen, T.T. (1992). "Plant Succession: theory and prediction". *Population and community biology series 11, published by Chapman & Hall, ISBN: 0 412 26900 7.*

Gloaguen, J.C. (1990). Post-burn succession on Brittany heathlands. *J. Veg. Sci., 1, 147-52.*

Goldstein, G., Ortega, J.K.E., Nerd, A., Nobel, P.S. (1991). Diel Patterns of Water Potential Components for the Crassulacean Acid Metabolism Plant *Opuntia ficus-indica* when Well Watered or Droughted. *Plant Physiology 95, 274-280.*

Gosz, J. R., Moore, D. I., Shore, G. A., Grover, H. D., Rison, W., Rison, C. (1995). Lightning estimates of precipitation location and quantity on the Sevilleta LTER, New Mexico. *Ecol. Applications, 5, 1141-1150.*

Graumlich, L.J. (1987). Precipitation variation in the Pacific Northwest (1675-1975) as reconstructed from tree rings. *Annals of the Association of American Geographers, 77:19-29.*

Green, G.N., and Jones, G.E. (1997). The Digital Geologic Map of New Mexico in ARC/INFO Format. *U.S. Geological Survey Open-File Report OFR 97-0052. U.S. Geological Survey, Denver, Colorado.*

Grier, C. C., Elliot, K. J., McCullough, D. G. (1992). Biomass distribution and productivity of Pinus edulis-Juniperus monosperma woodlands of north-central Arizona. *Forest Ecology and Management, 50, 331-350.*

Grime, J.P. (1979). Plant Strategies and Vegetation Processes. *Wiley, Chichester*.

Grover, H.D., and Musick, H.B. (1990). Shrubland Encroachment in Southern New Mexico, U.S.A.: An Analysis of Desertification Processes in the American Southwest. *Climatic Change, 17: 305-330.*

Grubb, P.J. (1988). The encoupling of disturbance and recruitment, two kinds of seed banks, and persistence of plant populations at the regional and local scale. *Ann. Zool. Fennici, 25, 23-36.*

Gruell, G.E. (1999). Historical and modern roles of fire in piñon-juniper. *Pages 24–28. In S. B. Monsen, R. Stevens, R.J. Tausch, and R.F. Miller (compilers). Proceedings: Ecology and Management of Piñonjuniper Communities within the Interior West. USDA Forest Service Proceedings RMRS-P-9.*

Grytnes, J.A., and Vetaas, O.R. (2002). Species richness and altitude: a comparison between null models and interpolated plant species richness along the Himalayan altitudinal gradient, Nepal. *Am. Nat., 159:294-304. doi:10.1086/338542*.

Grytnes, J.A., and Beaman, J.H. (2006). Elevational species richness patterns for vascular plants for Mount Kinabalu, Borneo. *J. Biogeogr., 33:1838-1849. doi:10.1111/j.1365-2699.2006.01554.x.*

Guan, H., and Wilson, J. L. (2009). A hybrid dual-source model for potential evaporation and transpiration partitioning. *J. Hydrol., 377, 405-416.*

Gueymard, C.A. (1989). A two-band model for the calculation of clear sky solar irradiance, illuminance, and photosynthetically active radiation at the Earth's surface. *Solar Energy, 43:253-65.*

Gueymard, C.A. (2001). Parameterized transmittance model for direct beam and circumsolar spectral irradiance. *Solar Energy, 71:325-46.*

Gueymard, C.A. (2008). REST2: High-performance solar radiation model for cloudlesssky irradiance illuminance and photosynthetically active radiation - validation with a benchmark dataset. *Solar Energy, 82:272-85.*

Gugliuzza, G., Inglese, P., Farina, V. (2002). Relationship between fruit thinning and irrigation on determining fruit quality of cactus pear fruits. *Acta Horticulturae, 581, 221-225.*

Gutiérrez-Jurado, H.A., Vivoni, E.R., Harrison, J.B.J., Guan, H. (2006). Ecohydrology of root zone water fluxes and soil development in complex semiarid rangelands. *Hydrological Processes, 20, 3289-3316.*

Hall, S.A., and Penner, W.L. (2013). Stable carbon isotopes, C_3-C_4 vegetation, and 12,800 years of climate change in central New Mexico, USA. *Palaeogeography, Palaeoclimatology, Palaeoecology, 369, 272-281.*

Han, H., and Felker, P. (1997). Field validation of water-use efficiency of the CAM plant Opuntia ellisiana in south Texas. *Journal of Arid Environments, 36: 133-148.*

Hanewinkel, M., Cullmann, D.A., Schelhaas, M.J., Nabuurs, G.J., Zimmermann, N.E. (2013). Climate change may cause severe loss in the economic value of European forest land. *Nature Climate Change, 3, 203-207. doi:10.1038/nclimate1687.*

Hayek, L-A.C., and Buzas, M.A. (1997). Surveying natural populations. Columbia University Press, New York Hietel E, Waldhardt R, Otte A (2004) Analysing land-cover changes in relation to environmental variables in Hesse, Germany. *Landscape Ecol., 19:473-489. Doi: 10.1023/B:LAND.0000036138.82213.80.*

He, Y., D'Odorico, P., De Wekker, S.F.J., Fuentes, J.D., Litvak, M. (2010). On the impact of shrub encroachment on microclimate conditions in the northern Chihuahuan desert. *Journal of Geophysical Research, vol. 115, D221120, doi:10.1029/2009JD013529.*

Hegland, S.J., Nielsen, A., Lázaro, A., Bjerknes, A., Totland, Ø. (2009). "How does climate warming affect plant-pollinator interactions?". *Ecology Letters, 12 (2): 184-195. doi:10.1111/j.1461-0248.2008.01269.x.*

Hirschi, M., Stoeckli, S., Dubrovsky, M., Spirig, C., Calanca, P., Rotach, M.W., Fischer, A.M., Duffy, B., Samietz, J. (2012). Downscaling climate change scenarios for apple pest and disease modeling in Switzerland. *Earth Syst. Dyn., 3:33-47.*

Holland, P.G., and Steyn, D.G. (1975). Vegetational responses to latitudinal variations in slope angle and aspect. *J. Biogeogr., 2: 179-183. doi:10.2307/3037989.*

Holmes, R.L., Adams, R.K., Fritts, H.C. (1986). Tree ring chronologies of western North America: California, eastern Oregon and northern Great Basin. Chronology Series VI. *Laboratory of Tree Ring Research, University of Arizona, Tucson, AZ.*

Holmgren, C. A., Norris, J., Betancourt, J.L. (2007). Inferences about winter temperatures and summer rains from the late Quaternary record of C4 perennial grasses and C_3 desert shrubs in the northern. *Journal of Quaternary science, 22(2), 141-161.*

Horn, H.S. (1976). Succession, in Theoretical Ecology. *Blackwell, Oxford, pp. 187-204.*

Horn, H.H. (1981). Succession, in theoretical Ecology: Principles and Applications. *Blackwell, Oxford, pp 253-71.*

Hughes, L. (2000). Biological consequences of global warming: Is the signal already apparent? *Trends Ecol. Evol., 15, 56-61.*

Hwang, T., Song, C., Vose, J. M., Band, L. E. (2011). Topography-mediated controls on local vegetation phenology estimated from MODIS vegetation index. *Landscape Ecol., doi: 10.1007/s10980-011-9580-8.*

Ineichen, P. (2006). Comparison of eight clear sky broadband models against 16 independent data banks. *Solar Energy, 80:468-78.*

Inglese, P., Gugliuzza, G., Liguori, G. (2009). Fruit Production of Cultivated Cacti: a Short Overview on Plant Ecophysiology and C Budget. *Proc. VIth IC on Cactus and Cochineal Eds.: F.A.P. Campos et al. Acta Hort. 811, ISHS 2009.*

IPCC. Special report on emissions scenarios, (2000). A special report of Working Group III of the Intergovernmental Panel on Climate Change. *Cambridge University Press, Cambridge, United Kingdom and New York, NY, USA, 2000.*

IPCC. Climate change (2007): the physical science basis. Contribution of Working Group I to the fourth assessment report of the Intergovernmental Panel on Climate Change. *Cambridge University Press, Cambridge, United Kingdom and New York, NY, USA, 2007.*

IPCC. Climate change, (2013): the physical science basis. Contribution of Working Group I to the fifth assessment report of the Intergovernmental Panel on Climate Change. *Cambridge University Press, Cambridge, United Kingdom and New York, NY, USA, 2013.*

Isard, S.A. (1986). Factors influencing soil moisture and plant community distribution on Niwot Ridge, Front Range, Colorado, U.S.A. *Arctic and Alpine Research, vol. 18, No. 1, pp. 83-96.*

Istanbulluoglu, E., and Bras, R.L. (2006). On the dynamics of soil moisture, vegetation, and erosion: Implications of climate variability and change. *Water Resources Research, vol. 42, W06418, doi:10.1029/2005WR004113, 2006.*

Istanbulluoglu, E., Yetemen, O., Vivoni, E. R., Gutierrez-Jurado, H. A., Bras, R. L. (2008). Eco-geomorphic implication of hillslope aspect: inferences from analysis of landscape morphology in central New Mexico. *Geophys. Res. Letters, 32, L14403, doi:10.1029/2008GL034477.*

Istanbulluoglu, E., Wang, T., Wedin, D. (2012). Evaluation of Ecohydrologic Model Parsimony at Local and Regional Scales in a Semiarid Grassland Site. *Ecohydrology, 5, 121-142.*

Ivanov, V.Y., Bras, R.L., Curtis, D.C. (2007). A weather generator for hydrological, ecological, and agricultural applications. *Water Resour. Res.;43: W10,40. doi:10.1029/2006WR005,364.*

Ivanov, V. Y., Bras, R. L., Vivoni, E. R. (2008a). Vegetation-hydrology dynamics in complex terrain of semiarid areas: 1. A mechanistic approach to modeling dynamic feedbacks. *Water Resour. Res., 44, W03429, doi:10.1029/2006WR005588.*

Ivanov, V. Y., Bras, R. L., Vivon, E. R. (2008b). Vegetation-hydrology dynamics in complex terrain of semiarid areas: 2. Energy-water controls of vegetation spatiotemporal dynamics and topographic niches of favorability. *Water Resour. Res., 44, W03430, doi:10.1029/2006WR005595.*

Jardine, J.T., and Forsling, C. L. (1922). Range and cattle management during drought. U.S. *Dept. Agr. Bull. 1031. 83 p.*

Jeltsch, F., Milton, S.J., Dean, W.R.J., van Rooyen, N. (1996). Tree spacing and coexistence in semi-arid savannas. *J. Ecol., 84, 583-595*.

Jeltsch, F., Milton, S.J., Dean, W.R.J., van Rooyen, N., Moloney, K.A. (1998). Modelling the impact of small-scale heterogeneities on tree-grass coexistence in semi-arid savannas. *J. Ecol., 86(5), 780-793*.

Jeltsch, F., Moloney, K., Milton, S.J. (1999). Detecting process from snapshot pattern: Lessons from tree spacing in the southern Kalahari. *Oikos, 85, 451-466.*

Johnsen, T.N. (1962). One seed juniper invasion of northern Arizona. *Ecol. Monogr. 32: 187-207.*

Johnson, H.B., Polley, H.W., Mayeux, H.S. (1993). Increasing CO_2 and plant-plant interactions: effects on natural vegetation. *Vegetatio 104/105:157-170.*

Johnson, D.D. (2005). The influence of environmental attributes on temporal and structural dynamics of western juniper woodland development and associated fuel loading characteristics. *M.S. Thesis, Oregon State University, Corvallis, OR.*

Johnson, D.D., and Miller, R.F. (2006). Structure and development of expanding western juniper woodlands as influenced by two topographic variables. *Forest Ecology and Management, 229:7-15.*

Kannan, R., and James., D.A. (2009). Effects of climate change on global biodiversity: a review of key literature. *Tropical Ecology, 50(1): 31-39.*

Kappelle, M., Van Uffelen, J-G., Cleef, A.M. (1995). Altitudinal zonation of montane Quercus forests along two transects in Chirripo National Park, Costa Rica. *Vegetatio, 119:119-153. doi:10.1007/BF00045594.*

Katz, R.W., and Parlange, M.B. (1998). Overdispersion phenomenon in stochastic modeling of precipitation. *J. Climate, 11:591-601.*

Kelly, A.E., and Goulden, M.L. (2008). Rapid shifts in plant distribution with recent climate change. *PNAS, vol. 105, no. 33, 11823-11826.*

Kendall, M.G. (1962). Rank correlation methods. *Hafner Publishing Company, New York.*

Kilsby, C.G., Jones, P., Burton, A., Ford, A., Fowler, H., Harpham, C. (2007). A daily weather generator for use in climate change studies. *Environ Model Software*, 22:1705-19.

Kim, Y., and Eltahir, E.A.B. (2004). Role of topography in facilitating coexistence of trees and grasses within savannas. *Water Resour. Res., 40, W07505, doi:10.1029/2003WR002578.*

Kimball, B.A., Kobayashi, K., Bindi, M. (2001). Responses of agricultural crops to free-air CO_2 enrichment. *Advances in Agronomy, vol. 77, pp. 293-368.*

Klausmeier, A. (1999). Regular and irregular patterns in semiarid vegetation. *Science, 284, 1826-1828.*

Klemmedson, J. O., and Wienhold, B. J. (1992). Aspect and species influences on nitrogen and phosphorus in Arizona chaparral soil-plant system. *Arid Soil Research and Rehabilitation, 6: 105-116.*

Knapp, P.A., and Soulé, P.T. (1996). Vegetation change and the role of atmospheric CO_2 enrichment on a relict site in central Oregon: 1960-1994. *Annals of the Association of American Geographers, 86:387-411.*

Knapp, P.A., and Soulé, P.T. (1998). Recent Juniperus occidentalis (western juniper) expansion on a protected site in central Oregon. *Global Change Biology, 4:347-357.*

Knapp, P. A., and Soulé, P. T. (1999). Geographical distribution of an 18th-century heart rot outbreak in western juniper (Juniperus occidentalis spp. Occidentalis Hook.). *Journal of Arid Environments, 41:247-256.*

Knapp, P. A., Soulé, P. T., and Grissino-Mayer, H. D. (2001). Post-drought growth responses of western juniper (Juniperus occidentalis var. occidentalis) in central Oregon. *Geophysical Research Letters, 28:2657-2660.*

Knapp, A.K., McCarron, J.K., Silletti, G.A., Hoch, G.I., Heisler, M.S., Lett, J.M., Blair, J.M., Briggs, J.M., Smith, M.D. (2008a). Ecological consequences of the replacement of the native grassland by Juniper virginiana and other woody plants. *In: Van Auken, Western North American Juniperus Communities: A Dynamic Vegetation Type. Springer, New York, pp. 156-169.*

Knapp, A.K., Briggs, J.M., Collins, S.L., Archer, S.R., Bret-Harte, M.S., Ewers, B.E., Peters, D.P., Young, D.R., Shaver, G.R., Pendall,E., Cleary, M.B. (2008b). Shrub encroachment in North American grasslands: shifts in growth form dominance rapidly alters control of ecosystem carbon inputs. *Global Change Biology, 14, 615-623.*

Knipe, D., and Herbel, C.H. (1966). Germination and growth of some semidesert grassland species treated with aqueous extract from creosotebush. *Ecol., 47(5), 775-781.*

Körner, C.H., Walther, G.R. (2001). Fingerprints of Climate Change - Concluding Remarks. *In Fingerprints of Climate Change; Walther, G.R., Burga, C.A., Edwards, P.J., Eds.; Kluwer: New York, NY, USA; pp. 305-316.*

Körner, C., and Basler, D. (2010). Phenology under global warming. *Science, 327, 1461_1462, doi:10.1126/science.1186473.*

Koutsoyiannis, D., (2003). Climate change, the Hurst phenomenon, and hydrological statistics. *Hydrol. Sci. J., 48(1, 6):3-24.*

Kramer, P.J., Boyer, J.S., (1995). Water Relations of Plants and Soils. *Academic Press: San Diego, CA, USA.*

Krinner, G., Viovy, N., de Noblet-Ducoudré, N., Ogée, J., Polcher, J., Friedlingstein, P., Ciais, P., Sitch, S., Prentice, I.C. (2005). A dynamic global vegetation model for studies of the coupled atmosphere-biosphere system. *Global Biogeochemical Cycles Volume 19, Issue 1. DOI: 10.1029/2003GB002199.*

Kucharik, C.J., Foley, J.A., Delire, C. (2000). Testing the performance of a Dynamic Global Ecosystem Model: Water balance, carbon balance, and vegetation structure. *Global Biogeochem. Cycles, 14(3), 795-825*.

Kurc, S.A., and Small, E.E. (2004). Dynamics of evapotranspiration in semiarid grassland and shrubland during the summer monsoon season, central New Mexico. *Water Resour. Res., 40, W09305, doi:10.1029/2004WR003068.*

Kutiel, P. (1992). Slope aspect effect on soil and vegetation in a Mediterranean ecosystem. *Israel Journal of Botany, 41: 243-250.*

Kutiel, P., and Lavee, H. (1999). Effect of slope aspect on soil and vegetation properties along an aridity transect. *Israel Journal of Plant Sciences, 47: 169-178.*

Kysely, J., Dubrovsky, M. (2005). Simulation of extreme temperature events by a stochastic weather generator: effects of interdiurnal and interannual variability reproduction. *Int. J. Climatol., 25:251-69.*

Laio, F., Porporato, A., Ridolfi, L., Rodriguez-Iturbe, I. (2001). Plants in water controlled ecosystems: Active role in hydrologic processes and response to water stress II. Probabilistic soil moisture dynamics. *Adv. Water Resour., 24, 707-723.*

Lajtha, K., and Whitford, W.G. (1989). The Effect of Water and Nitrogen Amendments on Photosynthesis, Leaf Demography, and Resource-Use Efficiency in Larrea tridentata, a Desert Evergreen Shrub. *Oecologia, 80(3), 341-348.*

LaMarche, V.C., Jr. (1974). Paleoclimatic inferences from long tree-ring records. *Science, 183:1043-1048.*

Larcher, W. (1995). Physiological Plant Ecology. *3rd ed. Springer-Verlag: New York, NY, USA, 1995.*

Le Houèrou, M. (1974). Fire and vegetation in the Mediterranean Basin. *Tall Timbers Fire Ecology Conference Proceedings, 13: 237-277.*

Lean, J., and Rowntree, P.R. (1997). Understanding the sensitivity of a GCM simulation of Amazonian deforestation to the specification of vegetation and soil characteristics. *J. Climate, 10, 1216-1235.*

Lee, T. J. (1992). The impact of vegetation on the atmospheric boundary layer and convective storms. *Ph.D. dissertation, Colorado State University, 137 pp*.

Lejeune, O., Tlidi, M., Couteron, P. (2002). Localized vegetation patches: A self-organized response to resource scarcity. *Phys. Rev., E 66: 010901-1*.

Lenihan, J.M., Drapek, R., Bachelet, D., Neilson, R.P. (2001). Climate Change Effects on Vegetation distribution, Carbon, and Fire in California. *Ecological Applications, 13:1667-1681*.

Lenihan, J.M., Bachelet, D., Neilson, R.P., Drapek, R. (2008). Response of vegetation distribution, ecosystem productivity, and fire to climate change scenarios for California. *Climatic Change, 87 (Suppl. 1): S215-S230. doi: 10.1007/s10584-007-9362-0.*

Leonard, M., Lambert, M.F., Metcalfe, A.V., Cowpertwait, P.S.P. (2008). A space–time Neyman–Scott rainfall model with defined storm extent. *Water Resour. Res.;44(W09402). doi:10.1029/2007WR006110.*

Levis, S., Coe, M.T., Foley, J.A. (1996). Hydrologic budget of a land surface model: A global application. *J. Geophys. Res., 101, 16921-16930.*

Lieberman, M., Lieberman, D., Hartshorn, G.S., Peralta, R. (1996). Tropical forest structure and composition on a large-scale altitudinal gradient in Costa Rica. *J. Ecol., 84:137-152. doi: 10.2307/2261350*.

Lieffers, V.J., and Larkin Lieffers, P.A. (1987). Slope, aspect and slope position as factors controlling grassland communities in the coulees of the Oldman River, Alberta. *Canadian Journal of Botany, 65 (7), 1371-1378.*

Liuzzo, L., Noto, L., Vivoni, E., La Loggia, G. (2010). Basin-Scale Water Resources Assessment in Oklahoma under Synthetic Climate Change Scenarios Using a Fully Distributed Hydrologic Model. *J. Hydrol. Eng., 15(2), 107-122*.

Loarie, S.R., Duffy, P.B., Hamilton, H., Asner, G.P., Field, C.B., Ackerly, D.D. (2009). The velocity of climate change. *Nature 462 (7276): 1052-1055. doi:10.1038/nature08649.*

Long, S.P., Ainsworth, E.A., Rogers, A., Ort, D.R. (2004). Rising atmospheric Carbon Dioxide: Plants FACE the future. *Annu. Rev. Plant. Biol.,* 55, 591-628.

Lovett, J.C. (1999). Tanzanian forest tree plot diversity and elevation. *J. Trop. Ecol., 15:689-694. doi:10.1017/S0266467499001108.*

Luttge, U. (1997). Physiological ecology of tropical plants. *Springer, Berlin*.

Mackay, D.S. (2001). Evaluation of hydrologic equlibrium in a mountainous watershed: incorporating forest canopy spatial adjustment to soil biogeochemical processes. *Advances in Water Resources, 24, 1211-1227.*

Mackenzie, F.T. (2003). Our changing planet: an introduction to earth system science and global environmental change. *Prentice Hall-Pearson Education. Inc., Upper Saddle River, New Jersey.*

Manfreda, S. (2009). Ecohydrology: A new interdisciplinary approach to investigate on climate soilvegetation interactions. *Ann. Arid Zone, 48, 219-228.*

Manfreda, S., and Caylor, K.K. (2013). On the Vulnerability of Water Limited Ecosystems to Climate Change. *Water, 5, 819-833; doi:10.3390/w5020819*.

Manfreda, S., Pizzolla, T., Caylor, K.K. (2013). Modelling Vegetation Patterns in Semiarid Environments. *Procedia Environmental Sciences, 19, 168-177*.

Kendall, M.G. (1962). Rank correlation methods. *Hafner Publishing Company, New York*.

Manning, L.J., Hall, J.W., Fowler, H.J., Kilsby, C.G., Tebaldi, C. (2009). Using probabilistic climate change information from a multimodel ensemble for water resources assessment. *Water Resour. Res. 45(W11411), doi:10.1029/2007WR006674*.

Marani, M. (2003). On the correlation structure of continuous and discrete point rainfall. *Water Resour. Res., 39(5). doi:10.1029/2002WR001456.*

Marani, M. (2005). Non-power-law-scale properties of rainfall in space and time. *Water Resour. Res., 41(W08413). doi:10.1029/2004WR003822.*

Maraun, D., Wetterhall, F., Ireson, A.M., Chandler, R.E., Kendon, E.J., Widmann, M., Brienen,S., Rust, H.W., Sauter, T., Themessl, M., Venema, V.K.C., Chun, K.P., Goodess, C.M., Jones, R.G., Onof, C., Vrac, M., Thiele-Eich, I. (2010). Precipitation downscaling under climate change: recent developments to bridge the gap between dynamical models and the end user. *Rev. Geophys., 48(RG3003).*

Margalef, R. (1958). Information theory in ecology. *Gen. Syst.,3, 36-71*.

Margalef, R. (1963). On certain unifying principles in ecology. *Amer. Nat., 97, 357-74.*

Margalef, R. (1968). Perspectives in Ecological Theory. *Univ. Of Chicago Press, Chicago.*

Martens, S.N., Breshears, D.D., Meyer, C.W. (2000). Spatial distributions of understory light along the grassland forest continuum: effects of cover, height, and spatial pattern of tree canopies. *Ecological Modeling, 126, 79-93*.

Martinez-Ramos, M., Alvarez-Buylla, E., Sarukhan, J. (1989). Tree demography and gap dynamics in a tropical rain forest. *Ecology, 70, 555-8*.

Martınez-Yrızar, A., Burquez, A., Maass, M. (2000). Structure and functioning of tropical deciduous forest in Western Mexico. In: Robichaux RH, Yetman DA (eds) The tropical deciduous forest of Alamos: biodiversity of a threatened ecosystem in Mexico. *The University of Arizona Press, Tucson, pp 19-35*.

Maselli, F., Chiesi, M., Rodolfi, A., Maracchi, G. (2007). Uso Di Serie Temporali NDVI Per Stimare l'effetto Dei Cambiamenti Climatici Sugli Ecosistemi Forestali (in Italian). *In Clima e Cambiamenti Climatici–Le Attività Di Ricerca Del CNR; Carli, B., Cavarretta, G., Colacino, M., Fuzzi, S., Eds.; Consiglio Nazionale delle Ricerche, Roma, Italy, 2007; pp. 701-704.*

Mata-Gonzalez, R., Pieper, R.D., Cardenas, M.M. (2002). Vegetation patterns as affected by aspect and elevation in small desert mountains. *The Southwestern Naturalist, 47 (3),440-448.*

McDonnel, M.J. (1988). Landscapes, birds, and plants: Dispersal patterns and vegetation change, in the Biogeography of the island Region of western Lake Erie. *The Ohio State Univ. Press., Columbus, pp. 214-220.*

McDowell, P.F., Webb, T., Bartlein, P.J. (1991). Long-term environmental change, in the Earth as Transformed by Human Action. *Cambridge Univ. Press, Cambridge.*

McDowell, M., Pockman, W.T., Allen, C.D., Breshears, D.D., Cobb, N., Kolb, T., Plaut, J., Sperry, J., West, A., Williams, D.G., and Yepez, E.A. (2008). Mechanisms of plant survival and mortality during drought: why do some plants survive while others succumb drought? *New Phytol., 178, 719-739.*

McKague, K., Rudra, R., Ogilvie, J. (2003). CLIMGEN – a convenient weather generator tool for Canadian climate stations. *In: Meeting of the CSAE/SCGR Canadian society for engineering in agricultural food and biological systems, Montreal, Quebec, July 6-9, 03-118, 2003. Web-site: <http://www.sipeaa.it/tools/ ClimGen/CSAE03-118.pdf>.*

McMahon, S.M., Harrison, S.P., Armbruster, W.S., Bartlein, P.J., Beale, C.M., Edwards, M.E., Kattge¸ J., Midgley, G., Morin, X., Prentice, I.C (2011). Improving assessment and modelling of climate change impacts on global terrestrial biodiversity. *Trends in Ecology and Evolution May, Vol. 26, No. 5.*

Meehl, G.A., Stocker, T.F., Collins,W.D., Friedlingstein, P., Gaye, A.T., Gregory, J.M., Kitoh, A., Knutti, R., Murphy, J.M., Noda, A., Raper, S.C.B., Watterson, I.G., Weaver, A.G., and Zhao, Z.C. (2007). Global Climate Projections, in: Climate Change 2007: The Physical Science Basis, Contribution of Working Group I to the Fourth Assessment Report of the Intergovernmental Panel on Climate Change, edited by: Solomon, S., Qin, D., Manning, M., Chen, Z., Marquis, M., Averyt, K. B., Tignor, M., and Miller, H. L. *Cambridge University Press, Cambridge, United Kingdom and New York, NY, USA.*

Meentemeyer, R.K., Moody, A., Franklin, J. (2001). Landscape-scale patterns of shrub-species abundance in California chaparral - The role of topographically mediated resource gradients. *Plant Ecol., 156(1), 19-41.*

Mehringer, P.J., and Wigand, P.E. (1984). Prehistoric distribution of western juniper. *Pages 1-9. In Proceedings-Western Juniper Management Short Course. Oregon State University Agricultural Extension Service, Bend, OR.*

Mehringer, P.J. (1985). Late-quaternary pollen records from the interior Pacific Northwest and northern Great Basin of the Untied States. *Pages 167-189. In W.M. Bryant and R.G. Hoolway (editors). Pollen Records of Late-Quaternary North American Sediments. American Association Stratigraphic Palynoligists. Dallas, TX.*

Mehringer, P.J. (1986). Prehistoric environments. *Pages 31-50. In W.L. D'Azevedo (editor). Volume II: Great Basin, Handbook of North American Indians. Washington, DC.*

Mehringer, P.J. (1987). Late Holocene environments on the northern periphery of the Great Basin. *Final Report, Bureau Land Management, Portland, OR.*

Mehringer, P.J., and Wigand, P.E. (1990). Comparison of late Holocene environments from woodrat middens and pollen. *Pages 294–325. In J.L. Betancourt, T.R. Van Devender, and P.S. Martin (editors). Packrat Middens: The Last 40,000 Years of Biotic Change. University of Arizona Press, Tucson, AZ.*

Menzel, A., Estrella, N., Fabian, P. (2001). Spatial and temporal variability of the phonological seasons in Germany from 1951 to 1996. *Glob. Change Biol., 7, 657-666.*

Merritt, W.S., Alila, Y., Barton, M., Taylor, B., Cohen, S., Neilsen, D. (2006). Hydrologic response to scenarios of climate change in sub watersheds of the Okanagan basin, British Columbia. *J. Hydrol., 326:79-108. doi:10.1016/j.jhydrol.2005.10.025.*

Miles, J. (1979). Vegetation Dynamics. *Chapman and Hall, London.*

Miles, J. (1987). Vegetation Succession: Past and present perceptions, in Colonization, Succession and Stability. *Blackwell, Oxford, pp 1-29.*

Miller, F.H. (1921). Reclamation of grass lands by Utah juniper on the Tusayan National Forest, Aribona. *J. For., 19: 647-651.*

Miller, R.F., Eddleman, L.E., Angell, R.F. (1987). The relationship of western juniper stem conducting tissue and basal circumference to leaf area and biomass. *Great Basin Naturalist, 47:349-354.*

Miller, R.F., and Shultz, L.M. (1987). Water relations and leaf morphology of Juniperus occidentalis in the northern Great Basin. *Forest Science, 33:690-706.*

Miller, R.F., and Wigand, P.E. (1994). Holocene changes in semiarid piñon-juniper woodlands: response to climate, fire and human activities in the U.S. Great Basin. *BioScience, 44:465-474.*

Miller, R.F., Svejcar, T.J., West, N.E. (1994). Implications of livestock grazing in the Intermountain sagebrush region: plant composition. *Pages 101–146. In M. Vavra, W.A. Laycock, and R.D. Piper (editors). Ecological Implications of Livestock Herbivory in the West. Society for Range Management, Denver, CO.*

Miller, R.F., and Rose, J.A. (1995). Historic expansion of Juniperus occidentalis (western juniper) in southeastern Oregon. *Great Basin Naturalist, 55:37-45.*

Miller, R.F., and Rose, J.A. (1999). Fire history and western juniper encroachment in sagebrush steppe. *Journal of Range Management, 52:550-559.*

Miller, R.F, Tausch, R.J., Waichler, W. (1999a). Oldgrowth juniper and piñon woodlands. *Pages 375-384. In S.B. Monsen, R. Stevens, R.J. Tausch, and*

R.F. Miller (compilers). Proceedings: Ecology and Management of Piñon-juniper Communities within the Interior West. USDA Forest Service Proceedings RMRS-P-9.

Miller, R.F., Willis, M., Rose, J.A., Rickensmyer, D., Anthony, B. (1999b). The affects of juniper woodlands on avian populations. *Pages 106–111. In History, Ecology, and Management of Juniper Woodlands. Range Field Day Annual Report, Oregon State Agricultural Experiment Station Special Report 1002.*

Miller, R.F., Svejcar, T.J., Rose, J.A. (2000). Impacts of western juniper on plant community composition and structure. *Journal of Range Management, 53:574-585.*

Miller, R.F. (2001). Managing western juniper for wildlife. *Woodland Fish and Wildlife MISC 0286 Washington State University Cooperative Extension, Pullman, WA.*

Miller, R. F., and Eddleman, L.E. (2001). Spatial and temporal changes of sage grouse habitat in the sagebrush biome. *Oregon State University Agricultural Experiment Station Technical Bulletin 151.*

Miller, R.F., and Tausch, R.J. (2001). The role of fire in piñon and juniper woodlands: a descriptive analysis. *Pages 15-30. In K.E.M. Galley and T.P. Wilson (editors). Proceedings of the Invasive Species: the Role of Fire in the Control and Spread of Invasive Species. Miscellaneous Publication No. 11, Tall Timbers Research Station, Tallahassee, FL.*

Miller, R.F., Baisan, C., Rose, J., Pacioretty, D. (2001). Pre- and post-settlement fire regimes in mountain big sagebrush steppe and aspen in the northwest Great Basin. *National Interagency Fire Center Final Report, Eastern Oregon Agricultural Research Center, Oregon State University, Burns, OR.*

Miller, R.F., Heyerdahl, E.K., Hopkins, K. (2003). Fire regimes, pre- and post-settlement vegetation, and the modern expansion of western juniper at Lava Beds National Monument, California. *Final Report to the USDI Lava Beds National Monument*.

Miller, R.F., Bates, J.D., Svejcar, T.J., Pierson, F.B., Eddleman, L.E. (2005). Biology, Ecology, and Management of Western Juniper. *Technical Bulletin 152, Oregon State University, Agricultural Experiment Station, pp 77.*

Miller, R.F., Bates, J.D., Svejcar, T.J., Pierson, F.B., Eddleman, L.E. (2007). Western Juniper Field Guide: Asking the Right Questions to Select Appropriate Management Actions. *Circular 1321, U.S. Department of the Interior, U.S. Geological SurveyCircular, pp 72.*

Miller, R.F., Tausch, R.J., McArthur E.D., Johnson D.D., Sanderson, S.C. (2008). Age Structure and Expansion of Piñon-Juniper Woodlands: A Regional Perspective in the Intermountain West. *USDA Forest Service RMRS-RP-69., pp. 21*.

Min, S. K., Xuebin Z., Francis W.Z., Gabriele C.H. (2011). Human contribution to more-intense precipitation extremes. *Nature, 470 (7334): 378-381*.

Montaldo, N., Rondena, R., Albertson, J. D., Mancini, M. (2005). Parsimonious modeling of vegetation dynamics for ecohydrologic studies of water-limited ecosystems. *Water Resour. Res., 41, W10416, doi:10.1029/2005WR004094.*

Montaldo, N., Albertson, J.D., Mancini, M. (2008). Vegetation dynamics and soil water balance in a water-limited Mediterranean ecosystem on Sardinia, Italy. *Hydrol. Earth Syst. Sci. Discuss., 5, 219-255*

Montaldo, N., Corona, R., Albertson, J.D. (2013). On the Separate Effects of Soil and Land Cover on Mediterranean Ecohydrology: Two Contrasting Case Studies in Sardinia, Italy. *Water Resources Research, Vol. 49, 2, 1123-1136.*

Monteith, J. L. (1965). Evaporation and environment. *Symp. Soc. Exp. Biol., 19, 205-224*.

Monteith, J.L. (1973). Principles of Environmental Physics. *Elsevier Publishing, New York.*

Mooney, H., Larigauderie, A., Cesario, M., Elmquist, T., Hoegh-Guldberg, O., Lavorel, S., Mace, G.M., Palmer, M., Scholes, R., Yahara, T. (2009). Biodiversity, climate change, and ecosystem services. *Curr Opin Environ Sustain, 1(1):46-54*.

Moratiel, R., Snyder, R.L., Duràn, J.M., Tarquis, A.M. (2011). Trends in climatic variables and future reference evapotranspiration in Duero Valley (Spain). *Natural Hazards and Earth System Sciences, 11, 1795-1805.*

Morin, X., and Thuiller, W. (2009). Comparing niche and process-based models to reduce prediction uncertainty in species range shifts under climate change. *Ecology, 90:1301-1313. doi:10.1890/08-0134.1.*

Muneer, T., Gul, M.S., Kubie, J. (2000). Models for estimating solar radiation and illuminance from meteorological parameters. *J. Solar Energy Eng., 122:146-53.*

Mutziger, A.J., Burt, C.M., Howes, D.J., Allen, R.G. (2005). Comparison of measured and modified FAO 56 modeled bare soil evaporation. *J. of Irrigation and Drainage Engineering, 131: 59-72.*

Myneni, R.B., Keeling, C.D., Tucker, C.J., Asrar, G., Nemani, R.R. (1997). Increased plant growth in the northern high latitudes from 1981 to 1991. *Nature, 386, 698-702.*

Myneni, R.B., Nemani, R.R., Running, S.W. (1997). Estimation of global leaf area index and absorbed par using radiative transfer models. *IEEE Trans. Geosci. Remote Sens., 35, 1380-1393.*

Nagendra, H. (2002). Opposite trends in response for the Shannon and Simpson indices of landscape diversity. *Applied Geography, 22, 175-186.*

Nash, J.E., and Sutcliffe, J.V. (1970). River flow forecasting through conceptual models: Part 1. A discussion of principles. *J. of Hydro., 10(3): 282-290.*

Nathan, R., Horvitz, N., He, Y., Kuparinen, A., Schurr, F.M., Katul, G.G. (2011). Spread of North American wind-dispersed trees in future environments. *Ecology Letters, (2011) 14: 211-219, doi: 10.1111/j.1461-0248.2010.01573.x*.

Nelder, J., and Mead, R. (1965). A Simplex method for function minimization. *Comput. J., 7:308-13.*

Nemani, R.R., Keeling, C.D., Hashimoto, H., Jolly, W.M., Piper, S.C., Tucker, C.J., Myneni, R.B., Running, S.W. (2003). Climate-Driven Increases in Global Terrestrial Net Primary Production from 1982 to 1999. *Science, 300, 1560; DOI: 10.1126/science.1082750*.

Nerd, A., Karady, A., Mizrahi, Y. (1989). Irrigation, fertilization and polyethylene covers influence bud development in prickly pear. *Horticultural Science, 24, 773-775.*

Nichols, W.F., Killinbeck, K.T., August, P.V. (1998). The influence of geomorphological heterogeneity on biodiversity II. A landscape perspective. *Conserv. Biol. 12:371–379. doi: 10.1046/j.1523-1739.1998.96237.x*.

Nielsen-Pincus, M. (2008). Lower Crooked River Watershed Assessment. *Crooked River Watershed Council, February 2008*.

Noble, I.R., and Slatyer, R.O. (1980). The use of vital attributes to predict successional changes in plant communities subject to recurrent disturbances. *Vegetatio, 43, 5-21.*

Nobel P.S., and Hartsock T.L. (1983). Relationships between Photosynthetically Active Radiation, Nocturnal Acid Accumulation, and CO_2 Uptake for a Crassulacean Acid Metabolism Plant, Opuntia ficus-indica. *Plant Physiol., 71:71-75.*

Nobel, P.S., and Hartsock, T.L. (1984). Physiological responses of *Opuntia ficus-indica* to growth temperature. *Physiologia Plantarum 60, 98-105*.

Nobel, P.S. (1988). Environmental Biology of Agaves and Cacti. *Cambridge University Press, Cambridge New York, USA, pp. 270.*

Nobel, P.S., and Bobich, E.G. (1995). Environmental biology. *Book: Cacti, Biology and Uses, edited by Nobel P.S.*

Nobel, P.S. (2002). Cacti: biology and uses. *University of California Press, Berkeley, pp. 280.*

Nobel, P.S., Bobich, E. (2002). Initial net CO_2 uptake responses and root growth for a CAM community placed in a closed environment. *Annals of Botany, 90, 593-598.*

Norby, R.J., Wullschleger, S.D., Gunderson, C.A., Johnson, D.W., Ceulemans, R. (1999). Tree responses to rising CO_2 in field experiments: Implications for the future forest. *Plant, Cell and Environment, 22(6): 683-714.*

Norby, R.J., and Zak, D.R. (2011). Ecological lessons from Free-Air CO_2 enrich-ment (FACE) experiments. *Annu. Rev. Ecol. Evol. Syst. 42, 181-203, http://dx.doi.org/10.1146/annurev-ecolsys-102209-144647.*

O'Brien, R.A., and Woudenberg, S.W. (1999). Description of piñon-juniper and juniper woodlands in Utah and Nevada from an inventory perspective. *Pages 55–59. In S.S.B. Monsen, R. Stevens, R.J. Tausch, and R.F. Miller (compilers). Proceedings: Ecology and Management of Piñon-juniper*

Communities within the Interior West. Provo, UT. USDA Forest Service Proceedings. RMRS-P-9.

Odum, E.P. (1969). The strategy of ecosystem development. *Science, 164, 262-70.*

Oliphant, J.O. (1968). On the cattle ranges of the Oregon country. *University of Washington Press, Seattle, WA.*

Olivero, A.M., and Hix, D.M. (1998). Influence of slope aspect and stand age on ground flora of southeastern Ohio forest ecosystems. *Plant Ecology, 139: 177-187.*

Onof, C., Chandler, E., Kakou, A., Northrop, P., Wheater, H.S., Isham, V. (2000). Rainfall modeling using Poisson-cluster processes: a review of developments. *Stochast Environ Res Risk Assess, 14:384-411.*

Parker, K.W. (1945). Juniper comes to the grasslands. *Am. Cattle Prod., 27: 112-114.*

Parlange, M.B., and Katz, R.W. (2000). An extended version of the Richardson model for simulating daily weather variables. *J. Appl. Meteorol., 39:610-22.*

Parmenter, R.R. (2008). Long-Term Effects of Summer Fire on Desert Grassland Plant Demographics in New Mexico. *Rangeland Ecol Manage, 61:156-168.*

Paul, M.N., and Litvak, M. (2009). Quantifying biome specific relationships of 1438 vegetation indices and monsoon event responses. *REU Summer Symposium.*

Peet, R.K., and Christensen, N.L. (1980). Succession: a population process. *Vegetation, 43, 131-40.*

Penuelas, J., Canadell, J.G., Ogaya, R. (2011). Increased water-use efficiency during the 20th century did not translate into enhanced tree growth. *Global Ecology and Biogeography, 20, 597-608.*

Perry, G.L.W., and Enright, N.J. (2002). Humans, fire and landscape pattern: understanding a maquis-forest complex, Mont Do, New Caledonia, using a spatial 'state-and-transition' model. *Journal of Biogeography, volume 29, Issue 9, pages 1143-1158.*

Peters, D., Bestelmeyer, P.C., Brandon, T., Herrick, J.E., Fredrickson, E.L., Monger, H.C., Havstad, K.M. (2006). Disentangling complex landscapes; new insights into arid and semiarid system dynamics. *Bioscience, 56, 491-501.*

Pianka, E.R. (2000). Evolutionary ecology. *Addison Wesley Longman, San Francisco.*

Pickett, S.T.A., and White, P.S. (1985). The Ecology of Natural Disturbance and Patch Dynamics. *Academic Press, Orlando.*

Pickett, S.T.A., Collins, S.L., Armesto, J.J. (1987). Models, mechanisms and pathways of succession. *Bot. Rev., 53, 335-71.*

Pickett, S.T.A., and Kolasa, J. (1989). Structure of theory in vegetation science. *Vegetation, 83, 7-15.*

Picone, R.M., Crisafulli, A., Zaccone, S. (2008). Habitat forestali di particolare valore naturalistico (DIR. 92/43/CEE) dei Monti Peloritani (Sicilia). *Atti del Terzo Congresso Nazionale di Selvicoltura. Taormina (ME), 16-19 ottobre 2008. Accademia Italiana di Scienze Forestali, Firenze, p. 243-248. doi: 10.4129/CNS2008.032*.

Pielke, R.A. (2001). Influence of the spatial distribution of vegetation and soils on the prediction of cumulus convective rainfall. *Rev. Geophys., 39(2), 151-177.*

Pierce, K.B. Jr, Lookingbill, T., Urban, D. (2005). A simple method for estimating potential relative radiation (PRR) for landscape-scale vegetation analysis. *Landscape Ecol., 20:137-147.*

Pignatti, S. (1994). Ecologia del Paesaggio (in Italian). *UTET: Torino, Italy, 1994.*

Pimienta-Barrios, E., Zañudo-Hernàndez, J., Nobel, P.S. (2005). Effects of young cladodes on the gas exchange of basal cladodes of Opuntia ficus-indica (Cactaceae) under wet and dry conditions. *Int. J. Plant Sci., 166 (6):961-968.*

Pizzolla, T., Acampora, A., Manfreda, S. (2012a). Effects of Morphology on Global Solar Radiation and Potential Evapotranspiration. *L'acqua, 2/2012, pp. 45-53.*

Pizzolla, T., Manfreda, S., Caylor, K.K., Fiorentino, M. (2012b). Il ruolo dell'esposizione e della pendenza dei versanti sullo stress idrico della vegetazione (in Italian). *XXXIII Convegno Naionale di Idraulica e Costruzioni Idrauliche, Brescia 10-15 settembre 2012.*

Pohl, K.A., Hadley, K.S., Arabas, K. (2002). A 545-year drought reconstruction for central Oregon. *Physical Geography, 23:302-320.*

Poiani, K.A.. and Johnson, W.C. (1993). A Spatial Simulation Model of Hydrology and Vegetation Dynamics in Semi-Permanent Prairie Wetlands. *Ecological Applications Vol. 3, No. 2, pp. 279-293.*

Polley, H.W., Johnson, H.B., Mayeux, H.S. (1992). Carbon dioxide and water fluxes of C_3 annuals and C_3 and C_4 perennials at subambient CO_2 concentrations. *Func. Ecol., 6, 693-703.*

Porporato, A, Laio, F., Ridolfi, L., Rodriguez-Iturbe, I. (2001). Plants in water-controlled ecosystems: Active role in hydrological processes and response to water stress, III, Vegetation water stress. *Adv. Water. Resour., 24, 725-744.*

Prentice, I.C. (1986). Some concepts and objectives of forest dynamics research, in Forest Dynamics Research in Western and Central Europe. *PUDOC, Wageningen, pp. 32-9.*

Prentice, I.C., van Tongeren, O., de Smidt, J.T. (1987). Simulation of heathland vegetation dynamics. *J. Ecol., 75, 203-19.*

Pumo, D., Viola, F., Noto, L.V. (2008). Ecohydrology in Mediterranean areas: a numerical model to describe growing seasons out of phase with precipitations. *Hydrol. Earth Syst. Sci., 12, 303-316.*

Pumo, D., Viola, F., Noto, L.V. (2010). Climate changes' effects on vegetation water stress in Mediterranean areas. *Ecohydrology, 3: 166-176. doi: 10.1002/eco.117.*

Rahbek, C. (1995). The elevational gradient of species richness: a uniform pattern? *Ecography, 18:200-205. doi:10.1111/j.1600-0587.1995.tb00341.x.*

Randin, C.F., Paulsen, J., Vitasse, Y., Kollas, C., Wohlgemuth, T., Zimmermann, N.E., Körner, C. (2013). Do the elevational limits of deciduous tree species match their thermal latitudinal limits? *Global Ecol. Biogeogr., 22, 913-923.*

Reid, K. D., Wilcox, B. P., Breshears, D. D., MacDonald, L. (1999). Runoff and erosion in a piñon-juniper woodland: Influence of vegetation patches. *Soil Sci. Soc. Am. J., 63:1869-1879.*

Ricard, J.P., and Messier, C. (1996). Abundance, growth, and allometry of red raspberry (*Rubus idaeus* L.) along a natural light gradient in a northern hardwood forest. *For. Ecol. Manag., 81, 153-160.*

Richardson, C.W., Wright, D.A. (1984). WGEN: a model for generating daily weather variables, *ARS 8, USDA-ARS, 1984.*

Richardson, A.D., Keenan, T.F., Migliavacca, M., Ryu, Y., Sonnentag, O, Toomey, M. (2013). Climate change, phenology, and phenological control of vegetation feedbacks to the climate system. *Agricultural and Forest Meteorology, 169, 156-173.*

Ricklefs, R.E., and Miller, G.L. (2000). Ecology. Freeman, New York Romero-Centeno R, Zavala-Hidalgo J, Gallegos A, O'Brien JJ (2003) Isthmus of Tehuantepec wind climatology and ENSO signal. *J. Clim., 16:2628-2639.*

Ridolfi, L., D'Odorico, P., Porporato, A., Rodriguez-Iturbe, I. (2000). Impact of climate variability on the vegetation water stress. *Water Resour. Res., 36(8), 2297-2307.*

Rietkerk, M., Dekker, S. C., Wassen, M. J., Verkroost, A. W. M., Bierkens, M. F. P. (2004). A Putative Mechanism for Bog Patterning. *Am. Nat., 163(5), 699-708.*

Rietkerk, M., Dekker, S.C., de Ruiter, P.C., van de Koppel, J. (2004). Self-organized patchiness and catastrophic shifts in ecosystems. *Science, 305, 1926-1929.*

Rigon, R., Bertoldi, G., Over, T.M. (2006). GEOtop: a distributed hydrological model with coupled water and energy budgets. *J. Hydrometeorol, 7:371-387.*

Rizvi, S. J. H., and Rizvi, V. (1992). Allelopathy: Basic and applied aspects. *Chapman & Hall, London. 480 pp.*

Roberts, C., and Jones, J.A. (2000). Soil patchiness in juniper-sagebrush-grass communities of central Oregon. *Plant and Soil, 223:45-61.*

Rodriguez-Iturbe, I., Cox, D., Isham, V. (1987). Some models for rainfall based on stochastic point processes. *Proc. Roy. Soc. Lond. Ser. A., 410:269-88.*

Rodriguez-Iturbe, I., Eagleson, P.S. (1987). Mathematical models of rainstorm events in space and time. *Water Resour Res., 23(1):181-90.*

Rodriguez-Iturbe, I., Cox, D., Isham, V. (1988). A point process model for rainfall: further developments. *Proc. Roy. Soc. Lond. Ser. A., 417:283-98.*

Rodriguez-Iturbe, I., D'Odorico, P., Porporato, A., Ridolfi, L. (1999). On the spatial and temporal links between vegetation, climate, and soil moisture. *Water Resour. Res., 35(12), 3709-3722.*

Rodriguez-Iturbe, I. (2000). Ecohydrology: A hydrologic perspective of climate-soil-vegetation dynamics. *Water Resour. Res., 36(1), 3-9.*

Runkle, J.R. (1989). Synchrony of regeneration, gaps and latitudinal differences in tree species diversity. *Ecology, 70, 546-47.*

Ryan, M. G. (1991). The effects of climate change on plant respiration. *Eco. Appl., 1(2), 157-167.*

Ryser, P. (1990). Influence of Gaps and Neighbouring Plants on Seedling Establishment in Lemistone Grassland. Experimental Field Studies in Northern Switzerland. *Inst. Der ETH, Stiftung Rubel, Zurich, Vol. 104.*

San José, J.J., Montes, R., Nikonova, N. (2007a). Diurnal patterns of carbon dioxide, water vapour and energy fluxes in pineapple [*Ananas comosus* (L.) Merr. Cv. Red Spanish] field using eddy covariance. *Photosynthetica, 45(3), 370-384.*

San José, J.J., Montes, R., Nikonova, N. (2007b). Seasonal patterns of carbon dioxide, water vapour and energy fluxes in pineapple. *Agricultural and Forest Meteorology, 147, 16-34.*

Saulnier, G.M., Beven, K., Obled, C. (1997). Including spatially variable effective soil depths in TOPMODEL. *Journal of Hydrology, 202, 158-172*.

Scanlon, T.M., Caylor, K.K., Levin, S.A., Rodriguez-Iturbe, I. (2007). Positive feedbacks promote power-law clustering of Kalahari vegetation. *Nature, 449 (7159), 209-U4*.

Schaefer, R.J., Thayer, D.J., and Burton, T.S. (2003). Forty-one years of vegetation change on permanent transects in northeastern California: implications for wildlife. *California Fish and Game, 89:55-71.*

Scheiner, S.M., and Rey Benayas, J.M. (1994). Global patterns of plant diversity. *Evol. Ecol., 8, 331-338.*

Schmidli, J., Frei, C., Vidale, P.L. (2006). Downscaling from GCM precipitation: a benchmark for dynamical and statistical downscaling methods. *Int. J. Climatol., 26:679-89.*

Schott, M.R., and Pieper, R.D. (1986). Succession in Pinyon-Juniper Vegetation in New Mexico. *Rangelands, 8(3): 126-128.*

Scifres, C.J. (1980). Brush Management Principles and Practices for Texas and the Southwest. *Texas A&M University Press, College Station.*

Scott, R.L., Huxman, T.A., Cable, W.L., Emmerich, W.E. (2006). Partitioning of evapotranspiration and its relation to carbon dioxide exchange in a Chihuahuan Desert shrubland. *Hydrol. Process., 20, 3227-3243.*

Seager, R., Ting, M., Held, I., Kushnir, Y., Lu, J., Vecchi, G., Huang, H.P., Harnik, N., Leetmaa, A., Lau, N.C., Li, C., Velez, J., Naik, N. (2007). Model

projections of an imminent transition to a more arid climate in Southwestern North America. *Science, 316:1181-4. doi:10.1126/science.1139601.*

Semenov, M.A., Barrow, E.M. (1997). Use of a stochastic weather generator in the development of climate change scenarios. *Climatic Change, 35:397-414.*

Semenov, M.A., Brooks, R.J., Barrow, E.M., Richardson, C.W. (1998). Comparison of the WGEN and LARS-WG stochastic weather generators for diverse climates. *Climate Res.,10:95-107.*

Shannon, C.E., and Weaver, W. (1949). The mathematical theory of communication. *Illinois: University of Illinois Press.*

Sharma, C.M., and Baduni, N.P. (2000). Effect of aspect on the structure of some natural stands of Abies pindrow in Himalayan moist temperate forest. *Environmentalist, 20:309-317. doi:10.1023/A:1006765529832.*

Sharpley, A.N., and Williams, J.R. (1990). EPIC-Erosion/Productivity impact calculator: 1. Model documentation. *Technical bulletin 1768, US Department of Agriculture, 235 p.*

Shreve, F. (1917). A map of the vegetation of the United States. *Geol. Rev., 3: 119-125.*

Simpson, E.H. (1949). Measurement of diversity. *Nature, 163, 688.*

Singh, R.S., and Singh, V. (2003). Growth and Development Influenced by Size, Age, and Planting Methods of Cladodes in Cactus Pear (Opuntia ficus-indica (L.) Mill.). *J. PACD, 47-54.*

Sitch, S., Smith, B., Prentice, I. C. (2003). Evaluation of ecosystem dynamics, plant geography and terrestrial carbon cycling in the LPJ dynamic global vegetation model. *Global Change Biol., 9, 161-185.*

Slingo, A. (1989). A GCM parameterization for the shortwave radiative properties of water clouds. *J. Atmos. Sci., 46(10):1419-27.*

Small, E. E. (2005). Climate controls on diffuse groundwater recharge in semiarid environments of the southwest United States. *Water Resour. Res., 41, W04012, doi:10.1029/2004WR003193.*

Smith, T.M., and Goodman, P.S. (1987). Successional dynamics in an Acacia nilotica-Euclea divinorum savannah in southern Africa. *J. Ecol., 75, 603-610.*

Snyman, H.A. (2005). Root distribution with changes in distance and depth of two-year-old cactus pears Opuntia ficus-indica and O. robusta plants. *South African Journal of Botany, 72, 434-441.*

Soil Survey Staff (1994). State Soil Geographic Database (STATSGO) data users guide. USDA Natural Resources Conservation Service Misc. Publ. 1492. *U.S. Government Printing Office, Washington, DC, pp. 88-1036.*

Solomon, S., Plattner, G.-K., Knutti, R., Friedlingstein, P. (2009). Irreversible climate change due to carbon dioxide emissions. *Proc. Nat. Acad. Sci. U.S.A., 106, 1704-1709.*

Soulé, P.T., and Knapp P.A. (1999). Western juniper expansion on adjacent disturbed and near relict sites. *Journal of Range Management 52:525-533.*

Soulé, P.T., Knapp, P.A., Grissino-Mayer, H.D. (2004). Human agency, environmental drivers, and western juniper establishment during the late Holocene. *Ecological Applications, 14:96-112.*

Sowder, J.E., and Mowat, E.L. (1958). Sivical characteristics of western juniper. *USDA Forest Service PNW Sivical Series 12.*

Srikanthan, R., and McMahon, T.A. (1982). Simulation of annual and monthly rainfalls a preliminary study at five Australian stations. *J. Appl. Meteorol., 21:1472-9.*

Srikanthan, R., and McMahon, T.A. (2001). Stochastic generation of annual, monthly and daily climate data: a review. *Hydrol Earth Syst Sci, 5:653-70.*

Stephens, G.L. (1978). Radiation profiles in extended water clouds: 2. Parameterization schemes. *J. Atmos. Sci., 35(11):2123-32.*

Sternberg, M., and Shoshany, M. (2001). Influence of slope aspect on Mediterranean woody formations: comparison of a semiarid and an arid site in Israel. *Ecol. Res., 16:335-345. doi: 10.1046/j.1440-1703.2001.00393.x.*

Stoutjesdijk, P.H., and Barkman, J.J. (1992). Microclimate: vegetation and fauna. *Opulus Press, Uppsala*.

Studer, S., Appenzeller, C., Defila, C. (2005). Inter-annual variability and decadal trends in alpine spring phenology: A multivariate analysis approach. *Clim. Change, 73, 395-414.*

Suzaki, T., Kume, A., Ino, Y. (2005). Effects of slope and canopy trees on light conditions and biomass of dwarf bamboo under a coppice canopy. *J. For Res., 10:151-156. doi:10.1007/s103 10-004-0123-x*.

Svoray, T., and Karnielli, A. (2010). Rainfall, topography and primary production relationships in a semiarid ecosystem. *Ecohydrology, 4, 56-66*.

Tague, C. L., and Band, L. E. (2004). RHESSys: Regional Hydro-Ecologic Simulation System: An object-oriented approach to spatially distributed modeling of carbon, water, and nutrient cycling. *Earth Interact., 8(19), 1-42, doi:10.1175/1087-3562(2004)8,1:RRHSSO.2.0.CO;2.*

Takle, E.S., and Brown, J.M. (1978). Note on the use of Weibull statistics to characterize wind-speed data. *J. Appl. Meteorol., 17:556-9.*

Tausch, R.J., and West, N.E. (1988). Differential establishment of piñon and juniper following fire. *American Midland Naturalist, 119:174-184.*

Tausch, R.J., and West, N.E. (1995). Plant species composition patterns with differences in tree dominance on a southwestern Utah piñon-juniper site. *Pages 16–23. In D.W. Shaw, E.F. Aldon, and C. LoSapio (technical coordinators). Proceedings: Desired future conditions for piñon-juniper ecosystems. USDA Forest Service, General Technical Report RM-258.*

Tausch, R.J. and Nowak, R.S. (1999). Fifty years of ecotone change between shrub and tree dominance in the Jack Springs piñon research natural area. *Pages 71-77. In E.D. McArthur, K. W. Ostler, C.L. Wambolt (compilers). Proceedings: Shrubland Ecotones. USDA Forest Service RMRS-P-11*.

Taylor, C.A. (2008). Ecological consequences of using prescribed fire and herbivory to manage Juniperus encroachment. *In: Van Auken, O.W. (Ed.). Wstern North American Juniperus Communities: A Dynamic Vegetation Type. Springer, New York, pp. 239-252.*

Tebaldi, C., Mearns, L., Nychka, D., Smith, R. (2004). Regional probabilities of precipitation change: a Bayesian analysis of multi-model simulations. *Geophys. Res. Lett., 31(L24213). doi:10.1029/2004GL021276.*

Tebaldi, C., Smith, R.L., Nychka, D., Mearns, L.O. (2005). Quantifying uncertainty in projections of regional climate change: a Bayesian approach to the analysis of multi-model ensembles. *J. Climate, 18:1524-40.*

Tebaldi, C., and Knutti, R. (2007). The use of the multi-model ensemble in probabilistic climate projections. *Philos. Trans. Roy. Soc. A., 365(1857):2053-75. doi:10.1098/rsta.2007.2076.*

Terry, R.G., Nowak, R.S., Tausch, R.J. (2000). Genetic variation in chloroplast and nuclear ribosomal DNA in Utah juniper (Juniperus oteosperma, Cupressaceae): evidence for interspecific gene flow. *American Journal of Botany, 87:250-258.*

Thomas, P.A. (1991). Response of Succulents to Fire: A Review. *Int. J. Wildland Fire, (1) 11-22.*

Thompson, R.S., and Hattori, E.M. (1983). Chapter 7. Packrat (Neotoma) middens from Gatecliff shelter and Holocene migrations of woodland plants. *Pages 157-167. In D.H. Thomas (editor). The Archaeology of Monitor Valley. 2. Gatecliff Shelter. Anthropology Paper, American Museum of Natural History No. 59.*

Thompson, R.S. (1984). Late Pleistocene and Holocene environments in the Great Basin. *Ph.D. Dissertation, University of Arizona, Tucson, AZ.*

Tian, Y.Q., Davies-Colley, R.J., Gong, P., Thorrold, B. W. (2001). Estimating solar radiation on slopes of arbitratry aspect. Short communication. *Agric. Forest Meteorol., 109, 67-74.*

Tilma, D. (1988). Plant Strategies and the Dynamics and Structure of Plant Communities. *Princeton Univ. Press, Princeton, New Jersey.*

Tilman, D. (1985). The resource ratio hypothesis of succession. *Amer. Nat., 125, 827-52.*

Tilman, D. (1987). Secondary succession and the pattern of plant dominance along experimental nitrogen gradients. *Ecological Monographs, 57, 189-214.*

Trenberth, K.E., Jones, P.A., Bojariu, R., Easterling, D., Klein Tank, A., Parker, D., Rahimzadeh, F., Renwick, J.A., Rusticucci, M., Soden, B., *et al.* (2007). Observations: Surface and Atmospheric Climate Change. In *Climate Change 2007: The Physical Science Basis. Contribution of Working Group I to the Fourth Assessment Report of the Intergovernmental Panel on Climate Ghange*; *Solomon, S., Qin, D., Manning, M., Chen, Z., Marquis, M., Averyt, K.B., Tignor, M., Miller, H.L., Eds.; Cambridge University Press: Cambridge, UK; New York, NY, USA.*

Turner, M.G., and Bratton, S.P. (1987). Fire, grazing, and the landscape heterogeneity of a Georgia barrier island, in Landscape Heterogeneity and Disturbance. *Springer-Verlag, New York, pp. 85-101.*

Turner, M.G. (1989). Landscape ecology: The effect of pattern on process. *Ann. Rev. Ecol., 20, 171-197.*

Urban, D.L., Miller, C., Halpin, P.N., Stephenson, N.L. (2000). Forest gradient response in Sierran landscapes: the physical template. *Landscape Ecol., 15:603-620. doi:10.1023/A:1008183331604.*

USDA Forest Service. (1981). Atlas of United States trees. Volume I: Conifers and important hardwoods. *USDA Forest Service Miscellaneous Publication No. 1146.*

Vale, T.R. (1982). Plants and people. Vegetation change in North America. *Resource Publs. In Geography, Assoc. Of American Geographers, Washington, D.C.*

Van Auken, O.W., and Bush, J.K. (1988). Competition between Schicachyrium scoparium and Prosopis glandulosa. *Am. J. Bot., 75. 782-789.*

Van Auken, O.W., and Brush, J.K. (1997). Growth of Prosopis glandulosa in response to changes in aboveground and belowground interference. *Ecology, 78: 1222-1229.*

Van Auken, O.W. (2000). Shrub Invasions of North American Semiarid Grasslands. *Annu. Rev. Ecol. Syst., 31:197-215.*

Van Auken, O.W. (2009). Causes and consequences of woody plant encroachment into western North American grasslands. *Journal of Environmental Management, 90, 2931-2942.*

Van Der Merwe, L.L., Wessels, A.B., Ferreira, D.I. (1997). Supplementary irrigation for spineless Cactus Pear. Proceedings of the III International Congress on Cactus Pear and Cochenille. *Acta Horticulturae, 438, 77-82.*

Van der Valk, A.G. (1985). Vegetation dynamics of prairie glacial marshes. *The Population Structure of Vegetation, Junk, Dordrecht, pp. 293-312.*

Van Devender, T.R., Thompson, R.S., Betancourt, J.L. (1987). Vegetation history of the deserts of southwestern North America; The nature and timing of the Late Wisconsin-Holocene transition. *Pages 323-352. In W.F. Ruddiman and H.E. Wright, Jr. (editors). North America and Adjacent Oceans During the Last Deglaciation. The Geology of North America K-3. Geological Society of America, Boulder, CO.*

van Wijk, M.T., and Rodriguez-Iturbe, I. (2002). Tree-grass competition in space and time: Insights from a simple cellular automata model based on ecohydrological dynamics. *Water Resour. Res., 38, 18-1-18-15.*

Vasek, F. C. and Thorne, R. F. (1977). Transmontane coniferous vegetation. *Pages 797-832. In M.G. Barbour and J. Major (editors). Terrestrial Vegetation of California. California Native Plant Society, Special Publication No. 9.*

Vazquez, J.A., and Givnish, T.J. (1998). Altitudinal gradients in tropical forest composition, structure, and diversity in the Sierra de Manantla. *J. Ecol., 86:999-1020. doi:10.1046/j.1365-2745.1998.00325.x*.

Viola, F., Liuzzo, L., Noto, L.V., Lo Conti, F., la Loggia, G. (2013). Spatial distribution of temperature trends in Sicily. *International Journal of Climatology, doi: 10.1002/joc.3657.*

Vogiatzakis, I.N., Griffiths, G.H., Mannion, A.M. (2003). Environmental factors and vegetation composition, LefkaOrimassif, Crete, S Aegean. *Glob. Ecol. Biogeogr., 12:131-146. doi: 10.1046/j.1466-822X.2003.00021.x.*

Wahl, E.W., and Lawson, T.L. (1970). The climate of the mid-nineteenth century United States compared to the current normals. *Monthly Weather Review, 98:259-265.*

Waichler, W.S., Miller, R.F., Doescher, P.S. (2001). Community characteristics of old-growth western juniper woodlands in the pumice zone of central Oregon. *Journal of Range Management, 54:518-527.*

Walter, H. (1973). Vegetation of the Earth. *Springer, New York*.

Walther, G.-R., Post, E., Convey, P., Menzel, A., Parmesan, C., Beebee, T.J.C., Fromentin, J.-M., Hoegh-Guldberg, O., Bairlein, F. (2002). Ecological responses to recent climate change. *Nature, 416, 389-395.*

Walton, J.C., Martinez-Gonzaleza, F., Worthingtonb, R. (2005). Desert vegetation and timing of solar radiation. *Journal of Arid Environments, 60, 697-707.*

Wang, G.L., and Eltahir, E.A.B. (2000). Biosphere-atmosphere interactions over West Africa. II: Multiple climate equilibria. *Q. J. R. Meteorol. Soc., 126(565), 1261-1280.*

Wang, G., and Feng, X. (2012). Response of Plants' Water Use Efficiency to Increasing Atmospheric CO_2 Concentration. *Environmental Science & Technology, 46, 8610-8620.*

Webb, T. (1986). Is vegetation in equilibrium with climate? How to interpret Late-Quaternary pollen data. *Vegetatio, 67, 75-91*.

Wells, P.K. (1983). Paleobiogeography of montane islands in the Great Basin since the last glaciopluvial. *Ecological Monographs, 53:341-382.*

Went, F. W. (1955). The ecology of desert plants. *Scient. Am., 192, 68-75*.

Wessman, C.A.S., Archer, S., Johnson, L.C., Asner, G.P. (2004). Woodland expansion in U.S. grasslands: assessing land-cover change and biogeochemical impacts. *In: Land Change Science: observing. Monitoring and understanding trajectories of change on the Earth's surface. Springer, New York,USA.*

West, N.E., and Van Pelt, N.S. (1986). Successional patterns in piñon-juniper woodlands. In Proc. Piñon-Juniper Conference. *Pages 43-52 in R.L. Everett (compiler). Proceedings: Piñon-juniper Conference. USDA Forest Service, General Technical Report INT-215.*

West, N.E. (1999). Juniper-pinyon savannas and woodlands of western North America. *Pages 288-308. In R.C. Anderson, J.S. Fralish, and J.M. Baskin (editors). Savannas, Barrens, and Rock Outcrop Plant Communities of North America. Cambridge University Press, London, England.*

White, P.S., and Pickett, S.T.A. (1985). Natural disturbance and patch dynamics: An introduction, in the Ecology of Natural Disturbance and Patch Dynamics. *Academic Press, Orlando, pp 3-13.*

White, C.S., Pendleton, R.L., Pendleton, B.K. (2006). Response of Two Semiarid Grasslands to a Second Fire Application. *Rangeland Ecol Manage, 59:98-106.*

Wigand, P.E. (1987). Diamond Pond, Harney County, Oregon: vegetation history and water table in the eastern Oregon desert. *Great Basin Naturalist, 47:427-458.*

Wigand, P.E., Hemphill, M.L., Sharpe, S., Patra, S. (1995). Great Basin semi-arid woodland dynamics during the late Quaternary. *Pages 51-70. In W.J. Waugh (editor). Proceedings: climate change in the four corners and adjacent regions: implications for environmental restoration and land-use planning. Mesa State College, Grand Junction CO. U.S. Department of Energy.*

Wilks, D.S. (1999). Interannual variability and extreme-value characteristics of several stochastic daily precipitation models. *Agric. Forest Meteorol., 93:153-69.*

Wilks, D.S., and Wilby, R.L. (1999). The weather generation game: a review of stochastic weather models. *Prog. Phys. Geograph., 23:329-57.*

Williams, C. A., and Albertson, J. D. (2004). Soil moisture controls on canopy-scale water and carbon fluxes in an African savanna. *Water Resour. Res., 40, W09302, doi:10.1029/2004WR003208.*

Williams, C. A., and Albertson, J. D. (2005). Contrasting short- and long-timescales effects of vegetation dynamics on water and carbon fluxes in water-limited ecosystems. *Water Resour. Res., 41, W06005, doi:10.1029/2004WR003750.*

Wilson, E.B., and Hilferty, M.M. (1931). Distribution of Chi-square. *Proc. Natl. Acad. Sci. USA, 17:684-8.*

Wolfram, S. (1983). Statistical mechanics of cellular automata. *Rev. Mod. Phys., 55, 601-644.*

Wolfram, S. (1984). Universality and complexity in cellular automata. *Physica D: Nonlinear Phenomena. Volume 10, Issues 1-2, Pages 1-35.*

Wolfram, S. (1986). Theory and Applications of Cellular Automata. *World Science Publishers, Singapore.*

Wright, H.A. (1980). The role and use of fire in the semidesert grass-shrub type. *Ogden, UT, USA: US Department of Agricolture, Forest Service, Intermountain Forest and Range Experiment Station, General Technical Report INT-85, 24 pp.*

Wright, H.A., and Bailey, A.W. (1982). Fire ecology. *United States and Canada. New York, NY, USA: John Wiley & Sons. 501 pp.*

Yarronton, G.A., and Morrison, R.G. (1974). Spatial dynamics of a primary succession: Nucleation. *J. Ecol., 62, 417-28.*

Yeakley, J.A., Hornberger, G.M., Swank, W.T., Bolstad, P.V., Vose, J.M. (2000). Soil moisture modelling in humid mountainous landscapes. In: Wilson JP, Gallant JC (eds) Terrain analysis: principles and applications. *Wiley, New York, pp 205-224*.

Yeaton, R.I., and Cody, M.L. (1979). The distribution of cacti along environmental gradients in the Sonoran and Mohave deserts. *Journal of Ecology, 67,529-541*.

Young, J.A., and Evans, R.A. (1981). Demography and fire history of a western juniper stand. *Journal of Range Management, 34:501-505.*

Zeng, X. D., Zeng, X., Barlage, M. (2008). Growing temperate shrubs over arid and semiarid regions in the Community Land Model-Dynamic Global Vegetation Model. *Global Biogeochem. Cycles, 22, GB3003, doi:10.1029/2007GB003014.*

Zhou, X., Istanbulluoglu, E., Vivoni, E.R. (2013). Modeling the ecohydrological role of aspect-controlled radiation on tree-grass-shrub coexistance in a semiarid climate. *Water Resources Research, 49(5): 2872-2895, doi: 10.1002/wrcr.20259.*

Biographical sketch

Domenico Caracciolo was born on 20 January 1986 in Palermo (Italy). In November 2008 he obtained the bachelor's degree in Environmental Engineering at University of Palermo, with full marks and honours (110/110 cum laude). In July 2010 he obtained the Master's degree in Environmental Engineering at University of Palermo, with full marks and honours (110/110 cum laude), with a thesis entitled "Analysis of the influence of the number and position of the raingauges on the hydrological response at the catchment scale". Since January 2011 he is a PhD student in Environmental and Hydraulic Engineering at University of Palermo. His research activities focus on physically based and distributed hydrological models and eco-hydrology. He is currently developing an eco-hydrological cellular automata model. During the three-year doctoral course, he spent six months (from 2nd October 2012 to 29th March 2013) at the University of Washington (Seattle - USA) as visiting scientist, within the research group of Dr. Erkan Istanbulluoglu.